# Omics-driven Drug Repurposing and Treatment Assessment in Human Viral Diseases

Dissertation

zur Erlangung des Doktorgrades (Dr. rer. nat.)

der Mathematisch-Naturwissenschaftlichen Fakultät

der Rheinischen Friedrich-Wilhelms-Universität Bonn

vorgelegt von

Rainer Knoll

aus

Bad Honnef, Deutschland

Bonn, 2024

Angefertigt mit Genehmigung und nach den Richtlinien der Mathematisch-Naturwissenschaftlichen Fakultät der Rheinischen Friedrich-Wilhelms-Universität Bonn.

Gutachter / Betreuer: Prof. Dr. Joachim L. Schultze

Gutachter: Prof. Dr. Jan Hasenauer

Tag der Promotion: 02.04.2025

Erscheinungsjahr: 2025

# Index

# Index of Figures



# Index of Tables

# Abbreviations

| | |
|---|---|
| ACE2 | angiotensin-converting enzyme 2 |
| AI | Artificially intelligence |
| AM | Alveolar macrophages |
| ART | Antiretroviral therapy |
| ATAC-seq | Assay for transposase-accessible chromatin using sequencing |
| BAL | Bronchoalveolar lavage |
| CD | Cluster of differentiation |
| cMap | Connectivity Map |
| COVID-19 | Coronavirus disease 2019 |
| CTSL | Cathepsin L |
| CyTOF | Cytometry by time of flight |
| DAMP | damage associated molecular patterns |
| DEG | Differentially expressed genes |
| DNA | Deoxyribonucleic acid |
| FDA | Federal Drug Administration |
| GSEA | Gene set enrichment analysis |
| hCMV | Human Cytomegalovirus |
| HIV | Human immunodeficiency virus |
| hsCRP | high sensitivity C-reactive protein |
| ICU | Intensive care unit |
| IFN | Interferon |
| IL | Interleukin |
| ILC | Innate lymphoid cells |
| iLINCS | Integrative LINCS |
| INSTI | integrase strand transfer inhibitor |
| LINCS | Library of Integrated Network-based Cellular Signatures |
| MDSC | myeloid derived-suppressor cells |
| miRNA | micro RNA |

| | |
|---|---|
| mRNA | messenger RNA |
| ncRNA | non-coding RNA |
| NES | Normalized enrichment score |
| NGS | Next generation sequencing |
| NNRTI | non-nucleoside reverse transcriptase inhibitor |
| NRTI | nucleoside reverse transcriptase inhibitor |
| PAMP | pathogen associated molecular patterns |
| PBMC | Peripheral blood mononuclear cells |
| PCA | Principal component analysis |
| PI | protease inhibitors |
| PLHIV | People living with HIV |
| PRR | Pattern recognition receptors |
| RNA | Ribonucleic acid |
| RNA-seq | RNA sequencing |
| SARS-CoV-2 | Severe acute respiratory syndrome |
| scRNA-seq | Single-cell RNA sequencing |
| SRP | signature reversion principle |
| TLR | Toll-like receptor |
| TMPRSS2 | transmembrane protease serine subtype 2 |
| WHO | World Health Organization |

# Relevant publications

- **2024**

**Knoll R***, Helbig ET*, Dahm K, Bolaji O, Hamm F, Dietrich O, van Uelft M, Müller S, Bonaguro L, Schulte-Schrepping J, Petrov L, Krämer B, Kraut M, Stubbemann P, Thibeault C, Brumhard S, Theis H, Hack G, De Domenico E, Nattermann J, Becker M, Beyer MD, Hillus D, Georg P, Loers C, Tiedemann J, Tober-Lau P, Lippert L, Pascual-Leone BM, Tacke F, Rohde G, Suttorp N, Witzenrath M, CAPNETZ Study Group, Pa-COVID-19 Study Group, Saliba AE, Ulas T, Polansky JK, Sawitzki B, Sander LE[#], Schultze JL[#], Aschenbrenner AC[#,§], Kurth F[#], "**The life-saving benefit of dexamethasone in severe COVID-19 is linked to a reversal of monocyte dysregulation**", Cell. 2024 Jul, doi: https://doi.org/10.1016/j.cell.2024.06.014.

Heumos L, Ehmele P, Treis T, Upmeier zu Belzen J, Namsaraeva A, Horvlava N, Shitov VA, Zhang X, Zappia L, **Knoll R**, Lang NJ, Hetzel L, Virshup I, Sikkema L, Roellin E, Curion F, Eils R, Schiller HB, Hilgendorff A, Theis FJ[§], "**An open-source framework for end-to-end analysis of electronic health record data**", N*ature Medicine*. 2024 Sep 12, doi: https://doi.org/10.1038/s41591-024-03214-0

- **2023**

**Knoll R**, Bonaguro L, Dos Santos JC, Warnat-Herresthal S, Jacobs-Cleophas MCP, Blümel E, Reusch N, Herbert M, Otten T, van der Heijden WA, van de Wijer L, Shalek AK, Händler K, Becker M, Beyer MD, Netea MG, Joosten LAB, van der Ven AJAM, Schultze JL[#], Aschenbrenner AC[#,§], "**Identification of drug candidates targeting monocyte reprogramming in people living with HIV**", Front Immunol. 2023 Nov 20;14:1275136. doi: 10.3389/fimmu.2023.1275136.

- **2022**

Vos WAJW*, Groenendijk AL*, Blaauw MJT, van Eekeren LE, Navas A, Cleophas MCP, Vadaq N, Matzaraki V, Dos Santos JC, Meeder EMG, Fröberg J, Weijers G, Zhang Y, Fu J, Ter Horst R, Bock C, **Knoll R**, Aschenbrenner AC, Schultze J, Vanderkerckhove L, Hwandih T, Wonderlich ER, Vemula SV, van der Kolk M, de Vet SCP, Blok WL, Brinkman K, Rokx C, Schellekens AFA, de Mast Q, Joosten LAB, Berrevoets MAH, Stalenhoef JE, Verbon A, van Lunzen J, Netea MG, van der Ven AJAM, "**The 2000HIV study: Design, multi-omics methods and participant characteristics**", Front Immunol. 2022 Dec 20;13:982746. doi: 10.3389/fimmu.2022.982746.

Baßler K*, Fujii W*, Kapellos TS*, Dudkin E*, Reusch N*, Horne A, Reiz B, Luecken MD, Osei-Sarpong C, Warnat-Herresthal S, Bonaguro L, Schulte-Schrepping J, Wagner A, Günther P, Pizarro C, Schreiber T, **Knoll R**, Holsten L, Kröger C, De Domenico E, Becker M, Händler K, Wohnhaas CT, Baumgartner F, Köhler M, Theis H, Kraut M, Wadsworth MH, Hughes TK, Ferreira HJ, Hinkley E, Kaltheuner IH, Geyer M, Thiele C, Shalek AK, Feißt A, Thomas D, Dickten H, Beyer M, Baum P, Yosef N, Aschenbrenner AC, Ulas T, Hasenauer J, Theis FJ, Skowasch D, Schultze JL, "**Alveolar macrophages in early stage COPD show functional deviations with properties of impaired immune activation**", Front Immunol. 2022 Jul 28;13:917232. doi: 10.3389/fimmu.2022.917232.

- **2021**

Krämer B*, **Knoll R***, Bonaguro L*, ToVinh M*, Raabe J*, Astaburuaga-García R, Schulte-Schrepping J, Kaiser KM, Rieke GJ, Bischoff J, Monin MB, Hoffmeister C, Schlabe S, De Domenico E, Reusch N, Händler K, Reynolds G, Blüthgen N, Hack G, Finnemann C, Nischalke HD, Strassburg CP, Stephenson E, Su Y, Gardner L, Yuan D, Chen D, Goldman J,

Rosenstiel P, Schmidt SV, Latz E, Hrusovsky K, Ball AJ, Johnson JM, Koenig1 P-A, Schmidt FI, Haniffa M, Heath JR, Kümmerer BM, Keitel V, Jensen B, Stubbemann P, Kurth F, Sander FE, Sawitzki B, Deutsche COVID-19 Omics Initiative (DeCOI), Aschenbrenner AC[#], Schultze JL[#], Nattermann J[#,§], "**Early IFN-α signatures and persistent dysfunction are distinguishing features of NK cells in severe COVID-19**", Immunity. 2021 Sep 4, doi: 10.1016/j.immuni.2021.09.002

**Knoll R**, Schultze JL, Schulte-Schrepping J, "**Monocytes and Macrophages in COVID-19**", Front Immunol. 2021 Jul 21;12:720109. doi: 10.3389/fimmu.2021.720109.

Aschenbrenner AC*, Mouktaroudi M*, Krämer B*, Oestreich M*, Antonakos N*, Nuesch-Germano M*, Gkizeli K*, Bonaguro L*, Reusch N*, Baßler K*, Saridaki M*, **Knoll R***, Pecht T*, Kapellos TS*, Doulou S*, Kröger C*, Herbert M*, Holsten L*, Horne A*, Gemünd ID*, Rovina N*, Agrawal S*, Dahm* K, van Uelft M*, Drews A*, Lenkeit L*, Bruse N*, Gerretsen J, Gierlich J, Becker M, Händler K, Kraut M, Theis H, Mengiste S, De Domenico E**,** Schulte-Schrepping J, Seep L, Raabe J, Hoffmeister C, ToVinh M, Keitel V, Rieke G, Talevi V, Skowasch D, Aziz NA, Pickkers P, van de Veerdonk FL, Netea MG[#], Schultze JL[#], Kox M[#], Breteler MMB[#], Nattermann J[#], Koutsoukou A[#], Giamarellos-Bourboulis EJ[#], Ulas T[#,§], German COVID-19 Omics Initiative (DeCOI)., "**Disease severity-specific neutrophil signatures in blood transcriptomes stratify COVID-19 patients.**", Genome Med. 2021 Jan 13;13(1):7. doi: 10.1186/s13073-020-00823-5.

Wendisch D*, Dietrich O*, Mari T*, von Stillfried S*, Ibarra IL, Mittermaier M, Mache C, Chua RL, **Knoll R**, Timm S, Brumhard S, Krammer T, Zauber H, Hiller AL, Pascual-Reguant A, Mothes R, Bülow RD, Schulze J, Leipold AM, Djudjaj S, Erhard F, Geffers R, Pott F, Kazmierski J, Radke J, Pergantis P, Baßler K, Conrad C, Aschenbrenner AC, Sawitzki B, Landthaler M, Wyler E, Horst D, Hippenstiel S, Hocke A, Heppner FL, Uhrig A, Garcia C, Machleidt F, Herold S, Elezkurtaj S, Thibeault C, Witzenrath M, Cochain C, Suttorp N, Drosten C, Goffinet C, Kurth F, Schultze JL, Radbruch H, Ochs M, Eils R, Müller-Redetzky H, Hauser AE, Luecken MD, Theis FJ, Conrad C, Wolff T[#], Boor P[#], Selbach M[#], Saliba AE[#], Sander LE[#,§], "**SARS-CoV-2 infection triggers profibrotic macrophage responses and lung fibrosis**", Cell. 2021 Dec 22;184(26):6243-6261.e27. doi: 10.1016/j.cell.2021.11.033.

Fujii W*, Kapellos TS*, Baßler K*, Händler K, Holsten L, **Knoll R**, Warnat-Herresthal S, Oestreich M, Hinkley ER, Hasenauer J, Pizarro C, Thiele C, Aschenbrenner AC, Ulas T, Skowasch D[#], Schultze JL[#,§], "**Alveolar macrophage transcriptomic profiling in COPD shows major lipid metabolism changes**", ERJ Open Research 2021 7: 00915-2020. doi: 10.1183/23120541.00915-2020.

- **2020**

Bernardes JP*, Mishra N*, Tran F*, Bahmer T, Best L, Blase JI, Bordoni D, Franzenburg J, Geisen U, Josephs-Spaulding J, Köhler P, Künstner A, Rosati E, Aschenbrenner AC, Bacher P, Baran N, Boysen T, Brandt B, Bruse N, Dörr J, Dräger A, Elke G, Ellinghaus D, Fischer J, Forster M, Franke A, Franzenburg S, Frey N, Friedrichs A, Fuß J, Glück A, Hamm J, Hinrichsen F, Hoeppner MP, Imm S, Junker R, Kaiser S, Kan YH, **Knoll R**, Lange C, Laue G, Lier C, Lindner M, Marinos G, Markewitz R, Nattermann J, Noth R, Pickkers P, Rabe KF, Renz A, Röcken C, Rupp J, Schaffarzyk A, Scheffold A, Schulte-Schrepping J, Schunk D, Skowasch D, Ulas T, Wandinger KP, Wittig M, Zimmermann J, Busch H[#], Hoyer BF[#], Kaleta C[#], Heyckendorf J[#], Kox M[#], Rybniker J[#], Schreiber S[#], Schultze JL[#], Rosenstiel P[#,§]; HCA Lung Biological Network; Deutsche COVID-19 Omics Initiative (DeCOI)., "**Longitudinal Multi-omics Analyses Identify Responses of Megakaryocytes, Erythroid Cells, and**

**Plasmablasts as Hallmarks of Severe COVID-19**", Immunity. 2020 Dec 15;53(6):1296-1314.e9. doi: 10.1016/j.immuni.2020.11.017.

*shared first authorship / #shared last authorship / §corresponding author

# Acknowledgements

This thesis is the highlight of my doctorate and would not have been possible without the support, guidance and motivation of many people. I am deeply grateful to everyone who has been a part of this journey and contributed to my personal and professional growth along the way.

First and foremost, I would like to extend my deepest gratitude to my mentors and supervisors, my first examiner Prof. Dr. Joachim L. Schultze and my group leader Dr. Anna C. Aschenbrenner. From the start of my doctorate, both trusted my abilities, saw my potential and gave me the opportunity to work and contribute in many fascinating projects enabling me to learn and grow. I am grateful for their continuous support, their guidance, their trust in my work and for the examination of this thesis.

I would also express my thanks to Prof. Dr. Jan Hasenauer for taking the time to examine my thesis. Additionally, I would like to thank Prof. Dr. Martin Hofmann-Apitius and Prof. Dr. Jacob Nattermann for being part of my dissertation committee.

Furthermore, to all of my past and present colleagues in the Aschenbrenner lab as well as the Systems Medicine department: Thank you for creating an environment of collaboration, learning, mutual support and fun which made my doctorate very much enjoyable! In particular, I would like to thank Charlotte Kröger, Jonas Schulte-Schrepping, Lorenzo Bonaguro, Nico Reusch, Victoria Isakzai, Sophie Müller, Emilia De Caro, Michael Kraut, Lisa Holsten, Kilian Dahm, Jannis Spintge, Elke Schubert, Heidi Theis, Martina van Uelft, Elena De Domenico, Kevin Baßler, Jacqueline Leidner, Shubhi Ambast, Jesse Asimeng, Karola Mai, Karoline Mauer and Thomas Ulas for their guidance, helpfulness, vivid discussions, mensa talks and coffee breaks.

Moreover, I wish to express my sincere gratitude to the many fruitful collaboration partners which made this thesis possible.

Finally, I am deeply grateful to my family for their support throughout every step of this journey. Their constant encouragement, understand and belief in me gave me the necessary motivation.

# 1. Summary

In this cumulative thesis, I present my research on transcriptomic-based drug repurposing in human viral infections describing an optimized workflow for drug prediction, *in vitro* validation and *in vivo* studies in clinical cohorts based on three publications.

In the first publication, I took lead in a larger team effort to introduce a newly designed drug repurposing approach based on whole blood transcriptomics data and drug signatures databases, which was applied to identify potential drug candidates for treatment of patients across COVID-19 severity groups stratified based on clinical parameters and transcriptomic phenotypes (Aschenbrenner et al. 2021). One of the drug candidates identified using this approach was dexamethasone, which was predicted to be effective in the most severe group of COVID-19 patients.

In the second publication, I present my findings on transcriptomic alterations in the monocyte compartment in chronically infected HIV patients using multi-omics technologies, demonstrate that these alterations originate from a certain disease state and identify potential drug candidates for the reversal of the disease signatures in monocytes (Knoll et al. 2023). In this study, I further extend the transcriptomics drug repurposing approach by refining the underlying disease signatures using single-cell omics for drug prediction and I validate promising drug candidates using *in vitro* stimulation experiments. Reading out direct drug-induced transcriptional alterations from these *in vitro* studies substantially strengthened the results from the drug repurposing approach.

In the third publication, I describe our framework on how to investigate repurposed drugs in clinical cohorts *in vivo* using single-cell transcriptomics towards precision medicine, exemplified with dexamethasone treatment in COVID-19 (Knoll et al. 2024). Dexamethasone caused strong transcriptional and immunomodulatory changes with a reversal of dysregulation in severe COVID-19 monocytes compared to treatment-naïve patients. Moreover, a treatment-specific monocyte response state was identified which stratified outcome and enabled prediction of treatment responses, stressing the potential of single-cell transcriptomics for companion diagnostics and mechanistic studies of repurposed drugs.

In conclusion, the research presented in this thesis describes the design and application of a transcriptomics-based drug repurposing pipeline for human viral infections. It highlights the significant potential of drug repurposing in context of data-driven disease severity stratification using optimized cell-state specific disease signatures. Moreover, it underscores the importance of *in vitro* validation for promising drug candidates to reverse disease signatures. This paves the way for a standardized analytical approach to evaluate drug indications in

clinical cohorts *in vivo*, utilizing single-cell transcriptomics for treatment response stratification, ultimately enabling precision medicine (Figure 1).

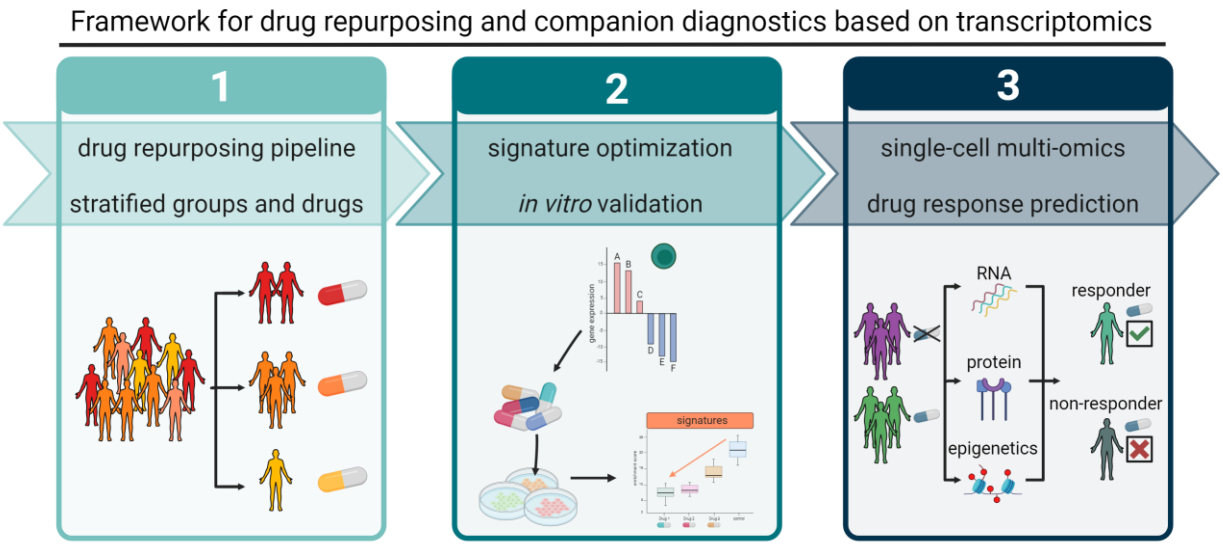


**Figure 1: Graphical overview of drug repurposing framework towards companion diagnostics based on transcriptomics data.**
Summary of the presented thesis consisting of three parts: 1) establishment of the drug repurposing pipeline and identification of drugs patient and therapy stratification, 2) signature optimization for drug repurposing from disease-driving cell states and *in vitro* validation of drug candidates and 3) single-cell multi-omics for assessment of repurposed drug effects as well as identification and prediction of treatment response as a basis for companion diagnostics.

# 2. Introduction

## 2.1. Evolution of omics for systems medicine

In biology, the term “omics” describes the comprehensive and complete analysis of biomolecules or processes of a specific type within a biological system. There are five major omics disciplines: 1) genomics; which studies the set of genes of an organism with respect to the structure, function and interaction, 2) transcriptomics; which studies all RNA molecules produced by genes, 3) proteomics; which describes all proteins translated from RNA including structure, function, interaction and modification, 4) metabolomics; which studies all metabolites and 5) epigenomics; which studies modifications to DNA and histones related to gene expression regulation. The related suffix “-ome” relates to all molecules and objects of the respective field, e.g. the transcriptome describes the entirety of RNA molecules such as messenger RNA (mRNA), non-coding (ncRNA) or micro RNA (miRNA) produced within cells or tissues at a specific time. Each omics discipline utilized high-throughput methodologies yielding comprehensive measurements of unprecedented resolution. Recent developments in the field of microfluidics and nanoliter reaction efficiency, further increase the resolution to apply omics at the level of individual cells, allowing to study physiological and pathological processes at the smallest structural and functional unit of life.

Profiling gene expression is considered to be one of the most powerful approaches to characterize disease-associated molecular alterations. First steps towards comprehensive measurements of the transcriptome were made with the invention of DNA microarrays in 1995, which allowed to probe thousands of genes with fluorescent dyes at a time (Figure 2, Schena et al. 1995). Although microarrays proofed to be very valuable in describing and classifying human diseases, their main drawback is that previously unknown transcripts cannot be tested as the probes need to be designed with known nucleotide sequences. More than a decade after the invention of microarrays, next generation sequencing (NGS) revolutionized the field of genomics and transcriptomics (Metzker 2010; Mardis 2011; Emrich et al. 2007). NGS technologies enabled rapid processing of increased sample sizes at unprecedented speed. As sequencing is performed from DNA, RNA need to be reverse transcribed to DNA in order to measure the RNA levels of a sample. With continuous technology optimization, sequencing costs were strongly reduced over the years, outpacing Moore’s Law. In 2001, the cost per megabase of DNA sequence was approximately $10,000 (Wetterstrand 2024). By 2022, technological advancements had driven this cost down by a staggering factor of $10^6$. For illustration, the sequencing costs of one human genome reduced from $100 Million to $1,000. Using NGS, all present RNA species of a sample could be measured in an unbiased and high throughput manner, leading to identification of previously unknown transcripts and biomarkers.

By that time, experiments were mostly performed on samples comprising a mixture of cells from a tissue, the so-called bulk transcriptomics. Bulk transcriptomics lead to valuable findings in characterization of human diseases, however, its main disadvantage is that gene expression is averaged across all cells in the sample. This can lead to a loss of signal from different cell types and rare subpopulations driving a disease can be overseen. Only few years after the invention of bulk RNA-sequencing (RNA-seq), a technological breakthrough in 2009 enabled the whole-transcriptome sequencing of a single-cell (Tang et al. 2009).

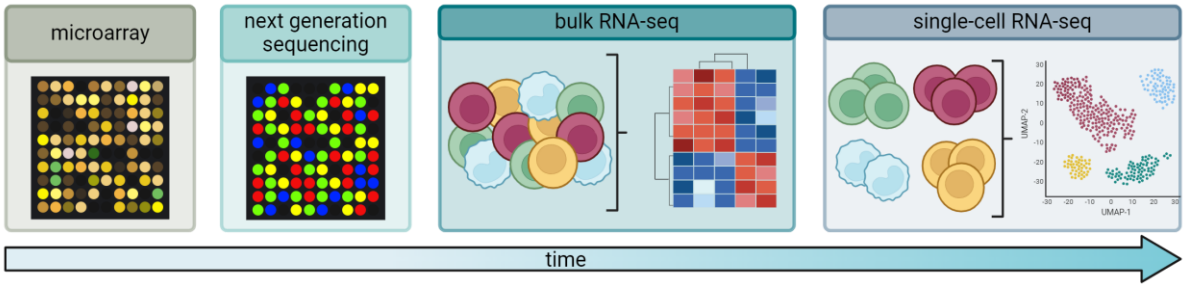


**Figure 2: Evolution of transcriptomic methods and technologies.**
Schematic overview of the development of omics methods and their application for transcriptomics over time. Microarray technology dominated the field after its invention in 1995, but was replaced with next generation sequencing (NGS) approaches a decade later. Their high throughput, unbiased quantification of gene expression and low cost were superior. NGS was first applied to measure the transcriptome of a mixture of cells per sample (bulk RNA-seq) but recent advancements let to higher resolutions, allowing the measurement of transcriptomes from single-cells (single-cell RNA-seq). Figure was created with Biorender.com.

Since then, improved and advanced single-cell (sc)RNA-seq technologies and protocols were developed, enhancing sample collection, processing, single-cell isolation, cDNA amplification, library preparation and sequencing (Svensson et al. 2018; De Domenico et al. 2020). With the technological developments, costs per sequenced cell strongly decreased while number of cells per experiment increased, allowing for the wide application in the scientific community which is reflected by the rapid increase of publications including scRNA-seq (Jovic et al. 2022) (Figure 3). The notable increase of single-cell studies in the recent years can, in part, be explained by the COVID-19 pandemic where single-cell transcriptomics proofed to be a powerful tool in unraveling the pathogenesis of the disease, which will be further addressed in the following section.

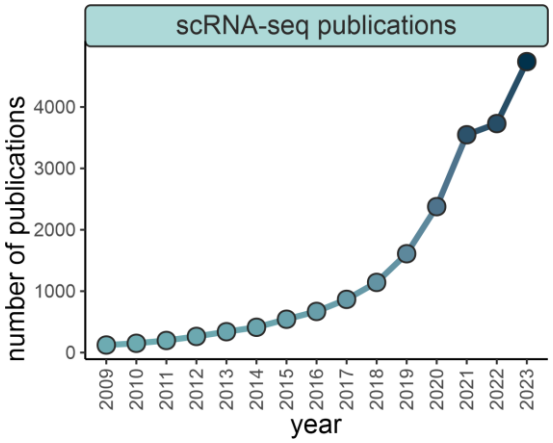


**Figure 3: Number of publications including single-cell RNA-seq (Pubmed search).**
Number of published studies that include scRNA-seq by year extracted by pubmed search (performed on pubmed.ncbi.nlm.nih.gov on 21.05.2024, searching for “single cell RNA seq”).

As the number of single cells analyzed in scRNA-seq datasets can reach several million (Cao et al. 2020; Sikkema et al. 2023; Li et al. 2023; Terekhova et al. 2023), the dimension and thereby the file size of these datasets continues to expand significantly. Managing such vast amounts of data effectively demands substantial computational resources for storage and processing. In addition to the required computing resources, novel computational solutions and algorithms are needed for informative analyses and biological interpretation (Lähnemann et al. 2020; Kiselev et al. 2019). At a rapid pace, novel methods, algorithms and tools for analysis are being developed, rigorously tested and fine-tuned for optimization (Zappia and Theis 2021). The vast amount of possibilities for the analysis of scRNA-seq data requires continuous exchange in the scientific community, well documented guidelines and best practices (Haque et al. 2017; Bonaguro et al., 2022; Heumos et al. 2023).

### 2.1.1. Studying the immune system using scRNA-seq

Due to its immense complexity and heterogeneity as well as its easy accessibility, the immune system represents a prime target for scRNA-seq (Papalexi and Satija 2018). The immune system comprises various cell types that can be broadly grouped into T cells, B cells, innate lymphoid cells (ILCs), macrophages, monocytes, dendritic cells (DCs) and granulocytes, each with distinct roles and functionalities. By employing scRNA-seq, molecular signatures and pathways specific for the respective cell groups can be characterized. This is powerful for dissecting the cellular heterogeneity of the immune system and identifying rare cell populations. For instance, different subsets of monocytes and DCs can be distinguished by their gene expression profiles and even previously unknown subsets can be identified (Villani et al. 2017). Moreover, scRNA-seq provides unprecedented insights during immune

responses in disease, enabling the discovery of transient cell states and molecular changes, that are difficult to capture using traditional methods. In example, Keren-Shaul et al. demonstrated the power of scRNA-seq by identifying a novel subset of microglia which associated with Alzheimer's disease and describing their markers and pathways (Keren-Shaul et al. 2017). These studies exemplify how scRNA-seq can be utilized to understand the immune system in health and disease, facilitating the discovery of novel cellular states, biomarkers and therapeutic targets (Figure 4).

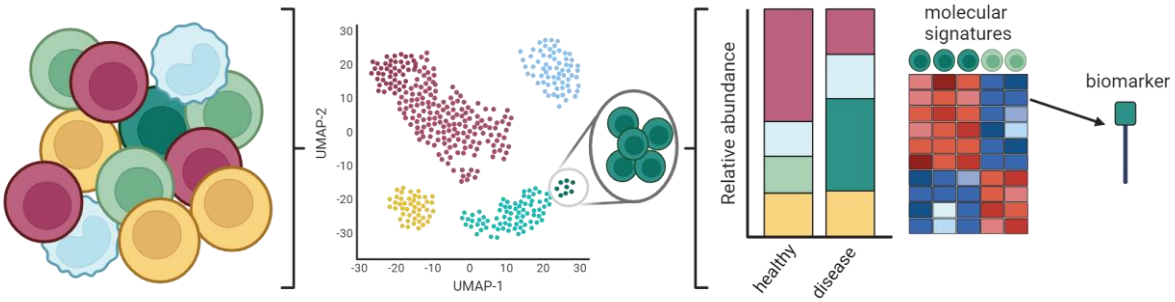


**Figure 4: Simplified overview of scRNA-seq dissection of the immune system.**
Simplified overview showing the potential of scRNA-seq to identify rare cellular states during immune responses in health and disease. Disease-associated states are more abundant in diseased patients and show distinct molecular signatures. These molecular signatures can give rise to new biomarkers for disease identification. Figure generated with Biorender.com.

## 2.2. The COVID-19 pandemic

In December 2019, several unexplained pneumonia cases emerged in Wuhan, China (WHO 2020). A novel coronavirus was quickly isolated from epithelial cells of infected patients, first named 2019-nCoV but in February 2020 renamed to severe acute respiratory syndrome coronavirus 2 (SARS-CoV-2) by the international Committee on Taxonomy of Viruses (Wu et al. 2020; Zhang and Holmes 2020). The disease caused by SARS-CoV-2 was termed coronavirus disease 2019 (COVID-19) by the World Health Organization (WHO) (Gandhi et al. 2020; Berlin et al. 2020). From China, a rapid spread of the virus and COVID-19 occurred around the globe, causing the most devastating pandemic of the recent decades with serious health, economic and social consequences worldwide (Nicola et al. 2020; Smit et al. 2023). As of April 2024, the WHO reported 775.3 million confirmed COVID-19 cases of which more than 7 million deceased (WHO 2024).

SARS-CoV-2 is an enveloped, positive-sense, single-stranded RNA virus of approx. 80nm in diameter belonging to the genus betacoronavirus (Yao et al. 2020). The virus enters the host cells by binding of its viral spike proteins to the host receptor angiotensin-converting enzyme 2 (ACE2) following membrane fusion (Jackson et al. 2021). In addition, the furin-like proteases, transmembrane protease serine subtype 2 (TMPRSS2) and cathepsin L (CTSL) play important roles for viral entry into the host cytoplasm (Hoffmann et al. 2020). Exploiting human (single-cell) transcriptome databases revealed that type II alveolar cells in the lower lung and even more upper bronchial and nasal epithelia, especially ciliated cells, showed expression of ACE2 (Hou et al. 2020; Sungnak et al. 2020; Wang et al. 2020; Ahn et al. 2021). A single-cell meta-analysis of 31 lung studies further assessed expression of *ACE2*, *TMPRSS2* and *CTSL* and identified risk factors such as age, sex and smoking to associate with higher expression of these genes (Muus et al. 2021). Besides the respiratory system as the primary infection site, ACE2 expression was also identified in cells of other organs such as in small intestine, colon, heart, muscle, kidney, testis and thyroid gland (Ziegler et al. 2020; Zou et al. 2020; Hikmet et al. 2020).

COVID-19 is a very heterogenous disease with disease courses ranging from asymptomatic to mild, severe and even critical courses with fatal outcome (Schultze and Aschenbrenner 2021). The most common features of COVID-19 are acute respiratory manifestations with symptoms such as cough, fever and in more severe cases pneumonia with hypoxemia, which can worsen to acute respiratory distress syndrome (ARDS) and/or multi-organ failure (Novel Coronavirus Pneumonia Emergency Response Epidemiology Team 2020; Osuchowski et al. 2021; Lamers and Haagmans 2022). Besides respiratory manifestations, many extrapulmonary manifestations have been reported, including neurologic, renal, hepatic, gastrointestinal, thromboembolism, cardiac, endocrine and dermatological manifestations

(Gupta et al. 2020; Osuchowski et al. 2021). In addition to these acute manifestations, about 10% of SARS-CoV-2 infected individuals develop long-lasting symptoms summarized under the term “long COVID” or “post-COVID-19 syndrome” (Davis et al. 2023; Mehandru and Merad 2022; Kedor et al. 2022). Symptoms include fatigue, cognitive impairment, memory loss, dyspnea, cough, chest pain and abdominal pain. This broad variety of symptoms makes it challenging to diagnose long COVID and several risk factors such as age, sex, ethnicity, comorbidities like type 2 diabetes, presence of autoantibodies and genetic polymorphisms have been reported (Davis et al. 2023; Su et al. 2022; National Center for Health Statistics. U.S 2024).

The rapid emergence and spread of COVID-19 around the globe led to a swift response by governments and especially the scientific community to diagnose the disease, to understand the immunopathology and to develop therapeutic strategies. At an unprecedented speed, testing kits were produced, both antibody- and PCR-based (Vandenberg et al. 2020; Filchakova et al. 2022), clinical trials for drugs such as for remdesivir or dexamethasone were conducted (RECOVERY Collaborative Group et al. 2021; Beigel et al. 2020; Salama et al. 2021) and vaccines were developed (Tregoning et al. 2021; Watson et al. 2022). As of April 2024, approx. 13.6 billion vaccine doses were administered (WHO 2024), preventing millions of deaths and paving the way to get COVID-19 under control. To understand the immunopathology of COVID-19, large-scale single-cell multi-omics studies have proven to be highly powerful in providing unprecedented level of details into disease progression, heterogeneity of severities and immune system alterations (Bernardes et al. 2020; Schulte-Schrepping et al. 2020; Krämer et al. 2021; Wendisch et al. 2021; Stephenson et al. 2021; Su et al. 2020; Georg et al. 2022; Liao et al. 2020; Chua et al. 2020; Arunachalam et al. 2020; Combes et al. 2021; Delorey et al. 2021; Ren et al. 2021; COvid-19 Multi-omics Blood ATlas (COMBAT) Consortium 2022; Sinha et al. 2022; Yoshida et al. 2022; Ziegler et al. 2021; Liu et al. 2021; Wilk et al. 2021; Woodall et al. 2024; Edahiro et al. 2023).

## 2.2.1. Monocytes and macrophages in COVID-19

**Knoll R**, Schultze JL, Schulte-Schrepping J, "**Monocytes and Macrophages in COVID-19**", Front Immunol. 2021 Jul 21;12:720109. doi: 10.3389/fimmu.2021.720109.

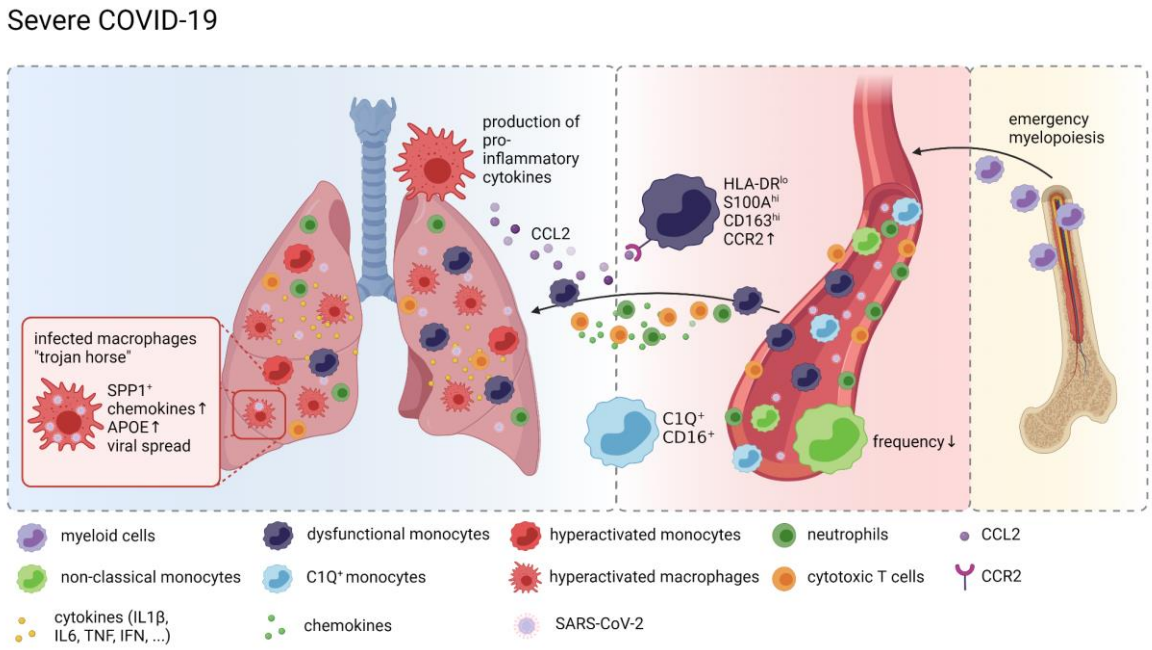


**Figure 5: Monocytes and macrophages in COVID-19.**
Graphical overview of the compositional and molecular alterations in monocyte and alveolar macrophage populations in COVID-19. Distinct monocyte and macrophage phenotypes were identified in the peripheral blood of patients with severe COVID-19 including immature cells indicating emergency myelopoiesis, dysfunctional HLA-DR$^{lo}$ classical monocytes and complement gene expressing non-classical monocytes. These cells are attracted to the lung by pro-inflammatory chemokines resulting in a continuous accumulation of hyperactivated MNPs producing more pro-inflammatory mediators recruiting more inflammatory cells, including cytotoxic T cells and neutrophils, thus further exacerbating inflammation and tissue damage. SARS-CoV-2 infected macrophages in the lung may act as trojan horses propagating SARS-CoV-2 infection and spreading hyperinflammation across the lung. Figure and legend taken from (Knoll et al. 2021).

COVID-19 has been associated with profound changes in the immune system, including increased levels of pro-inflammatory cytokines, neutrophilia, appearance of immature neutrophils, lymphopenia and myeloid dysregulation (Chen et al. 2020; Qin et al. 2020; Mehta et al. 2020; Schulte-Schrepping et al. 2020; Aschenbrenner et al. 2021; Cao 2020; Liao et al. 2020).

In (Knoll et al. 2021), we described monocyte and macrophage ontogeny and function, their general role in viral respiratory infections and summarized current findings about monocytes and macrophages in COVID-19.

The lung acts as a barrier between the outside world and the inside of the organism. With every inhalation, the organism is exposed to pathogens including viruses, bacteria and fungi (Prussin et al. 2015). Macrophages are the most abundant immune cells in the lung under

homeostatic conditions and act as a first line of defense to prevent infection. Depending on their location, macrophages can be distinguished into $CD11c^{neg}CD11b^{pos}$ interstitial macrophages (IM), which are residing in the lung parenchyma or $CD11c^{pos}CD11b^{neg}$ alveolar macrophages (AM), residing in the airspace lumen close to alveolar epithelial cells (Hussell and Bell 2014; Franke-Ullmann et al. 1996).

AMs originate from the yolk sac and populate the lung early after birth (Schulz et al. 2012; Guilliams et al. 2013). Due to self-renewal, the AM population in the lung is independent from bone marrow replacement and can persist lifelong (Tarling et al. 1987; Sawyer et al. 1982; Golde et al. 1974). Under homeostatic conditions, AMs have an anti-inflammatory and immunosuppressive phenotype characterized by clearance of debris, tissue remodeling, production of immunosuppressive prostaglandins and production of anti-inflammatory cytokines such as IL-10 and TGFβ (Hussell and Bell 2014; Coleman et al. 2013; Soroosh et al. 2013; Morris et al. 2003). AM phenotype is, however, strongly dependent on the local microenvironment can change between a e.g. pro- and anti-inflammatory state, described as AM plasticity (Coleman et al. 2013; Watanabe et al. 2019).

Upon infection, AMs switch to a pro-inflammatory state due to loss of anti-inflammatory signals such as CD200/CD200R and recognition of pathogen associated molecular patterns (PAMP) or damage associated molecular patterns (DAMP) *via* pattern recognition receptors (PRR) (Snelgrove et al. 2008; Steinmüller et al. 2000). Activated AMs have higher phagocytic activity, oxidative burst and enhanced production of pro-inflammatory cytokines and chemokines, leading to recruitment of other immune cells such as neutrophils, cytotoxic T cells and monocytes, that can differentiate into macrophages and enhance inflammation (Trapnell and Whitsett 2002; Baharom et al. 2017). To prevent prolonged inflammation with tissue damage, AMs switch to an anti-inflammatory state, enhancing tissue repair, removal of dying cells and secretion of anti-inflammatory mediators (Watanabe et al. 2019; Ortega-Gómez et al. 2013). If this tight balance between inflammation and resolution is lost, severe consequences for the organism can occur.

COVID-19 has a profound impact on the immune system leading to systemic elevation of cytokine and chemokine levels. The myeloid compartment plays an important role during the disease, as quantitative and phenotypic alterations varying by disease severity have been described.

In blood, reduced percentages of total monocytes were detected in severe COVID-19 using flow cytometry (Qin et al. 2020; Laing et al. 2020; Zhou et al. 2020). A significant reduction was described for non-classical monocytes in multiple studies using flow cytometry and/or single-cell transcriptomics (Gatti et al. 2020; Wilk et al. 2020; Schulte-Schrepping et al. 2020).

Patients admitted to ICU had expanded intermediate CD14+CD16+ monocytes with high expression of IL-6 compared to non-ICU patients (Zhou et al. 2020) and inflammatory myeloid cells were found to be increased in severe COVID-19 (Yim and Mizushima 2020).

Besides quantitative changes, monocytes in the blood also exhibited profound phenotypic alterations. Monocytes had higher expression of CD169, a clear sign of activation (Gatti et al. 2020) and featured inflammasome activation and increased pyroptosis from COVID-19 patients in ICU (Ferreira et al. 2021). Most importantly, monocytes from severely ill COVID-19 patients showed a reduced expression of the MHC-class-II receptor HLA-DR, which is a typical sign of immune suppression (Silvin et al. 2020; Schulte-Schrepping et al. 2020; Payen et al. 2020; Giamarellos-Bourboulis et al. 2020; Spinetti et al. 2020). This dysfunctional monocyte state strongly correlated with disease severity and outcome (Wang et al. 2020) as well as with levels of immunosuppressive factors such as IL-10, TGF-β, VEGFA and AREG (Kvedaraite et al. 2021). This cellular state was described by anti-inflammatory and immature gene expression as well as high levels of alarmins (S100A) (Silvin et al. 2020; Schulte-Schrepping et al. 2020; Su et al. 2020; Bernardes et al. 2020). Immunosuppression of HLA-DR$^{lo}$ monocytes was further demonstrated by their ability to suppress T cell proliferation via ARG-1 (Falck-Jones et al. 2021), showing similar characteristics to myeloid derived-suppressor cells (MDSC) which were previously described in chronic inflammation (Hegde et al. 2021). Patients with mild disease on the other hand had increased interferon-stimulated gene signatures in HLA-DR$^{hi}$ inflammatory monocytes (Schulte-Schrepping et al. 2020).

In the lung, infiltration of activated monocytes from the blood was observed in animal models and patients with COVID-19 (Nouailles et al. 2021; Sánchez-Cerrillo et al. 2020). In bronchoalveolar lavage fluid (BALF) of severe COVID-19 patients, a significant alteration in immune cell composition with increased proportions of macrophages was described (Liao et al. 2020). Tissue-resident AM were mostly depleted in severe COVID-19 but were replaced with inflammatory monocyte-derived macrophages, characterized by high expression of IL-1β, TNF, IL-6, CCL2, CCL3 and CCL4. High levels of CCL2 lead to the attraction of additional inflammatory and dysfunctional monocytes, enhancing inflammation. Trajectory analysis revealed the connection of hyperinflammatory monocytes to macrophages in the lung, showing higher levels of inflammasome- and fibrosis-related genes (Wauters et al. 2021). Macrophage states with gene expression associated with fibrosis such as *SPP1*, *TERM2* and *TGFB2* were also identified in other studies (Liao et al. 2020; Wendisch et al. 2021).

Overall, a strong inflammatory cascade can be described in COVID-19, starting with pro-inflammatory cytokine- and chemokine-release by hyperactivated macrophages in the lung, leading to infiltration of hyperinflammatory and dysfunctional monocytes, which exacerbates

tissue damage and further activate macrophages and fibrosis-associated programs (Figure 5).

For this publication, I was responsible for reviewing and summarizing current literature about alveolar and interstitial macrophages in respect to their ontogeny and function as well as the role of lung macrophages in viral respiratory infections. Moreover, I contributed to the collection of COVID-19 literature, designed the graphical overview figure and revised the manuscript.

## 2.3. The HIV/AIDS epidemic

Since the beginning of the Human Immunodeficiency Virus (HIV) epidemic, an estimated total of 85.6 million people have been infected with the virus and the HIV-related disease Acquire Immune Deficiency Syndrome (AIDS) caused approx. 40.4 million deaths (UNAIDS 2023). Although antiretroviral therapy (ART), the standard-of-care treatment, is highly effective in suppressing the virus and thereby strongly reducing morbidity, in 2022, there were 1.3 million new cases of HIV infection, about 39 million people living with HIV (PLHIV) and 630,000 HIV-related deaths (UNAIDS 2023). These numbers stress that the HIV/AIDS epidemic is still of major importance, continues to be a threat for public health and demands further studies for better disease characterization and treatment.

### 2.3.1. HIV origin, transmission, pathogenesis and treatment

HIV is a zoonosis and originates from the simian immunodeficiency virus (SIV) (Rambaut et al. 2004). It is proposed that the transmission occurred from consumption of infected primates by indigenous people in Central and West Africa (Kalish et al. 2005) with potential first cases of HIV around 1930-40 (Korber et al. 2000; Lemey et al. 2003). AIDS, the disease caused by HIV-infection, was first recognized and described as a mysterious disease in 1981 (Centers for Disease Control (CDC) 1981). Two years later, the virus was isolated at the Institute Pasteur (Barré-Sinoussi et al. 1983). Two subtypes of HIV are known: HIV-1, which originates from chimpanzees and spread world-wide as well as HIV-2, which originates from sooty mangabey and is mostly found in Central and West Africa and in a small area in India (Cho et al. 2022; Rambaut et al. 2004). In the subsequent text, any mention of HIV specifically refers to HIV-1 given its role in causing the epidemic.

HIV is a single-stranded RNA virus and belongs to the *Retroviridae* family (Seitz 2016). Transmission from human to human requires exposition to infected body fluids such as blood or sexual fluids, of note, ~80% of infections in adolescents or adults occur through vaginal or anal intercourse (Hladik and McElrath 2008; Cohen et al. 2011). HIV gains access to host cells via the CD4 receptor, a surface protein mostly expressed on T lymphocytes, but also on myeloid cells such as monocytes, macrophages and dendritic cells (Lekkerkerker et al. 2006; Chan and Kim 1998; Suligoi et al. 2010). As co-receptor, HIV uses the chemokine receptors CXCR4 or CCR5, which are expressed on T lymphocytes and myeloid cells, respectively (Dragic et al. 1996; Bleul et al. 1996). After fusion, the virus releases its core into the host cell where reverse transcription, host genome integration, virus gene transcription and translation as well as new virus assembly occurs (Barré-Sinoussi et al. 1983; Bukrinsky et al. 1992). The reverse transcription step is error-prone and leads to a very high mutation rate of virus DNA which can results in drug-resistance and immune evasion (Roberts et al. 1988). This

replication cycle is very rapid and about $10^{10}$ virions are produced per day (Perelson et al. 1996). In contrast to the productive form of infection, HIV can also latently infect cells, e.g. T cells (Chun et al. 1995). In a latent infection, the viral genome is integrated into the host genome, but no virus genes are transcribed and translated. However, reactivation of virus replication can occur at any time following cell activation (Pitman et al. 2018). By latently infecting resting long-lived memory T cells, HIV has a permanent reservoir. As these reservoirs are not showing active signs of HIV infection and are with 0.05% of resting T cells very small in numbers, it is not possible for the immune system to completely eradicate the source of virus.

HIV infection and progression can be separated into three phases in the absence of treatment: acute phase, asymptomatic phase and AIDS. After infection, HIV replication occurs mostly in activated CD4+ T cells in both circulation and tissue. Diagnosis of HIV infection is only possible by detection of virus RNA in blood, which can be measured about 10-12 days after infection using reverse transcription polymerase chain reaction (RT-PCR), before that, it is almost impossible (Fiebig et al. 2003; Lindbäck et al. 2000; Hecht et al. 2002). In this acute phase, a strong burst of viral replication is observed which results in up to 100 million viral RNA copies per ml plasma (Figure 6, (Fiebig et al. 2003; Lindbäck et al. 2000; Little et al. 1999)). Moreover, a progressive decline of CD4+ T cells numbers can be seen, down to half of their normal counts (Gupta 1993). During the acute phase, symptoms can last for 10 days and include fatigue, myalgias, mild rash, fever and headache (Kahn and Walker 1998; Cooper et al. 1985). After some time, viral load declines and HIV-specific cytotoxic T cells increase (Walker et al. 1987). In the following asymptomatic phase, viremia declines further to a lower level, while CD4+ T cell count is slightly rising, but never to levels before infection. Latent reservoirs act as permanent source for viral replication resulting in continuous immune activation and exhaustion (Fenwick et al. 2019). Over the years, persistent viremia induces a slow, but progressive loss of CD4+ T cells leading to an increased immunodeficiency (Ford et al. 2009). When the CD4+ T cell count is <200 cells per µl, the AIDS stage is reached. HIV-infected patients then become susceptible to opportunistic infections by bacteria, other viruses, fungi, and parasites and are more often diagnosed with cancer of different types (El-Atrouni et al. 2006; Crowe et al. 1991; Brooks et al. 2009) such as Kaposi sarcoma as described in the first description of AIDS (Centers for Disease Control (CDC) 1981). During this phase, viral load rapidly increases and further opportunistic diseases occur, leading to an inevitable death if no treatment occurs. HIV progression to AIDS is around 8-10 years but dependent on the individual patient.

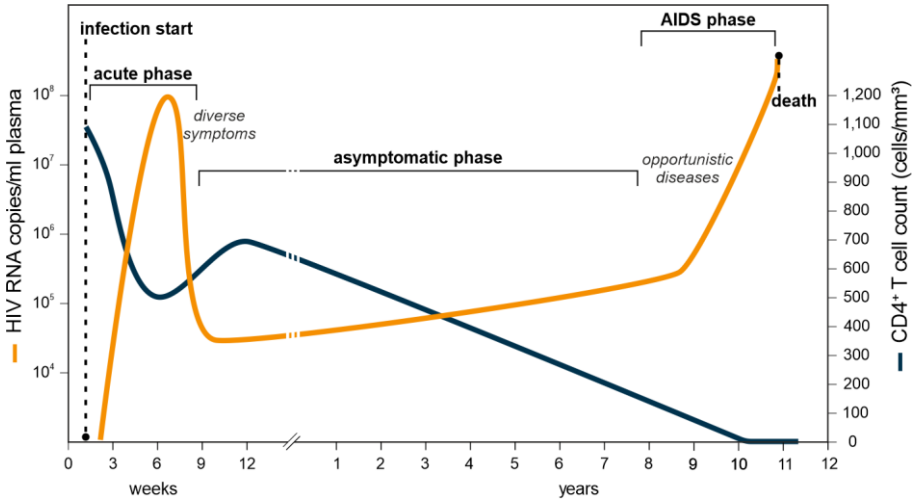


**Figure 6: Overview of the HIV progression in absence of treatment.**
Depiction of the disease course of HIV infection described with change of HIV RNA copies (per ml plasma) and CD4+ T cell count (cells per mm³) in the first weeks and following years after infection start. Three phases can be defined: the acute phase (first weeks) with diverse flu-like symptoms, peak of HIV RNA and strong reduction of CD4+ T cells, the asymptomatic phase (several years) with progressive decline of CD4+ T cells and increase of HIV RNA and the AIDS phase, characterized by very low CD4+ T cell count, rapidly increased HIV RNA and occurrence of opportunistic diseases, leading to the death approx. 11 years after infection. Adapted from (Bekker et al. 2023).

As untreated HIV infection leads to AIDS and death, the need for an effective treatment has been high. A first drug appeared in the 1990s (Concorde Coordinating Committee 1994) and more effective treatments and combinations of drugs were tested in the following years. The current standard-of-care is ART, which usually comprises a three-drug oral daily regimen with different combinations of nucleoside reverse transcriptase inhibitors (NRTI), integrase strand transfer inhibitor (INSTI), non-nucleoside reverse transcriptase inhibitor (NNRTI), protease inhibitors (PI) or entry inhibitors, each targeting unique steps of the HIV life cycle (Saag et al. 2020; Ryom et al. 2022). Treatment has a profound impact on HIV progression with clinical, immunological and psychological benefits, counteracting AIDS-related death, reducing HIV transmission and restoring quality of life (Antiretroviral Therapy Cohort Collaboration 2017; May et al. 2014; Cohen et al. 2016). The interruption of the HIV replication leads to a strong reduction in viremia, as well as a decline in CD4+ T cell destruction. The latter recover, first rapidly and then with a slow but steady increase, however, often to a level below pre-infection (Autran et al. 1997; Rajasuriar et al. 2010). Of great importance is the timing of treatment initiation. Studies showed that ART should be conducted as soon as feasible, proposing a “test and treat” strategy (Saag et al. 2020; INSIGHT START Study Group et al. 2015; TEMPRANO ANRS 12136 Study Group et al. 2015). If ART is initiated early, the acute HIV phase is shortened, maximum viral load is reduced and excessive CD4+ T cell destruction is prevented. For both timepoints, the AIDS stage is prevented. Nevertheless, immune activation is persistently elevated due to viral reservoirs and this lifelong latent infection leads to an

increased risk for cardiovascular, renal and neurological diseases as well as cancer, commonly termed non-AIDS-defining events (van der Heijden et al. 2021; Deeks et al. 2013; Hunt et al. 2016; Zicari et al. 2019; Strategies for Management of Antiretroviral Therapy (SMART) Study Group et al. 2006). As non-AIDS-defining events occur although ART is administered, new personalized drugs will be of great value.

### 2.3.2. Monocytes in HIV

Monocytes as part of the innate immune system play an important role in the defense response and clearance of pathogens including viruses (Shi and Pamer 2011). However, excessive recruitment of monocytes can also be detrimental and cause unwanted inflammation. In chronic HIV infection, the persistent inflammation and immune activation could be explained by viral reservoirs and increased susceptibility for coinfections with other pathogens such as human cytomegalovirus (hCMV). Of note, both explanations are associated with monocyte activation (Anzinger et al. 2014). Besides CD4+ T cells, macrophages and monocytes can also be infected with HIV via the co-receptor CCR5 and serve as viral reservoirs (Zhu et al. 2002; Bacchus et al. 2013; McElrath et al. 1989).

HIV infection leads to an increased number of intermediate and non-classical monocytes and the degree of non-classical monocyte expansion was linked to the rate of disease progression (Thieblemont et al. 1995; Ellery et al. 2007; Pulliam et al. 1997). Monocytes from PLHIV showed shortened telomers, a sign for increased cell division in the bone marrow during infection (Hearps et al. 2012). Indeed, monocyte turnover was found to be increased during HIV and SIV infection as well as HIV-positive aged individuals (Ziegler-Heitbrock 2014; Burdo et al. 2010; Hasegawa et al. 2009). Rhesus macaques positive for SIV confirmed increased turnover, however, the monocyte half-life was decreased so that the overall percentage was not changed in blood (He et al. 2018).

Besides increased turnover upon infection, monocytes also show a persistent activation in PLHIV (Hearps et al. 2012; Martin et al. 2013). Proinflammatory signaling was found to be increased in monocytes of PLHIV compared to HIV-negative controls with higher levels of CXCL10, CCL2 and neopterin (Hearps et al. 2012; McKibben et al. 2015). *In vitro* infection of monocytes with HIV and treatment with ART showed alterations in activation markers and proinflammatory genes such as *IL1B* (Bowman et al. 2020). Increased production of IL-1β from monocytes of PLHIV compared to healthy controls was confirmed with *ex vivo* stimulations using various pathogens (van der Heijden et al. 2021).

Across multiple studies, the most prominently reported reasoning for monocyte involvement in chronic inflammation of PLHIV are the elevated levels of the circulating and monocyte-associated soluble CD14 (sCD14) and soluble CD163 (sCD163) (Lyons et al. 2011; van der Heijden, Van de Wijer, et al. 2021; Sandler et al. 2011; Mensching and Hoelzemer 2022; Knudsen et al. 2022; Møller 2012; McKibben et al. 2015; van der Heijden, Wan, et al. 2021). CD14 acts as a receptor for bacterial LPS together with Toll-like receptor 4 (TLR4) (Wright et al. 1990) and can be cleaved from the surface of monocytes for solubilization (Stelter et al. 1996; Schütt et al. 1991). Similarly, activation of monocytes leads to shedding of the hemoglobin scavenger receptor CD163 from the cell surface in a soluble form (Møller 2012). As both receptors are expressed exclusively on monocytes and macrophages, they represent specific markers for these cell types and altered levels directly reflect monocyte involvement. Elevated levels of both sCD14 and sCD163 in PLHIV were associated with non-AIDS-related events (Rogacev et al. 2012; McKibben et al. 2015) and serve as predictors of mortality (Knudsen et al. 2016; Sandler et al. 2011). Moreover, increased sCD14 levels in PLHIV correlated with higher levels of serum amyloid A, D-dimers and markers of inflammation including IL-6 and high sensitivity C-reactive protein (hsCRP) (Lien et al. 1998; Méndez-Lagares et al. 2013), which were also associated with clinical outcome (Kuller et al. 2008; Duprez et al. 2012; De Luca et al. 2013; Shikuma et al. 2014). Non-AIDS-related events associated with profound monocyte involvement defined by elevated levels of sCD14 and sCD163 in PLHIV are mostly cardiovascular-related diseases. High levels of sCD14 were correlated with carotid artery intima-media thickness, a measurement for atherosclerosis (Sandler et al. 2011; Kelesidis et al. 2012; Merlini et al. 2012) and were associated with coronary artery calcification (Longenecker et al. 2014), while elevated levels of sCD163 increased the prevalence of atherosclerotic plaques (Burdo et al. 2011), noncalcified coronary plaques and arterial inflammation in PLHIV (Burdo et al. 2011; Fitch et al. 2013). Moreover, both elevated sCD14 and sCD16 were linked to carotid artery atheroma development in chronic HIV infection (Burdo et al. 2011; Hanna et al. 2017).

Besides sCD14 and sCD163, monocyte expression levels of CD11b and CX3CR1 associated with atherosclerosis and carotid intima-media thickness in PLHIV (Westhorpe et al. 2014; Hsue et al. 2012) and expression of tissue factor correlated with the coagulopathy marker D-dimer, which lead to the hypothesis that monocytes facilitate prothrombotic environments (Funderburg et al. 2010). Overall, a strong link of monocyte activation and marker expression was linked to multiple non-ADIS-related events, clearly highlighting the important role of monocytes in chronic inflammation in PLHIV (Rappaport and Volsky 2015; Burdo et al. 2011; Westhorpe et al. 2014; Hearps et al. 2011; Sandler et al. 2011; Anzinger et al. 2014).

In a recent study, Kazer et al. analyzed circulating immune cells during hyperacute HIV infection using single-cell transcriptomics (Kazer et al. 2020). Upon infection, monocytes in the blood were expanded and elevated levels of sCD14 were measured. They further described alterations in transcriptional programs of monocyte caused by HIV using gene modules. During HIV infection, monocytes had higher expression of genes related to antigen presentation, showed a strong interferon response signature and had elevated inflammatory programs. These transcriptional programs persisted throughout the first month of infection and showed their potential persisting role. The described programs were expressed by different states of monocytes, among others “inflammatory” as well as “anti-viral” monocytes, the latter showing high expression of interferon response genes such as *ISG15*, *IFIT3* and *IFIT2*.

Despite the clear involvement of monocytes in acute HIV infection, but also in chronic disease of PLHIV, extensive studies describing transcriptional and functional alterations of monocytes after long-term ART are still rare.

## 2.4. Drug repurposing

Newly emerging infectious diseases like COVID-19 impose a significant burden on society and the healthcare sector due to limited knowledge of immunopathology and the consequent lack of effective treatment strategies. Additionally, chronic infectious diseases, such as HIV, for which we have effective treatments available, some patients still develop comorbidities that diminish their quality of life, which could be mitigated with additional personalized treatments. In both cases, *de novo* drug development is often impractical, as it requires excessive time and financial investment with limited returns, which is reflected in a growing productivity gap in the pharmaceutical industry (Scannell et al. 2012; Ashburn and Thor 2004). Particularly for COVID-19, for which a quick and effective treatment was crucial, drug repurposing proofed to be exceptionally powerful (Rodrigues et al. 2022).

Drug repurposing or repositioning is a strategy to identify and apply previously approved or investigated drugs for purposes beyond their original indented indications (Pushpakom et al. 2019). There are three major advantages over *de novo* drug development (Figure 7). First, the risk of failure is lower since repurposed drugs were often already tested for safety in preclinical animal models or phase I trials in humans. Second, the development timeline is shortened from 12-16 years for new drugs to approx. 6 years for repurposed drugs because preclinical testing, safety assessments and chemical design have often been completed (Nosengo 2016). Third, the financial investment required by pharmaceutical companies is significantly reduced with costs estimated at $300 million for a repurposed drug compared to $2-3 billion for developing a new drug. Overall, repurposing of drugs has proven to be a less risky, faster and more cost-efficient approach for drug discovery compared to *de novo* drug development, offering a high return on investment.

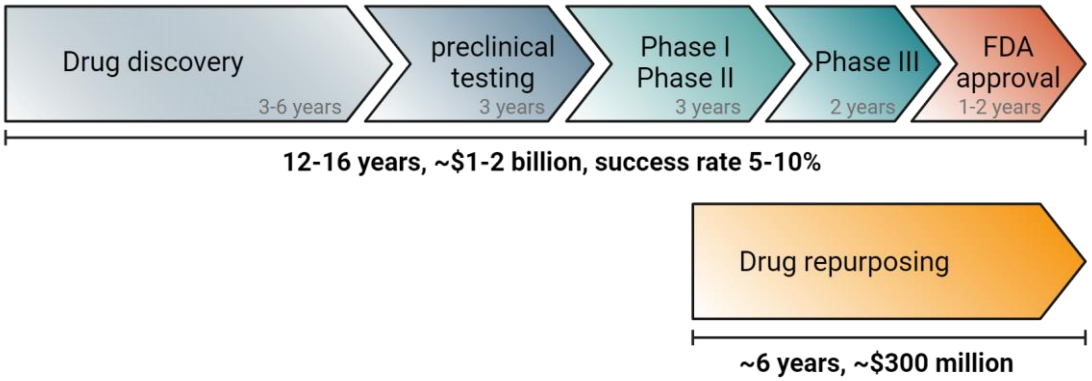


**Figure 7: Comparison of *de novo* drug development against drug repurposing.**
Development of new drugs takes approx. 12-16 years, costs $1-2 billion and has a low success rate until Federal Drug Administration (FDA) approval (Sun et al. 2022; Morgan et al. 2018). Drug repurposing on the other hand has a lower risk of failure, is approx. shortened by half due to previous existing preclinical testing and safety assessment and has a reduced cost of approx. $300 million. This figure was generated with Biorender.com and adapted from (Nosengo 2016).

Historically, repurposing of drugs was rather by serendipity with discovery of off-target or new on-target effects followed by commercial exploitation. The most successful and known example which was discovered without a systemic approach is sildenafil, originally developed as an antihypertensive drug but after evaluating the side effects, it was later repurposed for erectile dysfunction and marketed under the name Viagra® by Pfizer (Ghofrani et al. 2006). Another example is thalidomide, originally intended as a sedative against morning sickness which, however, showed severe side effects for pregnant women, leading to market withdrawal. Thalidomide was later repurposed for treatment of erythema nodosum leprosum and even showed efficacy against multiple myeloma (Ashburn and Thor 2004; Singhal et al. 1999). Inspired by these historic successes, more systematic approaches for identification of repurposed drugs were designed, resulting in numerous successful candidates, especially for COVID-19 (Table 1, Pushpakom et al. 2019; Rodrigues et al. 2022). These approaches share three steps before entering phase III clinical trials: 1) identification of drug candidates for a given indication, 2) mechanistic assessment of the drug effect in preclinical models and 3) evaluation of efficacy in phase II clinical trials. Of note, step 1 is the most critical and multiple systemic computational or experimental methods are available to facilitate this process. In this thesis, the focus is on the computational approach using signature matching.

**Table 1: Overview of successfully repurposed drugs.**
Selection of successfully repurposed drugs with original and new indication. This table was adapted from (Pushpakom et al. 2019) and extended for COVID-19 drugs from (Rodrigues et al. 2022).

| Drug name | Original indication | New indication | Date of approval |
|---|---|---|---|
| Zidovudine | Cancer | HIV/AIDS | 1987 |
| Sildenafil | Angina | Erectile dysfunction | 1998 |
| Thalidomide | Morning sickness | ENL and multiple myeloma | 1998 |
| Celecoxib | Pain and inflammation | Familial adenomatous polyps | 2000 |
| Atomoxetine | Parkinson disease | ADHD | 2002 |
| Rituximab | Cancer | Rheumatoid Arthritis | 2006 |
| Raloxifene | Osteoporosis | Breast cancer | 2007 |
| Fingolimod | Transplant rejection | Multiple sclerosis | 2010 |
| Aspirin | Analgesia | Colorectal cancer | 2015 |
| Remdesivir | Ebola virus | COVID-19 | 2020 |
| Baricitinib | Rheumatoid Arthritis | COVID-19 | 2020 |
| Dexamethasone | Allergies, asthma, arthritis | COVID-19 | 2021 |
| Paxlovid | SARS, HIV/AIDS, Hepatitis C | COVID-19 | 2022 |

### 2.4.1. Transcriptomics-based drug repurposing

For identification of potentially effective repurposed drugs, there are several computational approaches available, including data mining, modeling, machine learning or network analyses (Jarada et al. 2020). One of the most straightforward and simplistic yet highly efficient approaches is based on signature matching, known as the signature reversion principle (SRP, Figure 8, (Pushpakom et al. 2019; Iorio et al. 2013). In this method, disease-associated signatures, e.g. differentially expressed genes (DEG) between disease and healthy samples, are compared to transcriptomic signatures from drugs. These drug signatures are derived from comparing before and after treatment in tissues or cell lines. If a significant negative correlation is present, this drug might be able to reverse the disease signature and therefore reverse the disease phenotype. For the SRP analysis, publicly available and standardized drug signature databases are a prerequisite. First steps were made in 2006 by the Broad Institute, which established the Connectivity Map (cMap), comprising expression data from 164 distinct compounds at different concentrations across multiple cell lines (Lamb et al. 2006). Shortly after, the cMap was updated to the Library of Integrated Network-based Cellular Signatures (LINCS) by applying the L1000 platform (Subramanian et al. 2017). This resource initially comprised a total of 1.3 million profiles, generated from over 19,800 small molecules and 5,000 genetic perturbations, tested in replicates at varying concentrations and incubation times in up to 77 cell lines, resulting in over 437,000 unique signatures. In 2020, this database was updated to include over 3 million profiles and it continues to expand, offering an increasingly comprehensive resource for drug repurposing. Tools such as clue.io by the Broad Institute (Subramanian et al. 2017) or integrative LINCS (iLINCS, Pilarczyk et al. 2022), facilitate database query and SRP analysis. This principle proved to be highly effective, leading to the proposal of many promising repurposed drug candidates for various diseases, which were in part validated in either *in vitro* or *in vivo* models (Knoll et al. 2023; Aschenbrenner et al. 2021; Wagner et al. 2015; Huang et al. 2016; Malcomson et al. 2016; Shin et al. 2015). For instance, Dudley and colleagues applied the SRP to inflammatory bowel disease (IBD), a non-communicable inflammatory disease with limited treatment options (Dudley et al. 2011). Generating their own algorithm based on cMap, they not only confirmed the efficacy of prednisolone, the standard treatment for IBD, but also identified topiramate as a new potential candidate. Topiramate, an anticonvulsant commonly used to treat epilepsy, was validated in a rodent model of IBD where it improved colon tissue damage which is one of the most severe symptoms. Here, the authors applied the SRP on disease-signatures, however, the principle can also be applied for other purposes. Instead of a disease-signature, Wei et al. used glucocorticoid resistance signatures, which were calculated by comparing resistant acute lymphoblastic leukemia samples against responding samples and they

identified rapamycin as a potential modulator of resistance (Wei et al. 2006). In general, studies applying the SRP often group all patients of the respective disease together, however, therapy responses can be heterogeneous (Roden et al. 2011; Sweeney 1983). This variability in drug response is a core concept of precision medicine (Dugger et al. 2018; Goetz and Schork 2018). Therefore, combining SRP approaches with stratification of patients into severity groups or immunotypes can provide more insightful results and group-specific drug candidates (Figure 8, Aschenbrenner et al. 2021). Similarly, averaging the signal across all cells in a disease sample can result in loss of signal from rare and disease-driving cell types and states. A more precise generation of disease signature based on these specific disease-driving states, could improve drug candidate prediction (Knoll et al. 2023; He et al. 2023). And finally, *in vivo* validations of repurposed drug candidates in human clinical cohorts combined with single-cell omics technologies can provide valuable insights into the underlying pathways as well as compositional and transcriptional alterations (Knoll et al. 2024). Moreover, this validation enables the evaluation and prediction of treatment response, contributing to the development of more effective and precise therapies and highlights the potential of single-cell omics for development of companion diagnostics.

In this thesis, an optimized framework of drug repurposing comprising all improvements is presented.

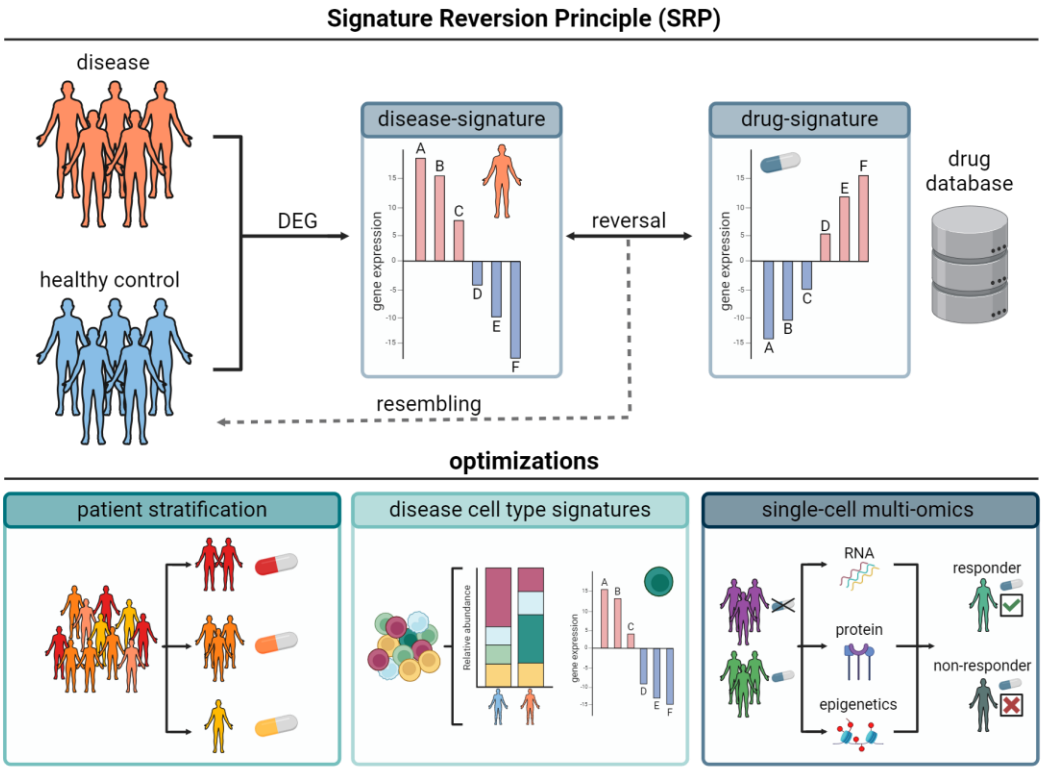


**Figure 8: Signature Reversion Principle (SRP) for drug repurposing and optimizations**
For drug repurposing, computational approaches based on the signature reversion principle (SRP) proofed to be powerful. DEG between diseases and healthy patients are calculated to generate a disease-signature and compared to all drug-signatures in the drug database. A drug, with a sufficiently reverse pattern could reverse the disease-signature and potentially the disease phenotype, restoring a healthy condition. The SRP can be optimized by stratifying patients into severity groups and predicting group-specific drugs, enhancing the disease-signature input by using a signature of disease-driving cell states and *in vivo* validation combined with single-cell multi-omics to decipher the mechanism and alterations by the repurposed drug as well as stratifying patients into drug-responder and non-responder. This figure was generated with Biorender.com.

# 3. Publications

## 3.1. Disease severity-specific neutrophil signatures in blood transcriptomes stratify COVID-19 patients

Aschenbrenner AC*, Mouktaroudi M*, Krämer B*, Oestreich M*, Antonakos N*, Nuesch-Germano M*, Gkizeli K*, Bonaguro L*, Reusch N*, Baßler K*, Saridaki M*, **Knoll R***, Pecht T*, Kapellos TS*, Doulou S*, Kröger C*, Herbert M*, Holsten L*, Horne A*, Gemünd ID*, Rovina N*, Agrawal S*, Dahm* K, van Uelft M*, Drews A*, Lenkeit L*, Bruse N*, Gerretsen J, Gierlich J, Becker M, Händler K, Kraut M, Theis H, Mengiste S, De Domenico E, Schulte-Schrepping J, Seep L, Raabe J, Hoffmeister C, ToVinh M, Keitel V, Rieke G, Talevi V, Skowasch D, Aziz NA, Pickkers P, van de Veerdonk FL, Netea MG[#], Schultze JL[#], Kox M[#], Breteler MMB[#], Nattermann J[#], Koutsoukou A[#], Giamarellos-Bourboulis EJ[#], Ulas T[#,§], German COVID-19 Omics Initiative (DeCOI)., "**Disease severity-specific neutrophil signatures in blood transcriptomes stratify COVID-19 patients.**", Genome Med. 2021 Jan 13;13(1):7. doi: 10.1186/s13073-020-00823-5.

*shared first authorship / [#]shared last authorship / [§]corresponding author

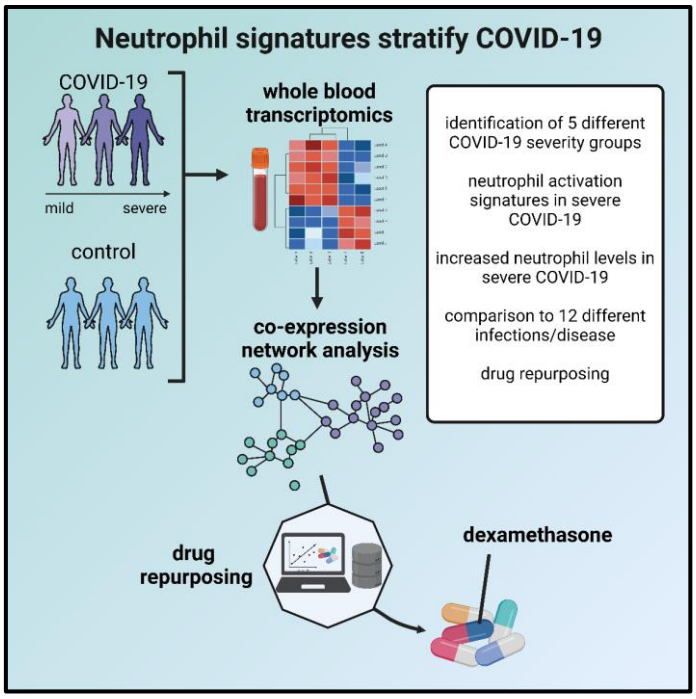


**Figure 9: Graphical abstract for "Disease severity-specific neutrophil signatures in blood transcriptomes stratify COVID-19 patients".**
Summary of the presented study generated with Biorender.com.

After first reported cases of COVID-19 worldwide, clinical observations revealed that there is a wide spectrum of disease manifestations, spanning from asymptomatic cases to mild and moderate with flu-like symptoms and severe cases with the need for mechanical ventilation, with some resulting in mortality (Knoll et al. 2024; Huang et al. 2020; Zhou et al. 2020; Wang et al. 2020). As the immune system plays an important role in viral infections, it was suggested that the heterogenous disease courses of COVID-19 can be explained by the differences in

the immune responses of the patients (Wang et al. 2020; Guan et al. 2020; Mathew et al. 2020; Su et al. 2020; Lucas et al. 2020).

In (Aschenbrenner et al. 2021), we performed bulk transcriptomics on whole blood samples from 39 COVID-19 patients and 10 control donors to better understand the heterogenous disease courses and to further identify potential treatment strategies (Figure 9).

First, all COVID-19 patients were grouped and compared against controls, resulting in strong transcriptional differences with 2,289 up- and 912 down-regulated genes. From these DEG, *CD177*, a gene highly expressed in neutrophils, was most eminent. To get a better picture of the heterogenous disease course of COVID-19, patients were stratified according to the WHO ordinal scale into mild (1-4) and severe (5-7). DEG analysis against controls was performed resulting in a greater number of DEG in whole blood samples from severe compared to mild COVID-19 patients. Functional enrichment revealed granulocyte/neutrophil activation for both severities, which was stronger in severe as well as reduced lymphocyte differentiation and T cell activation.

Of note, when inspecting the top 25% of the most variable expressed genes and clustering all samples in an unbiased fashion, clinical grouping such as by WHO scale did not fully explain the structure in the data. Therefore, we aimed for an unbiased stratification of patients into groups by CoCena², a co-expression-based network analysis approach. This analysis resulted in ten distinct expression modules and hierarchical clustering of the samples based on their group fold changes (GFC) for each module stratified the patients into six distinct transcriptional groups with five (G1-G5) comprising the COVID-19 patients and one (G6) consisting mostly of controls. Of the five COVID-19 groups, G1 included only male patients that were severely ill and together with G2 strongly enriched for inflammatory and neutrophil-associated terms. CIBERSORT deconvolution suggested an increased neutrophil-lymphocyte ration in G1 with the lowest in G6. This ratio was validated using flow cytometry. Another validation was performed by extracting neutrophils from a total of 34 COVID-19 samples (17 mild, 27 severe) and performing bulk transcriptomics. This analysis revealed that there were strong transcriptional alterations with signatures of pre-/immature neutrophils and simultaneous suppressive and inflammatory programs, which were also detected in the whole blood data.

To put COVID-19 into the context of other well studied diseases, whole blood transcriptome datasets from 12 additional studies were integrated to our COVID-19 dataset, including viral infections (chikungunya, HIV, influenza, Zika), bacterial infections (tuberculosis, bacterial sepsis, SIRRS) and other inflammatory diseases (systemic lupus erythematosus, Crohn's disease, rheumatoid arthritis, Ebola vaccination, neonatal-onset multisystem inflammatory disease and macrophage activation syndrome), comprising a total of 3,176 samples. Genes

were aligned to our COVID-19 co-expression network and GFCs were calculated for each sample. The lightgreen module, which associated mostly with the neutrophil signatures, was strongly expressed in the G1 COVID-19 group, but also slightly expressed in sepsis, influenza A, tuberculosis and HIV, revealing shared but also distinct transcriptional patterns. Similar shared but distinct patterns were observed for platelet activation, inflammatory responses with IL6 and TNF signaling as well as interferon-related signatures. The combination of distinct patterns reveled that COVID-19 underlies a unique SARS-CoV-2 immune response.

Despite the dysfunction of the immune system, clinical trials were mostly conducted to target the virus or its interaction partners directly, lacking immune-associated approaches. Moreover, as COVID-19 is a very heterogenous disease, patient group-specific therapies could strongly enhance disease courses, following the idea of precision medicine. To identify potentially beneficially drugs, we constructed a drug repurposing pipeline applying the SRP. Here, we used the COVID-19 group-specific signatures (DEG, G1-5 against G6) as an input for the clue.io and iLINCS platforms to collect a list of 940 unique drugs. Next, the gene signatures of these drugs were extracted from iLINCS (total of 62,897) and the top 300 up- and down-regulated genes were used as input for a gene set enrichment analysis (GSEA) on the whole blood COVID-19 data stratified by patient groups G1-G6. Using this pipeline, we wanted to identify drug-signatures that reverse the disease-signature, meaning that the genes down-regulated by a certain drug should mirror the up-regulated genes by the disease and *vice versa*. To asses this reversal we calculated the delta of the normalized enrichment score (ΔNES) and clustered the drug-signatures accordingly. Cluster 5 of the drug-signatures was very specific for the most severe G1 group and encompassed several drugs tested in clinical trials, such as dexamethasone, which is the current standard of care for hospitalized COVID-19 patients. Reoccurring targets of the drugs from this cluster 5 included pro-inflammatory genes such as *IL1B* and *CSTD* and associated mostly with the neutrophil-related lightgreen CoCena² module. The results from our drug repurposing pipeline highlighted the potential of transcriptome-based drug identification tailored for disease-groups and supported many drugs under investigation during that time such as dexamethasone.

In conclusion, we highlighted that COVID-19 is a heterogenous disease in which patients can be stratified into five distinct molecular phenotypes. Neutrophils with increased frequencies, immature signatures as well as inflammatory/suppressive features were a hallmark for severe COVID-19 being distinct from other inflammatory diseases. Our transcriptomic-based drug repurposing approach showed the potential to reverse disease-signatures and highlighted the importance of patient stratification for optimized and precise therapies.

For this publication, I conducted profound literature research, reviewed other models of drug repurposing using transcriptomic data and performed the mathematical conceptualization of our model which was realized by others. As part of the drug repurposing team, I applied the pipeline, interpreted the results and took the lead in writing and revising the corresponding manuscript part. Moreover, from the drug signatures of the most prominent drug cluster, I extracted the reoccurring target genes and highlighted them on the CoCena² network.

## 3.2. Identification of drug candidates targeting monocyte reprogramming in people living with HIV

**Knoll R,** Bonaguro L, Dos Santos JC, Warnat-Herresthal S, Jacobs-Cleophas MCP, Blümel E, Reusch N, Herbert M, Otten T, van der Heijden WA, van de Wijer L, Shalek AK, Händler K, Becker M, Beyer MD, Netea MG, Joosten LAB, van der Ven AJAM, Schultze JL[#], Aschenbrenner AC[#,§], "**Identification of drug candidates targeting monocyte reprogramming in people living with HIV**", Front Immunol. 2023 Nov 20;14:1275136. doi: 10.3389/fimmu.2023.1275136.

*shared first authorship / [#]shared last authorship / [§]corresponding author

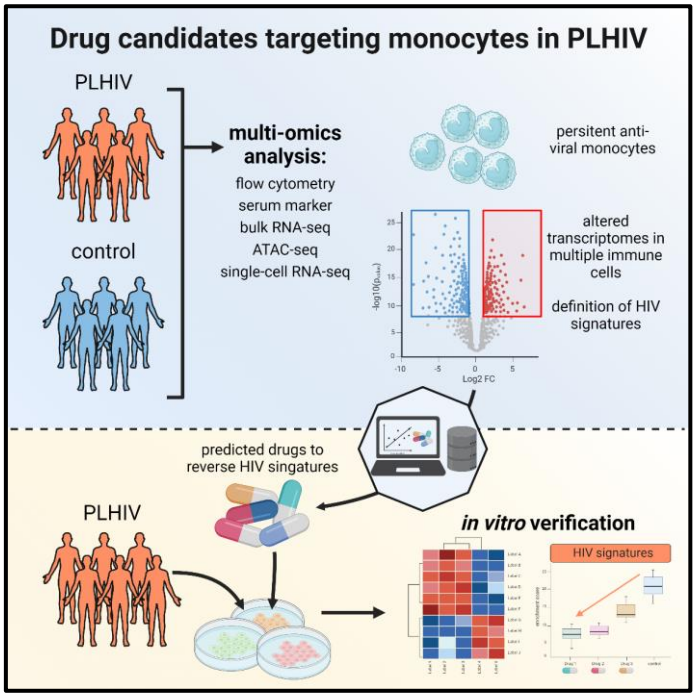


**Figure 10: Graphical abstract for "Identification of drug candidates targeting monocyte reprogramming in people living with HIV".**
Summary of the presented study generated with Biorender.com.

Even under long-term effective ART, PLHIV have higher risks for developing cardiovascular diseases, neurocognitive impairment and cancer due to persistent low-grade inflammation and immune dysfunction, stressing the need for optimized or additive treatment strategies (van der Heijden et al. 2021; Deeks et al. 2013; Hunt et al. 2016; Zicari et al. 2019). Despite the clearly important role of the adaptive immune system in HIV, recent studies suggested an alteration in the innate immune system in PLHIV, especially in monocytes (van der Heijden et al. 2021; Sandler et al. 2011; Mensching and Hoelzemer 2022).

In (Knoll et al. 2023), we applied multi-omics technologies to assess alterations in the immune cell compartment in a small cohort of PLHIV versus healthy controls, serving as a pilot study for a larger cohort study. We identified monocytes to be involved in persistent low-grade

inflammation and applied our SRP approach to identify and validate drug candidates that were predicted to reduce the observed inflammatory monocyte phenotype (Figure 10).

Five male PLHIV were recruited, matched with five healthy controls and blood was drawn to generate a multi-layer dataset including soluble factors in plasma, proteomics assessment, bulk transcriptomics of PBMCs and CD14+ monocytes, Assay for Transposases-Accessible Chromatin (ATAC-seq) of CD14+ monocytes and single-cell transcriptomics. First, transcriptional alterations were evaluated in all circulating immune cells. DEG analysis revealed 287 up- and 914 down-regulated genes in PLHIV, which we then clustered into four gene clusters. Clusters associated with PLHIV included early innate immune response genes with *S100A8* and *S100A9* (cluster 1) as well as typical interferon response genes such as *STAT1* and *ISG15* (cluster 2), reflecting an overall innate and myeloid pro-inflammatory gene program in PLHIV.

To inspect the involvement of myeloid cells in PLHIV in more detail, plasma levels of monocyte-specific soluble factors like sCD163 and sCD14 were assessed and reveled higher concentrations in PLHIV. Therefore, CD14+ monocytes were isolated and analyzed with bulk transcriptomics. Although few DEG were detected (65 up- and 6 down-regulated genes), a clear induction of type I interferon-related genes such as *CXCL10*, *STAT2*, *MX2* and *XAF1* was observed, which was also reflected in the functional enrichment with terms related to IFN response and response to virus enriched most prominently. Mapping back the induced genes in PLHIV from CD14+ monocytes to the transcriptional clusters identified in the PBMC analysis, a strong overlap to cluster 2 was seen.

To assess whether the alterations in PBMCs and monocytes of PLHIV are due to general transcriptional changes or result from a certain cell state, we analyzed PBMCs in more detail using scRNA-seq of the same donors. The resulting dataset comprised 31,566 cells with all expected immune cell present. DEG analysis highlighted strong transcriptional differences in PLHIV to healthy controls, especially in the monocyte compartment supporting previous results. Functional enrichment of the induced genes in monocytes of PLHIV showed IFN responses and response to virus as strongest enriched terms, matching our bulk transcriptomics analysis. Upregulation of genes was verified using protein measurements. To relate our findings from PLHIV to acute HIV, we integrated our data with our previous dataset from acute HIV infection, which was generated with the same microwell-based single-cell technology. From this integrated PBMC data, we subsetted the monocytes and annotated clusters based on the previously reported acute monocyte states. Acute HIV infection was associated with several inflammatory monocyte states, which were absent in PLHIV. Of note, the ‘anti-viral’ monocyte state that was present in acute HIV was equally detectable in PLHIV.

This state was characterized by high expression of interferon-related genes such as *IFIT3*, *IFIT2* and *ISG15* and showed strong enrichment for IFN response terms as well as response to virus, reminiscent of our previous results.

To identify drug candidates that have the potential to reverse the phenotype that we observed in monocytes of PLHIV, we applied our drug repurposing approach previously described in COVID-19. HIV signatures from PBMCs and monocytes were used as an input giving a list of 519 drug candidates, which resulted in 17,641 drug signatures. These signatures were used for enrichment on the bulk transcriptome PBMC and CD14+ monocyte datasets. Normalized enrichment scores (NES) were retrieved for the genes down-regulated and up-regulated from a drug signature and the delta of these values was calculated (ΔNES). Clustering of drug signature ΔNES values gave rise to 50 clusters, of which cluster 43 showed the highest score. The higher the score, the higher the potential to reverse the disease signature. Reoccurring target genes of drug candidates in that cluster were mostly related to interferons (*IFI27*, *OAS1*, *MX1*, *IFI44L*) and strongly enriched in the "anti-viral" monocyte state. Of the 32 drug candidates, five were chosen for an *in vitro* validation experiment: trametinib, sunitinib, sitagliptin and clofarabine, which have been studied in the context of HIV before, and the antibiotic doxycycline. For all of these five drugs, no immune-modulating functions have been reported. PBMCs of six independent PLHIV were extracted and stimulated with the respective drugs or DMSO as control overnight. As a readout for transcriptional changes, bulk transcriptomics was performed. Prominent transcriptional differences were induced by the treatments, which was reflected in the principle component analysis (PCA) and number of DEG. To validate our previous findings and to proof the potential of the drug repurposing approach, we tested the influence of the drug treatments on four gene signatures: 1) the reoccurring target genes of cluster 43 from the drug repurposing pipeline, 2) the marker genes of the "anti-viral" monocyte state from the single-cell analysis, 3) the IFN-γ response term and 4) the inflammatory response term. Sunitinib and doxycycline significantly reversed all four PLHIV-specific gene signatures, while trametinib also showed a strong and clofarabine a moderate reduction of the signatures. Sitagliptin did not show any reduction in our *in vitro* validation experiment.

In conclusion, we showed that monocytes play a major role in the persistent low-grade inflammation in PLHIV, with elevated interferon responses, mainly originating from a state previously described as "anti-viral" monocytes in acute infection. Moreover, we predicted and validated drugs *in vitro* that could reverse the monocyte-derived signatures in PLHIV with sunitinib and doxycycline as most potent repurposed drug candidates.

For this publication, I was responsible for the analysis of the multi-omics datasets including bulk and single-cell transcriptome, proteome, flow cytometry and ATAC-seq datasets, applying the drug repurposing pipeline as well as analyzing the drug *in vitro* validation bulk transcriptomic dataset. In particular, I conducted the DEG and functional analyses, the single-cell clustering, the cell type annotation, the integration of single-cell datasets, the *in silico* drug repurposing and its validation. Moreover, I took the lead in writing and reviewing the manuscript.

## 3.3. The life-saving benefit of dexamethasone in severe COVID-19 is linked to a reversal of monocyte dysregulation

**Knoll R***, Helbig ET*, Dahm K, Bolaji O, Hamm F, Dietrich O, van Uelft M, Müller S, Bonaguro L, Schulte-Schrepping J, Petrov L, Krämer B, Kraut M, Stubbemann P, Thibeault C, Brumhard S, Theis H, Hack G, De Domenico E, Nattermann J, Becker M, Beyer MD, Hillus D, Georg P, Loers C, Tiedemann J, Tober-Lau P, Lippert L, Pascual-Leone BM, Tacke F, Rohde G, Suttorp N, Witzenrath M, CAPNETZ Study Group, Pa-COVID-19 Study Group, Saliba AE, Ulas T, Polansky JK, Sawitzki B, Sander LE[#], Schultze JL[#], Aschenbrenner AC[#,§], Kurth F[#], "**The life-saving benefit of dexamethasone in severe COVID-19 is linked to a reversal of monocyte dysregulation**", Cell. 2024 Jul, doi: https://doi.org/10.1016/j.cell.2024.06.014.
*shared first authorship / [#]shared last authorship / [§]corresponding author

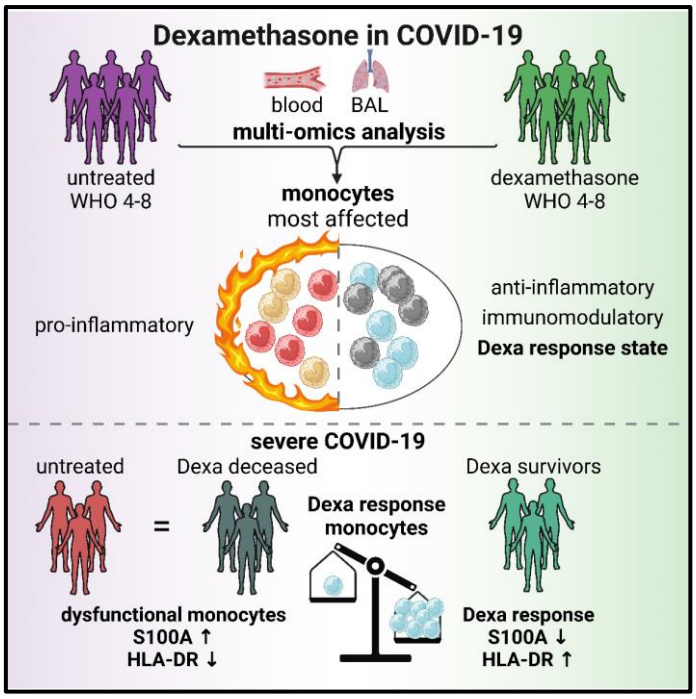


**Figure 11: Graphical abstract for "The life-saving benefit of dexamethasone in severe COVID-19 is linked to a reversal of monocyte dysregulation".**
Summary of the presented study generated with Biorender.com, taken from (Knoll et al. 2024).

Dexamethasone is the current standard-of-care against severe COVID-19 and was proven to be very effective by the RECOVERY trial and follow-up trials (RECOVERY Collaborative Group et al. 2021; WHO Rapid Evidence Appraisal for COVID-19 Therapies (REACT) Working Group et al. 2020; Tomazini et al. 2020). Nevertheless, there is still a substantial number of patients that are not responding to dexamethasone treatment, progress to a critical stage and decease. So far, biomarkers as predictors for treatment response to dexamethasone are lacking, which would be valuable for decision-making in personalized therapy, also known as companion diagnostics.

In (Knoll et al. 2024), we present a framework for identification of molecular changes and biomarkers defining treatment response of repurposed drugs using single-cell omics,

exemplified with dexamethasone in COVID-19. We analyzed blood-derived immune cells as well as immune cells from bronchoalveolar lavage (BAL) by multi-omics in a well-matched cohort of treatment naïve and dexamethasone-treated COVID-19 patients with either moderate or severe disease including deceased patients. Dexamethasone response was characterized by the induction of a monocytic response state and the reversal of the dysfunctional monocyte phenotype in severe COVID-19, but not in those with fatal outcome (Figure 11). Single-cell outcome-specific signatures were used for prediction of treatment response in two independent bulk whole blood transcriptome datasets and successfully stratified outcome, highlighting the potential as predictive biomarkers for treatment response.

From our central phenotyping platform study, we carefully selected patients that met the RECOVERY trial criteria for dexamethasone treatment and matched them with treatment naïve patients as controls. Whole blood and PBMC samples were taken on average 8 days after treatment and multi-omics was performed, including cytometry by time of flight (CyTOF), single-cell transcriptomics and multi-color flow cytometry. Compositional alterations were assessed using CyTOF, revealing a significant absolute increase of leukocytes in dexamethasone-treated patients with moderate disease as well as a relative decrease of monocytes, while there was no difference in severe patients. Treatment-related transcriptional alterations were inspected of a total of 114,181 single-cell PBMC transcriptomes. Molecular phenotypes of treatment-naïve COVID-19 patients matched previous studies including alterations in MHC-II (HLA), alarmin (S100A) and interferon genes. DEG analysis revealed most prominent changes by treatment in monocytes and B cells with many suppressed but also induced genes especially in monocytes. Common up-regulated genes across multiple cell types included *TSC22D3* and *TXNIP*, while *IFITM1* and *FTH1* were shared down-regulated genes. Functional enrichment indicated that dexamethasone acts via inhibition of NF-kB in multiple cell types.

As the monocyte compartment showed the most prominent regulation in response to dexamethasone-treatment, we aimed for a more detailed analysis. First, we investigated commonalities of treatment-effects between moderate and severe COVID-19 in monocytes, which resulted in a core up- and down-signature for dexamethasone treatment in COVID-19. This core signature was again related to NF-kB inhibition. Enrichment of an *in vitro* glucocorticoid signature strongly enriched in monocytes of treated patients. Of note, when assessing the enrichment by monocyte states, a strong enrichment was found in one specific state which we termed “Dexa response” state. This was validated using additional glucocorticoid signatures as well as investigating state specific markers, which included several known dexamethasone target genes such as *TSC22D3*, *SAP30*, *FKBP5* and *CD163*.

Of note, the “Dexa response” state was strongly increased in proportions for dexamethasone-treated patients, especially in moderate disease. Protein measurements by CyTOF and flow cytometry validated higher expression of CD163, a top marker of the “Dexa response” state, as well as higher frequencies of CD163+ monocytes in dexamethasone-treated patients. When the severe COVID-19 group was further stratified by outcome, a significant frequency increase of the “Dexa response” state was observed between treated survivors and those that deceased, the latter with barely detectable levels. As there were outcome-specific differences, we assessed transcriptional changes between severe survivors under dexamethasone treatment against untreated controls. Besides the core transcriptional signature, treatment was associated with a reversal of the dysfunctional monocyte state, previously reported in monocytes of severe COVID-19 patients. Dexamethasone treatment led to an induction of MHC-II genes and suppressed pro-inflammatory alarmins, chemokines and cytokines. Of note, dexamethasone non-survivors failed to reverse this dysregulation, resembling treatment-naïve severe COVID-19, indicating that outcome is associated with a monocytic dexamethasone response failure. To investigate this treatment effect in the lung, we sampled bronchoalveolar lavage (BAL) of severe COVID-19 patients. Marker genes related to the “Dexa response” state observed in blood were equally enriched in survivors that received dexamethasone, while untreated survivors as well as treated non-survivors showed a significantly reduced enrichment.

To see if the observed transcriptional alterations are underlying epigenetic changes, we sampled COVID-19 patients (WHO score 4-5) at day 2 after dexamethasone initiation and generated genome-wide DNA methylation profiles from sorted cell types for patients that responded to treatment and those that deteriorated, termed non-responders. PCA showed a difference of DNA methylation between responders and non-responders for CD14+ monocytes, which was not observed in CD19+ B cells and CD4+ and CD8+ memory T cells. Functional enrichment of promoter-associated differentially methylated positions (DMPs) showed associations towards pro-inflammatory programs in myeloid cells. Moreover, outcome-specific genes from the single-cell monocyte analysis showed significant differential methylations.

Lastly, we aimed to predict dexamethasone treatment response in two independent whole blood transcriptomics cohorts, which were sampled either 2 or 4 days after treatment initiation. After optimization, the outcome-specific single-cell monocyte signatures were enriched in the whole blood datasets, resulting in significant stratification by outcome. This highlighted the potential to identify dexamethasone non-responders already at a very early stage after treatment initiation using our identified signature and whole blood transcriptomics.

Taken together, we presented the framework on how to define treatment response of repurposed drugs by investigating treatment effects with single-cell multi-omics, exemplified with dexamethasone in COVID-19. Single-cell transcriptomics revealed immunosuppressive but also immunomodulatory effects of dexamethasone with strongest transcriptional and compositional changes in monocytes, where a core dexamethasone signature was identified. In monocytes, we identified a specific state that was associated with treatment response, stratifying outcome. Furthermore, dexamethasone lead to the reversal of the previously described dysfunctional monocyte phenotype in treated survivors, while non-survivors failed. Epigenetic investigations revealed pro-inflammatory changes already at an early stage in CD14+ monocytes, while other cell types did not show any differences. Lastly, we demonstrated how single-cell signatures were able to stratify patients by outcome in larger clinical cohorts using whole blood transcriptomics at an early time point after treatment start, highlighting the potential for single-cell omics signatures for companion diagnostics.

For this publication, I processed part of the samples, prepared the libraries for sequencing, was responsible for the entire blood single-cell transcriptomics analyses, as well as the BAL re-analyses of published datasets and took the lead in writing and reviewing the manuscript.

# 4. Conclusion

In my thesis, I outlined recent advancements in transcriptomic technologies, summarizes immunological alterations especially in monocytes in COVID-19 and chronic HIV and highlights drug repurposing based on transcriptomic data as a powerful approach for identification of new potential drug candidates in human diseases. In my work, I presented the optimized workflow of drug repurposing in human viral diseases based on transcriptomic data including the optimized strategy of drug candidate prediction for disease-specific patient groups, refinement of molecular disease-signatures from single-cell data, *in vitro* validation experiments and *in vivo* molecular characterization in human clinical cohorts with treatment response assessment and prediction based on multi-omics data towards the generation of companion diagnostics for precision medicine.

## 4.1. Characterization of human viral infections using omics

Transcriptomics, and especially single-cell transcriptomics, proofed to be exceptionally powerful in characterizing the immunopathology of human diseases, including infections (Kazer et al. 2020; Reyes et al. 2020; Bossel Ben-Moshe et al. 2019; Oelen et al. 2022), inflammatory diseases (Nehar-Belaid et al. 2020; Perez et al. 2022; Jaeger et al. 2021; Baßler et al. 2022), cancer (Bischoff et al. 2021; Barkley et al. 2022), cardiovascular diseases (Chaffin et al. 2022; Lake et al. 2023; Reichart et al. 2022) and neurodegenerative conditions (Mathys et al. 2019; Kamath et al. 2022; Keren-Shaul et al. 2017). In this thesis, I present the potential of high-resolution omics to investigate two human viral infectious diseases, namely acute COVID-19 and chronic HIV infection.

In acute COVID-19, we identified five whole blood transcriptome endotypes based on co-expression network analysis with specific transcriptomic signatures for each group (Aschenbrenner et al. 2021). The stratification into five groups showed that there are distinct molecular phenotypes in COVID-19, which are not fully explainable by clinical assessment. The most severe group was marked by strong neutrophil activation-associated signatures and showed the highest levels of neutrophils. Stratification of patients is of great importance as humans show a strong diversity, especially in the immune system (Brodin and Davis 2017; Liston et al. 2021). This immune variation arises from factors such as genetics, age, sex, diet and environment and can lead to different immune responses when challenged with pathogens like viruses. Consequently, every individual experiences varying degrees of disease severity, which can be hard to grasp by few measurements or the patient's medical records. Ideally, patient groups with similar molecular endotypes require personalized treatments to mitigate immunopathology (Dugger et al. 2018; Goetz and Schork 2018).

However, precision medicine approaches are often not available for the treatment of viral infections.

In chronic HIV, we highlighted the importance of monocytes in continuous immune activation and inflammation and identified a persistent anti-viral state, previously identified in acute HIV infection (Knoll et al. 2023). This finding would not have been possible without single-cell resolution. Although monocytes clearly play an important role in PLHIV as described previously (Hearps et al. 2012; Bowman et al. 2020; Lyons et al. 2011), most transcriptomic studies there are focusing on T cells, leaving monocytes understudied (Rato et al. 2017; Bradley et al. 2018; Buggert et al. 2018; Wang et al. 2020). As our cohort was limited in patient size, we are currently investigating another clinical study including up to 350 patients for single-cell transcriptomics in PLHIV.

Our transcriptomic clinical studies supported by other omics-layer as validations, proofed to be a robust and powerful strategy as they were absent of batch effects, showed great comparability to other studies and gave reliable and validated results based on multiple data layer.

Designing transcriptomics studies in a clinical setting offers exciting opportunities but requires thoughtful planning. Careful selection of eligible patients, considering factors like comorbidities, treatments, and the matching of age and sex for comparison groups helps to ensure robust results. Managing variables such as seasonality or technical effects further enhances the quality of the studies. For coherent analysis and comparison with other data sources, it is important to have standardized and well documented metadata. For this aim, multiple solutions are considered. Moreover, as transcriptomics research continues to evolve, increasing standardization and optimizing workflows will further enhance reproducibility and consistency, especially across different research centers and laboratory setups.

There are further developments in the field of transcriptomics, which may allow even more detailed analysis of the immunopathology of human diseases. These developments include the introduction of spatial transcriptomics (Marx 2021; Moses and Pachter 2022), multi-modal sequencing (Stoeckius et al. 2017; Reyes et al. 2019; Baysoy et al. 2023), which is the combination of transcriptomics with additional omics layer such as proteomics or epigenomics, and perturbation screens (Adamson et al. 2016; Dixit et al. 2016; Jaitin et al. 2016; Mimitou et al. 2019). Especially for the characterization of HIV reservoirs in T cells, which are highly heterogenous and rare, new single-cell multi-omics approaches have been suggested (Table 1). These methods aim for the analysis of enriched HIV-positive cells, defined by either HIV-RNA or HIV-DNA positivity, resulting in new insights of viral reservoirs which are believed to

be crucial for the success of future HIV cure strategies (Collora et al. 2022; Liu et al. 2020; Wu et al. 2023; Sun et al. 2023; Wei et al. 2023; Clark et al. 2023).

**Table 2: Methods for characterization of HIV-positive cells.**
Overview of published omics approaches for enhanced characterization of HIV-positive cells.

| Method | Omics | Authors | Journal | Date |
|---|---|---|---|---|
| SortSeq | Single-cell | Liu et al. | Science Translational Medicine | 2020 |
| ECCITE-seq | Transcriptomics, epigenomics, proteomics | Collora et al. | Immunity | 2022 |
| FIND-seq | Transcriptome | Clark et al. | Nature | 2023 |
| PheP-seq | proteomics | Sun et al. | Nature | 2023 |
| ASAPseq | Chromatin accessibility, proteomics | Wu et al. | Nature Immunology | 2023 |
| DOGMA-seq | Transcriptomics, epigenomics, proteomics | Wei et al. | Immunity | 2023 |

Until there are scalable and clinically applicable efficient and successful cure strategies available for HIV-positive patients, a complete characterization of the immune dysregulation of chronically infected PLHIV is required. For this aim, the 2000HIV study (Vos et al. 2022, clinicaltrials.gov: NCT03994835) was initiated with 1,895 HIV patients enrolled from the Dutch population comprising PLHIV on ART but also untreated HIV elite controllers. From all patients, in-depth multi-omics analyses were performed, including transcriptomics, proteomics, genomics, epigenomics and metabolomics. Moreover, single-cell transcriptomics was conducted on a subset of patients. In addition to the omics layers, other data layers such as immunophenotyping, immunological assays, viral reservoirs and clinical measurements were generated. The primary objectives of this study are to identify new candidate biomarkers that stratify non-AIDS-defining events, to describe extreme HIV phenotypes, such as rapid progressors and elite controllers, and to identify new therapeutic targets for repurposed or newly designed drugs. First insights of the 2000HIV study were reported and more are to come in the future (Blaauw et al. 2023; Vadaq et al. 2023; Vos, Navas, et al. 2024; Vos, Vadaq, et al. 2024; van Eekeren et al. 2024).

## 4.2. A framework for transcriptome-based drug repurposing

*De novo* design of drugs for human diseases is laborious, expensive and has low success rates (Sun et al. 2022; Scannell et al. 2012; Ashburn and Thor 2004). An alternative approach is to repurpose drugs approved for another indication (Rodrigues et al. 2022; Nosengo 2016). Drug repurposing has been proven to be efficient and less cost-effective intensive resulting in numerous successful new applications of drugs such as Sildenafil, Thalidomide, Aspirin and Dexamethasone (Pushpakom et al. 2019; Rodrigues et al. 2022). Many experimental and computational approaches for repurposing of drugs have been developed. Based on transcriptomic data, the reversal of disease signatures by drugs, by applying the SRP approach, led to promising predictions (Aschenbrenner et al. 2021; Knoll et al. 2023; Wagner et al. 2015; Huang et al. 2016; Malcomson et al. 2016; Shin et al. 2015).

In this thesis, I present an optimized framework for transcriptomics-driven identification of drugs that might be candidates for clinical applications in diseases caused by viral infections. This framework includes the stratification of patients into disease endotypes, refinement of the disease signatures using high-resolution single-cell data, *in vitro* validation experiments to test the efficacy of selected drug candidates and the usage of single-cell omics for treatment effect analysis and response prediction. In (Aschenbrenner et al. 2021) we introduced a transcriptomics-based drug repurposing approach which is based on the SRP and identified drugs for data-driven patient groups. As a result of human diversity, not all patients are benefitting from the same drug. This highlights the need for drug identification in stratified patient cohorts, following the concept of precision medicine (Dugger et al. 2018; Goetz and Schork 2018). Using disease-signatures from bulk transcriptomic data gave great insights, nevertheless further optimization could be achieved. By using single-cell data, a more fine-grained cell type-specific disease signature was generated (Knoll et al. 2023). As not all cell types contribute to immunopathology and disease severity, repurposing on optimized signatures can lead to more precise drug predictions. By this optimization approach, drugs predicted to be only moderately effective could be excluded. Although this refinement improves the prediction of drugs, the drug repurposing approach still generates a large and complex output. By ranking the signatures by their ability to reverse the disease signature, the focus can be narrowed to a select a few drugs for validation studies as the initial list of candidates would remain too long for evaluation in human clinical trials. To further refine the drug candidate list, *in vitro* stimulation experiments focusing on the top predicted drug candidates can be performed. By reading-out the drug influence through bulk transcriptomics, drug candidates that demonstrate strong potential to reverse the disease phenotype can be further selected. Therefore, testing the *in silico* predicted drugs with *in vitro* stimulation

experiments significantly narrows down the list of drugs candidates for further clinical evaluation.

Finally, if an identified drug candidate proves to be potent, its treatment effects and responses need to be tested and analyzed – e.g. by using single-cell omics – *in vivo* within human clinical cohorts. We assessed this step for the previously predicted (Aschenbrenner et al. 2021) and efficacy-tested (RECOVERY Collaborative Group et al. 2021; WHO Rapid Evidence Appraisal for COVID-19 Therapies (REACT) Working Group et al. 2020; Tomazini et al. 2020) drug dexamethasone in a clinical cohort study of COVID-19 patients (Knoll et al. 2024). We observed transcriptional and compositional alterations post-treatment and identified that these changes were confined to a specific monocyte state. Notably, these molecular treatment responses were directly correlated with clinical outcomes. Dexamethasone-treated COVID-19 survivors successfully reversed the previously described dysregulated severe phenotype in monocytes, whereas treated patients who deceased failed to achieve this reversal. Using the single-cell signatures, we were able to stratify whole blood bulk transcriptomics samples at earlier timepoints after treatment with high success into responder and non-responder in two independent cohorts. This analysis demonstrated that assessing dexamethasone treatment response with single-cell omics is powerful for treatment response analysis of clinical cohorts and can be used to stratify COVID-19 patients early after treatment initiation, distinguishing patients who benefit from those who do not. While we exemplified this framework for dexamethasone and COVID-19, we are convinced that this approach is not restricted to that drug and disease, but can be applied to evaluate other drug responses in various human diseases.

In the clinics, performing single-cell omics from every treated patient is still too expensive and not standardized. However, we demonstrated that this is not necessary. With single-cell omics from a medium-sized discovery cohort, we have the power and resolution to pinpoint the drug-induced changes and molecular responses in the immune system, leading to the generation of precise gene signatures. These gene signatures can then be used for treatment response stratification using methods that are more feasible in the clinics such as bulk transcriptomics or PCR. With our framework, we are paving the way for evaluation tests for treatment responses based on single-cell omics, which would be the exploratory step for the development of companion diagnostics. Companion diagnostic tests are used either before or during treatment, to evaluate if a diseased patient would benefit from a certain treatment and if not, another treatment might have to be suggested (Goetz and Schork 2018; Kang et al. 2023). Therefore, companion diagnostics are essential in personalized medicine. Although this is a great principle, so far, only 170 companion diagnostic tests, designed for 72 unique drugs, have been approved by the FDA (FDA 2024). Moreover, these tests are based on 43

unique biomarkers, with nearly all drugs being tested in cancer patients. To go beyond cancer, we suggest our framework for generation of companion diagnostics in viral infections. Our single-cell monocyte signature showed its potential and could be further optimized by reducing the number of genes in the signature so that a simpler test e.g. a PCR test could be developed for clinical purposes. However, FDA approval requires meeting stringent prerequisites and regulations including premarket approval, analytical and clinical validation, risk assessment, adherence to good manufacturing practices, compliance with quality system regulations and alignment with extensive guidance documents – all of which can present challenges (FDA, 2024).

Repurposing of drugs based on transcriptomics in human viral infections showed its great potential. Nevertheless, there are still further enhancements needed to improve the repurposing approach. Our approach uses the drug signature library from the Broad institute (Subramanian et al. 2017), which consists of over 437,000 unique drug signatures, representing a valuable resource. However, the drug signatures were generated mostly from cancer cell lines and are based on a bulk transcriptomic expression profile. Ideally, drug signatures extracted from immune cells or disease-relevant tissues using single-cell omics would strongly enhance the possibilities and accuracy of predicting repurposed drugs for various human disease. As this procedure would be applied for many drugs, a standardized protocol would be a prerequisite. In addition, the drug repurposing approach could benefit from additional computational methods or artificial intelligence (AI), to further narrow down the list of top predicted drugs. Additionally, larger cohorts of patients will improve repurposing and signature identification. Considering the exceptionally high number of patients included in the 2000HIV study as well as both bulk and single-cell transcriptomics layers included, performing a data-driven stratification followed by our drug repurposing approach presents a highly promising strategy.

Collectively, this work highlights the potential of transcriptomics-driven approaches for drug repurposing in human viral diseases, while showcasing how single-cell omics could guide exploratory analyses to develop future companion diagnostic tests, advancing precision medicine.

# 5. References


Adamson, B. *et al.* (2016) “A Multiplexed Single-Cell CRISPR Screening Platform Enables Systematic Dissection of the Unfolded Protein Response.,” *Cell*, 167(7), pp. 1867-1882.e21. doi:10.1016/j.cell.2016.11.048.

Ahn, J.H. *et al.* (2021) “Nasal ciliated cells are primary targets for SARS-CoV-2 replication in the early stage of COVID-19.,” *The Journal of Clinical Investigation*, 131(13). doi:10.1172/JCI148517.

Antiretroviral Therapy Cohort Collaboration (2017) “Survival of HIV-positive patients starting antiretroviral therapy between 1996 and 2013: a collaborative analysis of cohort studies.,” *The lancet. HIV*, 4(8), pp. e349–e356. doi:10.1016/S2352-3018(17)30066-8.

Anzinger, J.J. *et al.* (2014) “Monocytes as regulators of inflammation and HIV-related comorbidities during cART.,” *Journal of immunology research*, 2014, p. 569819. doi:10.1155/2014/569819.

Arunachalam, P.S. *et al.* (2020) “Systems biological assessment of immunity to mild versus severe COVID-19 infection in humans.,” *Science*, 369(6508), pp. 1210–1220. doi:10.1126/science.abc6261.

Aschenbrenner, A.C. *et al.* (2021) “Disease severity-specific neutrophil signatures in blood transcriptomes stratify COVID-19 patients.,” *Genome Medicine*, 13(1), p. 7. doi:10.1186/s13073-020-00823-5.

Ashburn, T.T. and Thor, K.B. (2004) “Drug repositioning: identifying and developing new uses for existing drugs.,” *Nature Reviews. Drug Discovery*, 3(8), pp. 673–683. doi:10.1038/nrd1468.

Autran, B. *et al.* (1997) “Positive effects of combined antiretroviral therapy on CD4+ T cell homeostasis and function in advanced HIV disease.,” *Science*, 277(5322), pp. 112–116. doi:10.1126/science.277.5322.112.

Bacchus, C. *et al.* (2013) “A single HIV-1 cluster and a skewed immune homeostasis drive the early spread of HIV among resting CD4+ cell subsets within one month post-infection.,” *Plos One*, 8(5), p. e64219. doi:10.1371/journal.pone.0064219.

Baharom, F. *et al.* (2017) “Human lung mononuclear phagocytes in health and disease.,” *Frontiers in Immunology*, 8, p. 499. doi:10.3389/fimmu.2017.00499.

Barkley, D. *et al.* (2022) “Cancer cell states recur across tumor types and form specific interactions with the tumor microenvironment.,” *Nature Genetics*, 54(8), pp. 1192–1201. doi:10.1038/s41588-022-01141-9.

Barré-Sinoussi, F. *et al.* (1983) “Isolation of a T-lymphotropic retrovirus from a patient at risk for acquired immune deficiency syndrome (AIDS).,” *Science*, 220(4599), pp. 868–871. doi:10.1126/science.6189183.

Baßler, K. *et al.* (2022) “Alveolar macrophages in early stage COPD show functional deviations with properties of impaired immune activation.,” *Frontiers in Immunology*, 13, p. 917232. doi:10.3389/fimmu.2022.917232.

Baysoy, A. *et al.* (2023) “The technological landscape and applications of single-cell multi-omics.,” *Nature Reviews. Molecular Cell Biology*, 24(10), pp. 695–713. doi:10.1038/s41580-023-00615-w.

Beigel, J.H. *et al.* (2020) “Remdesivir for the Treatment of Covid-19 - Final Report.,” *The New England Journal of Medicine*, 383(19), pp. 1813–1826. doi:10.1056/NEJMoa2007764.

Bekker, L.-G. *et al.* (2023) “HIV infection.,” *Nature reviews. Disease primers*, 9(1), p. 42. doi:10.1038/s41572-023-00452-3.

Berlin, D.A., Gulick, R.M. and Martinez, F.J. (2020) “Severe Covid-19.,” *The New England Journal of Medicine*, 383(25), pp. 2451–2460. doi:10.1056/NEJMcp2009575.

Bernardes, J.P. *et al.* (2020) “Longitudinal Multi-omics Analyses Identify Responses of Megakaryocytes, Erythroid Cells, and Plasmablasts as Hallmarks of Severe COVID-19.,” *Immunity*, 53(6), pp. 1296-1314.e9. doi:10.1016/j.immuni.2020.11.017.

Bischoff, P. *et al.* (2021) “Single-cell RNA sequencing reveals distinct tumor microenvironmental patterns in lung adenocarcinoma.,” *Oncogene*, 40(50), pp. 6748–6758. doi:10.1038/s41388-021-02054-3.

Blaauw, M.J.T. *et al.* (2023) “Traditional Cardiovascular Risk Factors Are Stronger Related to Carotid Intima-Media Thickness Than to Presence of Carotid Plaques in People Living With HIV.,” *Journal of the American Heart Association*, 12(20), p. e030606. doi:10.1161/JAHA.123.030606.

Bleul, C.C. *et al.* (1996) “The lymphocyte chemoattractant SDF-1 is a ligand for LESTR/fusin and blocks HIV-1 entry.,” *Nature*, 382(6594), pp. 829–833. doi:10.1038/382829a0.

Bonaguro, L. *et al.* (2022) “A guide to systems-level immunomics.,” *Nature Immunology*, 23(10), pp. 1412–1423. doi:10.1038/s41590-022-01309-9.

Bossel Ben-Moshe, N. *et al.* (2019) “Predicting bacterial infection outcomes using single cell RNA-sequencing analysis of human immune cells.,” *Nature Communications*, 10(1), p. 3266. doi:10.1038/s41467-019-11257-y.

Bowman, E.R. *et al.* (2020) “Macrophage maturation from blood monocytes is altered in people with HIV, and is linked to serum lipid profiles and activation indices: A model for studying atherogenic mechanisms.,” *PLoS Pathogens*, 16(10), p. e1008869. doi:10.1371/journal.ppat.1008869.

Bradley, T. *et al.* (2018) “Single-Cell Analysis of Quiescent HIV Infection Reveals Host Transcriptional Profiles that Regulate Proviral Latency.,” *Cell reports*, 25(1), pp. 107-117.e3. doi:10.1016/j.celrep.2018.09.020.

Brodin, P. and Davis, M.M. (2017) “Human immune system variation.,” *Nature Reviews. Immunology*, 17(1), pp. 21–29. doi:10.1038/nri.2016.125.

Brooks, J.T. *et al.* (2009) “HIV-associated opportunistic infections--going, going, but not gone: the continued need for prevention and treatment guidelines.,” *Clinical Infectious Diseases*, 48(5), pp. 609–611. doi:10.1086/596756.

Buggert, M. *et al.* (2018) “Identification and characterization of HIV-specific resident memory CD8+ T cells in human lymphoid tissue.,” *Science Immunology*, 3(24). doi:10.1126/sciimmunol.aar4526.

Bukrinsky, M.I. *et al.* (1992) “Active nuclear import of human immunodeficiency virus type 1 preintegration complexes.,” *Proceedings of the National Academy of Sciences of the United States of America*, 89(14), pp. 6580–6584. doi:10.1073/pnas.89.14.6580.

Burdo, T.H. *et al.* (2010) “Increased monocyte turnover from bone marrow correlates with severity of SIV encephalitis and CD163 levels in plasma.,” *PLoS Pathogens*, 6(4), p. e1000842. doi:10.1371/journal.ppat.1000842.

Burdo, T.H., Lo, J., *et al.* (2011) “Soluble CD163, a novel marker of activated macrophages, is elevated and associated with noncalcified coronary plaque in HIV-infected patients.,” *The Journal of Infectious Diseases*, 204(8), pp. 1227–1236. doi:10.1093/infdis/jir520.

Burdo, T.H., Lentz, M.R., *et al.* (2011) “Soluble CD163 made by monocyte/macrophages is a novel marker of HIV activity in early and chronic infection prior to and after anti-retroviral therapy.,” *The Journal of Infectious Diseases*, 204(1), pp. 154–163. doi:10.1093/infdis/jir214.

Cao, J. *et al.* (2020) “A human cell atlas of fetal gene expression.,” *Science*, 370(6518). doi:10.1126/science.aba7721.

Cao, X. (2020) “COVID-19: immunopathology and its implications for therapy.,” *Nature Reviews. Immunology*, 20(5), pp. 269–270. doi:10.1038/s41577-020-0308-3.

Centers for Disease Control (CDC) (1981) “Kaposi’s sarcoma and Pneumocystis pneumonia among homosexual men--New York City and California.,” *MMWR. Morbidity and Mortality Weekly Report*, 30(25), pp. 305–308.

Chaffin, M. *et al.* (2022) “Single-nucleus profiling of human dilated and hypertrophic cardiomyopathy.,” *Nature*, 608(7921), pp. 174–180. doi:10.1038/s41586-022-04817-8.

Chan, D.C. and Kim, P.S. (1998) “HIV entry and its inhibition.,” *Cell*, 93(5), pp. 681–684. doi:10.1016/s0092-8674(00)81430-0.

Chen, G. *et al.* (2020) “Clinical and immunological features of severe and moderate coronavirus disease 2019.,” *The Journal of Clinical Investigation*, 130(5), pp. 2620–2629. doi:10.1172/JCI137244.

Cho, M., Min, X. and Son, H.S. (2022) “Analysis of evolutionary and genetic patterns in structural genes of primate lentiviruses.,” *Genes & genomics*, 44(7), pp. 773–791. doi:10.1007/s13258-022-01257-6.

Chua, R.L. *et al.* (2020) “COVID-19 severity correlates with airway epithelium-immune cell interactions identified by single-cell analysis.,” *Nature Biotechnology*, 38(8), pp. 970–979. doi:10.1038/s41587-020-0602-4.

Chun, T.W. *et al.* (1995) “In vivo fate of HIV-1-infected T cells: quantitative analysis of the transition to stable latency.,” *Nature Medicine*, 1(12), pp. 1284–1290. doi:10.1038/nm1295-1284.

Clark, I.C. *et al.* (2023) “HIV silencing and cell survival signatures in infected T cell reservoirs.,” *Nature*, 614(7947), pp. 318–325. doi:10.1038/s41586-022-05556-6.

Cohen, M.S. *et al.* (2011) “Acute HIV-1 Infection.,” *The New England Journal of Medicine*, 364(20), pp. 1943–1954. doi:10.1056/NEJMra1011874.

Cohen, M.S. *et al.* (2016) “Antiretroviral Therapy for the Prevention of HIV-1 Transmission.,” *The New England Journal of Medicine*, 375(9), pp. 830–839. doi:10.1056/NEJMoa1600693.

Coleman, M.M. *et al.* (2013) “Alveolar macrophages contribute to respiratory tolerance by inducing FoxP3 expression in naive T cells.,” *American Journal of Respiratory Cell and Molecular Biology*, 48(6), pp. 773–780. doi:10.1165/rcmb.2012-0263OC.

Collora, J.A. *et al.* (2022) “Single-cell multiomics reveals persistence of HIV-1 in expanded cytotoxic T cell clones.,” *Immunity*, 55(6), pp. 1013-1031.e7. doi:10.1016/j.immuni.2022.03.004.

Combes, A.J. *et al.* (2021) “Global absence and targeting of protective immune states in severe COVID-19.,” *Nature*, 591(7848), pp. 124–130. doi:10.1038/s41586-021-03234-7.

Concorde Coordinating Committee (1994) “Concorde: MRC/ANRS randomised double-blind controlled trial of immediate and deferred zidovudine in symptom-free HIV infection. Concorde Coordinating Committee,” *Lancet* [Preprint].

Cooper, D.A. *et al.* (1985) “Acute AIDS retrovirus infection. Definition of a clinical illness associated with seroconversion.,” *The Lancet*, 1(8428), pp. 537–540. doi:10.1016/s0140-6736(85)91205-x.

COvid-19 Multi-omics Blood ATlas (COMBAT) Consortium (2022) “A blood atlas of COVID-19 defines hallmarks of disease severity and specificity.,” *Cell*, 185(5), pp. 916-938.e58. doi:10.1016/j.cell.2022.01.012.

Crowe, S.M. *et al.* (1991) “Predictive value of CD4 lymphocyte numbers for the development of opportunistic infections and malignancies in HIV-infected persons.,” *Journal of Acquired Immune Deficiency Syndromes*, 4(8), pp. 770–776.

Davis, H.E. *et al.* (2023) “Author Correction: Long COVID: major findings, mechanisms and recommendations.,” *Nature Reviews Microbiology*, 21(6), p. 408. doi:10.1038/s41579-023-00896-0.

Deeks, S.G., Tracy, R. and Douek, D.C. (2013) “Systemic effects of inflammation on health during chronic HIV infection.,” *Immunity*, 39(4), pp. 633–645. doi:10.1016/j.immuni.2013.10.001.

Delorey, T.M. *et al.* (2021) “COVID-19 tissue atlases reveal SARS-CoV-2 pathology and cellular targets.,” *Nature*, 595(7865), pp. 107–113. doi:10.1038/s41586-021-03570-8.

De Domenico, E. *et al.* (2020) “Optimized workflow for single-cell transcriptomics on infectious diseases including COVID-19.,” *STAR Protocols*, 1(3), p. 100233. doi:10.1016/j.xpro.2020.100233.

De Luca, A. *et al.* (2013) “The association of high-sensitivity c-reactive protein and other biomarkers with cardiovascular disease in patients treated for HIV: a nested case-control study.,” *BMC Infectious Diseases*, 13, p. 414. doi:10.1186/1471-2334-13-414.

Dixit, A. *et al.* (2016) “Perturb-Seq: Dissecting Molecular Circuits with Scalable Single-Cell RNA Profiling of Pooled Genetic Screens.,” *Cell*, 167(7), pp. 1853-1866.e17. doi:10.1016/j.cell.2016.11.038.

Dragic, T. *et al.* (1996) “HIV-1 entry into CD4+ cells is mediated by the chemokine receptor CC-CKR-5.,” *Nature*, 381(6584), pp. 667–673. doi:10.1038/381667a0.

Dudley, J.T. *et al.* (2011) “Computational repositioning of the anticonvulsant topiramate for inflammatory bowel disease.,” *Science Translational Medicine*, 3(96), p. 96ra76. doi:10.1126/scitranslmed.3002648.

Dugger, S.A., Platt, A. and Goldstein, D.B. (2018) “Drug development in the era of precision medicine.,” *Nature Reviews. Drug Discovery*, 17(3), pp. 183–196. doi:10.1038/nrd.2017.226.

Duprez, D.A. *et al.* (2012) “Inflammation, coagulation and cardiovascular disease in HIV-infected individuals.,” *Plos One*, 7(9), p. e44454. doi:10.1371/journal.pone.0044454.

Edahiro, R. *et al.* (2023) “Single-cell analyses and host genetics highlight the role of innate immune cells in COVID-19 severity.,” *Nature Genetics*, 55(5), pp. 753–767. doi:10.1038/s41588-023-01375-1.

van Eekeren, L.E. *et al.* (2024) “Liver Steatosis is Prevalent in Lean People With HIV and Associated With Exposure to Antiretroviral Treatment-A Cross-sectional Study.,” *Open forum infectious diseases*, 11(6), p. ofae266. doi:10.1093/ofid/ofae266.

El-Atrouni, W., Berbari, E. and Temesgen, Z. (2006) “HIV-associated opportunistic infections. Bacterial infections.,” *Le Journal medical libanais. The Lebanese medical journal*, 54(2), pp. 80–83.

Ellery, P.J. *et al.* (2007) “The CD16+ monocyte subset is more permissive to infection and preferentially harbors HIV-1 in vivo.,” *Journal of Immunology*, 178(10), pp. 6581–6589. doi:10.4049/jimmunol.178.10.6581.

Emrich, S.J. *et al.* (2007) “Gene discovery and annotation using LCM-454 transcriptome sequencing.,” *Genome Research*, 17(1), pp. 69–73. doi:10.1101/gr.5145806.

Falck-Jones, S. *et al.* (2021) “Functional monocytic myeloid-derived suppressor cells increase in blood but not airways and predict COVID-19 severity.,” *The Journal of Clinical Investigation*, 131(6). doi:10.1172/JCI144734.

FDA (2024) *List of Cleared or Approved Companion Diagnostic Devices (In Vitro and Imaging Tools)*. Available at: https://www.fda.gov/medical-devices/in-vitro-diagnostics/list-cleared-or-approved-companion-diagnostic-devices-in-vitro-and-imaging-tools (Accessed: July 11, 2024).

FDA (2024) *Principles for Codevelopment of an In Vitro Companion Diagnostic Device with a Therapeutic Product*. Available at: https://www.fda.gov/regulatory-information/search-fda-guidance-documents/principles-codevelopment-in-vitro-companion-diagnostic-device-therapeutic-product#:~:text=As%20described%20in%20the%20FDA,use%20indicated%20in%20the%20therapeutic (Accessed: October 14, 2024).

Fenwick, C. *et al.* (2019) “T-cell exhaustion in HIV infection.,” *Immunological Reviews*, 292(1), pp. 149–163. doi:10.1111/imr.12823.

Ferreira, A.C. *et al.* (2021) “SARS-CoV-2 engages inflammasome and pyroptosis in human primary monocytes.,” *Cell death discovery*, 7(1), p. 43. doi:10.1038/s41420-021-00428-w.

Fiebig, E.W. *et al.* (2003) “Dynamics of HIV viremia and antibody seroconversion in plasma donors: implications for diagnosis and staging of primary HIV infection.,” *AIDS*, 17(13), pp. 1871–1879. doi:10.1097/00002030-200309050-00005.

Filchakova, O. *et al.* (2022) “Review of COVID-19 testing and diagnostic methods.,” *Talanta*, 244, p. 123409. doi:10.1016/j.talanta.2022.123409.

Fitch, K.V. *et al.* (2013) “Noncalcified coronary atherosclerotic plaque and immune activation in HIV-infected women.,” *The Journal of Infectious Diseases*, 208(11), pp. 1737–1746. doi:10.1093/infdis/jit508.

Ford, E.S., Puronen, C.E. and Sereti, I. (2009) “Immunopathogenesis of asymptomatic chronic HIV Infection: the calm before the storm.,” *Current Opinion in HIV and AIDS*, 4(3), pp. 206–214. doi:10.1097/COH.0b013e328329c68c.

Franke-Ullmann, G. *et al.* (1996) “Characterization of murine lung interstitial macrophages in comparison with alveolar macrophages in vitro.,” *Journal of Immunology*, 157(7), pp. 3097–3104. doi:10.4049/jimmunol.157.7.3097.

Funderburg, N.T. *et al.* (2010) “Increased tissue factor expression on circulating monocytes in chronic HIV infection: relationship to in vivo coagulation and immune activation.,” *Blood*, 115(2), pp. 161–167. doi:10.1182/blood-2009-03-210179.

Gandhi, R.T., Lynch, J.B. and Del Rio, C. (2020) “Mild or Moderate Covid-19.,” *The New England Journal of Medicine*, 383(18), pp. 1757–1766. doi:10.1056/NEJMcp2009249.

Gatti, A. *et al.* (2020) “Decrease of Non-Classical and Intermediate Monocyte Subsets in Severe Acute SARS-CoV-2 Infection.,” *Cytometry. Part A: the Journal of the International Society for Analytical Cytology*, 97(9), pp. 887–890. doi:10.1002/cyto.a.24188.

Georg, P. *et al.* (2022) “Complement activation induces excessive T cell cytotoxicity in severe COVID-19.,” *Cell*, 185(3), pp. 493-512.e25. doi:10.1016/j.cell.2021.12.040.

Ghofrani, H.A., Osterloh, I.H. and Grimminger, F. (2006) “Sildenafil: from angina to erectile dysfunction to pulmonary hypertension and beyond.,” *Nature Reviews. Drug Discovery*, 5(8), pp. 689–702. doi:10.1038/nrd2030.

Giamarellos-Bourboulis, E.J. *et al.* (2020) “Complex Immune Dysregulation in COVID-19 Patients with Severe Respiratory Failure.,” *Cell Host & Microbe*, 27(6), pp. 992-1000.e3. doi:10.1016/j.chom.2020.04.009.

Goetz, L.H. and Schork, N.J. (2018) “Personalized medicine: motivation, challenges, and progress.,” *Fertility and Sterility*, 109(6), pp. 952–963. doi:10.1016/j.fertnstert.2018.05.006.

Golde, D.W., Byers, L.A. and Finley, T.N. (1974) “Proliferative capacity of human alveolar macrophage.,” *Nature*, 247(5440), pp. 373–375. doi:10.1038/247373a0.

Guan, W.-J. *et al.* (2020) “Comorbidity and its impact on 1590 patients with COVID-19 in China: a nationwide analysis.,” *The European Respiratory Journal*, 55(5). doi:10.1183/13993003.00547-2020.

Guilliams, M. *et al.* (2013) “Alveolar macrophages develop from fetal monocytes that differentiate into long-lived cells in the first week of life via GM-CSF.,” *The Journal of Experimental Medicine*, 210(10), pp. 1977–1992. doi:10.1084/jem.20131199.

Gupta, A. *et al.* (2020) “Extrapulmonary manifestations of COVID-19.,” *Nature Medicine*, 26(7), pp. 1017–1032. doi:10.1038/s41591-020-0968-3.

Gupta, K.K. (1993) “Acute immunosuppression with HIV seroconversion.,” *The New England Journal of Medicine*, 328(4), pp. 288–289. doi:10.1056/NEJM199301283280419.

Hanna, D.B. *et al.* (2017) “Association of Macrophage Inflammation Biomarkers With Progression of Subclinical Carotid Artery Atherosclerosis in HIV-Infected Women and Men.,” *The Journal of Infectious Diseases*, 215(9), pp. 1352–1361. doi:10.1093/infdis/jix082.

Haque, A. *et al.* (2017) “A practical guide to single-cell RNA-sequencing for biomedical research and clinical applications.,” *Genome Medicine*, 9(1), p. 75. doi:10.1186/s13073-017-0467-4.

Hasegawa, A. *et al.* (2009) “The level of monocyte turnover predicts disease progression in the macaque model of AIDS.,” *Blood*, 114(14), pp. 2917–2925. doi:10.1182/blood-2009-02-204263.

Hearps, A.C. *et al.* (2011) “HIV infection and aging of the innate immune system.,” *Sexual Health*, 8(4), pp. 453–464. doi:10.1071/SH11028.

Hearps, A.C. *et al.* (2012) “HIV infection induces age-related changes to monocytes and innate immune activation in young men that persist despite combination antiretroviral therapy.,” *AIDS*, 26(7), pp. 843–853. doi:10.1097/QAD.0b013e328351f756.

Hecht, F.M. *et al.* (2002) “Use of laboratory tests and clinical symptoms for identification of primary HIV infection.,” *AIDS*, 16(8), pp. 1119–1129. doi:10.1097/00002030-200205240-00005.

Hegde, S., Leader, A.M. and Merad, M. (2021) “MDSC: Markers, development, states, and unaddressed complexity.,” *Immunity*, 54(5), pp. 875–884. doi:10.1016/j.immuni.2021.04.004.

van der Heijden, W.A., Van de Wijer, L., *et al.* (2021) “Chronic HIV infection induces transcriptional and functional reprogramming of innate immune cells.,” *Journal of Clinical Investigation Insight*, 6(7). doi:10.1172/jci.insight.145928.

van der Heijden, W.A., Wan, J., *et al.* (2021) “Plasmatic coagulation capacity correlates with inflammation and abacavir use during chronic HIV infection.,” *JAIDS Journal of Acquired Immune Deficiency Syndromes*, 87(1), pp. 711–719. doi:10.1097/QAI.0000000000002633.

Heumos, L. *et al.* (2023) “Best practices for single-cell analysis across modalities.,” *Nature Reviews. Genetics*, 24(8), pp. 550–572. doi:10.1038/s41576-023-00586-w.

He, B. *et al.* (2023) “ASGARD is A Single-cell Guided Pipeline to Aid Repurposing of Drugs.,” *Nature Communications*, 14(1), p. 993. doi:10.1038/s41467-023-36637-3.

He, Z. *et al.* (2018) “Rapid Turnover and High Production Rate of Myeloid Cells in Adult Rhesus Macaques with Compensations during Aging.,” *Journal of Immunology*, 200(12), pp. 4059–4067. doi:10.4049/jimmunol.1800207.

Hikmet, F. *et al.* (2020) “The protein expression profile of ACE2 in human tissues.,” *Molecular Systems Biology*, 16(7), p. e9610. doi:10.15252/msb.20209610.

Hladik, F. and McElrath, M.J. (2008) “Setting the stage: host invasion by HIV.,” *Nature Reviews. Immunology*, 8(6), pp. 447–457. doi:10.1038/nri2302.

Hoffmann, M. *et al.* (2020) “SARS-CoV-2 Cell Entry Depends on ACE2 and TMPRSS2 and Is Blocked by a Clinically Proven Protease Inhibitor.,” *Cell*, 181(2), pp. 271-280.e8. doi:10.1016/j.cell.2020.02.052.

Hou, Y.J. *et al.* (2020) “SARS-CoV-2 Reverse Genetics Reveals a Variable Infection Gradient in the Respiratory Tract.,” *Cell*, 182(2), pp. 429-446.e14. doi:10.1016/j.cell.2020.05.042.

Hsue, P.Y. *et al.* (2012) “Carotid Intima-Media Thickness Progression in HIV-Infected Adults Occurs Preferentially at the Carotid Bifurcation and Is Predicted by Inflammation.,” *Journal of the American Heart Association*, 1(2). doi:10.1161/JAHA.111.000422.

Huang, C.-H. *et al.* (2016) “Identify potential drugs for cardiovascular diseases caused by stress-induced genes in vascular smooth muscle cells.,” *PeerJ*, 4, p. e2478. doi:10.7717/peerj.2478.

Huang, C. *et al.* (2020) “Clinical features of patients infected with 2019 novel coronavirus in Wuhan, China.,” *The Lancet*, 395(10223), pp. 497–506. doi:10.1016/S0140-6736(20)30183-5.

Hunt, P.W., Lee, S.A. and Siedner, M.J. (2016) “Immunologic biomarkers, morbidity, and mortality in treated HIV infection.,” *The Journal of Infectious Diseases*, 214 Suppl 2(Suppl 2), pp. S44-50. doi:10.1093/infdis/jiw275.

Hussell, T. and Bell, T.J. (2014) “Alveolar macrophages: plasticity in a tissue-specific context.,” *Nature Reviews. Immunology*, 14(2), pp. 81–93. doi:10.1038/nri3600.

INSIGHT START Study Group *et al.* (2015) “Initiation of antiretroviral therapy in early asymptomatic HIV infection.,” *The New England Journal of Medicine*, 373(9), pp. 795–807. doi:10.1056/NEJMoa1506816.

Iorio, F. *et al.* (2013) “Transcriptional data: a new gateway to drug repositioning?,” *Drug Discovery Today*, 18(7–8), pp. 350–357. doi:10.1016/j.drudis.2012.07.014.

Jackson, C.B. *et al.* (2021) “Mechanisms of SARS-CoV-2 entry into cells.,” *Nature Reviews. Molecular Cell Biology*, 23(1), pp. 3–20. doi:10.1038/s41580-021-00418-x.

Jaeger, N. *et al.* (2021) “Single-cell analyses of Crohn’s disease tissues reveal intestinal intraepithelial T cells heterogeneity and altered subset distributions.,” *Nature Communications*, 12(1), p. 1921. doi:10.1038/s41467-021-22164-6.

Jaitin, D.A. *et al.* (2016) “Dissecting Immune Circuits by Linking CRISPR-Pooled Screens with Single-Cell RNA-Seq.,” *Cell*, 167(7), pp. 1883-1896.e15. doi:10.1016/j.cell.2016.11.039.

Jarada, T.N., Rokne, J.G. and Alhajj, R. (2020) “A review of computational drug repositioning: strategies, approaches, opportunities, challenges, and directions.,” *Journal of cheminformatics*, 12(1), p. 46. doi:10.1186/s13321-020-00450-7.

Jovic, D. *et al.* (2022) “Single-cell RNA sequencing technologies and applications: A brief overview.,” *Clinical and translational medicine*, 12(3), p. e694. doi:10.1002/ctm2.694.

Kahn, J.O. and Walker, B.D. (1998) “Acute human immunodeficiency virus type 1 infection.,” *The New England Journal of Medicine*, 339(1), pp. 33–39. doi:10.1056/NEJM199807023390107.

Kalish, M.L. *et al.* (2005) “Central African hunters exposed to simian immunodeficiency virus.,” *Emerging Infectious Diseases*, 11(12), pp. 1928–1930. doi:10.3201/eid1112.050394.

Kamath, T. *et al.* (2022) “Single-cell genomic profiling of human dopamine neurons identifies a population that selectively degenerates in Parkinson’s disease.,” *Nature Neuroscience*, 25(5), pp. 588–595. doi:10.1038/s41593-022-01061-1.

Kang, S.L. *et al.* (2023) “Necessity of strengthening the current clinical regulatory for companion diagnostics: An institutional comparison of the FDA, EMA, and MFDS.,” *Molecular therapy. Methods & clinical development*, 30, pp. 447–458. doi:10.1016/j.omtm.2023.08.008.

Kazer, S.W. *et al.* (2020) “Integrated single-cell analysis of multicellular immune dynamics during hyperacute HIV-1 infection.,” *Nature Medicine*, 26(4), pp. 511–518. doi:10.1038/s41591-020-0799-2.

Kedor, C. *et al.* (2022) “A prospective observational study of post-COVID-19 chronic fatigue syndrome following the first pandemic wave in Germany and biomarkers associated with symptom severity.,” *Nature Communications*, 13(1), p. 5104. doi:10.1038/s41467-022-32507-6.

Kelesidis, T. *et al.* (2012) “Biomarkers of microbial translocation and macrophage activation: association with progression of subclinical atherosclerosis in HIV-1 infection.,” *The Journal of Infectious Diseases*, 206(10), pp. 1558–1567. doi:10.1093/infdis/jis545.

Keren-Shaul, H. *et al.* (2017) “A Unique Microglia Type Associated with Restricting Development of Alzheimer’s Disease.,” *Cell*, 169(7), pp. 1276-1290.e17. doi:10.1016/j.cell.2017.05.018.

Kiselev, V.Y., Andrews, T.S. and Hemberg, M. (2019) “Challenges in unsupervised clustering of single-cell RNA-seq data.,” *Nature Reviews. Genetics*, 20(5), pp. 273–282. doi:10.1038/s41576-018-0088-9.

Knoll, R., Schultze, J.L. and Schulte-Schrepping, J. (2021) “Monocytes and Macrophages in COVID-19.,” *Frontiers in Immunology*, 12, p. 720109. doi:10.3389/fimmu.2021.720109.

Knoll, R. *et al.* (2023) “Identification of drug candidates targeting monocyte reprogramming in people living with HIV.,” *Frontiers in Immunology*, 14, p. 1275136. doi:10.3389/fimmu.2023.1275136.

Knoll, R. *et al.* (2024) “The life-saving benefit of dexamethasone in severe COVID-19 is linked to a reversal of monocyte dysregulation.,” *Cell* [Preprint]. doi:10.1016/j.cell.2024.06.014.

Knudsen, A.D. *et al.* (2022) “Monocyte count and soluble markers of monocyte activation in people living with HIV and uninfected controls.,” *BMC Infectious Diseases*, 22(1), p. 451. doi:10.1186/s12879-022-07450-y.

Knudsen, T.B. *et al.* (2016) “Plasma Soluble CD163 Level Independently Predicts All-Cause Mortality in HIV-1-Infected Individuals.,” *The Journal of Infectious Diseases*, 214(8), pp. 1198–1204. doi:10.1093/infdis/jiw263.

Korber, B. *et al.* (2000) “Timing the ancestor of the HIV-1 pandemic strains.,” *Science*, 288(5472), pp. 1789–1796. doi:10.1126/science.288.5472.1789.

Krämer, B. *et al.* (2021) “Early IFN-α signatures and persistent dysfunction are distinguishing features of NK cells in severe COVID-19.,” *Immunity*, 54(11), pp. 2650-2669.e14. doi:10.1016/j.immuni.2021.09.002.

Kuller, L.H. *et al.* (2008) “Inflammatory and coagulation biomarkers and mortality in patients with HIV infection.,” *PLoS Medicine*, 5(10), p. e203. doi:10.1371/journal.pmed.0050203.

Kvedaraite, E. *et al.* (2021) “Major alterations in the mononuclear phagocyte landscape associated with COVID-19 severity.,” *Proceedings of the National Academy of Sciences of the United States of America*, 118(6). doi:10.1073/pnas.2018587118.

Lähnemann, D. *et al.* (2020) “Eleven grand challenges in single-cell data science.,” *Genome Biology*, 21(1), p. 31. doi:10.1186/s13059-020-1926-6.

Laing, A.G. *et al.* (2020) “A dynamic COVID-19 immune signature includes associations with poor prognosis.,” *Nature Medicine*, 26(10), pp. 1623–1635. doi:10.1038/s41591-020-1038-6.

Lake, B.B. *et al.* (2023) “An atlas of healthy and injured cell states and niches in the human kidney.,” *Nature*, 619(7970), pp. 585–594. doi:10.1038/s41586-023-05769-3.

Lamb, J. *et al.* (2006) “The Connectivity Map: using gene-expression signatures to connect small molecules, genes, and disease.,” *Science*, 313(5795), pp. 1929–1935. doi:10.1126/science.1132939.

Lamers, M.M. and Haagmans, B.L. (2022) “SARS-CoV-2 pathogenesis.,” *Nature Reviews Microbiology*, 20(5), pp. 270–284. doi:10.1038/s41579-022-00713-0.

Lekkerkerker, A.N., van Kooyk, Y. and Geijtenbeek, T.B.H. (2006) “Viral piracy: HIV-1 targets dendritic cells for transmission.,” *Current HIV Research*, 4(2), pp. 169–176. doi:10.2174/157016206776055020.

Lemey, P. *et al.* (2003) “Tracing the origin and history of the HIV-2 epidemic.,” *Proceedings of the National Academy of Sciences of the United States of America*, 100(11), pp. 6588–6592. doi:10.1073/pnas.0936469100.

Liao, M. *et al.* (2020) “Single-cell landscape of bronchoalveolar immune cells in patients with COVID-19.,” *Nature Medicine*, 26(6), pp. 842–844. doi:10.1038/s41591-020-0901-9.

Lien, E. *et al.* (1998) “Elevated levels of serum-soluble CD14 in human immunodeficiency virus type 1 (HIV-1) infection: correlation to disease progression and clinical events.,” *Blood*, 92(6), pp. 2084–2092. doi:10.1182/blood.V92.6.2084.

Lindbäck, S. *et al.* (2000) “Diagnosis of primary HIV-1 infection and duration of follow-up after HIV exposure. Karolinska Institute Primary HIV Infection Study Group.,” *AIDS*, 14(15), pp. 2333–2339. doi:10.1097/00002030-200010200-00014.

Liston, A. *et al.* (2021) “Human immune diversity: from evolution to modernity.,” *Nature Immunology*, 22(12), pp. 1479–1489. doi:10.1038/s41590-021-01058-1.

Little, S.J. *et al.* (1999) “Viral dynamics of acute HIV-1 infection.,” *The Journal of Experimental Medicine*, 190(6), pp. 841–850. doi:10.1084/jem.190.6.841.

Liu, C. *et al.* (2021) “Time-resolved systems immunology reveals a late juncture linked to fatal COVID-19.,” *Cell*, 184(7), pp. 1836-1857.e22. doi:10.1016/j.cell.2021.02.018.

Liu, R. *et al.* (2020) “Single-cell transcriptional landscapes reveal HIV-1-driven aberrant host gene transcription as a potential therapeutic target.,” *Science Translational Medicine*, 12(543). doi:10.1126/scitranslmed.aaz0802.

Li, Y.E. *et al.* (2023) “A comparative atlas of single-cell chromatin accessibility in the human brain.,” *Science*, 382(6667), p. eadf7044. doi:10.1126/science.adf7044.

Longenecker, C.T. *et al.* (2014) “Soluble CD14 is independently associated with coronary calcification and extent of subclinical vascular disease in treated HIV infection.,” *AIDS*, 28(7), pp. 969–977. doi:10.1097/QAD.0000000000000158.

Lucas, C. *et al.* (2020) “Longitudinal analyses reveal immunological misfiring in severe COVID-19.,” *Nature*, 584(7821), pp. 463–469. doi:10.1038/s41586-020-2588-y.

Lyons, J.L. *et al.* (2011) “Plasma sCD14 is a biomarker associated with impaired neurocognitive test performance in attention and learning domains in HIV infection.,” *JAIDS Journal of Acquired Immune Deficiency Syndromes*, 57(5), pp. 371–379. doi:10.1097/QAI.0b013e3182237e54.

Malcomson, B. *et al.* (2016) “Connectivity mapping (ssCMap) to predict A20-inducing drugs and their antiinflammatory action in cystic fibrosis.,” *Proceedings of the National Academy of Sciences of the United States of America*, 113(26), pp. E3725-34. doi:10.1073/pnas.1520289113.

Mardis, E.R. (2011) “A decade’s perspective on DNA sequencing technology,” *Nature*, 470(7333), pp. 198–203. doi:10.1038/nature09796.

Martin, G.E. *et al.* (2013) “Age-associated changes in monocyte and innate immune activation markers occur more rapidly in HIV infected women.,” *Plos One*, 8(1), p. e55279. doi:10.1371/journal.pone.0055279.

Marx, V. (2021) “Method of the Year: spatially resolved transcriptomics.,” *Nature Methods*, 18(1), pp. 9–14. doi:10.1038/s41592-020-01033-y.

Mathew, D. *et al.* (2020) “Deep immune profiling of COVID-19 patients reveals distinct immunotypes with therapeutic implications.,” *Science*, 369(6508). doi:10.1126/science.abc8511.

Mathys, H. *et al.* (2019) “Single-cell transcriptomic analysis of Alzheimer’s disease.,” *Nature*, 570(7761), pp. 332–337. doi:10.1038/s41586-019-1195-2.

May, M.T. *et al.* (2014) “Impact on life expectancy of HIV-1 positive individuals of CD4+ cell count and viral load response to antiretroviral therapy.,” *AIDS*, 28(8), pp. 1193–1202. doi:10.1097/QAD.0000000000000243.

McElrath, M.J., Pruett, J.E. and Cohn, Z.A. (1989) “Mononuclear phagocytes of blood and bone marrow: comparative roles as viral reservoirs in human immunodeficiency virus type 1 infections.,” *Proceedings of the National Academy of Sciences of the United States of America*, 86(2), pp. 675–679. doi:10.1073/pnas.86.2.675.

McKibben, R.A. *et al.* (2015) “Elevated levels of monocyte activation markers are associated with subclinical atherosclerosis in men with and those without HIV infection.,” *The Journal of Infectious Diseases*, 211(8), pp. 1219–1228. doi:10.1093/infdis/jiu594.

Mehandru, S. and Merad, M. (2022) “Pathological sequelae of long-haul COVID.,” *Nature Immunology*, 23(2), pp. 194–202. doi:10.1038/s41590-021-01104-y.

Mehta, P. *et al.* (2020) “COVID-19: consider cytokine storm syndromes and immunosuppression.,” *The Lancet*, 395(10229), pp. 1033–1034. doi:10.1016/S0140-6736(20)30628-0.

Méndez-Lagares, G. *et al.* (2013) “Long-term suppressive combined antiretroviral treatment does not normalize the serum level of soluble CD14.,” *The Journal of Infectious Diseases*, 207(8), pp. 1221–1225. doi:10.1093/infdis/jit025.

Mensching, L. and Hoelzemer, A. (2022) “NK Cells, Monocytes and Macrophages in HIV-1 Control: Impact of Innate Immune Responses.,” *Frontiers in Immunology*, 13, p. 883728. doi:10.3389/fimmu.2022.883728.

Merlini, E. *et al.* (2012) “T-cell phenotypes, apoptosis and inflammation in HIV+ patients on virologically effective cART with early atherosclerosis.,” *Plos One*, 7(9), p. e46073. doi:10.1371/journal.pone.0046073.

Metzker, M.L. (2010) “Sequencing technologies - the next generation.,” *Nature Reviews. Genetics*, 11(1), pp. 31–46. doi:10.1038/nrg2626.

Mimitou, E.P. *et al.* (2019) “Multiplexed detection of proteins, transcriptomes, clonotypes and CRISPR perturbations in single cells.,” *Nature Methods*, 16(5), pp. 409–412. doi:10.1038/s41592-019-0392-0.

Møller, H.J. (2012) “Soluble CD163.,” *Scandinavian Journal of Clinical and Laboratory Investigation*, 72(1), pp. 1–13. doi:10.3109/00365513.2011.626868.

Morgan, P. *et al.* (2018) “Impact of a five-dimensional framework on R&D productivity at AstraZeneca.,” *Nature Reviews. Drug Discovery*, 17(3), pp. 167–181. doi:10.1038/nrd.2017.244.

Morris, D.G. *et al.* (2003) “Loss of integrin alpha(v)beta6-mediated TGF-beta activation causes Mmp12-dependent emphysema.,” *Nature*, 422(6928), pp. 169–173. doi:10.1038/nature01413.

Moses, L. and Pachter, L. (2022) “Museum of spatial transcriptomics.,” *Nature Methods*, 19(5), pp. 534–546. doi:10.1038/s41592-022-01409-2.

Muus, C. *et al.* (2021) “Single-cell meta-analysis of SARS-CoV-2 entry genes across tissues and demographics.,” *Nature Medicine*, 27(3), pp. 546–559. doi:10.1038/s41591-020-01227-z.

National Center for Health Statistics. U.S (2024) *Long COVID Household Pulse Survey*. Available at: https://www.cdc.gov/nchs/covid19/pulse/long-covid.htm (Accessed: April 25, 2024).

Nehar-Belaid, D. *et al.* (2020) “Mapping systemic lupus erythematosus heterogeneity at the single-cell level.,” *Nature Immunology*, 21(9), pp. 1094–1106. doi:10.1038/s41590-020-0743-0.

Nicola, M. *et al.* (2020) “The socio-economic implications of the coronavirus pandemic (COVID-19): A review.,” *International Journal of Surgery*, 78, pp. 185–193. doi:10.1016/j.ijsu.2020.04.018.

Nosengo, N. (2016) “Can you teach old drugs new tricks?,” *Nature*, 534(7607), pp. 314–316. doi:10.1038/534314a.

Nouailles, G. *et al.* (2021) “Temporal omics analysis in Syrian hamsters unravel cellular effector responses to moderate COVID-19.,” *Nature Communications*, 12(1), p. 4869. doi:10.1038/s41467-021-25030-7.

Novel Coronavirus Pneumonia Emergency Response Epidemiology Team (2020) “The epidemiological characteristics of an outbreak of 2019 novel coronavirus diseases (COVID-19) in China,” *Zhonghua Liu Xing Bing Xue Za Zhi = Zhonghua Liuxingbingxue Zazhi*, 41(2), pp. 145–151. doi:10.3760/cma.j.issn.0254-6450.2020.02.003.

Oelen, R. *et al.* (2022) “Single-cell RNA-sequencing of peripheral blood mononuclear cells reveals widespread, context-specific gene expression regulation upon pathogenic exposure.,” *Nature Communications*, 13(1), p. 3267. doi:10.1038/s41467-022-30893-5.

Ortega-Gómez, A., Perretti, M. and Soehnlein, O. (2013) “Resolution of inflammation: an integrated view.,” *EMBO Molecular Medicine*, 5(5), pp. 661–674. doi:10.1002/emmm.201202382.

Osuchowski, M.F. *et al.* (2021) “The COVID-19 puzzle: deciphering pathophysiology and phenotypes of a new disease entity.,” *The Lancet. Respiratory medicine*, 9(6), pp. 622–642. doi:10.1016/S2213-2600(21)00218-6.

Papalexi, E. and Satija, R. (2018) “Single-cell RNA sequencing to explore immune cell heterogeneity.,” *Nature Reviews. Immunology*, 18(1), pp. 35–45. doi:10.1038/nri.2017.76.

Payen, D. *et al.* (2020) “A Longitudinal Study of Immune Cells in Severe COVID-19 Patients.,” *Frontiers in Immunology*, 11, p. 580250. doi:10.3389/fimmu.2020.580250.

Perelson, A.S. *et al.* (1996) “HIV-1 dynamics in vivo: virion clearance rate, infected cell life-span, and viral generation time.,” *Science*, 271(5255), pp. 1582–1586. doi:10.1126/science.271.5255.1582.

Perez, R.K. *et al.* (2022) “Single-cell RNA-seq reveals cell type-specific molecular and genetic associations to lupus.,” *Science*, 376(6589), p. eabf1970. doi:10.1126/science.abf1970.

Pilarczyk, M. *et al.* (2022) “Connecting omics signatures and revealing biological mechanisms with iLINCS.,” *Nature Communications*, 13(1), p. 4678. doi:10.1038/s41467-022-32205-3.

Pitman, M.C. *et al.* (2018) “Barriers and strategies to achieve a cure for HIV.,” *The lancet. HIV*, 5(6), pp. e317–e328. doi:10.1016/S2352-3018(18)30039-0.

Prussin, A.J., Garcia, E.B. and Marr, L.C. (2015) “Total virus and bacteria concentrations in indoor and outdoor air.,” *Environmental science & technology letters*, 2(4), pp. 84–88. doi:10.1021/acs.estlett.5b00050.

Pulliam, L. *et al.* (1997) “Unique monocyte subset in patients with AIDS dementia.,” *The Lancet*, 349(9053), pp. 692–695. doi:10.1016/S0140-6736(96)10178-1.

Pushpakom, S. *et al.* (2019) “Drug repurposing: progress, challenges and recommendations.,” *Nature Reviews. Drug Discovery*, 18(1), pp. 41–58. doi:10.1038/nrd.2018.168.

Qin, C. *et al.* (2020) “Dysregulation of Immune Response in Patients With Coronavirus 2019 (COVID-19) in Wuhan, China.,” *Clinical Infectious Diseases*, 71(15), pp. 762–768. doi:10.1093/cid/ciaa248.

Rajasuriar, R. *et al.* (2010) “Biological determinants of immune reconstitution in HIV-infected patients receiving antiretroviral therapy: the role of interleukin 7 and interleukin 7 receptor α and microbial translocation.,” *The Journal of Infectious Diseases*, 202(8), pp. 1254–1264. doi:10.1086/656369.

Rambaut, A. *et al.* (2004) “The causes and consequences of HIV evolution.,” *Nature Reviews. Genetics*, 5(1), pp. 52–61. doi:10.1038/nrg1246.

Rappaport, J. and Volsky, D.J. (2015) “Role of the macrophage in HIV-associated neurocognitive disorders and other comorbidities in patients on effective antiretroviral treatment.,” *Journal of Neurovirology*, 21(3), pp. 235–241. doi:10.1007/s13365-015-0346-y.

Rato, S. *et al.* (2017) “Single-cell analysis identifies cellular markers of the HIV permissive cell.,” *PLoS Pathogens*, 13(10), p. e1006678. doi:10.1371/journal.ppat.1006678.

RECOVERY Collaborative Group *et al.* (2021) “Dexamethasone in Hospitalized Patients with Covid-19.,” *The New England Journal of Medicine*, 384(8), pp. 693–704. doi:10.1056/NEJMoa2021436.

Reichart, D. *et al.* (2022) “Pathogenic variants damage cell composition and single cell transcription in cardiomyopathies.,” *Science*, 377(6606), p. eabo1984. doi:10.1126/science.abo1984.

Ren, X. *et al.* (2021) “COVID-19 immune features revealed by a large-scale single-cell transcriptome atlas.,” *Cell*, 184(7), pp. 1895-1913.e19. doi:10.1016/j.cell.2021.01.053.

Reyes, M. *et al.* (2019) “Simultaneous profiling of gene expression and chromatin accessibility in single cells.,” *Advanced Biosystems*, 3(11). doi:10.1002/adbi.201900065.

Reyes, M. *et al.* (2020) “An immune-cell signature of bacterial sepsis.,” *Nature Medicine*, 26(3), pp. 333–340. doi:10.1038/s41591-020-0752-4.

Roberts, J.D., Bebenek, K. and Kunkel, T.A. (1988) “The accuracy of reverse transcriptase from HIV-1.,” *Science*, 242(4882), pp. 1171–1173. doi:10.1126/science.2460925.

Roden, D.M. *et al.* (2011) “Pharmacogenomics: the genetics of variable drug responses.,” *Circulation*, 123(15), pp. 1661–1670. doi:10.1161/CIRCULATIONAHA.109.914820.

Rodrigues, L. *et al.* (2022) “Drug Repurposing for COVID-19: A Review and a Novel Strategy to Identify New Targets and Potential Drug Candidates.,” *Molecules*, 27(9). doi:10.3390/molecules27092723.

Rogacev, K.S. *et al.* (2012) “CD14++CD16+ monocytes independently predict cardiovascular events: a cohort study of 951 patients referred for elective coronary angiography.,” *Journal of the American College of Cardiology*, 60(16), pp. 1512–1520. doi:10.1016/j.jacc.2012.07.019.

Ryom, L. *et al.* (2022) “Major revision version 11.0 of the European AIDS Clinical Society Guidelines 2021.,” *HIV Medicine*, 23(8), pp. 849–858. doi:10.1111/hiv.13268.

Saag, M.S. *et al.* (2020) “Antiretroviral Drugs for Treatment and Prevention of HIV Infection in Adults: 2020 Recommendations of the International Antiviral Society-USA Panel.,” *The Journal of the American Medical Association*, 324(16), pp. 1651–1669. doi:10.1001/jama.2020.17025.

Salama, C. *et al.* (2021) “Tocilizumab in Patients Hospitalized with Covid-19 Pneumonia.,” *The New England Journal of Medicine*, 384(1), pp. 20–30. doi:10.1056/NEJMoa2030340.

Sánchez-Cerrillo, I. *et al.* (2020) “COVID-19 severity associates with pulmonary redistribution of CD1c+ DCs and inflammatory transitional and nonclassical monocytes.,” *The Journal of Clinical Investigation*, 130(12), pp. 6290–6300. doi:10.1172/JCI140335.

Sandler, N.G. *et al.* (2011) “Plasma levels of soluble CD14 independently predict mortality in HIV infection.,” *The Journal of Infectious Diseases*, 203(6), pp. 780–790. doi:10.1093/infdis/jiq118.

Sawyer, R.T., Strausbauch, P.H. and Volkman, A. (1982) “Resident macrophage proliferation in mice depleted of blood monocytes by strontium-89.,” *Laboratory Investigation*, 46(2), pp. 165–170.

Scannell, J.W. *et al.* (2012) “Diagnosing the decline in pharmaceutical R&D efficiency.,” *Nature Reviews. Drug Discovery*, 11(3), pp. 191–200. doi:10.1038/nrd3681.

Schena, M. *et al.* (1995) “Quantitative monitoring of gene expression patterns with a complementary DNA microarray.,” *Science*, 270(5235), pp. 467–470. doi:10.1126/science.270.5235.467.

Schulte-Schrepping, J. *et al.* (2020) “Severe COVID-19 Is Marked by a Dysregulated Myeloid Cell Compartment.,” *Cell*, 182(6), pp. 1419-1440.e23. doi:10.1016/j.cell.2020.08.001.

Schultze, J.L. and Aschenbrenner, A.C. (2021) “COVID-19 and the human innate immune system.,” *Cell*, 184(7), pp. 1671–1692. doi:10.1016/j.cell.2021.02.029.

Schulz, C. *et al.* (2012) “A lineage of myeloid cells independent of Myb and hematopoietic stem cells.,” *Science*, 336(6077), pp. 86–90. doi:10.1126/science.1219179.

Schütt, C., Schilling, T. and Krüger, C. (1991) “sCD14 prevents endotoxin inducible oxidative burst response of human monocytes.,” *Allergie und Immunologie*, 37(3–4), pp. 159–164.

Seitz, R. (2016) “Human immunodeficiency virus (HIV).,” *Transfusion medicine and hemotherapy : offizielles Organ der Deutschen Gesellschaft fur Transfusionsmedizin und Immunhamatologie*, 43(3), pp. 203–222. doi:10.1159/000445852.

Shikuma, C.M. *et al.* (2014) “Plasma monocyte chemoattractant protein-1 and tumor necrosis factor-α levels predict the presence of coronary artery calcium in HIV-infected individuals independent of traditional cardiovascular risk factors.,” *AIDS Research and Human Retroviruses*, 30(2), pp. 142–146. doi:10.1089/AID.2013.0183.

Shin, E. *et al.* (2015) “Drug Signature-based Finding of Additional Clinical Use of LC28-0126 for Neutrophilic Bronchial Asthma.,” *Scientific Reports*, 5, p. 17784. doi:10.1038/srep17784.

Shi, C. and Pamer, E.G. (2011) “Monocyte recruitment during infection and inflammation.,” *Nature Reviews. Immunology*, 11(11), pp. 762–774. doi:10.1038/nri3070.

Sikkema, L. *et al.* (2023) “An integrated cell atlas of the lung in health and disease.,” *Nature Medicine*, 29(6), pp. 1563–1577. doi:10.1038/s41591-023-02327-2.

Silvin, A. *et al.* (2020) “Elevated Calprotectin and Abnormal Myeloid Cell Subsets Discriminate Severe from Mild COVID-19.,” *Cell*, 182(6), pp. 1401-1418.e18. doi:10.1016/j.cell.2020.08.002.

Singhal, S. *et al.* (1999) “Antitumor activity of thalidomide in refractory multiple myeloma.,” *The New England Journal of Medicine*, 341(21), pp. 1565–1571. doi:10.1056/NEJM199911183412102.

Sinha, S. *et al.* (2022) “Dexamethasone modulates immature neutrophils and interferon programming in severe COVID-19.,” *Nature Medicine*, 28(1), pp. 201–211. doi:10.1038/s41591-021-01576-3.

Smit, J. *et al.* (2023) “Social and Economic Consequences of COVID-19,” *Publication for the special committee on COVID-19 pandemic: lessons learned and recommendations for the future (COVI)* [Preprint].

Snelgrove, R.J. *et al.* (2008) “A critical function for CD200 in lung immune homeostasis and the severity of influenza infection.,” *Nature Immunology*, 9(9), pp. 1074–1083. doi:10.1038/ni.1637.

Soroosh, P. *et al.* (2013) “Lung-resident tissue macrophages generate Foxp3+ regulatory T cells and promote airway tolerance.,” *The Journal of Experimental Medicine*, 210(4), pp. 775–788. doi:10.1084/jem.20121849.

Spinetti, T. *et al.* (2020) “Reduced Monocytic Human Leukocyte Antigen-DR Expression Indicates Immunosuppression in Critically Ill COVID-19 Patients.,” *Anesthesia and Analgesia*, 131(4), pp. 993–999. doi:10.1213/ANE.0000000000005044.

Steinmüller, C. *et al.* (2000) “Local activation of nonspecific defense against a respiratory model infection by application of interferon-gamma: comparison between rat alveolar and interstitial lung macrophages.,” *American Journal of Respiratory Cell and Molecular Biology*, 22(4), pp. 481–490. doi:10.1165/ajrcmb.22.4.3336.

Stelter, F. *et al.* (1996) “The myeloid differentiation antigen CD14 is N- and O-glycosylated. Contribution of N-linked glycosylation to different soluble CD14 isoforms.,” *European Journal of Biochemistry / FEBS*, 236(2), pp. 457–464. doi:10.1111/j.1432-1033.1996.00457.x.

Stephenson, E. *et al.* (2021) “Single-cell multi-omics analysis of the immune response in COVID-19,” *Nature Medicine* [Preprint]. doi:10.1038/s41591-021-01329-2.

Stoeckius, M. *et al.* (2017) “Simultaneous epitope and transcriptome measurement in single cells.,” *Nature Methods*, 14(9), pp. 865–868. doi:10.1038/nmeth.4380.

Strategies for Management of Antiretroviral Therapy (SMART) Study Group *et al.* (2006) “CD4+ count-guided interruption of antiretroviral treatment.,” *The New England Journal of Medicine*, 355(22), pp. 2283–2296. doi:10.1056/NEJMoa062360.

Subramanian, A. *et al.* (2017) “A next generation connectivity map: L1000 platform and the first 1,000,000 profiles.,” *Cell*, 171(6), pp. 1437-1452.e17. doi:10.1016/j.cell.2017.10.049.

Suligoi, B. *et al.* (2010) “The epidemic of HIV infection and AIDS, promotion of testing, and innovative strategies.,” *Annali dell'Istituto superiore di sanita*, 46(1), pp. 15–23. doi:10.4415/ANN_10_01_03.

Sungnak, W. *et al.* (2020) “SARS-CoV-2 entry factors are highly expressed in nasal epithelial cells together with innate immune genes.,” *Nature Medicine*, 26(5), pp. 681–687. doi:10.1038/s41591-020-0868-6.

Sun, D. *et al.* (2022) “Why 90% of clinical drug development fails and how to improve it?,” *Acta pharmaceutica Sinica. B*, 12(7), pp. 3049–3062. doi:10.1016/j.apsb.2022.02.002.

Sun, W. *et al.* (2023) “Phenotypic signatures of immune selection in HIV-1 reservoir cells.,” *Nature*, 614(7947), pp. 309–317. doi:10.1038/s41586-022-05538-8.

Su, Y. *et al.* (2020) “Multi-Omics Resolves a Sharp Disease-State Shift between Mild and Moderate COVID-19.,” *Cell*, 183(6), pp. 1479-1495.e20. doi:10.1016/j.cell.2020.10.037.

Su, Y. *et al.* (2022) “Multiple early factors anticipate post-acute COVID-19 sequelae.,” *Cell*, 185(5), pp. 881-895.e20. doi:10.1016/j.cell.2022.01.014.

Svensson, V., Vento-Tormo, R. and Teichmann, S.A. (2018) “Exponential scaling of single-cell RNA-seq in the past decade.,” *Nature Protocols*, 13(4), pp. 599–604. doi:10.1038/nprot.2017.149.

Sweeney, G.D. (1983) “Variability in the human drug response.,” *Thrombosis research. Supplement*, 4, pp. 3–15. doi:10.1016/0049-3848(83)90353-5.

Tang, F. *et al.* (2009) “mRNA-Seq whole-transcriptome analysis of a single cell.,” *Nature Methods*, 6(5), pp. 377–382. doi:10.1038/nmeth.1315.

Tarling, J.D., Lin, H.S. and Hsu, S. (1987) “Self-renewal of pulmonary alveolar macrophages: evidence from radiation chimera studies.,” *Journal of Leukocyte Biology*, 42(5), pp. 443–446. doi:10.1002/jlb.42.5.443.

TEMPRANO ANRS 12136 Study Group *et al.* (2015) “A trial of early antiretrovirals and isoniazid preventive therapy in africa.,” *The New England Journal of Medicine*, 373(9), pp. 808–822. doi:10.1056/NEJMoa1507198.

Terekhova, M. *et al.* (2023) “Single-cell atlas of healthy human blood unveils age-related loss of NKG2C+GZMB-CD8+ memory T cells and accumulation of type 2 memory T cells.,” *Immunity*, 56(12), pp. 2836-2854.e9. doi:10.1016/j.immuni.2023.10.013.

Thieblemont, N. *et al.* (1995) “CD14lowCD16high: a cytokine-producing monocyte subset which expands during human immunodeficiency virus infection.,” *European Journal of Immunology*, 25(12), pp. 3418–3424. doi:10.1002/eji.1830251232.

Tomazini, B.M. *et al.* (2020) “Effect of Dexamethasone on Days Alive and Ventilator-Free in Patients With Moderate or Severe Acute Respiratory Distress Syndrome and COVID-19: The CoDEX Randomized Clinical Trial.,” *The Journal of the American Medical Association*, 324(13), pp. 1307–1316. doi:10.1001/jama.2020.17021.

Trapnell, B.C. and Whitsett, J.A. (2002) “Gm-CSF regulates pulmonary surfactant homeostasis and alveolar macrophage-mediated innate host defense.,” *Annual Review of Physiology*, 64, pp. 775–802. doi:10.1146/annurev.physiol.64.090601.113847.

Tregoning, J.S. *et al.* (2021) “Progress of the COVID-19 vaccine effort: viruses, vaccines and variants versus efficacy, effectiveness and escape.,” *Nature Reviews. Immunology*, 21(10), pp. 626–636. doi:10.1038/s41577-021-00592-1.

UNAIDS (2023) *2023 UNAIDS Global AIDS Update Report*. Available at: https://thepath.unaids.org/ (Accessed: April 23, 2024).

Vadaq, N. *et al.* (2023) “High-throughput proteomic analysis reveals systemic dysregulation in virally suppressed people living with HIV.,” *Journal of Clinical Investigation Insight*, 8(11). doi:10.1172/jci.insight.166166.

Vandenberg, O. *et al.* (2020) “Considerations for diagnostic COVID-19 tests.,” *Nature Reviews Microbiology*, 19(3), pp. 171–183. doi:10.1038/s41579-020-00461-z.

Villani, A.-C. *et al.* (2017) “Single-cell RNA-seq reveals new types of human blood dendritic cells, monocytes, and progenitors.,” *Science*, 356(6335). doi:10.1126/science.aah4573.

Vos, W.A.J.W. *et al.* (2022) “The 2000HIV study: Design, multi-omics methods and participant characteristics.,” *Frontiers in Immunology*, 13, p. 982746. doi:10.3389/fimmu.2022.982746.

Vos, W.A.J.W., Vadaq, N., *et al.* (2024) “Cardiometabolic Differences in People Living with HIV Receiving Integrase Strand Transfer Inhibitors Compared to Non-nucleoside Reverse Transcriptase Inhibitors: Implications for Current ART Strategies.,” *Viruses*, 16(4). doi:10.3390/v16040582.

Vos, W.A.J.W., Navas, A., *et al.* (2024) “HIV immunological non-responders are characterized by extensive immunosenescence and impaired lymphocyte cytokine production capacity.,” *Frontiers in Immunology*, 15, p. 1350065. doi:10.3389/fimmu.2024.1350065.

Wagner, A. *et al.* (2015) “Drugs that reverse disease transcriptomic signatures are more effective in a mouse model of dyslipidemia.,” *Molecular Systems Biology*, 11(3), p. 791. doi:10.15252/msb.20145486.

Walker, B.D. *et al.* (1987) “HIV-specific cytotoxic T lymphocytes in seropositive individuals.,” *Nature*, 328(6128), pp. 345–348. doi:10.1038/328345a0.

Wang, Bolin *et al.* (2020) “Does comorbidity increase the risk of patients with COVID-19: evidence from meta-analysis.,” *Aging*, 12(7), pp. 6049–6057. doi:10.18632/aging.103000.

Wang, Dawei *et al.* (2020) “Clinical Characteristics of 138 Hospitalized Patients With 2019 Novel Coronavirus-Infected Pneumonia in Wuhan, China.,” *The Journal of the American Medical Association*, 323(11), pp. 1061–1069. doi:10.1001/jama.2020.1585.

Wang, Feng *et al.* (2020) “Systemically comparing host immunity between survived and deceased COVID-19 patients.,” *Cellular & Molecular Immunology*, 17(8), pp. 875–877. doi:10.1038/s41423-020-0483-y.

Wang, Yetao *et al.* (2020) “HIV-1-induced cytokines deplete homeostatic innate lymphoid cells and expand TCF7-dependent memory NK cells.,” *Nature Immunology*, 21(3), pp. 274–286. doi:10.1038/s41590-020-0593-9.

Wang, Yiliang *et al.* (2020) “A comprehensive investigation of the mRNA and protein level of ACE2, the putative receptor of SARS-CoV-2, in human tissues and blood cells.,” *International Journal of Medical Sciences*, 17(11), pp. 1522–1531. doi:10.7150/ijms.46695.

Watanabe, S. *et al.* (2019) “The role of macrophages in the resolution of inflammation.,” *The Journal of Clinical Investigation*, 129(7), pp. 2619–2628. doi:10.1172/JCI124615.

Watson, O.J. *et al.* (2022) “Global impact of the first year of COVID-19 vaccination: a mathematical modelling study.,” *The Lancet Infectious Diseases*, 22(9), pp. 1293–1302. doi:10.1016/S1473-3099(22)00320-6.

Wauters, E. *et al.* (2021) “Discriminating mild from critical COVID-19 by innate and adaptive immune single-cell profiling of bronchoalveolar lavages.,” *Cell Research*, 0, pp. 1–19. doi:10.1038/s41422-020-00455-9.

Wei, G. *et al.* (2006) “Gene expression-based chemical genomics identifies rapamycin as a modulator of MCL1 and glucocorticoid resistance.,” *Cancer Cell*, 10(4), pp. 331–342. doi:10.1016/j.ccr.2006.09.006.

Wei, Y. *et al.* (2023) “Single-cell epigenetic, transcriptional, and protein profiling of latent and active HIV-1 reservoir revealed that IKZF3 promotes HIV-1 persistence.,” *Immunity*, 56(11), pp. 2584-2601.e7. doi:10.1016/j.immuni.2023.10.002.

Wendisch, D. *et al.* (2021) “SARS-CoV-2 infection triggers profibrotic macrophage responses and lung fibrosis.,” *Cell*, 184(26), pp. 6243-6261.e27. doi:10.1016/j.cell.2021.11.033.

Westhorpe, C.L.V. *et al.* (2014) “Associations between surface markers on blood monocytes and carotid atherosclerosis in HIV-positive individuals.,” *Immunology and Cell Biology*, 92(2), pp. 133–138. doi:10.1038/icb.2013.84.

Wetterstrand (2024) *DNA Sequencing Costs:Data from the NHGRI Genome Sequencing Program (GSP)*. Available at: http://www.genome.gov/sequencingcostsdata (Accessed: May 17, 2024).

WHO (2020) *Pneumonia of unknown cause – China*. Available at: https://www.who.int/emergencies/disease-outbreak-news/item/2020-DON229 (Accessed: April 25, 2024).

WHO (2024) *WHO Coronavirus (COVID-19)dashboard > Cases [Dashboard]*. Available at: https://data.who.int/dashboards/covid19/cases (Accessed: April 25, 2024).

WHO Rapid Evidence Appraisal for COVID-19 Therapies (REACT) Working Group *et al.* (2020) “Association Between Administration of Systemic Corticosteroids and Mortality Among Critically Ill Patients With COVID-19: A Meta-analysis.,” *The Journal of the American Medical Association*, 324(13), pp. 1330–1341. doi:10.1001/jama.2020.17023.

Wilk, A.J. *et al.* (2020) “A single-cell atlas of the peripheral immune response in patients with severe COVID-19.,” *Nature Medicine*, 26(7), pp. 1070–1076. doi:10.1038/s41591-020-0944-y.

Wilk, A.J. *et al.* (2021) “Multi-omic profiling reveals widespread dysregulation of innate immunity and hematopoiesis in COVID-19.,” *The Journal of Experimental Medicine*, 218(8). doi:10.1084/jem.20210582.

Woodall, M.N.J. *et al.* (2024) “Age-specific nasal epithelial responses to SARS-CoV-2 infection.,” *Nature Microbiology*, 9(5), pp. 1293–1311. doi:10.1038/s41564-024-01658-1.

Wright, S.D. *et al.* (1990) “CD14, a receptor for complexes of lipopolysaccharide (LPS) and LPS binding protein.,” *Science*, 249(4975), pp. 1431–1433. doi:10.1126/science.1698311.

Wu, F. *et al.* (2020) “A new coronavirus associated with human respiratory disease in China.,” *Nature*, 579(7798), pp. 265–269. doi:10.1038/s41586-020-2008-3.

Wu, V.H. *et al.* (2023) “Profound phenotypic and epigenetic heterogeneity of the HIV-1-infected CD4+ T cell reservoir.,” *Nature Immunology*, 24(2), pp. 359–370. doi:10.1038/s41590-022-01371-3.

Yao, H. *et al.* (2020) “Molecular Architecture of the SARS-CoV-2 Virus.,” *Cell*, 183(3), pp. 730-738.e13. doi:10.1016/j.cell.2020.09.018.

Yim, W.W.-Y. and Mizushima, N. (2020) “Lysosome biology in autophagy.,” *Cell discovery*, 6(1), p. 6. doi:10.1038/s41421-020-0141-7.

Yoshida, M. *et al.* (2022) “Local and systemic responses to SARS-CoV-2 infection in children and adults.,” *Nature*, 602(7896), pp. 321–327. doi:10.1038/s41586-021-04345-x.

Zappia, L. and Theis, F.J. (2021) “Over 1000 tools reveal trends in the single-cell RNA-seq analysis landscape.,” *Genome Biology*, 22(1), p. 301. doi:10.1186/s13059-021-02519-4.

Zhang, Y.-Z. and Holmes, E.C. (2020) “A Genomic Perspective on the Origin and Emergence of SARS-CoV-2.,” *Cell*, 181(2), pp. 223–227. doi:10.1016/j.cell.2020.03.035.

Zhou, F. *et al.* (2020) “Clinical course and risk factors for mortality of adult inpatients with COVID-19 in Wuhan, China: a retrospective cohort study.,” *The Lancet*, 395(10229), pp. 1054–1062. doi:10.1016/S0140-6736(20)30566-3.

Zhou, Y. *et al.* (2020) “Pathogenic T-cells and inflammatory monocytes incite inflammatory storms in severe COVID-19 patients.,” *National science review*, 7(6), pp. 998–1002. doi:10.1093/nsr/nwaa041.

Zhu, T. *et al.* (2002) “Evidence for human immunodeficiency virus type 1 replication in vivo in CD14(+) monocytes and its potential role as a source of virus in patients on highly active antiretroviral therapy.,” *Journal of Virology*, 76(2), pp. 707–716. doi:10.1128/jvi.76.2.707-716.2002.

Zicari, S. *et al.* (2019) “Immune Activation, Inflammation, and Non-AIDS Co-Morbidities in HIV-Infected Patients under Long-Term ART.,” *Viruses*, 11(3). doi:10.3390/v11030200.

Ziegler-Heitbrock, L. (2014) “Monocyte subsets in man and other species.,” *Cellular Immunology*, 289(1–2), pp. 135–139. doi:10.1016/j.cellimm.2014.03.019.

Ziegler, C.G.K. *et al.* (2020) “SARS-CoV-2 Receptor ACE2 Is an Interferon-Stimulated Gene in Human Airway Epithelial Cells and Is Detected in Specific Cell Subsets across Tissues.,” *Cell*, 181(5), pp. 1016-1035.e19. doi:10.1016/j.cell.2020.04.035.

Ziegler, C.G.K. *et al.* (2021) “Impaired local intrinsic immunity to SARS-CoV-2 infection in severe COVID-19.,” *Cell*, 184(18), pp. 4713-4733.e22. doi:10.1016/j.cell.2021.07.023.

Zou, X. *et al.* (2020) “Single-cell RNA-seq data analysis on the receptor ACE2 expression reveals the potential risk of different human organs vulnerable to 2019-nCoV infection.,” *Frontiers of medicine*, 14(2), pp. 185–192. doi:10.1007/s11684-020-0754-0.

# 6. Appendix A-D

Appendix A:

**Monocytes and Macrophages in COVID-19**

**Knoll R**, Schultze JL, Schulte-Schrepping J, "**Monocytes and Macrophages in COVID-19**", Front Immunol. 2021 Jul 21;12:720109. doi: 10.3389/fimmu.2021.720109.

Appendix B:

**Disease severity-specific neutrophil signatures in blood transcriptomes stratify COVID-19 patients**

Aschenbrenner AC*, Mouktaroudi M*, Krämer B*, Oestreich M*, Antonakos N*, Nuesch-Germano M*, Gkizeli K*, Bonaguro L*, Reusch N*, Baßler K*, Saridaki M*, **Knoll R***, Pecht T*, Kapellos TS*, Doulou S*, Kröger C*, Herbert M*, Holsten L*, Horne A*, Gemünd ID*, Rovina N*, Agrawal S*, Dahm* K, van Uelft M*, Drews A*, Lenkeit L*, Bruse N*, Gerretsen J, Gierlich J, Becker M, Händler K, Kraut M, Theis H, Mengiste S, De Domenico E, Schulte-Schrepping J, Seep L, Raabe J, Hoffmeister C, ToVinh M, Keitel V, Rieke G, Talevi V, Skowasch D, Aziz NA, Pickkers P, van de Veerdonk FL, Netea MG[#], Schultze JL[#], Kox M[#], Breteler MMB[#], Nattermann J[#], Koutsoukou A[#], Giamarellos-Bourboulis EJ[#], Ulas T[#,§], German COVID-19 Omics Initiative (DeCOI)., "**Disease severity-specific neutrophil signatures in blood transcriptomes stratify COVID-19 patients.**", Genome Med. 2021 Jan 13;13(1):7. doi: 10.1186/s13073-020-00823-5.
*shared first authorship / [#]shared last authorship / [§]corresponding author

Appendix C:

**Identification of drug candidates targeting monocyte reprogramming in people living with HIV**

**Knoll R,** Bonaguro L, Dos Santos JC, Warnat-Herresthal S, Jacobs-Cleophas MCP, Blümel E, Reusch N, Herbert M, Otten T, van der Heijden WA, van de Wijer L, Shalek AK, Händler K, Becker M, Beyer MD, Netea MG, Joosten LAB, van der Ven AJAM, Schultze JL[#], Aschenbrenner AC[#,§], "**Identification of drug candidates targeting monocyte reprogramming in people living with HIV**", Front Immunol. 2023 Nov 20;14:1275136. doi: 10.3389/fimmu.2023.1275136.
*shared first authorship / [#]shared last authorship / [§]corresponding author

Appendix D:

**The life-saving benefit of dexamethasone in severe COVID-19 is linked to a reversal of monocyte dysregulation**

**Knoll R***, Helbig ET*, Dahm K, Bolaji O, Hamm F, Dietrich O, van Uelft M, Müller S, Bonaguro L, Schulte-Schrepping J, Petrov L, Krämer B, Kraut M, Stubbemann P, Thibeault C, Brumhard S, Theis H, Hack G, De Domenico E, Nattermann J, Becker M, Beyer MD, Hillus D, Georg P, Loers C, Tiedemann J, Tober-Lau P, Lippert L, Pascual-Leone BM, Tacke F, Rohde G, Suttorp N, Witzenrath M, CAPNETZ Study Group, Pa-COVID-19 Study Group, Saliba AE, Ulas T, Polansky JK, Sawitzki B, Sander LE[#], Schultze JL[#], Aschenbrenner AC[#,§], Kurth F[#], "**The life-saving benefit of dexamethasone in severe COVID-19 is linked to a reversal of monocyte dysregulation**", Cell. 2024 Jul, doi: https://doi.org/10.1016/j.cell.2024.06.014.
*shared first authorship / [#]shared last authorship / [§]corresponding author

frontiers in Immunology

REVIEW
published: 21 July 2021
doi: 10.3389/fimmu.2021.720109

# Monocytes and Macrophages in COVID-19

*Rainer Knoll*[1,2], *Joachim L. Schultze*[1,2,3] *and Jonas Schulte-Schrepping*[1,2*]

[1] Systems Medicine, Deutsches Zentrum für Neurodegenerative Erkrankungen (DZNE), Bonn, Germany, [2] Genomics & Immunoregulation, Life & Medical Sciences (LIMES) Institute, University of Bonn, Bonn, Germany, [3] PRECISE Platform for Single Cell Genomics and Epigenomics, Deutsches Zentrum für Neurodegenerative Erkrankungen (DZNE) and the University of Bonn, Bonn, Germany

COVID-19 is a contagious viral disease caused by SARS-CoV-2 that led to an ongoing pandemic with massive global health and socioeconomic consequences. The disease is characterized primarily, but not exclusively, by respiratory clinical manifestations ranging from mild common cold symptoms, including cough and fever, to severe respiratory distress and multi-organ failure. Macrophages, a heterogeneous group of yolk-sac derived, tissue-resident mononuclear phagocytes of complex ontogeny present in all mammalian organs, play critical roles in developmental, homeostatic and host defense processes with tissue-dependent plasticity. In case of infection, they are responsible for early pathogen recognition, initiation and resolution of inflammation, as well as repair of tissue damage. Monocytes, bone-marrow derived blood-resident phagocytes, are recruited under pathological conditions such as viral infections to the affected tissue to defend the organism against invading pathogens and to aid in efficient resolution of inflammation. Given their pivotal function in host defense and the potential danger posed by their dysregulated hyperinflammation, understanding monocyte and macrophage phenotypes in COVID-19 is key for tackling the disease's pathological mechanisms. Here, we outline current knowledge on monocytes and macrophages in homeostasis and viral infections and summarize concepts and key findings on their role in COVID-19. While monocytes in the blood of patients with moderate COVID-19 present with an inflammatory, interferon-stimulated gene (ISG)-driven phenotype, cellular dysfunction epitomized by loss of HLA-DR expression and induction of S100 alarmin expression is their dominant feature in severe disease. Pulmonary macrophages in COVID-19 derived from infiltrating inflammatory monocytes are in a hyperactivated state resulting in a detrimental loop of pro-inflammatory cytokine release and recruitment of cytotoxic effector cells thereby exacerbating tissue damage at the site of infection.

**Keywords: monocytes, macrophage, COVID-19, SARS-CoV-2, hyperinflammation, scRNA-seq, alveolar macrophage, viral infection**

OPEN ACCESS

***Edited by:***
*Thierry Roger, Centre Hospitalier Universitaire Vaudois (CHUV), Switzerland*

***Reviewed by:***
*Brandt D. Pence, University of Memphis, United States*
*Anna Smed-Sorensen, Karolinska Institutet (KI), Sweden*

****Correspondence:***
*Jonas Schulte-Schrepping*
*jschrepping@uni-bonn.de*

***Specialty section:***
*This article was submitted to Molecular Innate Immunity, a section of the journal Frontiers in Immunology*

***Received:*** *03 June 2021*
***Accepted:*** *07 July 2021*
***Published:*** *21 July 2021*

***Citation:***
*Knoll R, Schultze JL and Schulte-Schrepping J (2021) Monocytes and Macrophages in COVID-19. Front. Immunol. 12:720109. doi: 10.3389/fimmu.2021.720109*

## INTRODUCTION

COVID-19 (1, 2) is primarily a mild to moderate respiratory tract infection caused by severe acute respiratory syndrome coronavirus 2 (SARS-CoV-2), an enveloped, single-stranded RNA betacoronavirus (3–5). While 80% of the infections lead to asymptomatic or mild disease with common cold symptoms including dry cough, headache, loss of taste, dyspnea, fatigue and fever, contained by an efficient immune response (6–8), 15% of the patients go on to develop severe disease requiring intensive care and oxygen support and 5% develop critical disease with life-threatening pneumonia, acute respiratory distress syndrome (ARDS) and septic shock often culminating in multi-organ dysfunction and death (9).

Age, various comorbidities, including diabetes, obesity, lung and cardiovascular diseases, as well as genetic polymorphisms correlate with a higher risk of respiratory failure (10–13).

SARS-CoV-2, similar to SARS-CoV (14), enters host cells *via* the angiotensin-converting enzyme 2 (ACE2) receptor and uses the human protease TMPRSS2 as entry activator (15, 16). These genes are expressed in a wide range of cells, including nasal and bronchial epithelial cells, enterocytes, cardiomyocytes, vascular and testicular cells, placental trophoblasts, bile duct cells (17, 18) as well as macrophages (19, 20). Furthermore, additional entry molecules, such as Neuropilin (NRP1), have been discussed to facilitate viral cell entry (21, 22).

Although acute respiratory manifestations are the most common feature, COVID-19 can have multiple acute extra-pulmonary clinical effects likely to be related to vascular pathology (23), and also long-lasting complications referred to as the post-COVID syndrome or long COVID, including fatigue or neurological sequelae (24–27).

Control of viral infections and resolution of inflammation generally depends on dose and route of infection, viral virulence properties as well as host immune factors (28, 29). Tightly regulated interactions between epithelial cells and immune cells, orchestrated by cytokine signaling and direct cellular contacts, play a critical role, also in COVID-19 (30, 31). Moreover, viral clearance does not necessarily mean recovery to a healthy state. Hyperactivated and dysregulated immune cells pose a substantial danger for exacerbated tissue damage (32–34) and alter susceptibility to secondary bacterial superinfection (35, 36).

Severe COVID-19 has been associated with pronounced changes in peripheral immune activity (37, 38), including increased levels of acute phase reactants and pro-inflammatory cytokines (39, 40), neutrophilia and emergence of immature and low-density neutrophils (41, 42), increased neutrophil-to-lymphocyte ratio and lymphopenia (43) as well as myeloid inflammation (44) and reduced expression of the human leukocyte antigen DR isotype (HLA-DR) by circulating monocytes (42, 45).

A time-dependent, multi-stage disease model for COVID-19 has been proposed (28). Early and efficient activation of the immune system through induction of a potent interferon response is crucial for controlling the virus. However, a delayed and/or prolonged interferon response may lead to progressive tissue damage, which may ultimately result in a deleterious hyperinflammation characterized by excessive activation of mononuclear phagocytes (MNPs) and coagulation in combination with dysregulation of tissue repair mechanisms and fibrosis (46).

Together with dendritic cells (DC), macrophages and monocytes form the MNP system (47). In addition to being professional antigen-presenting cells (APC), MNPs sense and phagocytose pathogens, mediate leukocyte recruitment, initiate and shape immune responses and regulate inflammation.

Macrophages are a heterogeneous family of tissue-resident, phagocytic innate immune cells, including brain microglia, liver Kupffer cells and lung alveolar and interstitial macrophages, that play an important role in tissue homeostasis and immune defense (48). In case of infection, macrophages sense danger signals from microbial pathogens or tissue damage *via* a plethora of pattern recognition receptors (PRRs), and respond by release of inflammatory molecules that eliminate pathogens, initiate inflammation and recruitment of additional effector cells and promote tissue repair (32). However, as is the case for example in macrophage activation syndrome (MAS), an overwhelming macrophage response can be detrimental to the host (33).

Monocytes are blood-circulating, phagocytic innate immune cells classically divided into three subsets based on their respective expression of CD14 and CD16 [classical ($CD14^+CD16^-$), non-classical ($CD14dimCD16^+$), and intermediate ($CD14^+CD16^+$)] (48, 49). Under pathological conditions, including viral infections, monocytes, activated and recruited by inflammatory mediators, infiltrate affected tissues and acquire inflammatory macrophage and DC-like phenotypes to fulfil their effector functions of pro- and anti-inflammatory activities, antigen-presentation and tissue remodeling (50).

Here, we outline major findings concerning the role of monocytes and macrophages in COVID-19 and put them into the context of general knowledge of these cells in viral infections.

## ALVEOLAR AND INTERSTITIAL MACROPHAGE ONTOGENY AND FUNCTION

Every day, the lung inhales thousands of liters of air containing high amounts of pathogens including viruses, bacteria, and fungi (51). To prevent infection and its resulting complications for the organism, a tight control by the immune system is needed. In the lung, macrophages are the most abundant immune cell type under homeostatic conditions. Based on their exact location, they can be separated in at least two different populations; the interstitial macrophages (IMs) and alveolar macrophages (AMs) (52, 53).

**Abbreviations:** AMs, alveolar macrophages; APC, antigen-presenting cells; COPD, chronic obstructive pulmonary disease; COVID-19, Coronavirus disease 2019; DC, dendritic cells; IL, intereukin; IFN, interferon; IPF, idiopathic pulmonary fibrosis; ISG, interferon-stimulated genes; MNPs, mononuclear phagocytes; Mo-AMs, monocyte-derived AMs; Mo-DC, monocyte-derived DC; ORF, open reading frames; SARS-CoV-2, severe acute respiratory syndrome coronavirus 2; scRNA-seq, single-cell RNA-sequencing; snRNA-seq, single-nucleus RNA-sequencing.

IMs reside in the parenchyma between the microvascular endothelium and alveolar epithelium, while AMs have close contact to epithelial cells of alveoli and reside in the airspace lumen. However, a recent study by Neupane et al. showed that AMs are, in contrast to macrophages in other tissues, not sessile but can crawl in and between alveoli using the pores of Kohn (54). By expression of integrins, $CD11c^{neg}CD11b^{pos}$ IMs can be distinguished from $CD11c^{pos}CD11b^{neg}$ AMs (52).

In addition to mucus and the epithelial barrier, AMs are the first defenders against pathogens entering the respiratory system. They originate from the yolk sac and populate the lung early after birth (55, 56). AMs have proliferative capacity, thus can persist over the lifespan by self-renewal and are independent of replacement from the bone marrow (57–59). AMs detected in bronchoalveolar lavage fluid (BALF) after lung transplantation were almost exclusively donor derived (60). Following depletion of lung macrophages in mice, repopulation occurred almost entirely by *in situ* proliferation (61). In contrast, analysis of pulmonary MNPs in patients receiving bone marrow transplantation for hematologic disorders provided evidence for replenishment of AMs by monocytes of bone marrow origin (62). The current understanding of the plastic composition and complex ontogeny of pulmonary MNPs is best described by a dynamic interplay of cells derived from yolk sac macrophages, fetal liver, and adult monocytes given pathologic threats and vacant niches (63).

The functional phenotype of AMs strongly depends on the local microenvironment and can change with contact with epithelial cells, oxygen tension and surfactant-rich fluid, highlighting the relevance of AM plasticity (64, 65). Therefore, AMs can be pro-/anti-inflammatory, pro-/anti-fibrotic, pro-asthmatic, pro-resolving and/or tissue-reparative. In the physiological state, AMs are critical for homeostasis by removing apoptotic cells, foreign materials, and surfactant, thereby ensuring that the lungs remain free of debris. Of note, they typically show an immunosuppressive phenotype (52). The anti-inflammatory program is critical to prevent unwanted inflammation in the lung that can be of serious danger for the organism. Although AMs have antigen presenting capacities and express HLA-DR, they promote tolerance and suppress lymphocyte activation under homeostatic conditions by producing immunosuppressive prostaglandins and TGFβ, of which the latter together with retinoic acid may drive the development of $FOXP3^+$ regulatory T cells (Treg), further strengthening the anti-inflammation (66–68). By signaling through various receptors, such as by CD200R (69), SIRPα (70), mannose receptor CD206 (71), MACRO (72), TREM2 (73), and soluble mediators including Interleukin (IL)-10 (74), TGFβ (75) and PPARγ (76) AMs experience negative regulation. For instance, CD200 is expressed on the luminal side of respiratory epithelial cells and binding to CD200R on AMs leads to the suppression of pro-inflammatory genes in AMs (69).

Upon lung injury or infection, AMs can mount inflammatory responses (77). Destruction of airway epithelium can lead to a loss of exposure to regulatory ligands, such as CD200, resulting in a switch to a pro-inflammatory program in AMs (69). Recognition of pathogen associated molecular patterns (PAMP) of invading pathogens by AMs *via* PRRs further enhances this activation. These activated AMs are characterized by enhanced phagocytic capacity, higher oxidative burst and increased release of pro-inflammatory cytokines and chemokines, which results in inflammation and recruitment of other immune effector cells to the lung, including neutrophils (78). Recruited cells also include monocytes, which can differentiate into macrophage and DC-like cells, thus often referred to as monocyte-derived AMs (Mo-AMs) and DC (Mo-DC), upon arrival in peripheral tissues and can further enhance inflammation (79, 80). Their different ontogeny and functionality can influence the outcome of infection and inflammation.

Importantly, prolonged, and dysregulated inflammation caused by macrophages and monocytes can cause collateral tissue damage (81). To prevent prolonged inflammation and to limit tissue damage and fibrosis, AMs have evolved several strategies. These include phagocytosis of dying cells, e.g. neutrophils (82) preventing the release of their pro-inflammatory and toxic contents and triggering the secretion of TGFβ, IL-10, prostaglandin E2 and platelet-activating factor from AMs (83).

Respiratory pathologies such as asthma, chronic obstructive pulmonary disease (COPD), cystic fibrosis and idiopathic pulmonary fibrosis (IPF) are characterized by defective AM phagocytosis resulting in continuous inflammation (84–87).

Besides respiratory pathologies, cigarette smoking also presents a major risk factor for impaired AM function. AMs of smokers are expanded in numbers compared to non-smoking controls but show less phagocytic activity, glucose oxidation rate and cytokine production compared to non-smoking controls, which increases the risk of severe disease progression upon bacterial and viral infection (88–91).

After a successful inflammation, suppressive stimuli as described above are restored and AMs shift to an anti-inflammatory, tissue reparative phenotype restoring the homeostasis of the lung (65).

## THE ROLE OF LUNG MACROPHAGES IN VIRAL RESPIRATORY INFECTIONS

As described above, the lung is at permanent risk of infection by several pathogens, amongst them viruses such as rhinovirus, respiratory syncytial virus, influenza virus and coronavirus. Despite their obvious relevance, investigation of human lung MNPs during respiratory infections has been limited so far and most of our knowledge comes from animal models. For instance, Schneider et al. showed that AM-depleted WT mice infected with influenza A virus had impaired gas exchange and fatal hypoxia (92). Similar results were obtained in pigs which, after AM depletion by dichloromethlyene diphosphonate, were infected with seasonal human H1N1 influenza virus resulting in 40% mortality rate and increased suffering from severe respiratory signs, whereas infected control pigs showed less severe symptoms with no mortality (93).

Notably, various viruses, including Influenza, Chikungunya, human herpes and Zika virus, have been shown to utilize monocytes and macrophages as vessels for virus replication, dissemination, or long-term persistence within tissues. They enter the cells through endocytosis, phagocytosis, macropinocytosis or

membrane fusion and induce elevated expression of proinflammatory signaling and antiviral molecules (94–99). Direct infection of macrophages with SARS-CoV has also been shown, which, however, did not lead to dissemination or virus amplification but rather to an impaired type I interferon (IFN) response potentially worsening disease outcome (100).

Upon viral infection, AMs produce high levels of cellular mediators, including IL-1β, CCL3, CCL7 and CCL2, also known as monocyte chemotactic protein 1 (MCP1), which rapidly recruits CCR2-expressing bone marrow-derived monocytes into the lung. Furthermore, AMs are the main producers of type I IFN to trigger an antiviral response in influenza infection (101, 102). Of note, type I IFN production by AMs was higher than by plasmacytoid DCs (pDCs), coined as the natural "IFN producing cells", in response to virus, indicating that pDCs may play a subordinate role in the defense against viral infections in the lung (102). Moreover, alveolar epithelial cells also did not produce any type I IFN in response to influenza, further stressing the key role of AMs (103). Type I IFNs can signal autocrine and paracrine resulting in the activation of antiviral transcriptional programs including the transcription of ISG such as *ISG15*, *IFIT1* and *STAT2*, which can suppress viral replication (104, 105). Interestingly, not all virus infections trigger an increased type I IFN response. For instance, when human AMs were infected with coronavirus strain 229E (HCoV-299E), they secreted increased amounts of TNF, CCL5 and CCL4 (MIP-1β), causing inflammation, but IFN-β levels remained unchanged (106).

Viral infection triggers the migration of circulating monocytes to the lung guided by pro-inflammatory cytokines, such as CCL2 and CCL3, increasing the number of defending mononuclear phagocytes and enhancing inflammation (79). This is a necessary defense response, since viruses such as influenza can either reduce the numbers of resident AMs dramatically or impair their phenotype. When BALB/c mice were infected with influenza, 90% of resident AMs were lost in the first week after infection (107). This, however, was strain specific, since C57B1/6 mice did not show loss of AMs but rather an impaired phenotype. Nevertheless, both consequences were driven by IFN-γ and resulted in increased susceptibility to bacterial superinfections leading to significant body weight loss and mortality. Furthermore, a recent study by Neupane et al. showed that crawling of AMs, which is critical for AM function, was impaired after influenza infection. Again, this impairment was mediated by the IFN-γ pathway and resulted in increased risk for bacterial superinfections (54).

# THE ROLE OF MONOCYTES AND ALVEOLAR MACROPHAGES IN COVID-19

## The Involvement of Monocytes and Macrophages in SARS-CoV-2 Induced Hyperinflammation

COVID-19 is characterized by a systemic increase of numerous cytokines, including IL-1α, IL-1β, IL-6, IL-7, tumor necrosis factor (TNF), type I and II IFN, and the inflammatory chemokines CCL2, CCL3 and CXCL10 (40, 108, 109). Elevated levels of CCL2 and CCL7, two chemokines potent at the recruitment of $CCR2^+$ monocytes, have also been found in BALF from patients with severe COVID-19 (110).

The term "cytokine storm", historically described as an influenza-like syndrome that occurred after systemic infections and immunotherapies (111), has quickly become widely used, both in scientific publications and the media, to describe the cytokine response in COVID-19 (39). Although the increased systemic cytokine response in COVID-19 is undisputed, the term "cytokine storm" in COVID-19 pathophysiology is a topic of debate, as TNF, IL-6, and IL-8 concentrations in COVID-19 are less strong compared to sepsis, acute respiratory distress syndrome unrelated to COVID-19, trauma, cardiac arrest, and cytokine release syndrome (CRS) (112–115). Moreover, COVID-19 immune responses are highly dynamic as shown by time-dependent alterations of the systemic levels of many cytokines including IL-6 (40). Considering the co-occurrence of distinct systemic pro-inflammatory cytokine waves with the emergence of aberrant and immunosuppressive innate immune cells further complicates the exact terminology of immunopathology in severe COVID-19 and suggests a much more complex host-pathogen interaction better described by the term viral sepsis (28). In any case, the systemic cytokine profile observed in patients suffering from severe COVID-19 does resemble those observed in CRS, such as macrophage activation syndrome (MAS), which led early on to the working hypothesis that dysregulated activation of the MNP compartment contributes to COVID-19-associated hyperinflammation (33, 113).

The induction of cytokine production in MNPs in COVID-19 can either be triggered *via* recognition of damage-associated molecular patterns (DAMPS) released from epithelial cells affected by SARS-CoV-2 by PRRs or by direct recognition of viral pathogen-associated molecular patterns (PAMPs) *via* specific Toll-like receptors, i.e. TLR2 and TLR4, the retinoic acid-inducible gene I (RIG-I) or the melanoma differentiation associated gene (MDA)-5 (116–119). Furthermore, C-type lectin receptors, including DC-SIGN, L-SIGN, LSECtin, ASGR1, CLEC4K (Langerin) and CLEC10A (MGL), as well as Tweety family member 2 have been identified to interact with the SARS-CoV-2 spike protein inducing proinflammatory responses, but not allowing direct infection. Notably, however, these interactions were shown to promote virus transfer to $ACE^+$ cells (120, 121).

SARS-CoV-2 infection of lung-resident MNPs might result either from phagocytosis of infected alveolar epithelial cells followed by viral escape from the lysosome or by direct infection. *In vitro* experiments with human monocyte-derived DC and macrophages with SARS-CoV-2 have demonstrated that both cell types are permissive to SARS-CoV-2 as measured by quantification of SARS-CoV-2 nucleocapsid protein expression after *in vitro* infection, but did not support productive viral replication. Interestingly, expression of proinflammatory cytokines and chemokines however was only triggered in macrophages and not DC under these experimental

conditions (122). Additional independent infection experiments confirmed the abortive SARS-CoV-2 infection in human monocyte-derived DC and macrophages *in vitro* and corroborated the induction of antiviral and proinflammatory cytokines, including IFN-α/β, TNF, IL-1β, -6, and -10, as well as CXCL10, leading to type I IFN–mediated host cell death (123). Accordingly, investigation of cell tropism and immune activation profiles of SARS-CoV-2 in *ex vivo* organ cultures of human lung tissues revealed infection of type I and II pneumocytes as well as AMs (124), confirmed by detection of SARS-CoV-2 in AMs in autopsy samples from COVID-19 patients (125). Interestingly, analysis of murine AMs derived from human (h)ACE2 transgenic animals revealed different susceptibility to SARS-CoV-2 infection depending on their cytokine-induced polarization as *in vitro* treatment with IFN-γ and LPS caused increased infection rates compared to pre-treatment with IL-4 (126). Furthermore, *in vitro* treatment of PMA-differentiated THP-1 human macrophages and isolated $CD14^+$ monocytes with SARS-CoV-2 spike protein after LPS stimulation exposed a hyperresponsiveness to TLR signals by suppression of IRAK-M (127). Moreover, antibody-dependent mechanisms of infection present a conceivable alternative pathway and have been described for SARS-CoV (128, 129). Besides this body of evidence demonstrating the induction of inflammatory pathways in monocytes and macrophages upon recognition of SARS-CoV-2, metabolic alterations in these cells have been reported. *Ex vivo* infected human monocytes shifted their metabolism and became highly glycolytic leading to elevated glucose levels promoting SARS-CoV-2 replication and cytokine production (130). Moreover, monocytes derived from COVID-19 patients were shown to have increased lipid droplet accumulation, which was explained by the modulation of lipid synthesis and uptake investigated using *in vitro* infection models and again favored virus replication and inflammatory mediator production (131). Interestingly, the pharmacological inhibition of DGAT1, a key enzyme in lipid droplet formation, inhibited SARS-CoV-2 replication and production of pro-inflammatory mediators presenting a new opportunity for therapeutic intervention.

Corresponding to the systemic increase of cytokine and chemokine levels, quantitative and qualitative changes in immune cell populations, particularly in the myeloid compartment, have been observed in blood and lungs of patients with COVID-19 dependent on disease severity.

Flow cytometric analyses of peripheral blood reported reduced percentages of total monocytes in the blood of severe COVID-19 cases (38, 132, 133). Notably, this reduction was observed only transiently in a longitudinal study of immune cells in severe cases pointing to the highly time-sensitive immune response (134).

Beyond quantitative changes, striking disease-specific differences in monocyte phenotypes in the blood and monocyte–macrophage composition in the lung have been consistently reported. A significant expansion of $CD14^+CD16^+$ monocytes featuring high expression of IL-6 in the blood discriminated patients with COVID-19 admitted to ICUs from those who did not require intensive care (132). Moreover, significantly reduced numbers of non-classical and intermediate monocytes are found in acute patients with symptoms of severe SARS-CoV-2 infection (135) and circulating classical monocytes show clear signs of activation, including increased expression of CD169 (135). In addition, experimentally infected monocytes and those from patients with severe COVID-19 requiring intensive care feature inflammasome activation and increased pyroptosis associated with caspase-1 activation (136). Furthermore, increased proliferation of monocytes derived from patients with severe COVID-19 after *in vitro* challenge with lipopolysaccharide was discussed as an indicator for a release of immature myeloid cells from the bone marrow reminiscent of emergency myelopoiesis (137) and contributing to innate immune dysfunction (138). Most prominently and consistent across all studies, reduced HLA-DR expression on monocytes – a well-established marker of immune suppression – was reported in patients suffering from severe COVID-19 (41, 42, 134, 139, 140). Decreased HLA-DR expression appeared to be strongly associated with COVID-19 disease severity, exemplified by lower expression of HLA-DR by monocytes in patients admitted to the ICU versus non-ICU patients (140) and in non-survivors versus survivors (141). Furthermore, the presence of $HLA\text{-}DR^{lo}$ monocytes in severe cases of COVID-19 was found to be positively correlated with levels of the soluble immunosuppressive factors IL-10, TGF-β, VEGFA, and AREG (142). In addition, reduced HLA-DR and CD86 expression together with elevated levels of IL-1β, IL-6, IL-8, IL-10, IL-17 and IFN-γ were observed in children with multisystem inflammatory syndrome (MIS-C) associated with SARS-CoV-2 infection (143). Downregulation of HLA-DR is a molecular feature often described for monocytic myeloid-derived suppressor cells (MDSC) – a cellular state of monocytes described to develop during chronic inflammation, especially late-stage cancers, and defined by T cell immunosuppressive functions (144). Functional assessment of $HLA\text{-}DR^-$ monocytes derived from COVID-19 patients indeed confirmed their capacity to suppress T cell proliferation, partly *via* ARG-1, and thus supports the MDSC state beyond phenotypic description (145). Interestingly, the $HLA\text{-}DR^-$ monocytes specific for severe acute COVID-19 have furthermore been found to express CPT1, an enzyme essential for fatty acid oxidation, again highlighting the relevance of immunometabolic effects of SARS-CoV-2 infection (146).

## High-Resolution Single-Cell Omics Characterization of Monocytes and Macrophages in the Blood and Lungs of COVID-19 Patients

Application of high-resolution omics technologies with single-cell resolution, which were only developed and became widely applied within the last decade, has confirmed their great potential to rapidly decipher the immune response to an emerging pathogen during the COVID-19 pandemic. The first transcriptomic immune atlas of circulating peripheral blood mononuclear cells (PBMC) from 10 COVID-19 patients demonstrated globally decreased lymphocyte counts, while inflammatory myeloid cells were found to be more abundant (147). By now, at least 16 other studies have used scRNA-seq to characterize the immune response to SARS-CoV-2 (31, 41, 42, 45, 108, 148–158). While initial studies were based on low sample numbers limiting their

explanatory power, latest reports comprised samples derived from more than 100 individuals, included longitudinal samples or profiled matched samples from multiple tissues. Single-cell transcriptomic analysis of PBMC in 7 hospitalized COVID-19 patients revealed a depletion of $CD16^+$ monocytes in peripheral blood and the induction of an ISG signature in $CD14^+$ monocytes, but detected no substantial induction of pro-inflammatory cytokine genes, such as TNF, IL6, IL1β, CCL3, CCL4 or CXCL2 in these cells, suggesting that peripheral monocytes are no major contributors to the cytokine response in COVID-19 (155). The lack of expression of inflammatory cytokines in innate immune cells in the periphery of COVID-19 patients was confirmed by multiplex plasma cytokine analysis, mass cytometry, and scRNA-seq in a cohort of 76 COVID-19 patients and 69 healthy individuals from two cohorts. Despite significantly upregulated levels of inflammatory molecules in the plasma of COVID-19 patients and transiently induced expression of ISGs in peripheral immune cells, an impaired cytokine response in blood myeloid cells and pDCs, with markedly reduced expression of IL-6, TNF and IL-1β upon TLR stimulation, was observed emphasizing a tissue origin of the plasma cytokines (108). Interestingly, the lack of ISG-expressing cells associated with mild disease was linked to severe disease-specific production of antibodies suppressing cellular interferon responses (159). In a dual-center, two-cohort study, we combined scRNA-seq and single-cell proteomics of whole-blood and PBMC and determined changes in the immune cell composition and activation in mild versus severe COVID-19 over time. While non-classical monocyte numbers were diminished in COVID-19, $HLA\text{-}DR^{hi}CD11c^{hi}$ inflammatory monocytes with an ISG signature were elevated in mild COVID-19 and monocytes in severe COVID-19 featured strongly reduced HLA-DR expression, high expression levels of genes with anti-inflammatory and immature properties, including SELL (CD62L), CD163, MPO and PLAC8, as well as increased expression of S100A family members, e.g. S100A12 (42). Loss of non-classical monocytes, reduced HLA-DR expression in monocytes and massive release of S100A family members was observed in severe cases of COVID-19 in multiple additional studies (41, 151, 156, 157), albeit disease stratification into mild, moderate, severe and critical disease showed slight differences. In addition, calprotectin (S100A8/S100A9) plasma levels and decreased frequencies of non-classical monocytes were found to discriminate patients who develop a severe form of COVID-19 (41).

Although the analysis of blood was extremely instructive particularly when assessing systemic effects of COVID-19, the lung presents the primary site of infection for SARS-CoV-2 and investigating the local immune system response is key to understanding the pathology. Activated monocytes of the blood have been shown to infiltrate the lungs in patients with COVID-19 and in animal models of SARS-CoV-2 infection (160, 161). In their seminal study, Liao et al. characterized BALF from patients with varying severity of COVID-19 and healthy individuals using scRNA-seq and reported striking shifts in cellular composition with increased proportions of macrophages and neutrophils and lower proportions of DCs and T cells in samples from severe/critical COVID-19 compared to those from moderate disease and healthy individuals. Within the MNP compartment, they observed a depletion of tissue-resident AMs and a replacement by inflammatory monocyte-derived macrophages in patients with severe disease. Notably, cytokine and chemokine expression levels differed dependent on disease severity. While CXCL9, CXCL10 and CXCL11 expression levels were increased both in moderate and severe disease compared to healthy levels, IL1β, IL6, TNF as well as CCL2, CCL3, CCL4 and CCL7 were expressed at higher levels in lung macrophages from patients with severe COVID-19. CXCL16, which interacts with the chemokine receptor CXCR6 and attracts subsets of T cells, was specifically induced in patients with moderate disease. These distinct expression profiles suggest that lung macrophages in patients with severe COVID-19 may promote tissue infiltration of inflammatory monocytes enhancing local inflammation, whereas macrophages in patients with moderate COVID-19 preferentially attract T cells. Furthermore, macrophage subpopulations specific for severe disease presented with immunoregulatory features but also expression of the profibrotic genes TREM2, TGFB2, and SPP1 (45). In agreement with this study, scRNA-seq data of nasopharyngeal and bronchial samples from 19 COVID-19 patients revealed the presence of inflammatory non-tissue resident and monocyte-derived macrophages expressing various cytokines, including IL1, TNF, CCL2 and CCL3, as well as enhanced interactions between epithelial and immune cells as determined by ligand–receptor expression profiling, in critical compared to moderate disease (31). Interestingly, comparing macrophages from the lower to the upper airways demonstrated increased expression of inflammatory cytokines and chemokines in the bronchia. Furthermore, monocyte-to-macrophage trajectory analysis in scRNA-seq of BALF samples from COVID-19 patients exposed enrichment of chronic hyperinflammatory monocytes in critical COVID-19 presenting with elevated expression levels of inflammasome-related genes (NLRP3, IL1-β, IL10RA) and genes associated with fibrosis (FGL2, TGFB1, COTL1) potentially contributing to tissue damage in severe COVID-19 (154). Single-nucleus (sn)RNA-seq on lung autopsies from 19 COVID-19 decedents confirmed the lungs to be highly inflamed with dense infiltration of aberrantly activated monocyte-derived macrophages and alveolar macrophages in the tissue (153). Another cross-sectional scRNA-seq of 780,000 PBMC sampled from 130 patients collected across three medical centers in the UK revealed the presence of a non-classical monocyte population characterized by the expression of complement transcripts C1QA/B/C in COVID-19. The complement system is a key host-defense mechanism with capacity to exacerbate tissue injury through its proinflammatory effects. Notably, integration of these PBMC transcriptomes with data derived from BALF samples (45) followed by partition-based graph abstraction (PAGA) analysis demonstrated transcriptional similarity between the circulating $C1QA/B/C^+CD16^+$ monocytes and alveolar macrophages in COVID-19 emphasizing the altered composition of the lung MNP compartment (150). The consistent

reports of aberrant CD163$^{hi}$ and HLA-DR$^{lo}$ monocyte populations expressing the chemokine receptor CCR2 in the blood and hyperactivated airway monocytes and macrophages producing pro-inflammatory chemokines, including CCL2 and CCL3, were furthermore confirmed by high-dimensional phenotypic, transcriptomic, and functional profiling of immune cells from paired airway and blood samples obtained longitudinally from patients with severe COVID-19 (149).

Taken together, these data strongly suggest a model of a vicious cycle of pro-inflammatory cytokine release by hyperactivated lung MNPs resulting in erratic infiltration of pro-inflammatory effector cells, including dysregulated monocytes and cytotoxic T cells, which in turn exacerbates tissue damage and fuels macrophage activation (**Figure 1**).

## Detection of SARS-CoV-2 RNA in Single-Cell RNA Profiles of Monocytes and Macrophages

Since SARS-CoV-2 exploits the host cell transcriptional machinery to express viral genes, viral transcripts can be detected alongside human mRNA transcripts in scRNA-seq data, thereby allowing for identification of infected cells and their unique properties at single-cell resolution. Bost et al. developed a new computational pipeline, called Viral-Track, to quantify viral RNA in single-cell transcriptomic data. Application of their approach to scRNA-seq data of BALF from the aforementioned study by Liao et al. revealed the presence of viral reads in samples derived from patients with severe, but not mild disease, suggestive of a differential viral load in the lung (162). The highest levels of viral RNA were observed in ciliated and epithelial progenitor cells. However, viral RNA was also detected in a subset of macrophages characterized by expression of SPP1. Whether these transcripts resulted from direct infection of and viral replication within the myeloid cells or whether the cells phagocytosed cellular material carrying viral RNA could not be clarified by this approach. However, the results of the single-cell specific viral RNA quantification allowed for differential gene expression in infected *vs* bystander SPP1$^{+}$ macrophages, which revealed increased expression of chemokines (CCL7, CCL8, and CCL18) and APOE in virus-positive cells. The approach was further advanced by Wauters et al. who stratified SARS-CoV-2 infected cells in scRNA-seq data from BALF samples derived from patients with mild and critical COVID-19 by the presence of viral transcripts from distinct viral open reading frames (ORF). Detection of spike protein (S) specific transcripts in epithelial cells and consequentially reduced expression of ISGs suggests that S$^{+}$ epithelial cells have actively been infected. In contrast, transcripts

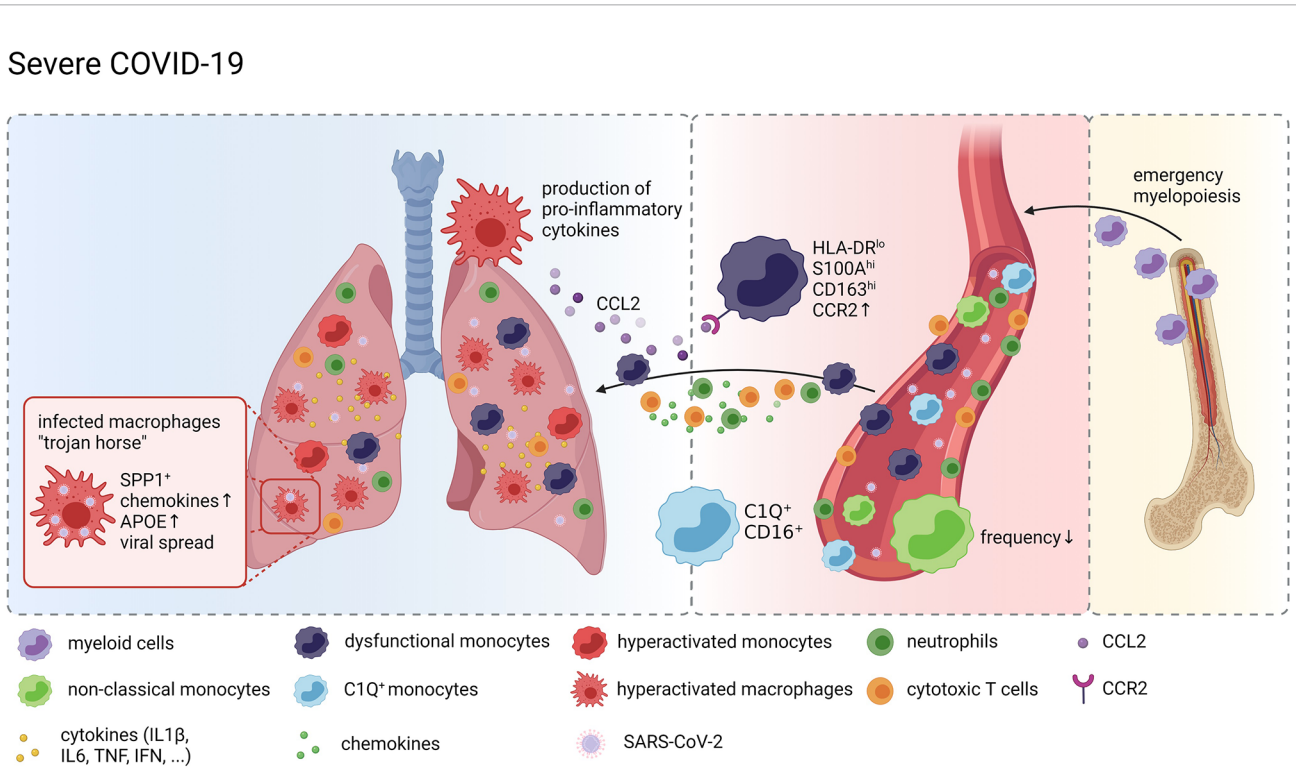


**FIGURE 1** | Monocytes and Macrophages in COVID-19. Graphical overview of the compositional and molecular alterations in monocyte and alveolar macrophage populations in COVID-19 created with BioRender.com. Distinct monocyte and macrophage phenotypes were identified in the peripheral blood of patients with severe COVID-19 including immature cells indicating emergency myelopoiesis, dysfunctional HLA-DR$^{lo}$ classical monocytes and complement gene expressing non-classical monocytes. These cells are attracted to the lung by pro-inflammatory chemokines resulting in a continuous accumulation of hyperactivated MNPs producing more pro-inflammatory mediators recruiting more inflammatory cells, including cytotoxic T cells and neutrophils, thus further exacerbating inflammation and tissue damage. SARS-CoV-2 infected macrophages in the lung may act as trojan horses propagating SARS-CoV-2 infection and spreading hyperinflammation across the lung.

of the nucleocapsid protein (N) and the ORF10 and ORF1a were detected in myeloid and lymphoid cells at much higher levels than in epithelial cells. Comparing $N^+$ *vs* $N^-$ alveolar and monocyte-derived macrophages determined genes involved in MHC class-II expression and ISG to be upregulated in response to the virus. Grant et al. followed an alternative approach to answer whether SARS-CoV-2 productively infects myeloid cells. Adding the negative-strand SARS-CoV-2 transcripts, which are transiently formed during viral replication, to the reference genome during alignment and quantification of their single-cell and bulk BALF transcriptome data allowed for evaluation of replicating SARS-CoV-2 in AMs. Besides the expected detection of positive and negative strand transcripts in epithelial cells, viral reads were also detected in subsets of macrophages suggesting that AMs harbor SARS-CoV-2 and allow viral replication *in vivo* (158), challenging the results on abortive infection gained from *in vitro* experiments. Interestingly, immunostaining of post-mortem tissue from patients who had died from COVID-19 revealed the presence of SARS-CoV-2 nucleoprotein in and the expression of ACE2 on populations of $CD169^+$ macrophages in lymph nodes and the spleen (20). Given the increasing body of evidence in support of active infection of and the indication of productive viral replication in AMs by SARS-CoV-2, Grant et al. have come up with the hypothesis that AMs may act as a Trojan horse, transferring the virus to adjacent lung regions, thereby slowly propagating SARS-CoV-2 infection and spreading hyperinflammation across the lung (**Figure 1**).

## OUTLOOK AND OPEN QUESTIONS

After more than a year into the pandemic, it is rather clear that the innate immune system and in particular monocytes and macrophages are linked to the heterogeneity of the COVID-19 disease courses. For example, HLA-$DR^{hi}$ monocytes are typically seen in mild cases, while HLA-$DR^{lo}$ $S100^+$ cells dominate in severe COVID-19. Future work needs to untangle which molecular mechanisms are responsible for these different cellular responses. For example, are certain signals from the microenvironment normally increasing the induction of HLA-DR molecules missing in patients with severe disease course? Are elevated levels of inhibitory factors such as certain prostaglandins or TGFβ responsible for the molecular phenotype of MNPs in severe COVID-19. Furthermore, is there a direct link between fibrotic lung disease as a result of severe COVID-19 with ARDS and changes in the MNP compartment or other immune cells like NK cells. And if this is the case, are the anti-fibrotic molecular programs of monocytes and macrophages not working or do these cells suddenly gain pro-fibrotic functionality. Are molecular changes seen in these cells early during the disease predictive for disease courses leading to irreversible tissue damage as it is proposed for some patients with Long COVID-19? Even if the pandemic will be under control due to world-wide vaccination programs and other medical measures, the sequelae of Long COVID-19 and its potential burden on long-term health requires further studies into the role of the immune system, in particular the innate immune system with monocytes, macrophages and granulocytes requiring special attention.

## AUTHOR CONTRIBUTIONS

All authors listed have made a substantial, direct, and intellectual contribution to the work, and approved it for publication.

## FUNDING

The work of JS was supported by the German Research Foundation (DFG) under Germany's Excellence Strategy (EXC2151–390873048), the EU project SYSCID (grant number 733100), the BMBF-funded grant iTREAT (01ZX1902B), ERA CVD (grant number 00160389), and the BMBF-funded excellence project Diet–Body–Brain (DietBB) (grant number 01EA1809A).

## REFERENCES

1. Berlin DA, Gulick RM, Martinez FJ. Severe Covid-19. *N Engl J Med* (2020) 383:2451–60. doi: 10.1056/NEJMcp2009575
2. Gandhi RT, Lynch JB, del Rio C. Mild or Moderate Covid-19. *N Engl J Med* (2020) 383:1757–66. doi: 10.1056/NEJMcp2009249
3. Kim D, Lee JY, Yang JS, Kim JW, Kim VN, Chang H. The Architecture of SARS-CoV-2 Transcriptome. *Cell* (2020) 181:914–21.e10. doi: 10.1016/j.cell.2020.04.011
4. Wu F, Zhao S, Yu B, Chen YM, Wang W, Song ZG, et al. A New Coronavirus Associated With Human Respiratory Disease in China. *Nature* (2020) 579:265–9. doi: 10.1038/s41586-020-2008-3
5. Zhang YZ. Holmes EC. A Genomic Perspective on the Origin and Emergence of SARS-CoV-2. *Cell* (2020) 181:223–7. doi: 10.1016/j.cell.2020.03.035
6. Huang C, Wang Y, Li X, Ren L, Zhao J, Hu Y, et al. Clinical Features of Patients Infected With 2019 Novel Coronavirus in Wuhan, China. *Lancet* (2020) 395:497–506. doi: 10.1016/S0140-6736(20)30183-5
7. Thevarajan I, Nguyen THO, Koutsakos M, Druce J, Caly L, van de Sandt CE, et al. Breadth of Concomitant Immune Responses Prior to Patient Recovery: A Case Report of Non-Severe COVID-19. *Nat Med* (2020) 26:453–5. doi: 10.1038/s41591-020-0819-2
8. Guan W, Ni Z, Hu Y, Liang W, Ou C, He J, et al. Clinical Characteristics of Coronavirus Disease 2019 in China. *N Engl J Med* (2020) 382:1708–20. doi: 10.1056/nejmoa2002032
9. Fu L, Wang B, Yuan T, Chen X, Ao Y, Fitzpatrick T, et al. Clinical Characteristics of Coronavirus Disease 2019 (COVID-19) in China: A Systematic Review and Meta-Analysis. *J Infect* (2020) 80:656–65. doi: 10.1016/j.jinf.2020.03.041
10. Zhang Q, Liu Z, Moncada-Velez M, Chen J, Ogishi M, Bigio B, et al. Inborn Errors of Type I IFN Immunity in Patients With Life-Threatening COVID-19. *Science* (2020) 370:eabd4570. doi: 10.1126/science.abd4570
11. Beck DB, Aksentijevich I. Susceptibility to Severe COVID-19. *Science* (2020) 370:404–5. doi: 10.1126/science.abe7591
12. Pairo-Castineira E, Clohisey S, Klaric L, Bretherick AD, Rawlik K, Pasko D, et al. Genetic Mechanisms of Critical Illness in COVID-19. *Nature* (2021) 591:92–8. doi: 10.1038/s41586-020-03065-y
13. Osuchowski MF, Winkler MS, Skirecki T, Cajander S, Shankar-Hari M, Lachmann G, et al. The COVID-19 Puzzle: Deciphering Pathophysiology

and Phenotypes of a New Disease Entity. *Lancet Respir Med* (2021) 9 (6):622–42. doi: 10.1016/s2213-2600(21)00218-6
14. Drosten C, Günther S, Preiser W, van der Werf S, Brodt H-R, Becker S, et al. Identification of a Novel Coronavirus in Patients With Severe Acute Respiratory Syndrome. *N Engl J Med* (2003) 348:1967–76. doi: 10.1056/nejmoa030747
15. Shang J, Wan Y, Luo C, Ye G, Geng Q, Auerbach A, et al. Cell Entry Mechanisms of SARS-CoV-2. *Proc Natl Acad Sci USA* (2020) 117:11727–34. doi: 10.1073/pnas.2003138117
16. Hoffmann M, Kleine-Weber H, Schroeder S, Krüger N, Herrler T, Erichsen S, et al. SARS-CoV-2 Cell Entry Depends on ACE2 and TMPRSS2 and Is Blocked by a Clinically Proven Protease Inhibitor. *Cell* (2020) 181:271–80.e8. doi: 10.1016/j.cell.2020.02.052
17. Hikmet F, Méar L, Edvinsson Å, Micke P, Uhlén M, Lindskog C. The Protein Expression Profile of ACE2 in Human Tissues. *Mol Syst Biol* (2020) 16: e9610. doi: 10.15252/msb.20209610
18. Sungnak W, Huang N, Bécavin C, Berg M, Queen R, Litvinukova M, et al. SARS-CoV-2 Entry Factors are Highly Expressed in Nasal Epithelial Cells Together With Innate Immune Genes. *Nat Med* (2020) 26:681–7. doi: 10.1038/s41591-020-0868-6
19. Song X, Hu W, Yu H, Zhao L, Zhao Y, Zhao X, et al. Little to No Expression of Angiotensin-Converting Enzyme-2 on Most Human Peripheral Blood Immune Cells But Highly Expressed on Tissue Macrophages. *Cytom Part A* (2020) 2020:1–10. doi: 10.1002/cyto.a.24285
20. Xiang Q, Feng Z, Diao B, Tu C, Qiao Q, Yang H, et al. SARS-CoV-2 Induces Lymphocytopenia by Promoting Inflammation and Decimates Secondary Lymphoid Organs. *Front Immunol* (2021) 12:661052. doi: 10.3389/fimmu.2021.661052
21. Daly JL, Simonetti B, Klein K, Chen KE, Williamson MK, Antón-Plágaro C, et al. Neuropilin-1 Is a Host Factor for SARS-CoV-2 Infection. *Science* (2020) 370:861–5. doi: 10.1126/science.abd3072
22. Cantuti-Castelvetri L, Ojha R, Pedro LD, Djannatian M, Franz J, Kuivanen S, et al. Neuropilin-1 Facilitates SARS-CoV-2 Cell Entry and Infectivity. *Science* (2020) 370:856–60. doi: 10.1126/science.abd2985
23. Gupta A, Madhavan MV, Sehgal K, Nair N, Mahajan S, Sehrawat TS, et al. Extrapulmonary Manifestations of COVID-19. *Nat Med* (2020) 26:1017–32. doi: 10.1038/s41591-020-0968-3
24. Fraser E. Long Term Respiratory Complications of Covid-19. *BMJ* (2020) 370:m3001. doi: 10.1136/bmj.m3001
25. Helms J, Kremer S, Merdji H, Clere-Jehl R, Schenck M, Kummerlen C, et al. Neurologic Features in Severe SARS-CoV-2 Infection. *N Engl J Med* (2020) 382:2268–70. doi: 10.1056/NEJMc2008597
26. Carfì A, Bernabei R, Landi F. Persistent Symptoms in Patients After Acute COVID-19. *JAMA - J Am Med Assoc* (2020) 324:603–5. doi: 10.1001/jama.2020.12603
27. Nalbandian A, Sehgal K, Gupta A, Madhavan MV, McGroder C, Stevens JS, et al. Post-Acute COVID-19 Syndrome. *Nat Med* (2021) 27:601–15. doi: 10.1038/s41591-021-01283-z
28. Schultze JL, Aschenbrenner AC. COVID-19 and the Human Innate Immune System. *Cell* (2021) 184:1671–92. doi: 10.1016/j.cell.2021.02.029
29. Rouse BT, Sehrawat S. Immunity and Immunopathology to Viruses: What Decides the Outcome? *Nat Rev Immunol* (2010) 10:514–26. doi: 10.1038/nri2802
30. Branchett WJ, Lloyd CM. Regulatory Cytokine Function in the Respiratory Tract. *Mucosal Immunol* (2019) 12:589–600. doi: 10.1038/s41385-019-0158-0
31. Chua RL, Lukassen S, Trump S, Hennig BP, Wendisch D, Pott F, et al. COVID-19 Severity Correlates With Airway Epithelium–Immune Cell Interactions Identified by Single-Cell Analysis. *Nat Biotechnol* (2020) 38:970–9. doi: 10.1038/s41587-020-0602-4
32. Merad M, Martin JC. Pathological Inflammation in Patients With COVID-19: A Key Role for Monocytes and Macrophages. *Nat Rev Immunol* (2020) 20:355–62. doi: 10.1038/s41577-020-0331-4
33. Schulert GS, Grom AA. Pathogenesis of Macrophage Activation Syndrome and Potential for Cytokine-Directed Therapies. *Annu Rev Med* (2015) 66:145–59. doi: 10.1146/annurev-med-061813-012806
34. Karki R, Sharma BR, Tuladhar S, Williams EP, Zalduondo L, Samir P, et al. Synergism of TNF-α and IFN-γ Triggers Inflammatory Cell Death, Tissue Damage, and Mortality in SARS-CoV-2 Infection and Cytokine Shock Syndromes. *Cell* (2021) 184:149–68.e17. doi: 10.1016/j.cell.2020.11.025
35. Goulding J, Godlee A, Vekaria S, Hilty M, Snelgrove R, Hussell T. Lowering the Threshold of Lung Innate Immune Cell Activation Alters Susceptibility to Secondary Bacterial Superinfection. *J Infect Dis* (2011) 204:1086–94. doi: 10.1093/infdis/jir467
36. Oliver BGG, Lim S, Wark P, Laza-Stanca V, King N, Black JL, et al. Rhinovirus Exposure Impairs Immune Responses to Bacterial Products in Human Alveolar Macrophages. *Thorax* (2008) 63:519–25. doi: 10.1136/thx.2007.081752
37. Chen G, Wu D, Guo W, Cao Y, Huang D, Wang H, et al. Clinical and Immunological Features of Severe and Moderate Coronavirus Disease 2019. *J Clin Invest* (2020) 130:2620–9. doi: 10.1172/JCI137244
38. Qin C, Zhou L, Hu Z, Zhang S, Yang S, Tao Y, et al. Dysregulation of Immune Response in Patients With Coronavirus 2019 (COVID-19) in Wuhan, China. *Clin Infect Dis* (2020) 71:762–8. doi: 10.1093/cid/ciaa248
39. Mehta P, McAuley DF, Brown M, Sanchez E, Tattersall RS, Manson JJ. COVID-19: Consider Cytokine Storm Syndromes and Immunosuppression. *Lancet* (2020) 395:1033–4. doi: 10.1016/S0140-6736(20)30628-0
40. Lucas C, Wong P, Klein J, Castro TBR, Silva J, Sundaram M, et al. Longitudinal Analyses Reveal Immunological Misfiring in Severe COVID-19. *Nature* (2020) 584:463–9. doi: 10.1038/s41586-020-2588-y
41. Silvin A, Chapuis N, Dunsmore G, Goubet AG, Dubuisson A, Derosa L, et al. Elevated Calprotectin and Abnormal Myeloid Cell Subsets Discriminate Severe From Mild COVID-19. *Cell* (2020) 182:1401–18.e18. doi: 10.1016/j.cell.2020.08.002
42. Schulte-Schrepping J, Reusch N, Paclik D, Baßler K, Schlickeiser S, Zhang B, et al. Severe COVID-19 Is Marked by a Dysregulated Myeloid Cell Compartment. *Cell* (2020) 182:1419–40.e23. doi: 10.1016/j.cell.2020.08.001
43. Cao X. COVID-19: Immunopathology and its Implications for Therapy. *Nat Rev Immunol* (2020) 20:269–70. doi: 10.1038/s41577-020-0308-3
44. Aschenbrenner AC, Mouktaroudi M, Krämer B, Oestreich M, Antonakos N, Nuesch-Germano M, et al. Disease Severity-Specific Neutrophil Signatures in Blood Transcriptomes Stratify COVID-19 Patients. *Genome Med* (2021) 13:7. doi: 10.1186/s13073-020-00823-5
45. Liao M, Liu Y, Yuan J, Wen Y, Xu G, Zhao J, et al. Single-Cell Landscape of Bronchoalveolar Immune Cells in Patients With COVID-19. *Nat Med* (2020) 26:842–4. doi: 10.1038/s41591-020-0901-9
46. Siddiqi HK, Mehra MR. COVID-19 Illness in Native and Immunosuppressed States: A Clinical–Therapeutic Staging Proposal. *J Hear Lung Transplant* (2020) 39:405–7. doi: 10.1016/j.healun.2020.03.012
47. van Furth R, Cohn ZA. The Origin and Kinetics of Mononuclear Phagocytes. *J Exp Med* (1968) 128:415–35. doi: 10.1084/JEM.128.3.415
48. Bassler K, Schulte-Schrepping J, Warnat-Herresthal S, Aschenbrenner AC, Schultze JL. The Myeloid Cell Compartment-Cell by Cell. *Annu Rev Immunol* (2019) 37:269–93. doi: 10.1146/annurev-immunol-042718-041728
49. Kapellos TS, Bonaguro L, Gemünd I, Reusch N, Saglam A, Hinkley ER, et al. Human Monocyte Subsets and Phenotypes in Major Chronic Inflammatory Diseases. *Front Immunol* (2019) 10:2035. doi: 10.3389/fimmu.2019.02035
50. Guilliams M, Mildner A, Yona S. Developmental and Functional Heterogeneity of Monocytes. *Immunity* (2018) 49:595–613. doi: 10.1016/j.immuni.2018.10.005
51. Prussin AJ, Garcia EB, Marr LC. Total Concentrations of Virus and Bacteria in Indoor and Outdoor Air. *Environ Sci Technol Lett* (2015) 2:84–8. doi: 10.1021/acs.estlett.5b00050
52. Hussell T, Bell TJ. Alveolar Macrophages: Plasticity in a Tissue-Specific Context. *Nat Rev Immunol* (2014) 14:81–93. doi: 10.1038/nri3600
53. Franke-Ullmann G, Pförtner C, Walter P, Steinmüller C, Lohmann-Matthes ML, Kobzik L. Characterization of Murine Lung Interstitial Macrophages in Comparison With Alveolar Macrophages *In Vitro*. *J Immunol* (1996) 157:3097–104.
54. Neupane AS, Willson M, Chojnacki AK, Vargas E Silva Castanheira F, Morehouse C, Carestia A, et al. Patrolling Alveolar Macrophages Conceal Bacteria From the Immune System to Maintain Homeostasis. *Cell* (2020) 183:110–25.e11. doi: 10.1016/j.cell.2020.08.020
55. Schulz C, Perdiguero EG, Chorro L, Szabo-Rogers H, Cagnard N, Kierdorf K, et al. A Lineage of Myeloid Cells Independent of Myb and Hematopoietic Stem Cells. *Science* (2012) 335:86–90. doi: 10.1126/science.1219179
56. Guilliams M, De Kleer I, Henri S, Post S, Vanhoutte L, De Prijck S, et al. Alveolar Macrophages Develop From Fetal Monocytes That Differentiate

Into Long-Lived Cells in the First Week of Life. *via GM-CSF. J Exp Med* (2013) 210:1977–92. doi: 10.1084/jem.20131199
57. Tarling JD, Lin HS, Hsu S. Self-Renewal of Pulmonary Alveolar Macrophages: Evidence From Radiation Chimera Studies. *J Leukoc Biol* (1987) 42:443–6. doi: 10.1002/jlb.42.5.443
58. Sawyer RT, Strausbauch PH, Volkman A. Resident Macrophage Proliferation in Mice Depleted of Blood Monocytes by Strontium-89. *Lab Investig* (1982) 46:165–70.
59. Golde DW, Byers LA, Finley TN. Proliferative Capacity of Human Alveolar Macrophage. *Nature* (1974) 247:373–5. doi: 10.1038/247373a0
60. Eguíluz-Gracia I, Schultz HHL, Sikkeland LIB, Danilova E, Holm AM, Pronk CJH, et al. Long-Term Persistence of Human Donor Alveolar Macrophages in Lung Transplant Recipients. *Thorax* (2016) 71:1006–11. doi: 10.1136/thoraxjnl-2016-208292
61. Hashimoto D, Chow A, Noizat C, Teo P, Beasley MB, Leboeuf M, et al. Tissue-Resident Macrophages Self-Maintain Locally Throughout Adult Life With Minimal Contribution From Circulating Monocytes. *Immunity* (2013) 38:792–804. doi: 10.1016/j.immuni.2013.04.004
62. Thomas ED, Ramberg RE, Sale GE, Sparkes RS, Golde DW. Direct Evidence for a Bone Marrow Origin of the Alveolar Macrophage in Man. *Science* (1976) 192:1016–8. doi: 10.1126/science.775638
63. Guilliams M, van de Laar L. A Hitchhiker's Guide to Myeloid Cell Subsets: Practical Implementation of a Novel Mononuclear Phagocyte Classification System. *Front Immunol* (2015) 6:406. doi: 10.3389/fimmu.2015.00406
64. Joshi N, Walter JM, Misharin AV. Alveolar Macrophages. *Cell Immunol* (2018) 330:86–90. doi: 10.1016/j.cellimm.2018.01.005
65. Watanabe S, Alexander M, Misharin AV, Budinger GRS. The Role of Macrophages in the Resolution of Inflammation. *J Clin Invest* (2019) 129:2619–28. doi: 10.1172/JCI124615
66. Coleman MM, Ruane D, Moran B, Dunne PJ, Keane J, Mills KHG. Alveolar Macrophages Contribute to Respiratory Tolerance by Inducing FoxP3 Expression in Naive T Cells. *Am J Respir Cell Mol Biol* (2013) 48:773–80. doi: 10.1165/rcmb.2012-0263OC
67. Soroosh P, Doherty TA, Duan W, Mehta AK, Choi H, Adams YF, et al. Lung-Resident Tissue Macrophages Generate Foxp3+ Regulatory T Cells and Promote Airway Tolerance. *J Exp Med* (2013) 210:775–88. doi: 10.1084/jem.20121849
68. Lipscomb MF, Lyons CR, Nunez G, Ball EJ, Stastny P, Vial W, et al. Human Alveolar Macrophages: HLA-DR-Positive Macrophages That are Poor Stimulators of a Primary Mixed Leukocyte Reaction. *J Immunol* (1986) 136(2):497–504.
69. Snelgrove RJ, Goulding J, Didierlaurent AM, Lyonga D, Vekaria S, Edwards L, et al. A Critical Function for CD200 in Lung Immune Homeostasis and the Severity of Influenza Infection. *Nat Immunol* (2008) 9:1074–83. doi: 10.1038/ni.1637
70. Janssen WJ, McPhillips KA, Dickinson MG, Linderman DJ, Morimoto K, Xiao YQ, et al. Surfactant Proteins A and D Suppress Alveolar Macrophage Phagocytosis *via* Interaction With Sirpα. *Am J Respir Crit Care Med* (2008) 178:158–67. doi: 10.1164/rccm.200711-1661OC
71. Zhang J, Tachado SD, Patel N, Zhu J, Imrich A, Manfruelli P, et al. Negative Regulatory Role of Mannose Receptors on Human Alveolar Macrophage Proinflammatory Cytokine Release *In Vitro*. *J Leukoc Biol* (2005) 78:665–74. doi: 10.1189/jlb.1204699
72. Ghosh S, Gregory D, Smith A, Kobzik L. MARCO Regulates Early Inflammatory Responses Against Influenza: A Useful Macrophage Function With Adverse Outcome. *Am J Respir Cell Mol Biol* (2011) 45:1036–44. doi: 10.1165/rcmb.2010-0349OC
73. Gao X, Dong Y, Liu Z, Niu B. Silencing of Triggering Receptor Expressed on Myeloid Cells-2 Enhances the Inflammatory Responses of Alveolar Macrophages to Lipopolysaccharide. *Mol Med Rep* (2013) 7:921–6. doi: 10.3892/mmr.2013.1268
74. Fernandez S, Jose P, Avdiushko MG, Kaplan AM, Cohen DA. Inhibition of IL-10 Receptor Function in Alveolar Macrophages by Toll-Like Receptor Agonists. *J Immunol* (2004) 172:2613–20. doi: 10.4049/jimmunol.172.4.2613
75. Morris DG, Huang X, Kaminski N, Wang Y, Shapiro SD, Dolganov G, et al. Loss of Integrin αvβ6-Mediated TGF-β Activation Causes Mmp 12-Dependent Emphysema. *Nature* (2003) 422:169–73. doi: 10.1038/nature01413
76. Gautier EL, Chow A, Spanbroek R, Marcelin G, Greter M, Jakubzick C, et al. Systemic Analysis of Pparγ in Mouse Macrophage Populations Reveals Marked Diversity in Expression With Critical Roles in Resolution of Inflammation and Airway Immunity. *J Immunol* (2012) 189:2614–24. doi: 10.4049/jimmunol.1200495
77. Lambrecht BN. Alveolar Macrophage in the Driver's Seat. *Immunity* (2006) 24:366–8. doi: 10.1016/j.immuni.2006.03.008
78. Steinmüller C, Franke-Ullmann G, Lohmann-Matthes ML, Emmendörffer A. Local Activation of Nonspecific Defense Against a Respiratory Model Infection by Application of Interferon-γ: Comparison Between Rat Alveolar and Interstitial Lung Macrophages. *Am J Respir Cell Mol Biol* (2000) 22:481–90. doi: 10.1165/ajrcmb.22.4.3336
79. Trapnell BC, Whitsett JA. GM-CSF Regulates Pulmonary Surfactant Homeostasis and Alveolar Macrophage-Mediated Innate Host Defense. *Annu Rev Physiol* (2002) 64:775–802. doi: 10.1146/annurev.physiol.64.090601.113847
80. Baharom F, Rankin G, Blomberg A, Smed-Sörensen A. Human Lung Mononuclear Phagocytes in Health and Disease. *Front Immunol* (2017) 8:499. doi: 10.3389/fimmu.2017.00499
81. Laskin DL, Sunil VR, Gardner CR, Laskin JD. Macrophages and Tissue Injury: Agents of Defense or Destruction? *Annu Rev Pharmacol Toxicol* (2011) 51:267–88. doi: 10.1146/annurev.pharmtox.010909.105812
82. Ortega-Gómez A, Perretti M, Soehnlein O. Resolution of Inflammation: An Integrated View. *EMBO Mol Med* (2013) 5:661–74. doi: 10.1002/emmm.201202382
83. Fadok VA, Bratton DL, Konowal A, Freed PW, Westcott JY, Henson PM. Macrophages That Have Ingested Apoptotic Cells *In Vitro* Inhibit Proinflammatory Cytokine Production Through Autocrine/Paracrine Mechanisms Involving TGF-β, PGE2, and PAF. *J Clin Invest* (1998) 101:890–8. doi: 10.1172/JCI1112
84. Fitzpatrick AM, Holguin F, Teague WG, Brown LAS. Alveolar Macrophage Phagocytosis is Impaired in Children With Poorly Controlled Asthma. *J Allergy Clin Immunol* (2008) 121(6):1372–8. doi: 10.1016/j.jaci.2008.03.008
85. Hodge S, Hodge G, Scicchitano R, Reynolds PN, Holmes M. Alveolar Macrophages From Subjects With Chronic Obstructive Pulmonary Disease are Deficient in Their Ability to Phagocytose Apoptotic Airway Epithelial Cells. *Immunol Cell Biol* (2003) 81:289–96. doi: 10.1046/j.1440-1711.2003.t01-1-01170.x
86. Vandivier RW, Richens TR, Horstmann SA, DeCathelineau AM, Ghosh M, Reynolds SD, et al. Dysfunctional Cystic Fibrosis Transmembrane Conductance Regulator Inhibits Phagocytosis of Apoptotic Cells With Proinflammatory Consequences. *Am J Physiol - Lung Cell Mol Physiol* (2009) 297(4):L677–86. doi: 10.1152/ajplung.00030.2009
87. Morimoto K, Janssen WJ, Terada M. Defective Efferocytosis by Alveolar Macrophages in IPF Patients. *Respir Med* (2012) 106:1800–3. doi: 10.1016/j.rmed.2012.08.020
88. Aoshiba K, Tamaoki J, Nagai A. Acute Cigarette Smoke Exposure Induces Apoptosis of Alveolar Macrophages. *Am J Physiol - Lung Cell Mol Physiol* (2001) 281(6):L1392–401. doi: 10.1152/ajplung.2001.281.6.l1392
89. Gleeson LE, O'Leary SM, Ryan D, McLaughlin AM, Sheedy FJ, Keane J. Cigarette Smoking Impairs the Bioenergetic Immune Response to Mycobacterium Tuberculosis Infection. *Am J Respir Cell Mol Biol* (2018) 59:572–9. doi: 10.1165/rcmb.2018-0162OC
90. Sussan TE, Gajghate S, Thimmulappa RK, Ma J, Kim JH, Sudini K, et al. Exposure to Electronic Cigarettes Impairs Pulmonary Anti-Bacterial and Anti-Viral Defenses in a Mouse Model. *PloS One* (2015) 10:e0116861. doi: 10.1371/journal.pone.0116861
91. Wallace WAH, Gillooly M, Lamb D. Intra-Alveolar Macrophage Numbers in Current Smokers and non-Smokers: A Morphometric Study of Tissue Sections. *Thorax* (1992) 47:437–40. doi: 10.1136/thx.47.6.437
92. Schneider C, Nobs SP, Heer AK, Kurrer M, Klinke G, van Rooijen N, et al. Alveolar Macrophages Are Essential for Protection From Respiratory Failure and Associated Morbidity Following Influenza Virus Infection. *PloS Pathog* (2014) 10:e1004053. doi: 10.1371/journal.ppat.1004053
93. Kim HM, Lee Y-W, Lee K-J, Kim HS, Cho SW, van Rooijen N, et al. Alveolar Macrophages Are Indispensable for Controlling Influenza Viruses in Lungs of Pigs. *J Virol* (2008) 82:4265–74. doi: 10.1128/jvi.02602-07

94. Yilla M, Harcourt BH, Hickman CJ, McGrew M, Tamin A, Goldsmith CS, et al. SARS-Coronavirus Replication in Human Peripheral Monocytes/Macrophages. *Virus Res* (2005) 107:93–101. doi: 10.1016/j.virusres.2004.09.004
95. Smith MS, Bentz GL, Alexander JS, Yurochko AD. Human Cytomegalovirus Induces Monocyte Differentiation and Migration as a Strategy for Dissemination and Persistence. *J Virol* (2004) 78:4444–53. doi: 10.1128/jvi.78.9.4444-4453.2004
96. Nottet HS, Persidsky Y, Sasseville VG, Nukuna AN, Bock P, Zhai QH, et al. Mechanisms for the Transendothelial Migration of HIV-1-Infected Monocytes Into Brain. *J Immunol* (1996) 156:1284–95.
97. Desforges M, Miletti TC, Gagnon M, Talbot PJ. Activation of Human Monocytes After Infection by Human Coronavirus 229E. *Virus Res* (2007) 130:228–40. doi: 10.1016/j.virusres.2007.06.016
98. Al-Qahtani AA, Lyroni K, Aznaourova M, Tseliou M, Al-Anazi MR, Al-Ahdal MN, et al. Middle East Respiratory Syndrome Corona Virus Spike Glycoprotein Suppresses Macrophage Responses *via* DPP4-Mediated Induction of IRAK-M and Pparγ. *Oncotarget* (2017) 8:9053–66. doi: 10.18632/oncotarget.14754
99. Nikitina E, Larionova I, Choinzonov E, Kzhyshkowska J. Monocytes and Macrophages as Viral Targets and Reservoirs. *Int J Mol Sci* (2018) 19:2821. doi: 10.3390/ijms19092821
100. Cheung CY, Poon LLM, Ng IHY, Luk W, Sia S-F, Wu MHS, et al. Cytokine Responses in Severe Acute Respiratory Syndrome Coronavirus-Infected Macrophages In Vitro: Possible Relevance to Pathogenesis. *J Virol* (2005) 79:7819–26. doi: 10.1128/jvi.79.12.7819-7826.2005
101. Wang J, Nikrad MP, Travanty EA, Zhou B, Phang T, Gao B, et al. Innate Immune Response of Human Alveolar Macrophages During Influenza a Infection. *PloS One* (2012) 7:e29879. doi: 10.1371/journal.pone.0029879
102. Kumagai Y, Takeuchi O, Kato H, Kumar H, Matsui K, Morii E, et al. Alveolar Macrophages Are the Primary Interferon-α Producer in Pulmonary Infection With RNA Viruses. *Immunity* (2007) 27:240–52. doi: 10.1016/j.immuni.2007.07.013
103. Wang J, Nikrad MP, Phang T, Gao B, Alford T, Ito Y, et al. Innate Immune Response to Influenza A Virus in Differentiated Human Alveolar Type II Cells. *Am J Respir Cell Mol Biol* (2011) 45:582–91. doi: 10.1165/rcmb.2010-0108OC
104. Wong MT, Chen SSL. Emerging Roles of Interferon-Stimulated Genes in the Innate Immune Response to Hepatitis C Virus Infection. *Cell Mol Immunol* (2016) 13:11–35. doi: 10.1038/cmi.2014.127
105. Hambleton S, Goodbourn S, Young DF, Dickinson P, Mohamad SMB, Valappil M, et al. STAT2 Deficiency and Susceptibility to Viral Illness in Humans. *Proc Natl Acad Sci USA* (2013) 110:3053–8. doi: 10.1073/pnas.1220098110
106. Joel Funk C, Wang J, Ito Y, Travanty EA, Voelker DR, Holmes KV, et al. Infection of Human Alveolar Macrophages by Human Coronavirus Strain 229E. *J Gen Virol* (2012) 93:494–503. doi: 10.1099/vir.0.038414-0
107. Califano D, Furuya Y, Metzger DW. Effects of Influenza on Alveolar Macrophage Viability Are Dependent on Mouse Genetic Strain. *J Immunol* (2018) 201:134–44. doi: 10.4049/jimmunol.1701406
108. Arunachalam PS, Wimmers F, Mok CKP, Perera RAPM, Scott M, Hagan T, et al. Systems Biological Assessment of Immunity to Mild Versus Severe COVID-19 Infection in Humans. *Science* (2020) 369:1210–20. doi: 10.1126/SCIENCE.ABC6261
109. Hadjadj J, Yatim N, Barnabei L, Corneau A, Boussier J, Smith N, et al. Impaired Type I Interferon Activity and Inflammatory Responses in Severe COVID-19 Patients. *Science* (2020) 369:718–24. doi: 10.1126/science.abc6027
110. Zhou Z, Ren L, Zhang L, Zhong J, Xiao Y, Jia Z, et al. Heightened Innate Immune Responses in the Respiratory Tract of COVID-19 Patients. *Cell Host Microbe* (2020) 27:883–90.e2. doi: 10.1016/j.chom.2020.04.017
111. Fajgenbaum DC, June CH. Cytokine Storm. *N Engl J Med* (2020) 383:2255–73. doi: 10.1056/nejmra2026131
112. Kox M, Waalders NJB, Kooistra EJ, Gerretsen J, Pickkers P. Cytokine Levels in Critically Ill Patients With COVID-19 and Other Conditions. *JAMA - J Am Med Assoc* (2020) 324:1565–7. doi: 10.1001/jama.2020.17052
113. Monneret G, Benlyamani I, Gossez M, Bermejo-Martin JF, Martín-Fernandez M, Sesques P, et al. COVID-19: What Type of Cytokine Storm Are We Dealing With? *J Med Virol* (2021) 93:197–8. doi: 10.1002/jmv.26317
114. Sinha P, Matthay MA, Calfee CS. Is a "Cytokine Storm" Relevant to COVID-19? *JAMA Intern Med* (2020) 180:1152–4. doi: 10.1001/jamainternmed.2020.3313
115. Leisman DE, Ronner L, Pinotti R, Taylor MD, Sinha P, Calfee CS, et al. Cytokine Elevation in Severe and Critical COVID-19: A Rapid Systematic Review, Meta-Analysis, and Comparison With Other Inflammatory Syndromes. *Lancet Respir Med* (2020) 8:1233–44. doi: 10.1016/S2213-2600(20)30404-5
116. Khanmohammadi S, Rezaei N. Role of Toll-Like Receptors in the Pathogenesis of COVID-19. *J Med Virol* (2021) 93:2735–9. doi: 10.1002/jmv.26826
117. Yang D, Geng T, Harrison AG, Wang P. Differential Roles of RIG-I-Like Receptors in SARS-CoV-2 Infection. *bioRxiv Prepr Serv Biol* (2021). doi: 10.1101/2021.02.10.430677
118. Zhao Y, Kuang M, Li J, Zhu L, Jia Z, Guo X, et al. SARS-CoV-2 Spike Protein Interacts With and Activates TLR4. *Cell Res* (2021) 31:818–20. doi: 10.1038/s41422-021-00495-9
119. Zheng M, Karki R, Williams EP, Yang D, Fitzpatrick E, Vogel P, et al. TLR2 Senses the SARS-CoV-2 Envelope Protein to Produce Inflammatory Cytokines. *Nat Immunol* (2021) 22:829–38. doi: 10.1038/s41590-021-00937-x
120. Thépaut M, Luczkowiak J, Vivès C, Labiod N, Bally I, Lasala F, et al. Dc/L-SIGN Recognition of Spike Glycoprotein Promotes SARS-CoV-2 Trans-Infection and can be Inhibited by a Glycomimetic Antagonist. *PloS Pathog* (2021) 17:e1009576. doi: 10.1371/journal.ppat.1009576
121. Lu Q, Liu J, Zhao S, Gomez Castro MF, Laurent-Rolle M, Dong J, et al. SARS-CoV-2 Exacerbates Proinflammatory Responses in Myeloid Cells Through C-Type Lectin Receptors and Tweety Family Member 2. *Immunity* (2021) 54:1304–1319.e9. doi: 10.1016/j.immuni.2021.05.006
122. Yang D, Chu H, Hou Y, Chai Y, Shuai H, Lee ACY, et al. Attenuated Interferon and Proinflammatory Response in SARS-CoV-2-Infected Human Dendritic Cells is Associated With Viral Antagonism of STAT1 Phosphorylation. *J Infect Dis* (2020) 222:734–45. doi: 10.1093/infdis/jiaa356
123. Zheng J, Wang Y, Li K, Meyerholz DK, Allamargot C, Perlman S. Severe Acute Respiratory Syndrome Coronavirus 2-Induced Immune Activation and Death of Monocyte-Derived Human Macrophages and Dendritic Cells. *J Infect Dis* (2021) 223:785–95. doi: 10.1093/infdis/jiaa753
124. Chu H, Chan JFW, Wang Y, Yuen TTT, Chai Y, Hou Y, et al. Comparative Replication and Immune Activation Profiles of SARS-CoV-2 and SARS-CoV in Human Lungs: An Ex Vivo Study With Implications for the Pathogenesis of COVID-19. *Clin Infect Dis* (2020) 71:1400–9. doi: 10.1093/cid/ciaa410
125. Martines RB, Ritter JM, Matkovic E, Gary J, Bollweg BC, Bullock H, et al. Pathology and Pathogenesis of SARS-CoV-2 Associated With Fatal Coronavirus Disease, United States. *Emerg Infect Dis* (2020) 26:2005–15. doi: 10.3201/eid2609.202095
126. Lv J, Wang Z, Qu Y, Zhu H, Zhu Q, Tong W, et al. Distinct Uptake, Amplification, and Release of SARS-CoV-2 by M1 and M2 Alveolar Macrophages. *Cell Discovery* (2021) 7:24. doi: 10.1038/s41421-021-00258-1
127. Pantazi I, Al-Qahtani AA, Alhamlan FS, Alothaid H, Matou-Nasri S, Sourvinos G, et al. SARS-CoV-2/ACE2 Interaction Suppresses IRAK-M Expression and Promotes Pro-Inflammatory Cytokine Production in Macrophages. *Front Immunol* (2021) 12:683800. doi: 10.3389/FIMMU.2021.683800
128. Liu L, Wei Q, Lin Q, Fang J, Wang H, Kwok H, et al. Anti-Spike IgG Causes Severe Acute Lung Injury by Skewing Macrophage Responses During Acute SARS-CoV Infection. *JCI Insight* (2019) 4:e123158. doi: 10.1172/jci.insight.123158
129. Jaume M, Yip MS, Cheung CY, Leung HL, Li PH, Kien F, et al. Anti-Severe Acute Respiratory Syndrome Coronavirus Spike Antibodies Trigger Infection of Human Immune Cells *via* a pH- and Cysteine Protease-Independent Fc R Pathway. *J Virol* (2011) 85:10582–97. doi: 10.1128/jvi.00671-11
130. Codo AC, Davanzo GG, Monteiro L de B, de Souza GF, Muraro SP, Virgilio-da-Silva JV, et al. Elevated Glucose Levels Favor SARS-CoV-2 Infection and Monocyte Response Through a HIF-1α/Glycolysis-Dependent Axis. *Cell Metab* (2020) 32:437–46.e5. doi: 10.1016/j.cmet.2020.07.007
131. da Silva Gomes Dias S, Soares VC, Ferreira AC, Sacramento CQ, Fintelman-Rodrigues N, Temerozo JR, et al. Lipid Droplets Fuel SARS-CoV-2 Replication and Production of Inflammatory Mediators. *PloS Pathog* (2020) 16:e1009127. doi: 10.1371/journal.ppat.1009127

132. Zhou Y, Fu B, Zheng X, Wang D, Zhao C, Qi Y, et al. Pathogenic T-Cells and Inflammatory Monocytes Incite Inflammatory Storms in Severe COVID-19 Patients. *Natl Sci Rev* (2020) 7:998–1002. doi: 10.1093/nsr/nwaa041
133. Laing AG, Lorenc A, del Molino del Barrio I, Das A, Fish M, Monin L, et al. A Dynamic COVID-19 Immune Signature Includes Associations With Poor Prognosis. *Nat Med* (2020) 26:1623–35. doi: 10.1038/s41591-020-1038-6
134. Payen D, Cravat M, Maadadi H, Didelot C, Prosic L, Dupuis C, et al. A Longitudinal Study of Immune Cells in Severe COVID-19 Patients. *Front Immunol* (2020) 11:580250. doi: 10.3389/fimmu.2020.580250
135. Gatti A, Radrizzani D, Viganò P, Mazzone A, Brando B. Decrease of Non-Classical and Intermediate Monocyte Subsets in Severe Acute SARS-CoV-2 Infection. *Cytom Part A* (2020) 97:887–90. doi: 10.1002/cyto.a.24188
136. Ferreira AC, Soares VC, de Azevedo-Quintanilha IG, Dias S da SG, Fintelman-Rodrigues N, Sacramento CQ, et al. SARS-CoV-2 Engages Inflammasome and Pyroptosis in Human Primary Monocytes. *Cell Death Discov* (2021) 7:43. doi: 10.1038/s41420-021-00428-w
137. Schultze JL, Mass E, Schlitzer A. Emerging Principles in Myelopoiesis at Homeostasis and During Infection and Inflammation. *Immunity* (2019) 50:288–301. doi: 10.1016/j.immuni.2019.01.019
138. Mann ER, Menon M, Knight SB, Konkel JE, Jagger C, Shaw TN, et al. Longitudinal Immune Profiling Reveals Key Myeloid Signatures Associated With COVID-19. *Sci Immunol* (2020) 5:eabd6197. doi: 10.1126/SCIIMMUNOL.ABD6197
139. Giamarellos-Bourboulis EJ, Netea MG, Rovina N, Akinosoglou K, Antoniadou A, Antonakos N, et al. Complex Immune Dysregulation in COVID-19 Patients With Severe Respiratory Failure. *Cell Host Microbe* (2020) 27:992–1000.e3. doi: 10.1016/j.chom.2020.04.009
140. Spinetti T, Hirzel C, Fux M, Walti LN, Schober P, Stueber F, et al. Reduced Monocytic Human Leukocyte Antigen-DR Expression Indicates Immunosuppression in Critically Ill COVID-19 Patients. *Anesth Analg* (2020) 131:993–9. doi: 10.1213/ANE.0000000000005044
141. Wang F, Hou H, Yao Y, Wu S, Huang M, Ran X, et al. Systemically Comparing Host Immunity Between Survived and Deceased COVID-19 Patients. *Cell Mol Immunol* (2020) 17:875–7. doi: 10.1038/s41423-020-0483-y
142. Kvedaraite E, Hertwig L, Sinha I, Ponzetta A, Myrberg IH, Lourda M, et al. Major Alterations in the Mononuclear Phagocyte Landscape Associated With COVID-19 Severity. *Proc Natl Acad Sci USA* (2021) 118(6): e2018587118. doi: 10.1073/pnas.2018587118
143. Carter MJ, Fish M, Jennings A, Doores KJ, Wellman P, Seow J, et al. Peripheral Immunophenotypes in Children With Multisystem Inflammatory Syndrome Associated With SARS-CoV-2 Infection. *Nat Med* (2020) 26:1701–7. doi: 10.1038/s41591-020-1054-6
144. Hegde S, Leader AM, Merad M. MDSC: Markers, Development, States, and Unaddressed Complexity. *Immunity* (2021) 54:875–84. doi: 10.1016/j.immuni.2021.04.004
145. Falck-Jones S, Vangeti S, Yu M, Falck-Jones R, Cagigi A, Badolati I, et al. Functional Monocytic Myeloid-Derived Suppressor Cells Increase in Blood But Not Airways and Predict COVID-19 Severity. *J Clin Invest* (2021) 131(6): e144734. doi: 10.1172/JCI144734
146. Thompson EA, Cascino K, Ordonez AA, Zhou W, Vaghasia A, Hamacher-Brady A, et al. Metabolic Programs Define Dysfunctional Immune Responses in Severe COVID-19 Patients. *Cell Rep* (2021) 34:108863. doi: 10.1016/j.celrep.2021.108863
147. Wen W, Su W, Tang H, Le W, Zhang X, Zheng Y, et al. Immune Cell Profiling of COVID-19 Patients in the Recovery Stage by Single-Cell Sequencing. *Cell Discov* (2020) 6:6. doi: 10.1038/s41421-020-0168-9
148. Lee JS, Park S, Jeong HW, Ahn JY, Choi SJ, Lee H, et al. Immunophenotyping of Covid-19 and Influenza Highlights the Role of Type I Interferons in Development of Severe Covid-19. *Sci Immunol* (2020) 5:1554. doi: 10.1126/sciimmunol.abd1554
149. Szabo PA, Dogra P, Gray JI, Wells SB, Connors TJ, Weisberg SP, et al. Longitudinal Profiling of Respiratory and Systemic Immune Responses Reveals Myeloid Cell-Driven Lung Inflammation in Severe COVID-19. *Immunity* (2021) 54:797–814.e6. doi: 10.1016/j.immuni.2021.03.005
150. Stephenson E, Reynolds G, Botting RA, Calero-Nieto FJ, Morgan MD, Tuong ZK, et al. Single-Cell Multi-Omics Analysis of the Immune Response in COVID-19. *Nat Med* (2021) 27:904–16. doi: 10.1038/s41591-021-01329-2
151. Su Y, Chen D, Yuan D, Lausted C, Choi J, Dai CL, et al. Multi-Omics Resolves a Sharp Disease-State Shift Between Mild and Moderate COVID-19. *Cell* (2020) 183:1479–95.e20. doi: 10.1016/j.cell.2020.10.037
152. Cao Y, Su B, Guo X, Sun W, Deng Y, Bao L, et al. Potent Neutralizing Antibodies Against SARS-CoV-2 Identified by High-Throughput Single-Cell Sequencing of Convalescent Patients' B Cells. *Cell* (2020) 182:73–84.e16. doi: 10.1016/j.cell.2020.05.025
153. Melms JC, Biermann J, Huang H, Wang Y, Nair A, Tagore S, et al. A Molecular Single-Cell Lung Atlas of Lethal COVID-19. *Nature* (2021) 33:15. doi: 10.1038/s41586-021-03569-1
154. Wauters E, Van Mol P, Garg AD, Jansen S, Van Herck Y, Vanderbeke L, et al. Discriminating Mild From Critical COVID-19 by Innate and Adaptive Immune Single-Cell Profiling of Bronchoalveolar Lavages. *Cell Res* (2021) 31:272–90. doi: 10.1038/s41422-020-00455-9
155. Wilk AJ, Rustagi A, Zhao NQ, Roque J, Martínez-Colón GJ, McKechnie JL, et al. A Single-Cell Atlas of the Peripheral Immune Response in Patients With Severe COVID-19. *Nat Med* (2020) 26:1070–6. doi: 10.1038/s41591-020-0944-y
156. Bernardes JP, Mishra N, Tran F, Rosenstiel P. Longitudinal Multi-Omics Analyses Identify Responses of Megakaryocytes, Erythroid Cells, and Plasmablasts as Hallmarks of Severe COVID-19. *Immunity* (2020) 53:1296–314.e9. doi: 10.1016/j.immuni.2020.11.017
157. Zhang JY, Wang XM, Xing X, Xu Z, Zhang C, Song JW, et al. Single-Cell Landscape of Immunological Responses in Patients With COVID-19. *Nat Immunol* (2020) 21:1107–18. doi: 10.1038/s41590-020-0762-x
158. Grant RA, Morales-Nebreda L, Markov NS, Swaminathan S, Querrey M, Guzman ER, et al. Circuits Between Infected Macrophages and T Cells in SARS-CoV-2 Pneumonia. *Nature* (2021) 590:635–41. doi: 10.1038/s41586-020-03148-w
159. Combes AJ, Courau T, Kuhn NF, Hu KH, Ray A, Chen WS, et al. Global Absence and Targeting of Protective Immune States in Severe COVID-19. *Nature* (2021) 591:124–30. doi: 10.1038/s41586-021-03234-7
160. Nouailles G, Wyler E, Pennitz P, Postmus D, Kazmierski J, Pott F, et al. Longitudinal Omics in Syrian Hamsters Integrated With Human Data Unravel Complexity 1 of Moderate Immune Responses to SARS-CoV-2 2 3. *bioRxiv* (2020) 2020:12. doi: 10.1101/2020.12.18.423524
161. Sánchez-Cerrillo I, Landete P, Aldave B, Sánchez-Alonso S, Sánchez-Azofra A, Marcos-Jiménez A, et al. COVID-19 Severity Associates With Pulmonary Redistribution of CD1c+ DCs and Inflammatory Transitional and Nonclassical Monocytes. *J Clin Invest* (2020) 130:6290–300. doi: 10.1172/JCI140335
162. Bost P, Giladi A, Liu Y, Bendjelal Y, Xu G, David E, et al. Host-Viral Infection Maps Reveal Signatures of Severe COVID-19 Patients. *Cell* (2020) 181:1475–1488.e12. doi: 10.1016/j.cell.2020.05.006


**Conflict of Interest:** The authors declare that the research was conducted in the absence of any commercial or financial relationships that could be construed as a potential conflict of interest.

*Copyright © 2021 Knoll, Schultze and Schulte-Schrepping. This is an open-access article distributed under the terms of the Creative Commons Attribution License (CC BY). The use, distribution or reproduction in other forums is permitted, provided the original author(s) and the copyright owner(s) are credited and that the original publication in this journal is cited, in accordance with accepted academic practice. No use, distribution or reproduction is permitted which does not comply with these terms.*

Aschenbrenner et al. Genome Medicine (2021) 13:7
https://doi.org/10.1186/s13073-020-00823-5

Genome Medicine

RESEARCH Open Access

# Disease severity-specific neutrophil signatures in blood transcriptomes stratify COVID-19 patients

Anna C. Aschenbrenner[1,2,3,4†], Maria Mouktaroudi[5†], Benjamin Krämer[6†], Marie Oestreich[3†], Nikolaos Antonakos[5†], Melanie Nuesch-Germano[3†], Konstantina Gkizeli[5†], Lorenzo Bonaguro[3†], Nico Reusch[3†], Kevin Baßler[3†], Maria Saridaki[5†], Rainer Knoll[3†], Tal Pecht[3†], Theodore S. Kapellos[3†], Sarandia Doulou[3†], Charlotte Kröger[3†], Miriam Herbert[3†], Lisa Holsten[3†], Arik Horne[3†], Ioanna D. Gemünd[3†], Nikoletta Rovina[7†], Shobhit Agrawal[8†], Kilian Dahm[3†], Martina van Uelft[3†], Anna Drews[2†], Lena Lenkeit[3†], Niklas Bruse[9†], Jelle Gerretsen[9], Jannik Gierlich[3], Matthias Becker[2], Kristian Händler[2], Michael Kraut[2], Heidi Theis[2], Simachew Mengiste[3], Elena De Domenico[2], Jonas Schulte-Schrepping[3], Lea Seep[3], Jan Raabe[6], Christoph Hoffmeister[6], Michael ToVinh[6], Verena Keitel[10], Gereon Rieke[6], Valentina Talevi[11], Dirk Skowasch[12], N. Ahmad Aziz[11,13], Peter Pickkers[9], Frank L. van de Veerdonk[4], Mihai G. Netea[4,14†], Joachim L. Schultze[1,2,3†], Matthijs Kox[9†], Monique M. B. Breteler[11,15†], Jacob Nattermann[6,16†], Antonia Koutsoukou[7†], Evangelos J. Giamarellos-Bourboulis[5†], Thomas Ulas[1,2*†] and German COVID-19 Omics Initiative (DeCOI)

## Abstract

**Background:** The SARS-CoV-2 pandemic is currently leading to increasing numbers of COVID-19 patients all over the world. Clinical presentations range from asymptomatic, mild respiratory tract infection, to severe cases with acute respiratory distress syndrome, respiratory failure, and death. Reports on a dysregulated immune system in the severe cases call for a better characterization and understanding of the changes in the immune system.

(Continued on next page)

* Correspondence: t.ulas@uni-bonn.de
Anna C. Aschenbrenner, Maria Mouktaroudi, Benjamin Krämer, Marie Oestreich, Nikolaos Antonakos, Melanie Nuesch-Germano, Konstantina Gkizeli, Lorenzo Bonaguro, Nico Reusch, Kevin Baßler, Maria Saridaki, Rainer Knoll, Tal Pecht, Theodore S. Kapellos, Sarandia Doulou, Charlotte Kröger, Miriam Herbert, Lisa Holsten, Arik Horne, Ioanna D. Gemünd, Nikoletta Rovina, Shobhit Agrawal, Kilian Dahm, Martina van Uelft, Anna Drews, Lena Lenkeit, and Niklas Bruse shared the first authorship.
Mihai G. Netea, Joachim L. Schultze, Matthijs Kox, Monique M.B. Breteler, Jacob Nattermann, Antonia Koutsoukou, Evangelos J. Giamarellos-Bourboulis, and Thomas Ulas shared the last authorship.
[1]Systems Medicine, German Center for Neurodegenerative Diseases (DZNE), Bonn, Germany
[2]PRECISE Platform for Single Cell Genomics and Epigenomics at the German Center for Neurodegenerative Diseases and the University of Bonn, Bonn, Germany
Full list of author information is available at the end of the article

© The Author(s). 2021 **Open Access** This article is licensed under a Creative Commons Attribution 4.0 International License, which permits use, sharing, adaptation, distribution and reproduction in any medium or format, as long as you give appropriate credit to the original author(s) and the source, provide a link to the Creative Commons licence, and indicate if changes were made. The images or other third party material in this article are included in the article's Creative Commons licence, unless indicated otherwise in a credit line to the material. If material is not included in the article's Creative Commons licence and your intended use is not permitted by statutory regulation or exceeds the permitted use, you will need to obtain permission directly from the copyright holder. To view a copy of this licence, visit http://creativecommons.org/licenses/by/4.0/. The Creative Commons Public Domain Dedication waiver (http://creativecommons.org/publicdomain/zero/1.0/) applies to the data made available in this article, unless otherwise stated in a credit line to the data.

(Continued from previous page)

**Methods:** In order to dissect COVID-19-driven immune host responses, we performed RNA-seq of whole blood cell transcriptomes and granulocyte preparations from mild and severe COVID-19 patients and analyzed the data using a combination of conventional and data-driven co-expression analysis. Additionally, publicly available data was used to show the distinction from COVID-19 to other diseases. Reverse drug target prediction was used to identify known or novel drug candidates based on finding from data-driven findings.

**Results:** Here, we profiled whole blood transcriptomes of 39 COVID-19 patients and 10 control donors enabling a data-driven stratification based on molecular phenotype. Neutrophil activation-associated signatures were prominently enriched in severe patient groups, which was corroborated in whole blood transcriptomes from an independent second cohort of 30 as well as in granulocyte samples from a third cohort of 16 COVID-19 patients (44 samples). Comparison of COVID-19 blood transcriptomes with those of a collection of over 3100 samples derived from 12 different viral infections, inflammatory diseases, and independent control samples revealed highly specific transcriptome signatures for COVID-19. Further, stratified transcriptomes predicted patient subgroup-specific drug candidates targeting the dysregulated systemic immune response of the host.

**Conclusions:** Our study provides novel insights in the distinct molecular subgroups or phenotypes that are not simply explained by clinical parameters. We show that whole blood transcriptomes are extremely informative for COVID-19 since they capture granulocytes which are major drivers of disease severity.

**Keywords:** COVID-19, Blood transcriptomics, Transcriptome, Co-expression analysis, Stratification, Molecular disease phenotypes, Granulocytes, Neutrophils, Drug repurposing

## Background

Pandemic spread of the recently emerged coronavirus, severe acute respiratory syndrome-coronavirus 2 (SARS-CoV-2), has resulted in over 84 million confirmed infected individuals and over 1.8 million deaths worldwide (WHO, covid19.who.int, as of January 6, 2021) from the resulting severe respiratory illness, called coronavirus disease 2019 (COVID-19) [1–3]. Based on clinical observations, it has become clear that there is great variety in disease manifestation, ranging from asymptomatic cases, to flu-like symptoms, to severe cases needing mechanical ventilation, to those who do not survive [4–8]. Increasing evidence suggests that the immune system plays a pivotal role in determining the severity of the disease course and it has been suggested that different molecular phenotypes might be responsible for the heterogeneous outcome of COVID-19 [9–14]. Identifying these molecular phenotypes might not only be important for a better understanding of the pathophysiology of the disease, but also to better define patient subgroups that are more likely to benefit from specific therapies [15–20]. Indeed, while vaccines are still under development, finding an effective and patient-tailored therapeutic management for COVID-19 patients including targeting derailed immune mechanisms [21–23] is key to mitigate the clinical burden as well as to prevent further disease fatalities [18, 19].

The analysis of peripheral blood-derived immune parameters in inflammatory and infectious diseases either by classical testing, including flow cytometry and serum protein measurements, or by omics technologies, including transcriptomics, has been proven very valuable in the past [24–32]. In COVID-19 patients, monitoring peripheral blood as a proxy for the ongoing changes within the circulating cells of the immune system has revealed lymphopenia to correlate with disease severity [33]. Single-cell analysis of blood-derived cells revealed downregulation of MHC molecules on monocytes and granulocytes [34], immune cell exhaustion [35], and a dysregulated myeloid cell compartment [34, 36] including dendritic cells [37] in a disease stage-dependent manner. Serial immune response analyses revealed four immune signatures represented by growth factors, two cytokine-defined phenotypes as well as a chemokine-defined phenotype [14]. While an early elevation in cytokine levels was associated with worse disease outcomes, patients with moderate COVID-19 displayed a progressive reduction in antiviral and antifungal immune responses [14]. Moreover, impaired type I interferon responses were seen in severe COVID-19 cases [38]. In another study, three distinct patient immunotypes were related to a poor clinical trajectory when combining flow cytometry, single-cell proteomics, and clinical observations [12]. Furthermore, several studies reported increased IL-6 serum levels to be a hallmark of COVID-19 [9, 13, 39–41], but also TNF and IL-8 [41]. A very recent large multi-omics longitudinal observational study identified a sharp transition between mild and moderate disease, indicating that targeting such a shift therapeutically might be beneficial for these patients [13].

Indeed, while one can envision mild and/or early cases to benefit from antiviral drug treatments currently under clinical investigation, more severe cases may benefit from treatment to mitigate the excessive systemic immune reactions resulting in progressing pneumonia and

even respiratory failure associated with severe COVID-19 [4–9]. The detrimental role of the systemic inflammation in the late phase of the disease has become clear, as the elevated inflammatory signaling has been associated with disease morbidity [6, 9, 13, 38–42]. Thus, a better understanding of the dysregulation of the host response to the infection leading to immunopathology is urgently needed to dissect and comprehend the immune parameters accompanying the heterogeneous disease severity seen upon SARS-CoV-2 infection.

Based on previous experience with other infectious diseases [24–30], we hypothesized that whole blood transcriptomes should allow us to (1) determine immune cellular characteristics and functions in COVID-19 patients, (2) reveal heterogeneous molecular phenotypes of patients with similar clinical presentation, (3) define commonalities and differences of COVID-19 in comparison to other inflammatory conditions, and (4) predict potential drug repurposing that might counteract observed immune dysregulations.

Here, by using blood transcriptomes, we provide evidence for molecular subtypes within the immune response of COVID-19 patients beyond distinguishing mild and severe cases only. In addition, molecular changes in blood of severely affected patients are strikingly associated with changes in the granulocyte compartment. Furthermore, blood transcriptomes of molecular subtypes of COVID-19 patients seem to be unique in comparison to more than 2600 samples derived from other infections, inflammatory conditions, and controls. Finally, reverse drug target prediction using patients' blood transcriptomes revealed known as well as additional new potential targets for further evaluation. Our data might also serve as a starting point for a large-scale assembly of molecular data collected during currently ongoing and future therapy trials for COVID-19 patients based on whole blood transcriptomes.

## Methods

### Human cohorts

#### *Whole blood samples for RNA-seq analysis*

The study was conducted between March 13 and March 30, 2020. A total of 6 ml of blood was sampled from patients with community-acquired pneumonia (CAP) by SARS-CoV-2 within the first 24 h of hospital admission. CAP was defined as the presence of diffuse infiltrates in chest X-ray or chest computed tomography and positive molecular testing of respiratory secretions for SARS-CoV-2. Exclusion criteria were infection by the human immunodeficiency virus, neutropenia, and any previous intake of immunosuppressive medication (corticosteroids, anti-cytokine biologicals, and biological response modifiers). The studies were conducted under the 23/12.08.2019 approval of the Ethics Committee of Sotiria Athens General Hospital and the 26.02.2019 approval of the Ethics Committee of ATTIKON University General Hospital. Written informed consent was provided by patients or by first-degree relatives in case of patients unable to consent. Patients were classified based on the WHO ordinal scale: mild = WHO1–4 and severe = WHO5–7. "Immune classification" of the patients is based on the criteria used in Giamarellos-Bourboulis et al. [40]: MAS for patients with > 4.420 ng/ml ferritin, dysregulation for patients with < 4.420 ng/ml ferritin with < 5000 molecules of HLA-DR+/CD14+ cells, and intermediate for those patients lying in between MAS and dysregulation. The following information was recorded: white blood cell count and differential, administered treatment, and 28-day outcome. Patients were sampled within 24 h upon admission to the hospital. A volume of 2.5 ml of the collected blood was transferred into one PAXgene tube and stored at − 80 °C. The remaining was used for flow cytometry analysis. A similar amount of blood was sampled from 10 controls, matched for age, sex, and Charlson's comorbidity index. They were subject to testing of the nasopharyngeal secretion for SARS-CoV-2 and all confirmed to be asymptomatic and seronegative.

For the second cohort, whole blood samples were collected for RNA-seq analysis in PAXgene tubes from 30 patients upon admission to the Intensive Care Unit of the Radboud University Medical Center in Nijmegen, the Netherlands. The study was carried out in accordance with the applicable rules concerning the review of research ethics committees and informed consent. All patients or legal representatives were informed about the study details and could decline to participate. COVID-19 was diagnosed by a positive SARS-CoV-2 RT-PCR test in nasopharyngeal and throat swabs and/or by typical chest CT-scan findings. Exclusion criteria were hematological malignancies and/or active chemotherapy, solid organ transplant, autoimmune diseases, and pre-existent use of high-dose corticosteroids.

#### *Granulocyte samples for RNA-seq analysis*

This study was approved by the Institutional Review Board of the University Hospital Bonn (073/19 and 134/20). After providing written informed consent, 16 COVID-19 patients (44 samples) were included in the study. In-patients who were not able to consent at the time of study enrollment, consent was obtained after recovery. COVID-19 patients who tested positive for SARS-CoV-2 RNA in nasopharyngeal swabs were recruited at the Medical Clinic I of the University Hospital Bonn between March 30 and May 17, 2020. Longitudinal samples were included from day 1 to 20 after onset of symptoms and grouped into day 1–10 and 11–20 according to previous reports [34, 43].

Granulocytes were isolated from EDTA-treated or heparinized peripheral blood by density centrifugation over Pancoll or Ficoll-Paque density centrifugation (density: 1.077 g/ml). Granulocyte fractions were then treated with 10 ml RBC lysis buffer (Biolegend) for 10 min. After RBC lysis, cells were washed with DPBS and recovered by centrifugation at 300×*g* for 10 min. Granulocyte pellets were then lysed with 500 µl of QIAzol (Qiagen), shortly vortexed, and incubated 5 min at RT prior storage at − 80 °C until RNA extraction.

### Rhineland Study as control samples within the integrated dataset for disease comparison

#### *Study population*

The Rhineland Study is an ongoing community-based cohort study in which all inhabitants of two geographically defined areas in the city of Bonn, Germany, aged 30–100 years are being invited to participate. Persons living in these areas are predominantly German with Caucasian ethnicity. Participation in the study is possible by invitation only. The only exclusion criterion is insufficient German language skills to give informed consent.

#### *Ethical approval*

Approval to undertake the Rhineland Study was obtained from the ethics committee of the University of Bonn, Medical Faculty. The study is carried out in accordance with the recommendations of the International Conference on Harmonization (ICH) Good Clinical Practice (GCP) standards (ICH-GCP). Written informed consent was obtained from all participants in accordance with the Declaration of Helsinki.

#### *Blood withdrawal*

Overnight fasting blood was collected from all participants between 7:00 and 9:30 AM, including a PAXgene tube for RNA extraction.

### Flow cytometry techniques

Whole blood cells were incubated for 15 min in the dark with anti-CD45 PC5 (emission 667 nm, Beckman Coulter). Fluorospheres (Beckman Coulter) were used for the determination of absolute counts. Cells were analyzed after running through the CYTOMICS FC500 flow cytometer (Beckman Coulter Co, Miami, FL). Isotypic IgG controls stained also with anti-CD45 were used for each patient. Gating to identify neutrophils and lymphocytes was done by the characteristic sideward scattering of CD45-positive cells (Additional file 2: Figure S8).

### Whole blood RNA isolation

Total RNA was isolated from whole blood samples stored and stabilized in PAXgene RNA tubes using the Qiagen PAXgene Blood miRNA kit according to the manufacturer's guidelines. Eluted RNA was dissolved in RNase-free water. The quality and quantity of RNA were evaluated by visualization of 28S and 18S band integrity on a Tapestation 4200 system (Agilent).

### RNA-sequencing

Total RNA was converted into double-stranded cDNA libraries using the TruSeq Stranded Total RNA with Ribo-Zero Globin kit (Illumina). In brief, ribosomal and globin mRNA were depleted from 750 ng purified total RNA using biotinylated, target-specific oligos combined with Ribo-Zero rRNA removal beads; remaining RNA was fragmented using divalent cations under elevated temperature. First-strand was generated using SuperScript2 RT (Invitrogen) supplemented with actinomycin D, followed by second-strand synthesis with dUTP replacing dTTP. 3′ ends were adenylated and index adapters were ligated before subsequent PCR amplification to yield the final library. Remaining overhangs were converted into blunt ends via exonuclease/polymerase activities, and enzymes were removed. Selective enrichment of DNA fragments with ligated adaptor molecules was performed using Illumina PCR primers in a 15-cycle PCR reaction, followed by purification cDNA using SPRIBeads (Beckman Coulter). Libraries were quantified by Qubit dsDNA HS Assay (Thermo Fisher Scientific), and fragment size distribution was determined using the HS D1000 assay on a Tapestation 4200 system (Agilent). High-throughput sequencing was carried out with a NovaSeq™ 6000 Sequencing System S2 (50bp paired-end reads), and data was converted into fastq files using bcl2fastq2 v2.20.

### RNA-sequencing analysis

Sequenced reads were aligned and quantified using STAR: ultrafast universal RNA-seq aligner (v2.7.3a) [44] and the human reference genome, GRCh38p13, from the Genome Reference Consortium. Raw counts were imported using DESeqDataSetFromHTSeqCount function from DESeq2 (v1.26.0) [45] and rlog transformed according to DESeq2 pipeline. DESeq2 was used for the calculation of normalized counts for each transcript using default parameters. All normalized transcripts with a maximum over all row mean lower than 10 were excluded resulting in 37,526 present transcripts. Differentially expressed genes were calculated for the scenario status (COVID-19 vs controls), mild/severe (severe COVID-19 vs controls, mild COVID-19 vs controls, and severe vs mild COVID-19), and new_cluster (1vs6, 2vs6, 3vs6, 4vs6, and 5vs6) separately using a $p$ value cutoff of 0.05, an adjusted $p$ value (IHW) < 0.05 (independent hypothesis weighting), and a FC of 2. All present transcripts were used as input for principal component analysis. The top 25% most variable transcripts within the dataset were selected and visualized in a heat map.

DEGs were visualized as DE bar plots and were used as input for volcano plots.

### Gene ontology enrichment analysis (GOEA)

To test for functional enrichment within all three scenarios, we performed GOEA for up- or downregulated transcripts in the respective comparison using gene ontology set of biological processes. Gene set "c5.bp.v7.0.symbols.gmt" was obtained from the Molecular Signatures Database (MSigDB) [46]. compareCluster and enrichGo functions from the R package ClusterProfiler (v3.12.0) [47] were used to determine significant enrichment ($q$ value $< 0.05$) of biological processes. All present genes were used as background (universe).

### Filtering for transcription factors, epigenome, surfaceome, and secretome

All present transcripts were filtered and sorted by their variance in the dataset. The 20 most variable genes of each category were selected and visualized using a heat map. Transcription factor lists were extracted from [48], the epigenome gene list was literature-driven, and surface and secretome markers were extracted from the Human Protein Atlas [49].

### Clustering of patients according to clinical parameters

The contribution of each clinical parameter to the transcriptome in COVID-19 patients was determined using linear modeling of each parameter separately with PC1. Clinical parameters with rounded up adjusted $r$-square $\geq 0.2$ were used for agglomerative hierarchical clustering of the COVID-19 patients. A dissimilarity matrix based on Gower distance was calculated using the daisy function from the cluster packages (version 2.1.0). Agglomerative hierarchical clustering was performed using the hclust function, defining the method with a setting forward.D2 method linkage. We evaluated the clustering by extracting cluster statistics using the function cluster.stats from the package fpc (version 2.2-5). The number of clusters was chosen at the value at which the lowest distance among patients within clusters (i.e., low value of within-cluster sum of squares distance) and preserving a high distance among clusters (i.e., high average silhouette width) was achieved, while still maintaining a comparable number of individuals among the clusters.

### Linear support vector regression

Linear support vector regression [50] was employed to computationally deconvolute the study's whole blood samples. Gene expression tables were normalized with DESeq2 and were utilized as the input mixture file. LM22-subsetted signatures for B cells, T cells, NK cells, monocytes, dendritic cells, eosinophils, and neutrophils were generated as described on https://cibersort.stanford.edu/tutorial.php. The algorithm was subsequently run with 1000 permutations, and the proportions of cell types were visualized with ggplot2 (v3.2.1) [51].

### CoCena$^2$: Construction of Co-expression network analysis—automated

To define differences and similarities in transcript expression patterns among the different groups, CoCena$^2$ (Construction of Co-expression network analysis—automated) was performed based on Pearson's correlation. CoCena$^2$ is a network-based approach to identify clusters of genes that are co-expressed in a series of observed conditions based on data retrieved from RNA-sequencing. The tool offers a variety of functions that allow subsequent in-depth analysis of the biological context associated with the found clusters. First, we have calculated the variance for each gene in the complete dataset. Nine thousand three hundred seventy-eight of all present genes show a variance of at least 3rd quantile of all variances. Therefore, we selected the 10,000 most variable genes as input for the analysis.

To identify genes whose expression patterns are highly similar across all tested samples, pairwise Pearson's correlation coefficients are calculated using the R package Hmisc (v4.1-1). The underlying assumption of the Pearson correlation to the data is that it is normally distributed, which is a valid assumption to make in the context of gene expression when looking at expression patterns within different experimental conditions. The correlation between each pair of genes is the basis for the subsequent network construction. Therefore, the tool focuses mainly on positively correlated gene pairs, since the rate of confirmation of an edge representing an association of genes is higher than that of a non-existing association.

In order to refine the structure of the upcoming network and to unravel the condition-specific signatures, a correlation cutoff is proposed to mark the minimal correlation a pair of genes must exhibit for their co-expression to be taken into account. The cutoff is determined based on different criteria:

1) Scale-free topology

Gene expression networks have been argued to have a scale-free topology [52], meaning that the majority of vertices has a low number of adjacent edges, also referred to as the vertex' degree, whereas only very few vertices have a high degree. The degree distribution of scale-free networks asymptotically follows a power law. To assess the scale-free topology of a network constructed by a given correlation cutoff, a log-log plot of the degree distribution is constructed and the $R^2$ value

of the resulting linear regression is used to evaluate the scale-free criterion.

2) Number of graph components

A graph component is a subset of nodes, such that there is a path from every node within the component to any other node in that same component but none connecting the nodes to any outside of that component. Even though there exist functional collections of genes that cooperate to fulfill a common task, these collections are not expected to be operating independently within the cell. Thus, the cutoff proposal favors graphs with a small number of components.

3) Number of edges

To avoid a highly connected graph with great lack of structure—"hairball," the cutoff is chosen such that the number of edges is minimized while respecting the abovementioned criteria.

A Pearson correlation coefficient cutoff of 0.857 (6085 nodes and 252,584 edges) was chosen to construct scale-free networks.

The undirected co-expression network is constructed based on the gene pairs which show a higher correlation in their expression pattern than the set cutoff. A series of network-based clustering algorithms is available to then identify clusters of strong co-expression within the network. An option "auto" is provided, which tests the different clustering algorithms and picks the one that achieves the highest modularity score. Unbiased clustering was performed using the "label propagation" algorithm in igraph (v1.2.1) [the igraph software package for complex network research] and was repeated 1000 times. Modules with less than 40 genes were discarded. Genes assigned to more than 5 different clusters during the iterations received no cluster assignment.

To assess the expression strength of the found gene clusters in the different studied conditions, the group fold changes (GFCs) of the conditions are calculated for each gene by calculating the mean expression of a gene over all samples and then computing the fold change of the mean gene expression within each condition from the overall mean. The GFCs of all genes within one cluster are then added and divided by the total number of genes per cluster, resulting in condition-specific GFCs per cluster. By using the GFC, it is possible to illustrate a directional change for all conditions including the control samples in respect to the overall GFC. Agglomerative hierarchical clustering was performed by the hclust function (cluster package, version 2.1.0), using a dissimilarity matrix of samples based on the GFC values of each sample defined with the daisy function for calculating the Euclidean distances. The number of clusters was set to achieve a low within-cluster sum of squares distance and a high average silhouette, while preserving a comparable number of individuals within each cluster. The clinical parameters and the GFC results are displayed in a heat map where conditions are clustered by their GFCs revealing similar and opposing patterns (Cluster/Condition heat map). The expression pattern of the modules can be further used for additional analysis, e.g., stratification in another cohort.

Utilizing the R package *clusterProfiler*, CoCena[2] automatically analyzes the gene clusters with respect to different kinds of gene set enrichments: the genes within each cluster are scanned for enrichment in KEGG [53], Hallmark [54], Gene Ontology terms [55], and Reactome [56]. Using the R package *pcaGoPromoter* [57], the genes are also analyzed for enrichment of transcription factor binding sides, and if the predicted transcription factors are present in the data, their expression profile is visualized to facilitate evaluation of their possible role.

To investigate the interactions between protein-coding and long non-coding RNAs, we utilized the enricher function from the clusterProfiler package. We performed an enrichment analysis for lncRNA species, using the protein-coding genes that belong to the lightgreen cluster as the input gene list and all the network protein-coding genes as background. The annotation table defining lncRNA to protein-coding RNA was downloaded from the RNA interactome database RNAInter [58], filtered to only include interactions of lncRNA detected by the RNA-sequencing, had an experimental validation score of at least 0.5, and was involved in regulating the function of granulocytes [59]. Next, to obtain a comprehensive understanding of the lncRNA that may be relevant for this specific network module, the lncRNA found by the enrichment analysis with $p$ value < 0.1 were sorted according to the highest number of genes. Thereafter, Spearman's correlation among the gene expression of each lncRNA and its corresponding protein-coding RNAs was performed, and significant protein-coding RNA genes were plotted in a heat map. The CoCena[2] network was visualized by using the ggplot function from the ggplot2 package. Annotations were generated by filtering the edges of the network for the 5 top connected transcription factors, epigenetic regulators, and surface and secretome markers in each cluster. GO enrichment analysis was performed on each cluster by utilizing the enrichGO function from the clusterProfiler package to assess the overall functionality of the cluster using the genes of each cluster as the input and all the in the network as background. The top GO term and top connected genes of each cluster were compiled representing their general characteristic.

### Granulocyte dataset analysis

Granulocyte raw data was aligned and quantified using STAR (v2.7.3a) and the human reference genome, GRCh38p13, from the Genome Reference Consortium. Raw counts were imported using DESeqDataSetFromHTSeqCount function and rlog transformed. DESeq2 was used for the calculation of normalized counts for each transcript using default parameters. All normalized transcripts with a maximum over all row mean lower than 10 were excluded resulting in 27,781 present transcripts. Differentially expressed genes were calculated for the severe vs mild for day 1–10 and 11–20 (post 1st symptoms groups) separately using a $p$ value cutoff of 0.05, an adjusted $p$ value (IHW) < 0.05 (independent hypothesis weighting), and a FC of 2. All present transcripts were used as input for principal component analysis. DEGs were visualized as DE bar plots.

To visualize the module expression over the time between mild and severe case, the granulocyte data was grouped by the modules identified in Fig. 2 and the function geom_smooth with default parameters was used to calculate the estimated curve for the module gene expression over the time and a confidence band representing the uncertainty in the estimate.

### Data integration for disease comparison

To describe the differences and similarities between COVID-19 and other diseases, we searched in databases for genomics data such as Gene Expression Omnibus (GEO) [60] and ArrayExpress [61] for studies that fulfill certain criteria: (I) having at least 20 samples, (II) the disease of study was of relevance (other infections, such as bacterial and viral, plus diseases that mainly involve immune dysregulation, such as autoimmune disease), and (III) library preparation and sequencing technology differ as little as possible from our COVID-19 protocol, except for the influenza dataset which comes from a microarray experiment (GSE111368). The fastq files of 18 additional studies (PRJNA588242, GSE101705, GSE107104, GSE112087, GSE127792, GSE128078, GSE129882, GSE133378, GSE143507, GSE57253, GSE63042, GSE66573, GSE79362, GSE84076, GSE89403, GSE90081, GSE97590, GSE99992, and the Rhineland study) were downloaded and aligned with STAR. The counts were imported into R (v3.6.2) and were modeled for each gene using DESeq2. Merged raw counts from the RNA-seq studies were combined with the microarray study and were filtered for the genes present in the COVID-19 co-expression network, and ribosomal protein-coding genes and mitochondrial genes were removed, yielding a total of 5770 genes and 3176 samples. To account for differences in sequencing depth across studies as well as between RNA-seq and microarray data, a quantile normalization was performed on the filtered data. Group fold changes were calculated, where the grouping variable was set to be the disease status.

To explore COVID-19 associated expression of genes within the integrated dataset, the data was intersected with the gene modules previously retrieved from the COVID-19 CoCena$^2$ network, and the mean group fold changes were determined per cluster and condition and visualized in a heat map.

The modules were analyzed for enriched immune cell markers as provided by CIBERSORT and BD Rhapsody, and those that showed neutrophil enrichment were screened for genes representative of different neutrophil subtypes as recently described [34].

### Enrichment of signature from scRNA data of granulocytes

The signatures of different neutrophil states in COVID-19 as previously described [34] were enriched for the different clusters from CoCena$^2$.

To get a more fine-grained differentiation of the specific neutrophil states for Fig. 3, the authors kindly provided additional signatures from the scRNA dataset using a Wilcoxon rank sum test for differential gene expression implemented in Seurat. Genes had to be expressed in > 10% of the cells of a cluster, to exceed a logarithmic threshold > 0.1, and to have > 5% difference in the minimum detection between two clusters. The following additional comparisons were performed: 8 and 9 (pre- and immature neutrophils combined) vs the rest, and 1, 3, 4, and 6 (neutrophil states from control patients) vs the rest. To get unique signature genes for clusters 0, 2, and 5 (COVID-19-specific clusters), we took the following approach for each cluster: (1) calculate DEG for cluster 0 vs all other clusters, (2) calculate DEG for cluster 0 vs 2 and 5, (3) take intersection of these two calculations, and (4) remove genes that occur in more than one of these intersections of cluster 0, 2, or 5.

### Gene set enrichment analysis (GSVA)

The GSVA R package (v1.34.0) [62] was used to test the enrichment of neutrophil signatures [34] in the normalized gene expression table. The *gsva* method was used for the run and data were visualized in a heat map with the pheatmap (v1.0.12) package.

### Overview of drugs

An overview of currently used, recommended, or investigated drugs for treatment of COVID-19 patients was compiled from drug lists and lists of drugs in clinical trials downloaded from https://www.drugbank.ca/covid-19, https://www.pharmgkb.org/page/COVID, and https://clinicaltrials.gov/ct2/results?cond=COVID-19 (last update: 5 June 2020). Classification of the drugs was performed based on the ATC code, as well as additional

research on the drugs action. Drug target genes were identified using the DrugBank database [63] (Additional file 7: Table S6). The number of drugs currently recommended or investigated, and the number of clinical trials within the respective drug classes were visualized using the ggplot2 package [64, 65]. The target genes of the drugs currently recommended or investigated with a minimum frequency of 4 were visualized in a word cloud using the wordcloud package (version 2.6).

### Drug prediction

To identify drugs, which reverse the gene expression signature observed in the comparisons of the COVID-19-specific clusters compared to the control cluster, the drug prediction databases iLINCS (http://www.ilincs.org/ilincs/) and CLUE (https://clue.io/) were accessed. As input for the drug prediction, the top 1000 (iLINCS) or the top 100 (CLUE) DEGs were used. Drugs reversing the COVID-19 gene expression signature (defined by a negative score) were pooled together with drugs under investigation in current literature, resulting in a list of 940 unique drugs. Using the iLINCS API (https://github.com/uc-bd2k/ilincsAPI/blob/master/usingIlincsApis.Rmd), every gene expression signature from each drug listed in the signature libraries iLINCS chemical perturbagens (LINCSCP), iLINCS targeted proteomics signatures (LINCSTP), Disease-related signatures (GDS), Connectivity Map signatures (CMAP), DrugMatrix signatures (DM), Transcriptional signatures from EBI Expression Atlas (EBI), Cancer therapeutics response signatures (CTRS), and Pharmacogenomics transcriptional signatures (PG) was downloaded. Labeling was performed in the following principle: "drug name"_"database"_"database ID". Signatures were ordered by fold change, and only the top 300 genes were used. This resulted in a total of 62,897 unique drug signatures each with an up- and downregulated set. Subsequently, GSEA [66] was performed on the sequencing data for every up- and downregulated set for each drug and each cluster comparison. The resulting normalized enrichment scores (NES) were used to calculate the delta NES for each drug, defined as ΔNES = NES (down) – NES (up), ergo the difference of the NES from the downregulated set and the NES from the upregulated set of each respective drug. These ΔNES values were then *k*-mean clustered ($k = 40$). The clusters showing the highest ΔNES values for all comparisons and the cluster showing only high ΔNES in the comparison G1 vs G6 (most severe) were chosen and selected ones of the uniquely present drugs shown. The leading edge genes of the downregulation signatures of these drugs for the G1 vs G6 comparison were examined, and the frequency was counted. Recurring target genes were plotted on the CoCena[2] network.

Patterns of differential gene expression of genes targeted by drugs which are currently approved or under investigation for the treatment of COVID-19 patients were visualized using ggplot2. To this end, target genes of each drug and their first-degree neighbors were extracted from several databases and the gene co-expression networks, respectively. Regulation patterns of expression of these genes in different COVID-19 patient groups, as compared to the control group, were classified as up-/downregulated or not significant (n.s.) when pairwise comparisons of gene expression of COVID-19 patients and controls were not statistically significant. The same methodology was applied to genes not included in the drug-target list to identify genes which are not targeted by current drugs but could be potentially targeted by newly identified drugs.

## Results

### Whole blood transcriptomes reveal diversity of COVID-19 patients not explained by disease severity

To investigate the host immune response of COVID-19 patients in a systematic approach, whole blood transcriptomes were analyzed from 39 patients and 10 control donors recruited at the same hospital by RNA-sequencing (RNA-seq, Fig. 1a, Additional file 1: Table S1). Two-dimensional data representation using principal component analysis (PCA) showed separation of COVID-19 and control samples (Additional file 2: Figure S1A). Differential expression analysis identified 2289 upregulated and 912 downregulated genes comparing COVID-19 and control samples ($FC > |2|$, $padj < 0.05$; Fig. 1b). Upregulated genes showed greater fold changes than the downregulated genes (Fig. 1c). Of note, *CD177*, markedly expressed in neutrophils [67, 68], was the most prominently upregulated gene with the lowest *p* value. Heightened expression was further found for several granulocyte- and monocyte-associated molecules, such as Eosinophil-derived neurotoxin (*RNASE2*), Haptoglobin (*HP*), Neutrophil elastase (*ELANE*), Olfactomedin 4 (*OLFM4*), Myeloperoxidase (*MPO*), Resistin (*RETN*), matrix metalloproteinases (*MMP8*, *MMP9*), and alarmins (*S100A8*, *S100A9*, *S100A12*), as well as for cell cycle progression-associated genes (*G0S2*, *CDC6*, *CDC25A*), type I interferon (IFN)-induced genes (*IFI27*, *IFITM3*, *SIGLEC1* (CD169)), but also genes with immunosuppressive functions (*IL10*, *SOCS3*, *ARG1* (Arginase)). Downregulated genes included many lymphocyte-associated factors, such as *NELL2*, *RORC*, *KLRB1*, *TCF7* (TCF1), *RCAN3* (Calcipressin-3), *BACH2*, or *LEF1* (Fig. 1c, Additional file 3: Table S2). Functional analysis of the differentially expressed genes (DEGs) by gene ontology enrichment analysis (GOEA) revealed granulocyte and complement activation-associated terms enriched in the upregulated DEGs and lymphocyte

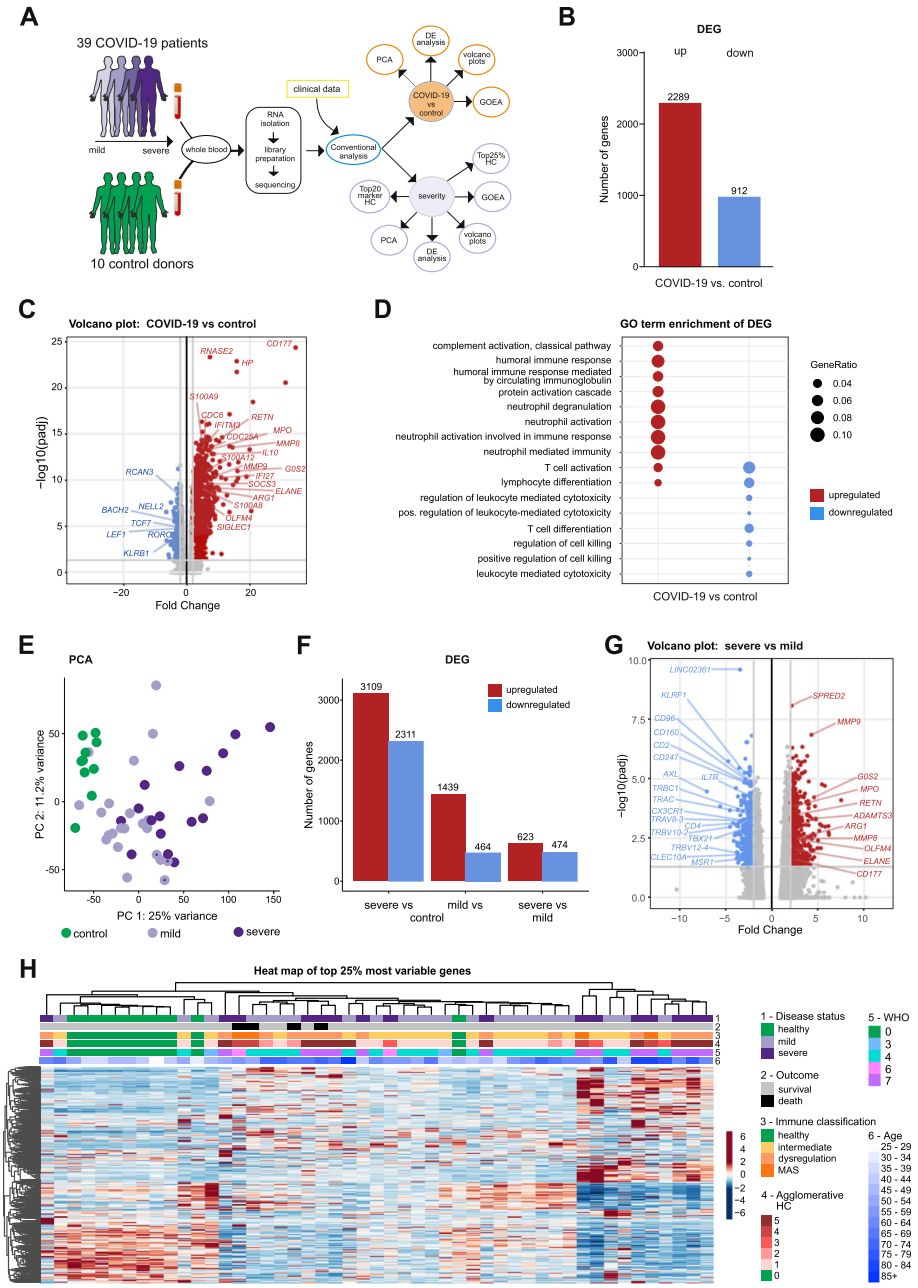


**Fig. 1** Whole blood transcriptomes reveal diversity of COVID-19 patients not explained by disease severity. **a** Schematic workflow for analysis of whole blood transcriptome data. **b** Number of significantly upregulated (red) and downregulated (blue) genes (FC > |2|, FDR-adj. *p* value < 0.05) comparing COVID-19 and control samples. **c** Volcano plot depicting fold changes (FC) and FDR-adjusted *p* values comparing COVID-19 and control samples. Differentially expressed up- (red) and downregulated genes (blue) are shown and selected genes are highlighted. **d** Plot of top 10 most enriched GO terms for significantly up- and downregulated genes, showing ratio of significantly regulated genes within enriched GO terms (GeneRatio). **e** PCA plot depicting relationship of all samples based on dynamic gene expression of all genes comparing mild and severe COVID-19 as well as control samples. **f** Number of significantly upregulated (red) and downregulated (blue) genes (FC > |2|, FDR-adj. *p* value < 0.05) comparing mild and severe COVID-19 as well as control samples. **g** Volcano plot depicting fold changes and FDR-adjusted *p* values comparing mild and severe COVID-19 as well as control samples. Differentially expressed up- (red) and downregulated genes (blue) are shown and selected genes are highlighted. **h** Hierarchical clustering map of 25% most variable genes between control patients and COVID-19 mild or severe patients, with additional annotation of disease outcome, hierarchical agglomerative clustering of clinical parameters COVID-19, the groups defined by agglomerative clustering, WHO ordinal score, and age bins

differentiation and T cell activation for the downregulated DEGs (Fig. 1d). Interestingly, the T cell activation-associated genes accounting for the enrichment of this term for the upregulated DEGs included *IL10* and *CD274* (PD-L1) pointing at suppressive T cell functionality (Additional file 3: Table S2).

Given the heterogeneous nature of clinical manifestation of COVID-19, we sought to stratify the transcriptomic profiles by disease severity based on WHO ordinal scale. Classification scores of 1–4 was considered as "mild" and 5–7 as "severe." Indeed, samples from patients with mild disease clustered more closely to the control samples, while those of severe cases scattered away in the PCA (Fig. 1e). Consequently, there was a greater number of DEGs in blood samples from severe COVID-19 patients than in mild patients when compared to controls (Fig. 1f). Many of the DEGs found in the COVID-19 vs control comparison (Fig. 1c) were also found when separating the COVID-19 samples by severity (Additional file 2: Figure S1B,C). Both, severe and mild COVID-19 in comparison to controls shared neutrophil-specific *CD177* and *HP* expression among the most upregulated DEGs, as well as lymphocyte-associated genes such as *ABLIM1*, *NELL2*, *RCAN3*, *RORC*, *BACH2*, and *KLRB1*, among the downregulated genes (Additional file 2: Figure S1B,C). GOEA reflected these findings (Additional file 2: Figure S1D). Although all samples from COVID-19 patients showed functional enrichment for granulocyte/neutrophil activation-associated terms in general, direct comparison of severe and mild COVID-19 patients revealed this to be a heightened characteristic of the immunoprofiles in severe COVID-19 (Additional file 2: Figure S1D). Upregulated DEGs in the severe vs mild sample comparison included *CD177*, Neutrophil elastase (*ELANE*), Olfactomedin 4 (*OLFM4*), Myeloperoxidase (*MPO*), Resistin (*RETN*), and matrix metalloproteinases *MMP8* and *MMP9*. Whereas the type I IFN-response genes, such as *IFI27* or *IFITM3*, were not differentially regulated in severe vs mild samples, expression of immunosuppression-associated factor Arginase (*ARG1*) was more pronounced in severe COVID-19 patients (Fig. 1g, Additional file 3: Table S2). Moreover, blood transcriptomes from severe cases showed decreased expression of lymphocyte-associated genes, such as the T cell receptor chains (*TRAC*, *TRBC1*), CD3 zeta chain (*CD247*), *CD4*, *CD2*, *TBX21* (TBET), and *IL7R*, as well as monocyte-associated genes, such as the fractalkine receptor (*CX3CR1*) or the macrophage scavenger receptor (*MSR1*) (Fig. 1g, Additional file 3: Table S2). Differences in gene expression were not restricted to granulocyte and T cell functions only: assessing the changes in defined gene groups, e.g., transcription factors, epigenetic regulators, and surface or secreted molecules, we observed many significant changes in genes that are not restricted to granulocytes or T cells, clearly indicating that other cell types are also transcriptionally altered in COVID-19 patients (Additional file 2: Figure S1E).

Distribution of the COVID-19 samples in the PCA revealed heterogeneity in the transcriptomic profiles (Fig. 1e), which might be due to clinical heterogeneity (Additional file 1: Table S1). In order to investigate this further, the top 25% of the most variable expressed genes were visualized in a heat map and samples sorted by unbiased hierarchical clustering based on their transcriptomic profiles, which resulted in more than three clusters suggesting higher transcriptional heterogeneity as explained by mild and severe COVID-19 cases vs control (Fig. 1h). Strikingly, neither disease, disease severity, nor the inclusion of outcome or immune classification [40] sufficiently explained the structure in the data. In order to get a better clinical understanding of the transcriptional data, we included further clinical parameters and grouped the COVID-19 patients accordingly (Fig. 1h). We therefore performed agglomerative hierarchical clustering using the clinical parameters that contributed most to the transcriptional differences observed across the first principal component of the dataset ($r$-adjusted square $\geq 0.1$, Additional file 2: Figure S1F). The COVID-19 patients were clustered into five clinical groups, which was the optimal number of clusters at which the intra-group variance was low and the "clusters distance" remained high (Additional file 2: Figure S1G,H). Interestingly, neither COVID-19 disease status, immune classification, nor our clinical parameter-based grouping of the COVID-19 patients aligned with overall transcriptional variability in the data (Fig. 1h), indicating that hidden information in the blood transcriptome may guide further patient stratification.

## Co-expression analysis discloses COVID-19 subgroups with distinct molecular signatures

Classical approaches to analyze the transcriptome data by using differential gene expression analysis based on sample groups defined by a selection of clinical parameters precluded dissection of the heterogeneity of the host immune response towards SARS-CoV-2 infection, which is evident in the high-parameter space of the transcriptome (Fig. 1). Co-expression analysis on the other hand identifies similarly regulated genes across samples and groups these genes into modules, which can then be explored for each patient sample individually or for entire patient groups. Applying such an approach using our established CoCena$^2$ pipeline [https://github.com/Ulas-lab/CoCena2] (Fig. 2a) for all 49 samples (39 COVID-19, 10 control) independent of their clinical annotation disclosed 10 co-expression modules, designated by color indianred to darkgrey, across a total of 6085 genes

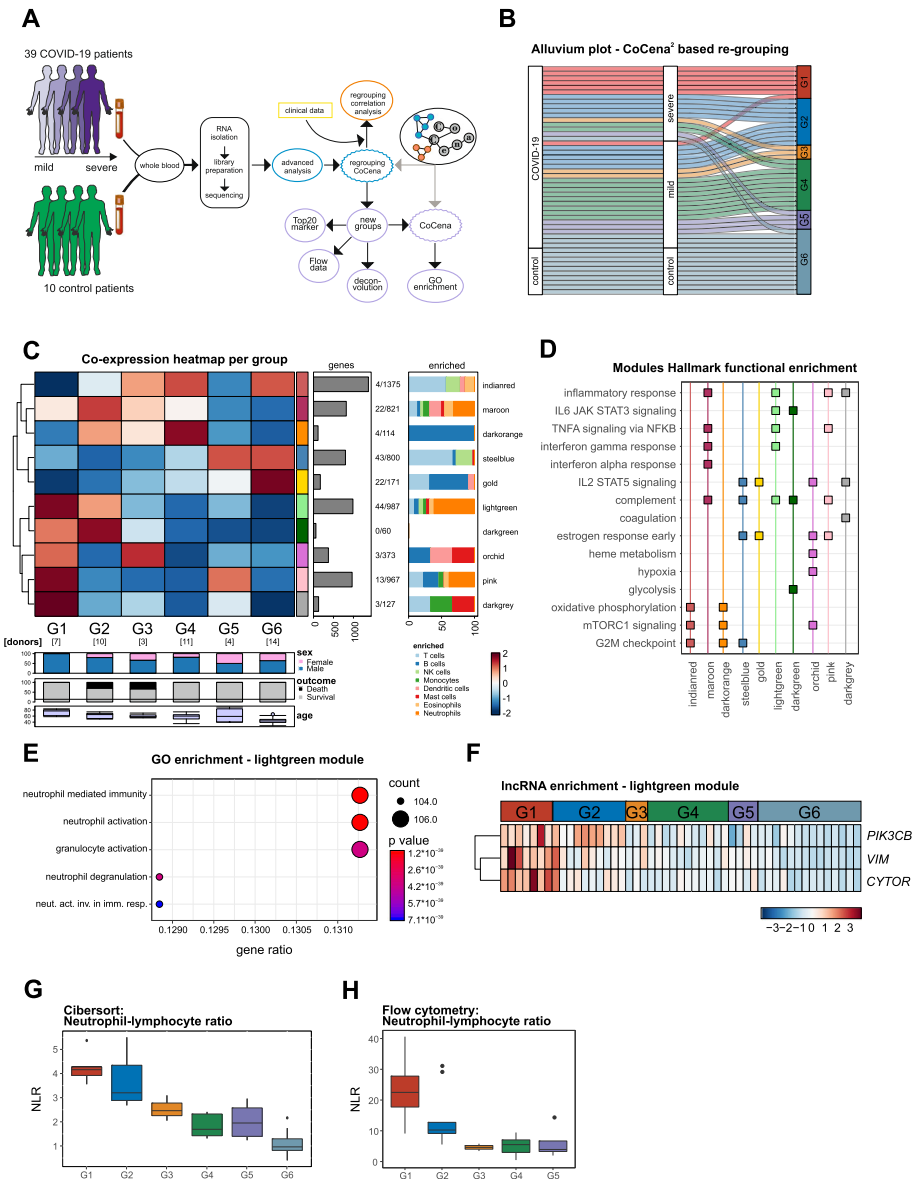


**Fig. 2** Co-expression analysis discloses COVID-19 subgroups with distinct molecular signatures. **a** Schematic overview of the analysis performed on the whole blood samples. **b** Alluvium plot visualizing the distribution of the samples according to different grouping; disease status, severity, and data-driven sample groups. **c** Group fold change heat map and hierarchical clustering for the six data-driven sample groups and the gene modules identified byCoCena[2] analysis. **d** Functional enrichment of CoCena[2]-derived modules using the Hallmark gene set database. Selected top terms were visualized. **e** Functional enrichment of CoCena[2] module lightgreen using GO gene set database. Top 5 terms were visualized. **f** Heat map presenting the normalized expression values of the lncRNA CYTOR, and protein-coding RNAs PIK3CB and VIM from the lightgreen CoCena[2] module. **g** Neutrophil-lymphocyte ratio plot after cell type deconvolution at lineage level. **h** Neutrophil-lymphocyte ratio across the six data-driven sample groups. Box plots show median with variance, with lower and upper hinges representing the 25th and 75th percentile, respectively

included in the analysis (Additional file 2: Figure S2A). Hierarchical clustering of the samples based on their group fold changes (GFCs) for each module revealed a data-driven patient stratification assorting the samples into six groups (Additional file 2: Figure S2B), which were subsequently used in all following analyses: five different COVID-19 sample-containing groups, which only partially grouped by disease severity and illustrated heterogeneity of the immune response in COVID-19 patients, plus one group containing all control as well as four COVID-19 samples (Fig. 2b + Additional file 2: Figure S2C). Overlaying this information onto the original PCA reflected structured sample stratification as the newly defined groups clustered together (Additional file

2: Figure S2D). GFC analysis of the newly generated groups revealed group-specific enrichment of co-expressed gene modules (Fig. 2c). GOEA on each of the modules identified associated gene signatures displaying distinct functional characteristics, which distinguish the different sample groups G1–G6 (Fig. 2d + Additional file 2: Figure S3, Additional file 4: Table S3). For example, "inflammatory response" was enriched in modules maroon, lightgreen, pink, and darkgrey, all characteristic for sample groups G1 and G2 to different extents, indicating these to possibly undergoing a more vigorous inflammatory immune reaction (Fig. 2c, d). Of note, G1 and G2 harbor a great fraction of samples from patients with severe COVID-19 (Fig. 2b). Only a slight increase in the inflammation-associated module maroon, an increase in expression in the genes of darkorange (enriched in oxidative phosphorylation, mTORC1 signaling, and cell cycle-associated genes), and a loss of expression in the gold module (connected to estrogen response genes and IL2 signaling) were indicative of the G4 sample group. G6, encompassing all control samples, was not associated with any modules connected to inflammatory processes, but showed higher expression of indianred, steelblue, and gold, all functionally enriched basic cellular and metabolic processes. Extended analysis of the lightgreen module, containing 987 genes, revealed a prominent enrichment of granulocyte/neutrophil activation-related signatures (Fig. 2e, Additional file 4: Table S3). To further explore this neutrophil activation signature association, we investigated possible co-expression patterns of long non-coding RNAs (lncRNA) that were reported as regulators of granulocyte function [59]. *CYTOR* (also known as *Morrbid*) is a lncRNA that mediates survival of neutrophils, eosinophils, and classical monocytes in response to pro-survival cytokines [59], and interacts with the protein-coding RNAs for the catalytic PI3K isoform phosphatidylinositol-4,5-bisphosphate 3-kinase catalytic subunit beta (*PIK3CB*) and the filament Vimentin (*VIM*) [69]. Interestingly, expression of *CYTOR* was significantly increased in severe COVID-19 patient group G1 ($p < 0.001$) and correlated with both *PIK3CB* ($r = 0.53$, $p < 0.001$) and *VIM* ($r = 0.55$, $p < 0.001$) (Fig. 2f).

Next, we asked whether the enrichment for neutrophil activation-associated signatures in G1 and G2 is attributed to an increased relative number of granulocytes within the whole blood sample. Deconvolution of the expression values using linear support vector regression [50] showed increased relative percentages of neutrophils especially in G1 and G2 (Additional file 2: Figure S2E). G5, on the other hand, clearly displayed an increased percentage of monocytes. At the same time, lymphocyte enrichment was found to be reduced in the COVID-19 sample groups, most prominently in G1 and G2 (Additional file 2: Figure S2E). The linear deconvolution results were then validated by flow cytometry. Blood composition of COVID-19 donors confirmed an increased number of neutrophils and a decreased number of lymphocytes especially in G1 and G2 (Additional file 2: Figure S2F). As a result, the neutrophil-lymphocyte ratio (NLR), a clinical marker proposed for disease severity as it has been associated with an increased systemic inflammation [70, 71], was markedly elevated in G1 and G2 compared to the control sample-containing G6, both in the computationally deconvoluted results (Fig. 2g) as well as measured by flow cytometry (Fig. 2h). Interestingly, in context of the observation that men more often progress to severe COVID-19 than women [72], G1 encompasses samples from solely male patients (Additional file 2: Figure S2C). Analysis of the top 20 differentially expressed transcription factors, epigenetic regulators, and surface or secreted proteins for the six sample groups confirmed an increased inflammatory state, again most remarkably for G1 and G2, evident from the transcription factors of the STAT family, *STAT1*, *STAT3*, *STAT5B*, and *STAT6*; the surface marker *CSF3R* (G-CSF) or *FCGR3B* (CD16b); the secreted factors *GRN* or *IL1B*; or the epigenetic regulator *PADI4* (PAD4) (Additional file 2: Figure S2H).

We confirmed our findings of distinct molecular phenotypes in the blood of COVID-19 patients in a second independent cohort. Thirty patients, severely affected by SARS-CoV-2 infection, were sampled upon admission to the ICU. We stratified the obtained blood transcriptomes based on the module signatures from the co-expression analysis (Fig. 2c). The samples of the second cohort were filtered for the genes present in the COVID-19 co-expression network, group fold changes were calculated across all patients individually, and sample groups G1–G6 assigned according to their combinatorial module expression (Additional file 2: Figure S4A). Controls from the first cohort were included for comparison. Interestingly, in these ICU patients, we noted the transcriptome profiles from the second cohort to show greatest similarity to G1 and G2, which is in line with their severe phenotypes and our findings from the first cohort. Hierarchical clustering of the samples based on their group fold changes for each module stratified the samples of the second cohort into four groups (Additional file 2: Figure S4B). The control samples from the first cohort built one separate group, which we designated again as G6. To allow for group-specific comparison to the stratification within the first cohort (Fig. 2c), we calculated the mean GFCs of the four groups identified in the second cohort (Additional file 2: Figure S4C). Second cohort samples of the first group showed enrichment in modules lightgreen, pink, and darkgrey and were thus assigned most similar to G1; the third group of the new samples showed enrichment in modules maroon and darkorange, most similar to G2; and the remaining samples were stratified into an intermediate

group exhibiting stronger expression of genes from the darkorange as well as pink module indicating characteristics of both G1 and G2 (Additional file 2: Figure S4C).

Collectively, co-expression analysis (CoCena[2]) in whole blood transcriptomes reveals at least five molecular phenotypes of the host's immune response in COVID-19 patients with at least two different groups in clinically described severe COVID-19 patients. The two molecularly defined groups G1 and G2 are transcriptionally characterized by a pronounced neutrophilic signature, at the same time distinct in other cellular characteristics. Such molecular classification might serve as a basis for identifying clinical surrogates for patient stratification. Since whole blood transcriptomics captures functional changes in the host's peripheral immune response across all cell types, we next sought a more detailed investigation of the granulocyte compartment within the framework of the newly identified subgroups.

## Granulocytes from severe COVID-19 patients show a simultaneous increase in inflammatory and suppressive signatures

To investigate whether the activation signatures seen in whole blood of COVID-19 patients are not only due to disease-associated increase of the neutrophil population, granulocytes were sequenced and transcriptomes were analyzed from 16 longitudinally sampled patients (8 mild, 9 severe), resulting in 17 mild and 27 severe COVID-19 samples (Fig. 3a). Evaluation of the relative cell type composition within each sample using linear deconvolution predicted the samples to mainly consist of neutrophils, with comparable fractions of 79% on average (Additional file 2: Figure S5A). Exploratory analysis by PCA showed a separation between mild and severe COVID-19 patients' granulocyte samples, especially for the day 1–10 groups (Fig. 3b). Differential expression analysis identified 314 upregulated and 703 downregulated genes comparing severe and mild samples from day 1 to 10 after first symptoms, while comparison at a late disease stage showed less differences on gene level (445 up- and 1924 downregulated genes; FC > |2|, padj < 0.05; Fig. 3c, Additional file 5: Table S4). Whole blood transcriptome analysis showed enrichment of neutrophil activation-associated signatures (Fig. 2). Excluding the bias of alterations in neutrophil population size across conditions, gene set enrichment analysis on granulocyte samples now uncovered that differentially expressed genes between severe and mild COVID-19 patients are indeed characterized by an increase in granulocyte activation-associated factors (Additional file 2: Figure S5B). *CD177* is part of the granulocyte activation gene set and was indeed markedly increased in severe (day 1–10) compared to mild (day 1–10) COVID-19 samples (Fig. 3d). Also, the alarmin *S100A12* exhibited heightened expression in granulocytes from severe COVID-19 patients (Fig. 3d).

Next, we used the CoCena[2] modules from the whole blood analysis (Fig. 2c) to identify modules that are actually driven by alterations in neutrophil activation instead of a mere increase in the neutrophil population. To investigate the expression patterns in a longitudinal fashion, mean expression over time and a confidence interval were calculated for each module in the mild and severe cases, respectively. Modules being mainly expressed in the severe groups G1 and G2 (darkgreen, darkgrey, lightgreen, maroon, and pink) showed a shift towards upregulation of genes in the severe group compared to the mild group, except for module darkgrey (Fig. 3e). The other modules, darkorange, gold, indianred, orchid, and steelblue, presented mostly the opposite trend, being expressed at higher levels in the mild compared to the severe COVID-19 cases (Additional file 2: Figure S5C).

Recently, heterogeneity of neutrophils with distinct subsets associated with disease severity and phase was revealed by single-cell RNA-seq analysis in blood of COVID-19 patients [34]. Enrichment of the three signatures that related to severe COVID-19 in our granulocyte samples demonstrated that the findings obtained in the single-cell study were also discernible in bulk data, and the results in accordance with the reported phenotypes: premature/immature, severe inflammatory, and severe suppressive subset marker genes were markedly enriched in granulocytes from severe COVID-19 patients in the present study (Additional file 2: Figure S5D). Further analysis of this observation on the gene level displayed the heightened expression of pre-/immature neutrophil-associated markers in severe COVID-19 patients' granulocytes, such as FUT4 (CD15), metalloproteinase *MMP8*, alarmins (*S100A8/9*), NET formation-involved *PADI4*, or *NLRC4*, for which activating mutations have been reported to overtly trigger the inflammasome and thereby increase the risk to develop autoinflammatory syndrome [73, 74] (Fig. 3f). Marker genes attributed to the "mild mature activated" neutrophil subset [34], such as *ITGA4* or *SLC38A1*, were indeed elevated as well in the mild COVID-19 patients' granulocytes of this study. In line with the single-cell study, signs of an interferon response were observed irrespective of disease severity (*IFIT1*, *IFIT3*), while only severe COVID-19 patients' granulocytes featured expression of genes with suppressive functionality, such as *ARG1* or *CD274* (PD-L1) (Fig. 3f).

We next assessed the granulocyte samples based on the module signatures from the whole blood analysis. The granulocyte samples were filtered for the genes present in the COVID-19 co-expression network (Fig. 2c) and the group fold changes were calculated across all

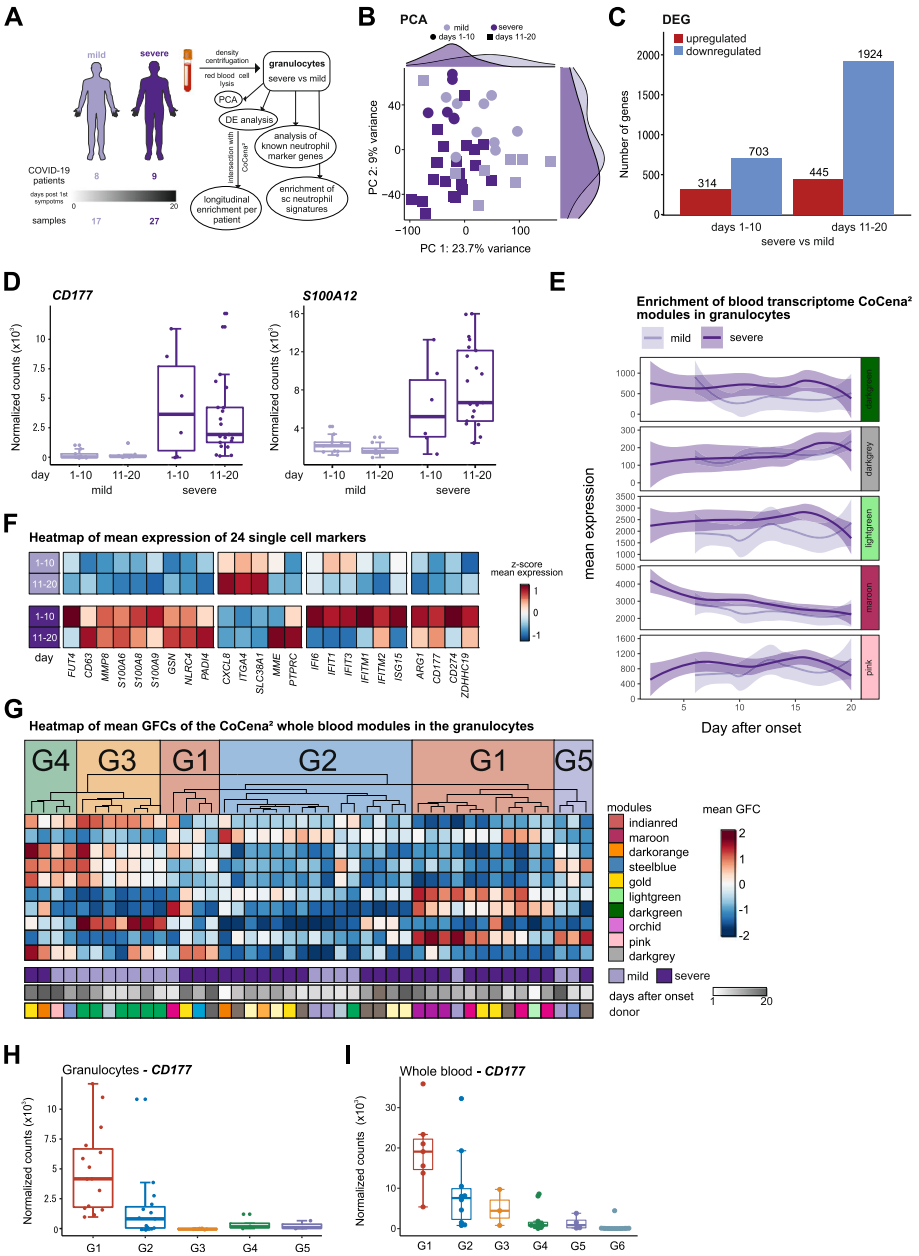


**Fig. 3** Granulocytes from severe COVID-19 patients show a simultaneous increase in inflammatory and suppressive signatures. **a** Schema of sample processing and analysis. **b** PCA of all genes within the dataset mapped by COVID-19 severity status. **c** Bar plot of DEGs between severe and mild COVID-19 patients at day 1–10 (left) and day 11–20 (right) (FC > |2|, FDR-adj. *p* value < 0.05). **d** Boxplot of CD177 (left) and S100A12 (right) in mild and severe COVID-19 patients at day 1–10 and 11–20. **e** Mean of group fold changes (GFCs) of the modules darkgreen, darkgrey, lightgreen, maroon, and pink in the granulocyte samples of mild (light purple) and severe (purple) COVID-19 cases over time. **f** Heat map of mean expression of 24 markers in mild (top) and severe (bottom) patients ordered by days after disease onset bins (day 1–10 and 11–20). **g** Heat map of mean GFCs of the CoCena$^2$ whole blood modules in the granulocyte samples from each individual patient. Patients are clusters by the mean GFC module expression. Severity patterns found in the whole blood CoCena$^2$ network were identified and patient groups were assigned accordingly (G1–G5). **h** Box plot of CD177 expression in granulocytes grouped by G1–G5. **i** Box plot of CD177 expression in whole blood grouped by G1–G6

patients individually; sample groups G1–G5 were assigned according to their combinatorial module expression (Figs. 2c + 3g). For example, samples attributed to G1 showed high enrichment scores in modules lightgreen, darkgreen, and pink, whereas those assigned as G2 additionally expressed the maroon module. Samples with the indianred/darkorange combination were designated as G4. Re-analysis of *CD177*, *NLRC4*, *ARG1*,

and *CD274* (PD-L1) as a function of the assigned sample groups (Fig. 3g) showed increased expression in G1 and G2 in relation to the other groups (Fig. 3h + Additional file 2: Figure S5E). Interestingly, the stratified patient groups in the whole blood data also depicted increased expression in G1 and G2 in comparison to the control-containing G6 (Fig. 3i + Additional file 2: Figure S5F).

Analysis of granulocyte samples from COVID-19 patients proved that, in addition to the relative increase in neutrophils in severe COVID-19 cases, there are indeed alterations in the transcriptional program of these cells themselves. We found enrichment of signatures typical of pre-/immature neutrophils and evidence of simultaneous inflammatory and suppressive features, arguing for a dysregulation in the peripheral granulocyte compartment. Importantly, transferring these findings back to the whole blood analysis showed that the granulocyte phenotypes were still observable within the whole blood transcriptomes.

### Integration with signatures from other diseases reveals COVID-19-specific characteristics

Putting COVID-19 into context of other known diseases, we compiled whole blood transcriptomes from 12 further diseases, including several viral and bacterial infections as well as immune-related disorders into one large dataset encompassing a total of 3176 samples including the 39 COVID-19 samples from this study (Fig. 4a, Additional file 2: Figure S6A, Additional file 6: Table S5). All in all, the dataset contains four other viral infection studies (chikungunya [30], HIV [27], influenza [75], and Zika [76], $n = 695$), seven bacterial infection studies (tuberculosis [24–27, 77], bacterial sepsis and systemic inflammatory response syndrome (SIRS, $n = 1578$) [28]), six inflammatory/autoimmune studies (systemic lupus erythematosus [78], Crohn's disease, rheumatoid arthritis [79], Ebola vaccination [29], neonatal-onset multisystem inflammatory disease (NOMID), and macrophage activation syndrome (NLRC4-MAS) [74], $n = 326$), and control samples from nine different studies ($n = 538$). To investigate how the COVID-19-specific co-expression modules can be linked to other diseases, the combined dataset was filtered for the genes present in the COVID-19 co-expression network (Fig. 2c) and the group fold changes were calculated across all samples (Fig. 4b). Additionally, cell type-specific signatures [50] and single cell-derived neutrophil subset signatures [34] (Additional file 7: Table S6) were intersected with all CoCena$^2$ modules. This analysis revealed that the lightgreen module shows a high (61%) neutrophil enrichment followed by module pink (38%) and maroon (32%), which is in line with a high functional enrichment for neutrophil activation in lightgreen (Fig. 2e, Additional file 4: Table S3). Genes within module lightgreen were most prominently upregulated in the severe COVID-19 group (G1) as well as in sepsis, in patients with influenza A and with tuberculosis and HIV infection, but less so in individually occurring HIV and tuberculosis (Fig. 4b). Enrichment of the neutrophil subset signatures revealed increased expression of genes found in pre-/immature neutrophils and those of inflammatory neutrophils associated with severe COVID-19. Many genes within module lightgreen are known to be related to induction of neutrophil extracellular traps (NET) (e.g., *PKC* [80], *PADI4* [81], *LTB4* [82]). Moreover, a link between excessive NET formation and tissue damage has been reported in sepsis [83]. Module darkgrey shares a similar expression pattern across the disease spectrum with lightgreen though being upregulated in infection with any of the four included influenza strains and contains genes involved in platelet activation. The NET-platelet-thrombin axis has been reported to be involved in the promotion of intravascular coagulation in sepsis [84]. The pink module shows the second highest neutrophil enrichment, which is dominated by the enrichment of pre-/immature neutrophil subtype signatures. It is strongly increased in sepsis, tuberculosis, and after Ebola vaccination as well as in autoinflammatory diseases such as rheumatoid arthritis, NLRC4-MAS, and NOMID, and shows slight overlap with the severe COVID-19 patients in group G1. It contains many epigenetic modifiers, such as *HDAC5*, *SETD1B*, or *KMT2D*, as well as *KLF2*, shown to regulate NF-κB-mediated immune functions, such as inflammation, erythropoiesis, and lung development [85]. Maroon is the third module with predicted neutrophil enrichment, which features genes from the "severe suppressive" subset alongside the "severe inflammatory" and pre-/immature subset signatures. It is associated with COVID-19 groups G2–4 and shares this characteristic with blood transcriptomes from the response to infection with chikungunya and Zika virus or from HIV patients suffering from tuberculosis.

A combination of single sample gene set variation analysis (ssGSVA), a non-parametric, unsupervised approach to estimate variation of gene set enrichment within each single sample, and Hallmark enrichment for each disease or inflammatory condition in the compiled dataset accentuated the findings on COVID-19 blood transcriptomes in context of the other diseases (Fig. 4c). "Interferon alpha and gamma responses" were enriched in acute viral infections with chikungunya and Zika virus as well as in HIV with or without concomitant tuberculosis or after Ebola vaccination, and this enrichment was shared with COVID-19 G2. "Inflammatory response," "IL6 and TNFA signaling" is an attribute of both G1 and G2, to a lesser degree of G5, also tuberculosis/HIV, and to some extent of sepsis and influenza A. More prominently enriched in sepsis were "complement,"

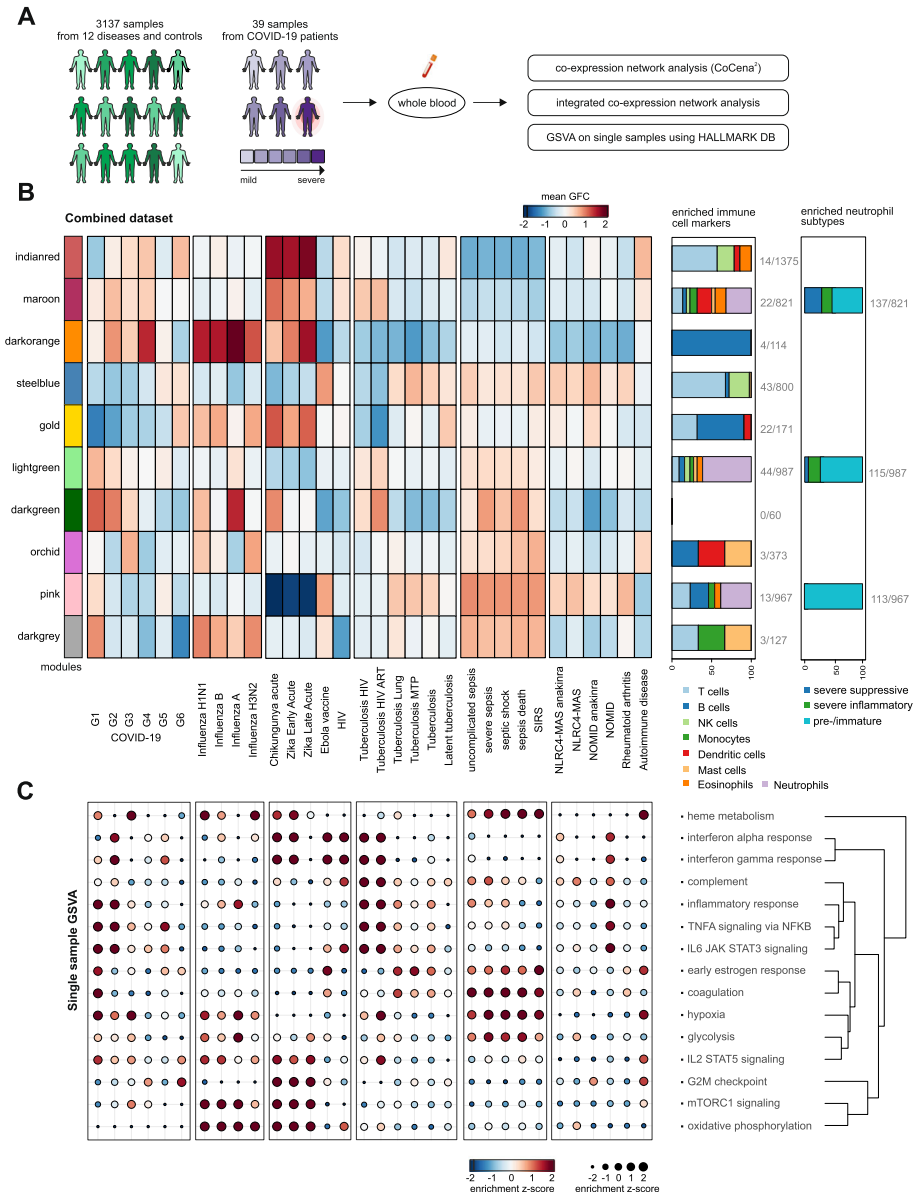


**Fig. 4** Integration with signatures from other diseases reveals COVID-19-specific characteristics. **a** Schema of analysis of the integrated dataset. The integrated dataset was analyzed with regard to expression patterns of the clusters previously identified in the whole blood COVID-19-specific co-expression network. **b** Heat map of mean group fold changes of CoCena[2] module comparison between COVID-19 and other diseases. From left to right, the diseases are ordered by category (COVID-19, viral infections, bacterial infections, and others). On the right side of the heat map, the first box plot shows the enriched immune cell markers in each module. The second box plot shows the enrichment of genes upregulated in specific neutrophil subtypes based on cross-referencing with single-cell data [34]. Both box plots show enriched cell types in percent of total hits; absolute hits with respect to cluster size are stated aside. **c** Gene set variation analysis was conducted for every single patient based on Hallmark gene sets as shown in Fig. 2d. The result was standardized to retrieve the *z*-scores; a disease mean was calculated and displayed as a dot plot with size and color correlating to the *z*-score. The labels on the *x*-axis are the same as in **b**

"coagulation," "heme metabolism," and "glycolysis" — shared by COVID-19 G1+G3, whereas "oxidative phosphorylation" and "mTORC1 signaling" were seen for all four influenza strains, chikungunya, and Zika virus infections — shared to some extent with COVID-19 G3+G4.

Although we observed overlaps of gene modules enriched in COVID-19 with several other infectious and immune-related diseases, each of our molecularly defined COVID-19 patient groups was characterized by a specific combination of these modules, clearly indicating the unique biology of this SARS-CoV-2 infection-mediated immune response, which needs to be considered when developing patient-stratified therapy regimens.

### COVID-19 patient subgroup-specific signatures can be used to predict potential drug repurposing

Despite the immunologically driven nature of COVID-19, most drugs that are currently investigated in clinical trials to combat or ameliorate COVID-19 are targeting the virus and its direct interaction partners (Additional file 2: Figure S7A+B, Additional file 8: Table S7). Compounds as well as the number of clinical trials performed with anti-inflammatory, immunosuppressive, and immunomodulatory properties are immensely outnumbered by other approaches. Examining the listed target genes of currently investigated drugs in our stratified patient groups, we found 162 included in our co-expression network analysis, most of which being differentially expressed in the severe patient group G1 in comparison to G6 (Figs. 2c + 5a). In addition, many of the regulated genes in our patient signatures are clearly not affected by the drugs that are currently investigated against COVID-19. The immunopathologies seen in COVID-19 patients, especially past their second week of symptoms, demand a host-directed, immune system-focused therapy.

To identify potentially beneficial drugs, we designed an in silico signature-based drug repurposing approach (Fig. 5b). To generate input signatures of interest, we characterized our stratified sample groups by identifying differentially expressed genes between groups G1–G5 and the control group G6 (Additional file 2: Figure S7C). Most transcriptional differences were observed for G1 (up: 4032, down: 4729) and G2 (up: 2336, down: 2767), whereas group G3 (up: 1193, down: 1921), G5 (up: 1089, down: 1216), and especially G4 (up: 727, down: 547) were less different to G6. Only a minor fraction of 137 DEGs was shared by all 5 comparisons. The most overlap of DEGs was observed between G1 and G2, the two groups comprising mostly severe COVID-19 patients. Nevertheless, G2 was still characterized by a large number of specific DEGs (Additional file 2: Figure S7C). GOEA of the upregulated DEGs of each comparison revealed enrichment of genes in the context of "neutrophil activation" and "coagulation" in all comparisons (Additional file 2: Figure S7D). Humoral and B cell-mediated immunity terms on the other hand were enriched the strongest in G4-specific upregulated DEGs (Additional file 2: Figure S7D). Differential expression analysis for the stratified sample groups once more emphasized that neutrophils play a central role in the host's immune response against SARS-CoV-2 infection. Neutrophils, as the most abundant circulating leukocytes, have become a therapeutic target of interest in multiple disease settings in recent years [86]. Two interesting target genes discussed in this context and already addressed in clinical trials are CXCR2 and C5AR1. Consistent with the increased NLR in G1 and G2, we observed significant upregulation of *CXCR2* and *C5AR1* in both groups (Additional file 2: Figure S7E).

Using patient cluster-specific DEGs as input (Additional file 2: Figure S7C, Additional file 9: Table S8), we searched for compounds that evoke a reverse signature in human cells via the NIH Library of Integrated Network-Based Cellular Signatures (iLINCS) [87] and the Broad Institute's Repurposing Hub [88]. The best counteracting signatures for each comparison were combined with signatures for all currently investigated drugs and downloaded for further analysis, resulting in about 63,000 signatures from 940 compounds/drugs. We performed gene set enrichment analysis for all signatures against our COVID-19 patient comparisons and calculated the difference of the up- and downregulated normalized enrichment score (ΔNES). A positive ΔNES indicates drug signatures that reverse our COVID-19 signatures, whereas drugs with a negative ΔNES induce signatures similar to the ones observed in COVID-19. Signatures were then grouped by *k*-means clustering revealing groups of drug signatures that reverse specific patient subgroup signatures (e.g., cluster 5) or those that have the highest impact on all patient subgroups (e.g., cluster 13, Fig. 5c). Among the top signatures in cluster 13 are methylprednisolone ($\Delta NES_{G1} = 7.13$), immunoglobulins ($\Delta NES_{G1} = 6.62$), methotrexate ($\Delta NES_{G1} = 4.21$), and pevonedistat ($\Delta NES_{G1} = 4.81$) which are all under investigation (clinicaltrials.gov), thereby proving that our in silico signature-based drug repurposing approach can indeed predict drugs that have already been deemed potentially beneficial in this disease (Additional file 2: Figure S7F). Extracting the leading edge of the most frequently targeted genes by the drugs included in cluster 13 revealed alarmins, such as *S100A8* or *S100A6*, and *SERPINB1*, critical for neutrophil survival by protecting the cell from proteases released into the cytoplasm during stress [89–91]. Visualizing these genes in the co-expression network deducted from the blood transcriptomes of our COVID-19 patient cohort identified most of them as part of cluster lightgreen and maroon (Additional file 2: Figure S7G). Sample group G1-specific drug signature cluster 5 also encompasses a considerable number of drugs currently being tested in clinical trials to fight COVID-19 (Fig. 5d + Additional file 2: Figure S7A, Additional file 10: Table S9). Interestingly, a lot of drug signatures in cluster 5 were related to female hormones, such as alpha-estradiol ($\Delta NES_{G1} = 2.83$), estradiol-cypionate ($\Delta NES_{G1} = 2.78$), estriol ($\Delta NES_{G1} = 2.78$), or chlormadinone acetate used in birth control pills ($\Delta NES_{G1} = 2.74$), but also for example dexamethasone ($\Delta NES_{G1} = 2.65$) that was recently reported to reduce mortality in severe COVID-19 cases requiring intubation, while showing no benefit for patients with milder disease courses [92]. The most frequently

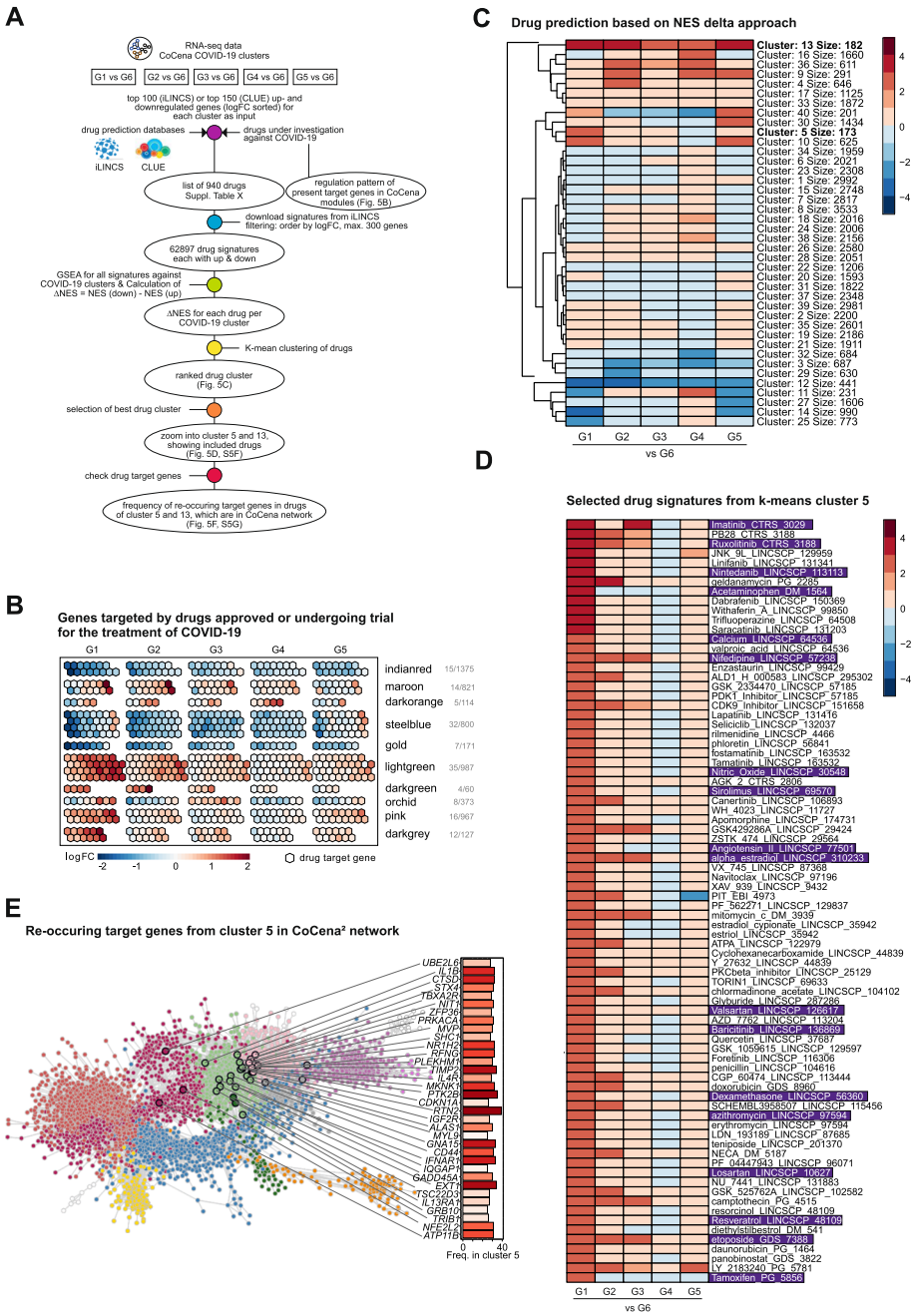


**Fig. 5** Patient subgroup-specific signatures can be used to predict potential drug targets. **a** Schematic workflow of the drug prediction analysis. Drug signatures were collected using the platforms iLINCS and CLUE. Signatures were selected by highest counteracting ΔNES score and combined with signatures of drugs under investigation from the literature. **b** Visualization of genes targeted by drugs approved or undergoing trial for the treatment of COVID-19 patients included in the whole blood co-expression network. Numbers of such genes from each module are designated on the right of the panel. Genes are represented as hexagons and colored by the expression fold change between COVID-19 patient severity group (G1–G5) and the control group (G6) (upregulated: red, downregulated: blue, not regulated: grey). **c** Drug predictions based on ΔNES score of drug signatures in regard to diseased patient group-specific gene expression patterns (G1–5 vs G6). Signatures were clustered by *k*-means clustering. A high ΔNES score accounts for drug signatures which counteract the gene expression of the patient group they are compared to. Drug signatures with a negative ΔNES score induce a gene expression pattern similar to the input. The number of signatures within a cluster determines its size. **d** Display of selected drug signatures from *k*-means cluster 5 from **c** showing the highest ΔNES score in the most severe COVID-19 patient group G1 and the least effect in patient group G4. **e** Visualization of recurring target genes in the G1 vs G6 comparison of cluster 5 signatures and their frequency mapped onto the CoCena$^2$ network

targeted genes within the signatures of cluster 5 included protein tyrosine kinase 2 beta (*PTK2B*), playing an important role for integrin-mediated neutrophil degranulation [93, 94]; lysosomal protease cathepsin D (*CTSD*) expressed in neutrophils and monocytes; and the inflammatory mediator interleukin-1β (*IL1B*) (Fig. 5e). The majority of these target genes cluster in the G1-specific lightgreen and pink, as well as in the maroon CoCena$^2$ modules. Drugs predicted to be effective for each module are presented as a resource as supplementary information for further inspection (Additional file 10: Table S9).

We used stratified blood transcriptomes from COVID-19 patients in an in silico signature-based approach to identify potential drugs for therapeutic repurposing. Many of our identified hits are indeed already being tested in clinical trials. Further, it became evident that, apart from common therapeutic avenues to address the immune dysregulation in COVID-19 patients, there are patient groups that may benefit from treatments targeting more precisely their immune phenotype and this phenotyping could be used for enrichment of patient groups in clinical trials.

## Discussion

The global spread of SARS-CoV-2 resulting in hundreds of thousands of COVID-19 cases urgently demands a more thorough molecular understanding of the pathophysiology of the disease [15, 20, 95, 96]. While vaccines are still under development [97–102], therapeutic management of the COVID-19 patients is key to mitigate the clinical burden as well as to prevent deaths. It has become clear that there is great variety in the occurrence of disease manifestation, and dysregulation of local and systemic immune responses have been implicated in disease heterogeneity [12–14, 22, 37, 38, 42, 95, 103, 104]. Here, by applying classical bioinformatics approaches and data-driven co-expression network analysis (CoCena$^2$) on blood transcriptomes of COVID-19 patients, we provide evidence for the existence of distinct molecular phenotypes that are not solely explained by current clinical and immunological parameters. Particularly in severe COVID-19, we detected dramatic transcriptional changes in the blood compartment with loss of T cell activation and concurrent gain of a rather unique combination of neutrophil activation signals, which was not simply due to changes in cell numbers since isolated neutrophils showed the same transcriptional changes. CoCena$^2$ allowed us to group functionally related genes into 10 major transcriptional modules with distinct expression patterns across five, on this basis newly defined COVID-19 patient groups, of which two (G1, G2) were related to severe disease courses. While pronounced neutrophil-related alterations were observed in both subgroups of severe COVID-19 patients (G1, G2), genes associated with coagulation and platelet function were mainly elevated in patients with the most highly elevated number of neutrophils as measured by flow cytometry, an information that was also deduced by linear support vector regression from transcriptome data. Assessment of non-coding RNA species from whole blood transcriptomes also allowed the identification for additional regulatory circuits. For example, we identify *CYTOR*, a lncRNA associated with granulocyte survival [59] strongly upregulated in COVID-19 patient group G1, which was accompanied by strong induction of CYTOR interactors such as *VIM* and *PIK3CB* [69]. These findings strongly support the notion that whole blood transcriptomics might not only be suitable for better understanding the systemic immune response in COVID-19 patients, but can also be used to predict novel therapeutic targets involving distinct pathophysiological mechanisms observed in COVID-19. In a "reverse transcriptome approach," we used the specific changes observed in the COVID-19-related transcriptional modules as the bait and searched for inverse correlation in thousands of drug-based transcriptome signatures to predict potential drug candidates. Most interestingly, we identified drug candidates that might be beneficial for all COVID-19 patients, but also candidates that might only be suitable for a subgroup of patients. Lastly, by comparing the transcriptional modules identified in whole blood of COVID-19 patients, we identified unique differences to other viral and bacterial infections, for which similar data were available, suggesting that blood transcriptomes might also be used diagnostically or for outcome prediction in larger clinical cohorts, treatment, or vaccine trials in the near future.

Classical bioinformatic assessment of blood transcriptome data comparing defined groups, in this study represented by control individuals and samples derived from either mild or severe COVID-19 patients, already revealed important biology of the systemic immune response. For example, the most significantly elevated transcript was *CD177*, a cell surface molecule on neutrophils, which was enhanced in both mild and severe cases (Fig. 1, Additional file 2: Figure S1), was recently identified by proteomics in bronchoalveolar lavage of COVID-19 patients [105], and has also been introduced as a hallmark for Kawasaki syndrome [106], a syndrome that has been observed in several studies being increased in children and adolescents during the SARS-CoV-2 pandemic [107–112]. In acute Kawasaki syndrome, elevated expression of *CD177* was associated with resistance to treatment with intravenous immunoglobulin (IVIG), a therapy in COVID-19 patients that is currently investigated in clinical trials around the world (18 trials, clinicaltrials.gov). Integrating the assessment of CD177 into these trials might help to stratify patients and better predict individual therapy outcome.

Hierarchical clustering of the most variable genes in the dataset already hinted towards further heterogeneity among patients beyond the current clinical differentiation into mild and severe patients (Fig. 1). Indeed, co-expression network analysis in a data-driven fashion allowed us to define five patient subgroups (G1–5) defined by 10 distinct transcriptional modules, which was corroborated in a second independent cohort (Fig. 2 + Additional file 2: Figure S4). Gene transcription observed in severe COVID-19 patients in G1 clearly differed from severe G2 COVID-19 patients particularly in modules darkgrey, pink, orchid, and maroon (Fig. 2c). For example, biological mechanisms related to the darkgrey module included blood coagulation, platelet activation, aggregation, and degranulation, as well as cell-cell adhesion and integrin-mediated signaling. These are all mechanisms that are integral to several of the complications observed in a subset of severe COVID-19 patients including increased disseminated intravascular coagulation [113–115], venous thromboembolism [113, 116], stroke [117, 118], or acute cor pulmonale [119]; neutrophil extracellular traps have been reported to contribute to immunothrombosis seen in pulmonary autopsies [120, 121]. All in all, these findings support the need for advanced molecular subtyping of COVID-19 patients, as proposed here based on blood transcriptomes. This is only one prominent example of the rich information within the new structure of molecular COVID-19 phenotypes that we provide here. For further inspection of the data, we refer the reader to the online tool that allows to extract module and group specific gene expression information (https://www.fastgenomics.org/).

In addition to many other infectious and non-infectious diseases [24–32], whole blood transcriptomics revealed important insights into the patient structure in COVID-19 and comparative analysis provides first evidence for the unique changes elicited by this disease within the host in comparison to other infections (Fig. 4). While cases in G2–4 shared changes with other viral infections such as influenza, chikungunya, or Zika, mainly including interferon signature genes (*IFI16*, *IFI35*, *IFIT1*, maroon module), partial overlap to bacterial sepsis was observed for G1–G3, albeit the major sepsis module (pink) was not prominently enriched in COVID-19 patients indicating that there are distinct differences in pathology of these two diseases. Although we could establish an integrative model using historical and publicly available blood transcriptome data, we also realized that limited standardization of the experimental procedures (sample processing, library production, sequencing) between different whole blood transcriptomics studies led to the exclusion of several additional important studies. In this context, it will be of great interest whether blood transcriptomics, as it was shown for tuberculosis [24, 25], can be utilized in large enough cohorts and clinical trials for disease risk or outcome prediction in COVID-19. We propose to collect whole blood transcriptomics data in a central registry for direct inspection by the research community and provide a prototype model for such a registry on FASTGenomics. Transcriptome data have been successfully used to predict a role for specific gene networks in the drug response to certain cancer types [122–126]. Considering the strong influence of the systemic immune response on severity and outcome of COVID-19, we wanted to establish whether the global assessment of molecular subgroups of COVID-19 patients could be utilized to predict novel drug targets for this disease addressing the dysregulated peripheral immune response of the host (Fig. 5). Using two major databases providing transcriptome signatures to many known drugs, CLUE [126] and iLINCS [125], we designed an in silico signature-based drug repurposing approach, allowing us to identify candidate drugs [127] that might reverse immune pathophysiology as observed in blood transcriptomes. Some of the candidate drugs identified are currently already in clinical trials, for example imatinib (NCT04394416, NCT04357613, NCT04346147, NCT04422678), ruxolitinib (20 trials listed), or nintedanib (NCT04338802, NCT04541680), for which prediction was particularly high in G1 patients. These trials might benefit from assessing molecular phenotypes of immune cells thereby determining whether patients with G1 type transcriptomes benefit most from such treatment. First study reports have recently declared strong benefit for dexamethasone treatment in severe COVID-19 cases requiring intubation, while no effect on mortality was seen for those patients who did not require respiratory support [23, 92]. Of note, drugs predicted to potentially reverse the transcriptome signatures of the severely affected G1 group may have adverse effects in milder COVID-19 cases from G4 as observed in the contrasting regulation patterns in many of the clusters (Fig. 5c). Interestingly and in line with the reports on sexual dimorphism in COVID-19 severity and mortality [128], G1 included only male patients and many of the drugs predicted to reverse the G1-specific signatures were related to female hormones (Fig. 5d). However, we also predicted drugs for all COVID-19 patients already in clinical trials such as immunoglobulins (> 150 trials, clinicaltrials.gov), or methylprednisolone (19 trials), findings further supporting the value of our prediction approach. Despite these promising results, strongly suggesting that reverse transcriptomics is not only of value in cancer [122–124] but might also be used to identify drugs targeting the immune pathophysiology in COVID-19, we would also like to point out current limitations of our findings that need to be addressed in future studies. Predictions, as well as

also the molecular phenotypes for patient stratification, will further benefit from and focused by validation studies in independent COVID-19 patient cohorts, which is to be fostered by a central database for COVID-19 patients' blood transcriptome data. These additional studies will also be able to further address disease severity in combination with different patient demographics and additional clinical parameters. Nevertheless, we used samples from different countries, illustrating the generalizability. Furthermore, the molecularly derived and prioritized drug candidates presented here might be tested in very recently introduced pre-clinical models [129] prior to starting clinical trials. Irrespective of the current shortcomings, we favor such drug candidate identification, since it is based on interrogation of molecular data directly derived from patients' immune cells involved in the ongoing processes in the disease and therefore may increase the likelihood of a beneficial effect in patients.

## Conclusions

Collectively, we provide first evidence for whole blood transcriptomics to potentially become a valuable tool for distinguishing the peripheral immune response seen in COVID-19 from that in other infections in cases for which pathogen detection might be difficult, for monitoring and potentially predicting outcome of the disease, to further dissect molecular phenotypes of COVID-19, particularly of the host's immune system, also along the disease course over time, and to support drug target prediction for subgroups of patients. Clearly, in contrast to more sophisticated higher resolution methods, whole blood transcriptomes can be easily obtained in large clinical cohort studies and large clinical treatment trials yet providing an enormous information content about the molecular reactions of the host's immune system. We therefore propose a blood transcriptome registry following the model we introduce here on the FASTGenomics platform that would allow the scientific community to utilize the information for new clinical studies and to address further large-scale studies into pathophysiological mechanisms of the disease and enhance the chances of trials to demonstrate a clinical benefit in patients.

## Supplementary Information

The online version contains supplementary material available at https://doi.org/10.1186/s13073-020-00823-5.

**Additional file 1: Table S1.** Cohort statistics.

**Additional file 2: Supplementary Figures S1-S8.**

**Additional file 3: Table S2.** Differential genes.

**Additional file 4: Table S3.** CoCena modules.

**Additional file 5: Table S4.** Granulocytes anno, differential genes and neutrophil subtypes.

**Additional file 6: Table S5.** Overview of datasets.

**Additional file 7: Table S6.** Immune cell type signatures.

**Additional file 8: Table S7.** Drugs overview.

**Additional file 9: Table S8.** Differential genes of groups G1-G6.

**Additional file 10: Table S9.** Predicted drugs.

### Acknowledgements

We thank Claudia Finnemann for perfect technical assistance.

*Deutsche COVID-19 Omics Initiative (DeCOI)*

Janine Altmüller, Angel Angelov, Robert Bals, Alexander Bartholomäus, Anke Becker, Michael Bitzer, Ezio Bonifacio, Peer Bork, Nicolas Casadei, Thomas Clavel, Maria Colome-Tatche, Andreas Diefenbach, Alexander Dilthey, Nicole Fischer, Konrad Förstner, Sören Franzenburg, Julia-Stefanie Frick, Gisela Gabernet, Julien Gagneur, Tina Ganzenmüller, Marie Gauder, Siri Göpel, Alexander Goesmann, Torsten Hain, André Heimbach, Michael Hummel, Angelika Iftner, Thomas Iftner, Stefan Janssen, Jörn Kalinowski, René Kallies, Birte Kehr, Andreas Keller, Sarah Kim-Hellmuth, Christoph Klein, Oliver Kohlbacher, Karl Köhrer, Jan Korbel, Denise Kühnert, Ingo Kurth, Markus Landthaler, Yang Li, Kerstin Ludwig, Oliwia Makarewicz, Manja Marz, Alice McHardy, Christian Mertes, Sven Nahnsen, Markus Nöthen, Peter Nürnberg, Uwe Ohler, Stephan Ossowski, Jörg Overmann, Klaus Pfeffer, Anna R. Poetsch, Alfred Pühler, Nikolaus Rajewsky, Markus Ralser, Olaf Rieß, Stephan Ripke, Ulisses Nunes da Rocha, Philip Rosenstiel, Antoine-Emmanuel Saliba, Leif Erik Sander, Birgit Sawitzki, Philipp Schiffer, Wulf Schneider, Eva-Christina Schulte, Joachim L. Schultze, Alexander Sczyrba, Yogesh Singh, Michael Sonnabend, Oliver Stegle, Jens Stoye, Fabian Theis, Janne Vehreschild, Jörg Vogel, Max von Kleist, Andreas Walker, Jörn Walter, Dagmar Wieczorek, Sylke Winkler, John Ziebuhr

### Authors' contributions

Conceptualization: ACA, FLvdV, MGN, JLS, MK, and TU; methodology: MO, MN-G, LB, NR, KB, RK, TSK, CK, MH, LH, IG, SA, KD, LL, NB, MB, KH, MK, HT, SM, EDD, and TU; formal analysis: ACA, MO, MN-G, LB, NR, KB, RK, TP, TSK, CK, MH, LH, AH, IG, SA, KD, LL, NB, JG, JS-S, LS, and TU; investigation: ACA, MO, MN-G, LB, NR, KB, RK, TP, TSK, CK, MH, LH, AH, IG, SA, KD, LL, NB, JS-S, JLS, and TU; resources: MM, BK, NK, KG, MS, SD, NR, JR, KMK, MTV, GR, VT, DS, AA, PP, MK, MMBB, JN, AK, and EJG-B; writing—original draft: ACA, MO, MN-G, LB, NR, KB, RK, TP, TSK, CK, MH, LH, AH, IG, KD, MvU, AD, JLS, and TU; writing—review and editing: ACA, BK, MO, MN-G, LB, NR, KB, RK, AD, FLvdV, MGN, JLS, MK, MMBB, JN, EJG-B, and TU; visualization: ACA, MO, MN-G, LB, NR, KB, RK, TP, TSK, CK, MH, LH, AH, IG, SA, KD, MvU, LL, NB, JLS, and TU; supervision: ACA, JLS, MK, MMBB, JN, and TU; funding acquisition: ACA, JLS, MMBB, and EJG-B. All authors read and approved the final manuscript.

### Funding

ACA was supported by an intramural grant from the Department of Genomics & Immunoregulation at the LIMES Institute. The work of JLS and MMBB was supported by the German Research Foundation (DFG) under Germany's Excellence Strategy – EXC2151 – 390873048 as well as by the Diet-Body-Brain Competence Cluster in Nutrition Research funded by the Federal Ministry of Education and Research (grant numbers 01EA1410C and 01EA1809C). JLS was further supported by the DFG under SCHU 950/8-1; GRK 2168, TP11; SFB704, the EU project SYSCID under grant number 733100. MGN was supported by a Spinoza grant of the Netherlands Organisation for Scientific Research and an ERC Advanced Grant (833247). The study was funded in part by the Hellenic Institute for the Study of Sepsis. EJG-B received funding from the FrameWork 7 program HemoSpec and from the Horizon2020 Marie-Curie project European Sepsis Academy (granted to the National and Kapodistrian University of Athens). JN was supported by the DFG (SFB TR57, SPP1937), the DZIF, and the Hector-Foundation (M89). Design of the study; collection, analysis, and interpretation of data; and writing of the manuscript were done independently from the funding bodies. Open Access funding enabled and organized by Projekt DEAL.

### Availability of data and materials

The data that support the findings of this study, including transcriptome data from 95 patients (123 samples) at multiple time points who granted informed consent to share such data, are made available at the European

Genome-Phenome Archive (EGA) under accession number EGAS00001004503, which is hosted by the EBI and the CRG. The Rhineland Study's dataset is not publicly available because of data protection regulations. Access to data can be provided to scientists in accordance with the Rhineland Study's Data Use and Access Policy. Requests for further information or to access the Rhineland Study's dataset should be directed to RS-DUAC@dzne.de. All scripts and all processed data are available under https://github.com/schultzelab/COVID-19-blood-bulk-RNA-Seq [130]. In addition to data deposition on EGA and Github, we provide an interactive platform for data inspection and analysis via FASTGenomics (fastgenomics.org). The FAST Genomics platform also provides normalized count tables of the datasets generated in this study. CoCena[2] is also available under https://github.com/Ulas-lab/CoCena2 [131].

The publicly available datasets analyzed during the current study are available from the

*EGA repository*

https://ega-archive.org/studies/EGAS00001004503 [132]

*GEO repository*

GSE111368 (https://www.ncbi.nlm.nih.gov/geo/query/acc.cgi?acc=GSE111368) [75]

GSE101705 (https://www.ncbi.nlm.nih.gov/geo/query/acc.cgi?acc=GSE101705) [26]

GSE107104 (https://www.ncbi.nlm.nih.gov/geo/query/acc.cgi?acc=GSE107104) [27]

GSE112087 (https://www.ncbi.nlm.nih.gov/geo/query/acc.cgi?acc=GSE112087) [78]

GSE127792 (https://www.ncbi.nlm.nih.gov/geo/query/acc.cgi?acc=GSE127792) [133]

GSE128078 (https://www.ncbi.nlm.nih.gov/geo/query/acc.cgi?acc=GSE128078) [134]

GSE129882 (https://www.ncbi.nlm.nih.gov/geo/query/acc.cgi?acc=GSE129882) [76]

GSE133378 (https://www.ncbi.nlm.nih.gov/geo/query/acc.cgi?acc=GSE133378) [32]

GSE143507 (https://www.ncbi.nlm.nih.gov/geo/query/acc.cgi?acc=GSE143507)

GSE57253 (https://www.ncbi.nlm.nih.gov/geo/query/acc.cgi?acc=GSE57253) [74]

GSE63042 (https://www.ncbi.nlm.nih.gov/geo/query/acc.cgi?acc=GSE63042) [28]

GSE66573 (https://www.ncbi.nlm.nih.gov/geo/query/acc.cgi?acc=GSE66573) [135]

GSE79362 (https://www.ncbi.nlm.nih.gov/geo/query/acc.cgi?acc=GSE79362) [24]

GSE84076 (https://www.ncbi.nlm.nih.gov/geo/query/acc.cgi?acc=GSE84076) [77]

GSE89403 (https://www.ncbi.nlm.nih.gov/geo/query/acc.cgi?acc=GSE89403) [25]

GSE90081 (https://www.ncbi.nlm.nih.gov/geo/query/acc.cgi?acc=GSE90081) [79]

GSE97590 (https://www.ncbi.nlm.nih.gov/geo/query/acc.cgi?acc=GSE97590) [29]

GSE99992 (https://www.ncbi.nlm.nih.gov/geo/query/acc.cgi?acc=GSE99992) [30]

*BioProject repository*

PRJNA588242 (https://www.ncbi.nlm.nih.gov/bioproject/PRJNA588242) [136].

## Ethics approval and consent to participate

The studies were conducted under the following ethics approvals: The 23/12.08.2019 approval of the Ethics Committee of Sotiria Athens General Hospital and the 26.02.2019 approval of the Ethics Committee of ATTIKON University General Hospital. Written informed consent was provided by patients or by first-degree relatives in case of patients unable to consent. Study samples from Nijmegen, the Netherlands, were obtained in accordance with the applicable rules concerning the review of research ethics committees and informed consent. All patients or legal representatives were informed about the study details and could decline to participate. The Bonn study was approved by the Institutional Review Board of the University Hospital Bonn (073/19 and 134/20). After providing written informed consent, 16 COVID-19 patients were included in the study. In-patients who were not able to consent at the time of study enrollment provided consent after recovery. Approval to undertake the Rhineland Study was obtained from the ethics committee of the University of Bonn, Medical Faculty. The study is carried out in accordance with the recommendations of the International Conference on Harmonization (ICH) Good Clinical Practice (GCP) standards (ICH-GCP). The research conformed to the principles of the Helsinki Declaration.

## Consent for publication

Not applicable.

## Competing interests

EJG-B has received honoraria (paid to the University of Athens) from AbbVie USA, Abbott CH, Angelini Italy, Biotest Germany, InflaRx GmbH, MSD Greece, and XBiotech Inc. He has received independent educational grants from AbbVie, Abbott, Astellas Pharma, AxisShield, bioMérieux Inc., InflaRx GmbH, and XBiotech Inc.

The remaining authors declare that they have no competing interests.

## Author details

[1]Systems Medicine, German Center for Neurodegenerative Diseases (DZNE), Bonn, Germany. [2]PRECISE Platform for Single Cell Genomics and Epigenomics at the German Center for Neurodegenerative Diseases and the University of Bonn, Bonn, Germany. [3]Genomics and Immunoregulation, Life & Medical Sciences (LIMES) Institute, University of Bonn, Bonn, Germany. [4]Department of Internal Medicine and Radboud Center for Infectious Diseases (RCI), Radboud University Medical Center, Nijmegen, The Netherlands. [5]4th Department of Internal Medicine, National and Kapodistrian University of Athens, Medical School, Athens, Greece. [6]Department I of Internal Medicine, University Hospital of Bonn (UKB), Bonn, Germany. [7]1st Department of Pulmonary Medicine and Intensive Care Unit, National and Kapodistrian University of Athens, Medical School, Athens, Greece. [8]West German Genome Center (WGGC), University of Bonn, Bonn, Germany. [9]Department of Intensive Care Medicine and Radboud Center for Infectious Diseases (RCI), Radboud University Medical Center, Nijmegen, The Netherlands. [10]Department of Gastroenterology, Hepatology and Infectious Diseases, University Hospital Düsseldorf, Heinrich Heine University Düsseldorf, Düsseldorf, Germany. [11]Population Health Sciences, German Center for Neurodegenerative Diseases (DZNE), Bonn, Germany. [12]Department of Internal Medicine II, Section of Pneumology, University Hospital of Bonn (UKB), Bonn, Germany. [13]Department of Neurology, Faculty of Medicine, University of Bonn, Bonn, Germany. [14]Immunology & Metabolism, Life and Medical Sciences (LIMES) Institute, University of Bonn, Bonn, Germany. [15]Institute for Medical Biometry, Informatics and Epidemiology (IMBIE), Faculty of Medicine, University of Bonn, Bonn, Germany. [16]German Center for Infection Research (DZIF), Bonn, Germany.

Received: 15 July 2020 Accepted: 18 December 2020
Published online: 13 January 2021

## References

1. Grubaugh ND, Petrone ME, Holmes EC. We shouldn't worry when a virus mutates during disease outbreaks. Nat Microbiol. 2020;5(4):529–530.
2. Fauver JR, Petrone ME, Hodcroft EB, Shioda K, Ehrlich HY, Watts AG, et al. Coast-to-coast spread of SARS-CoV-2 during the early epidemic in the United States. Cell. 2020;181(5):990–996.e5.
3. Zhou P, Yang X Lou, Wang XG, Hu B, Zhang L, Zhang W, et al. A pneumonia outbreak associated with a new coronavirus of probable bat origin. Nature. 2020;579(7798):270–3.
4. Brignola C, Campieri M, Farruggia P, Tragnone A, Pasquali S, Iannone P, et al. The possible utility of steroids in the prevention of relapses of Crohn's disease in remission: a preliminary study. J Clin Gastroenterol. 1988;10(6):631–4.
5. Guan W, Ni Z, Hu Y, Liang W, Ou C, He J, et al. Clinical characteristics of coronavirus disease 2019 in China. N Engl J Med. 2020;382(18):1708–20.
6. Huang C, Wang Y, Li X, Ren L, Zhao J, Hu Y, et al. Clinical features of patients infected with 2019 novel coronavirus in Wuhan, China. Lancet. 2020;395(10223):497–506.
7. Zhou F, Yu T, Du R, Fan G, Liu Y, Liu Z, et al. Clinical course and risk factors for mortality of adult inpatients with COVID-19 in Wuhan, China: a retrospective cohort study. Lancet. 2020;395(10229):1054–62.
8. Wang D, Hu B, Hu C, Zhu F, Liu X, Zhang J, et al. Clinical characteristics of 138 hospitalized patients with 2019 novel coronavirus-infected pneumonia in Wuhan, China. JAMA. 2020;323(11):1061–9.

9. Ong EZ, Chan YFZ, Leong WY, Lee NMY, Kalimuddin S, Haja Mohideen SM, et al. A dynamic immune response shapes COVID-19 progression. Cell Host Microbe. 2020;27(6):879–882.e2.
10. Wang B, Li R, Lu Z, Huang Y. Does comorbidity increase the risk of patients with covid-19: evidence from meta-analysis. Aging (Albany NY). 2020;12(7):6049–57.
11. Guan WJ, Liang WH, Zhao Y, Liang HR, Chen ZS, Li YM, et al. Comorbidity and its impact on 1590 patients with Covid-19 in China: a nationwide analysis. Eur Respir J. 2020;55(5):2000547.
12. Mathew D, Giles JR, Baxter AE, Oldridge DA, Greenplate AR, Wu JE, et al. Deep immune profiling of COVID-19 patients reveals distinct immunotypes with therapeutic implications. Science. 2020;369(6508):eabc8511.
13. Su Y, Chen D, Yuan D, Lausted C, Choi J, Dai CL, et al. Multi-omics resolves a sharp disease-state shift between mild and moderate COVID-19. Cell. 2020; 183(6):1479–1495.e20.
14. Lucas C, Wong P, Klein J, Castro TBR, Silva J, Sundaram M, et al. Longitudinal analyses reveal immunological misfiring in severe COVID-19. Nature. 2020; 584(7821):463-9.
15. Gandhi RT, Lynch JB, del Rio C. Mild or moderate Covid-19. N Engl J Med. 2020;383(18):1757-66.
16. Dugger SA, Platt A, Goldstein DB. Drug development in the era of precision medicine. Nat Rev Drug Discov. 2018;17(3):183-96.
17. Zumla A, Maeurer M, Chakaya J, Hoelscher M, Ntoumi F, Rustomjee R, et al. Towards host-directed therapies for tuberculosis. Nat Rev Drug Discov. 2015; 14(8):511-2.
18. Mullard A. Coordinating the COVID-19 pipeline. Nat Rev Drug Discov. 2020; 19(5):298.
19. Ledford H. Dozens of coronavirus drugs are in development — what happens next? Nature. 2020;581(7808):247-8.
20. Berlin DA, Gulick RM, Martinez FJ. Severe Covid-19. N Engl J Med. 2020; 383(25):2451-60.
21. Dimopoulos G, de Mast Q, Markou N, Theodorakopoulou M, Komnos A, Mouktaroudi M, et al. Favorable anakinra responses in severe Covid-19 patients with secondary hemophagocytic lymphohistiocytosis. Cell Host Microbe. 2020;28(1):117–123.e1.
22. Jamilloux Y, Henry T, Belot A, Viel S, Fauter M, El Jammal T, et al. Should we stimulate or suppress immune responses in COVID-19? Cytokine and anti-cytokine interventions, Autoimmun Rev. 2020;19(7):102567.
23. RECOVERY Collaborative Group H, Horby P, Lim WS, Emberson JR, Mafham M, Bell JL, et al. Dexamethasone in hospitalized patients with covid-19 - preliminary report. N Engl J Med. 2020:NEJMoa2021436.
24. Zak DE, Penn-Nicholson A, Scriba TJ, Thompson E, Suliman S, Amon LM, et al. A blood RNA signature for tuberculosis disease risk: a prospective cohort study. Lancet. 2016;387(10035):2312–22.
25. Thompson EG, Du Y, Malherbe ST, Shankar S, Braun J, Valvo J, et al. Host blood RNA signatures predict the outcome of tuberculosis treatment. Tuberculosis. 2017;107:48–58.
26. Leong S, Zhao Y, Joseph NM, Hochberg NS, Sarkar S, Pleskunas J, et al. Existing blood transcriptional classifiers accurately discriminate active tuberculosis from latent infection in individuals from south India. Tuberculosis. 2018;109:41–51.
27. Verma S, Du P, Nakanjako D, Hermans S, Briggs J, Nakiyingi L, et al. Tuberculosis in advanced HIV infection is associated with increased expression of IFNγ and its downstream targets. BMC Infect Dis. 2018;18(1): 220.
28. Tsalik EL, Langley RJ, Dinwiddie DL, Miller NA, Yoo B, van Velkinburgh JC, et al. An integrated transcriptome and expressed variant analysis of sepsis survival and death. Genome Med. 2014;6(11):111.
29. Rechtien A, Richert L, Lorenzo H, Martrus G, Hejblum B, Dahlke C, et al. Systems vaccinology identifies an early innate immune signature as a correlate of antibody responses to the Ebola vaccine rVSV-ZEBOV. Cell Rep. 2017;20(9):2251–61.
30. Michlmayr D, Pak TR, Rahman AH, Amir ED, Kim E, Kim-Schulze S, et al. Comprehensive innate immune profiling of chikungunya virus infection in pediatric cases. Mol Syst Biol. 2018;14(8):e7862.
31. Hill JA, Ikoma M, Zerr DM, Basom RS, Peddu V, Huang M-L, et al. RNA sequencing of the in vivo human herpesvirus 6B transcriptome to identify targets for clinical assays distinguishing between latent and active infections. J Virol. 2019;93(3):e01419–18.
32. Bartholomeus E, De Neuter N, Lemay A, Pattyn L, Tuerlinckx D, Weynants D, et al. Diagnosing enterovirus meningitis via blood transcriptomics: an alternative for lumbar puncture? J Transl Med. 2019;17(1):282.
33. Yang X, Yu Y, Xu J, Shu H, Xia J, Liu H, et al. Clinical course and outcomes of critically ill patients with SARS-CoV-2 pneumonia in Wuhan, China: a single-centered, retrospective, observational study. Lancet Respir Med. 2020;8(5):475–81.
34. Schulte-Schrepping J, Reusch N, Paclik D, Baßler K, Schlickeiser S, Zhang B, et al. Severe COVID-19 is marked by a dysregulated myeloid cell compartment. Cell. 2020;182(6):1419–1440.e23.
35. Zhang J-Y, Wang X-M, Xing X, Xu Z, Zhang C, Song J-W, et al. Single-cell landscape of immunological responses in patients with COVID-19. Nat Immunol. 2020;21(9):1107–18.
36. Wilk AJ, Rustagi A, Zhao NQ, Roque J, Martínez-Colón GJ, McKechnie JL, et al. A single-cell atlas of the peripheral immune response in patients with severe COVID-19. Nat Med. 2020;26(7):1070–6.
37. Arunachalam PS, Wimmers F, Mok CKP, Perera RAPM, Scott M, Hagan T, et al. Systems biological assessment of immunity to mild versus severe COVID-19 infection in humans. Science. 2020;369(6508):1210–20.
38. Hadjadj J, Yatim N, Barnabei L, Corneau A, Boussier J, Smith N, et al. Impaired type I interferon activity and inflammatory responses in severe COVID-19 patients. Science. 2020;369(6504):718–24.
39. Chen G, Wu D, Guo W, Cao Y, Huang D, Wang H, et al. Clinical and immunological features of severe and moderate coronavirus disease 2019. J Clin Invest. 2020;130(5):2620–9.
40. Giamarellos-Bourboulis EJ, Netea MG, Rovina N, Akinosoglou K, Antoniadou A, Antonakos N, et al. Complex immune dysregulation in COVID-19 patients with severe respiratory failure. Cell Host Microbe. 2020;27(6):992–1000.e3.
41. Del Valle DM, Kim-Schulze S, Huang H-H, Beckmann ND, Nirenberg S, Wang B, et al. An inflammatory cytokine signature predicts COVID-19 severity and survival. Nat Med. 2020;26(10):1636–43.
42. Merad M, Martin JC. Pathological inflammation in patients with COVID-19: a key role for monocytes and macrophages. Nat Rev Immunol. 2020;20(6): 355–62.
43. Messner CB, Demichev V, Wendisch D, Michalick L, White M, Freiwald A, et al. Ultra-high-throughput clinical proteomics reveals classifiers of COVID-19 infection. Cell Syst. 2020;11(1):11–24.e4.
44. Dobin A, Davis CA, Schlesinger F, Drenkow J, Zaleski C, Jha S, et al. STAR: ultrafast universal RNA-seq aligner. Bioinformatics. 2013;29(1):15–21.
45. Love MI, Huber W, Anders S. Moderated estimation of fold change and dispersion for RNA-seq data with DESeq2. Genome Biol. 2014;15(12):550.
46. Liberzon A, Subramanian A, Pinchback R, Thorvaldsdóttir H, Tamayo P, Mesirov JP. Molecular signatures database (MSigDB) 3.0. Bioinformatics. 2011;27(12):1739–40.
47. Yu G, Wang LG, Han Y, He QY. ClusterProfiler: an R package for comparing biological themes among gene clusters. Omi A J Integr Biol. 2012;16(5):284–7.
48. Fulton DL, Sundararajan S, Badis G, Hughes TR, Wasserman WW, Roach JC, et al. TFCat: the curated catalog of mouse and human transcription factors. Genome Biol. 2009;10(3):R29.
49. Uhlén M, Fagerberg L, Hallström BM, Lindskog C, Oksvold P, Mardinoglu A, et al. Tissue-based map of the human proteome. Science. 2015;347(6220): 1260419.
50. Newman AM, Liu CL, Green MR, Gentles AJ, Feng W, Xu Y, et al. Robust enumeration of cell subsets from tissue expression profiles. Nat Methods. 2015;12(5):453–7.
51. Ito K, Murphy D. Tutorial: application of ggplot2 to pharmacometric graphics. CPT Pharmacometrics Syst Pharmacol. 2013;2(10):e79.
52. Aloy P, Russell RB. Taking the mystery out of biological networks. EMBO Rep. 2004;5(4):349–50.
53. Kanehisa M, Goto S. KEGG: Kyoto Encyclopedia of Genes and Genomes. Nucleic Acids Res. 2000;28(1):27–30.
54. Liberzon A, Birger C, Thorvaldsdóttir H, Ghandi M, Mesirov JP, Tamayo P. The molecular signatures database hallmark gene set collection. Cell Syst. 2015;1(6):417–25.
55. Gene Ontology Consortium. Gene Ontology Consortium: going forward. Nucleic Acids Res. 2015;43(Database issue):D1049–56.
56. Fabregat A, Jupe S, Matthews L, Sidiropoulos K, Gillespie M, Garapati P, et al. The reactome pathway knowledgebase. Nucleic Acids Res. 2018;46(D1):D649–55.
57. Hansen M, Gerds TA, Nielsen OH, Seidelin JB, Troelsen JT, Olsen J. PcaGoPromoter - an R package for biological and regulatory interpretation of principal components in genome-wide gene expression data. PLoS One. 2012;7(2):e32394.
58. Lin Y, Liu T, Cui T, Wang Z, Zhang Y, Tan P, et al. RNAInter in 2020: RNA interactome repository with increased coverage and annotation. Nucleic Acids Res. 2020;48(D1):D189–97.

59. Tian X, Tian J, Tang X, Ma J, Wang S. Long non-coding RNAs in the regulation of myeloid cells. J Hematol Oncol. 2016;9(1):99.
60. Clough E, Barrett T. The Gene Expression Omnibus database. Methods Mol Biol. 2016;1418:93–110.
61. Athar A, Füllgrabe A, George N, Iqbal H, Huerta L, Ali A, et al. ArrayExpress update - from bulk to single-cell expression data. Nucleic Acids Res. 2019; 47(D1):D711–5.
62. Hänzelmann S, Castelo R, Guinney J. GSVA: gene set variation analysis for microarray and RNA-Seq data. BMC Bioinformatics. 2013;14:7.
63. Wishart DS, Feunang YD, Guo AC, Lo EJ, Marcu A, Grant JR, et al. DrugBank 5.0: a major update to the DrugBank database for 2018. Nucleic Acids Res. 2018;46(D1):D1074–82.
64. Wickham H. ggplot2: Elegant Graphics for Data Analysis. Springer-Verlag New York. 2016. ISBN 978-3-319-24277-4. https://cran.r-project.org/web/packages/ggplot2/citation.html.
65. Neth H, Gradwohl N. unikn: Graphical elements of the University of Konstanz's corporate design. Soc Psychol Decis Sci. 2019; [cited 2020 Jun 24]. Available from: https://www.spds.uni-konstanz.de/publication-page/unikn-graphical-elements-university-konstanzs-corporate-design.
66. Korotkevich G, Sukhov V, Sergushichev A. Fast gene set enrichment analysis. bioRxiv. 2019:060012 [cited 2020 Jun 24]. Available from: https://www.biorxiv.org/content/10.1101/060012v2.
67. Lalezari P, Murphy GB, Allen FH. NB1, a new neutrophil-specific antigen involved in the pathogenesis of neonatal neutropenia. J Clin Invest. 1971; 50(5):1108–15.
68. Grieshaber-Bouyer R, Nigrovic PA. Neutrophil heterogeneity as therapeutic opportunity in immune-mediated disease. Front Immunol. 2019;10:346.
69. Zhang Y, Xiang C, Wang Y, Duan Y, Liu C, Jin Y, et al. lncRNA LINC00152 knockdown had effects to suppress biological activity of lung cancer via EGFR/PI3K/AKT pathway. Biomed Pharmacother. 2017;94:644–51.
70. Shang W, Dong J, Ren Y, Tian M, Li W, Hu J, et al. The value of clinical parameters in predicting the severity of COVID-19. J Med Virol. 2020;92(10): 2188–92.
71. Yan X, Li F, Wang X, Yan J, Zhu F, Tang S, et al. Neutrophil to lymphocyte ratio as prognostic and predictive factor in patients with coronavirus disease 2019: a retrospective cross-sectional study. J Med Virol. 2020;92(11):2573–81.
72. Wenham C, Smith J, Morgan R. COVID-19: the gendered impacts of the outbreak. Lancet. 2020;395(10227):846–8.
73. Romberg N, Al Moussawi K, Nelson-Williams C, Stiegler AL, Loring E, Choi M, et al. Mutation of NLRC4 causes a syndrome of enterocolitis and autoinflammation. Nat Genet. 2014;46(10):1135–9.
74. Canna SW, De Jesus AA, Gouni S, Brooks SR, Marrero B, Liu Y, et al. An activating NLRC4 inflammasome mutation causes autoinflammation with recurrent macrophage activation syndrome. Nat Genet. 2014;46(10):1140–6.
75. Dunning J, Blankley S, Hoang LT, Cox M, Graham CM, James PL, et al. Progression of whole-blood transcriptional signatures from interferon-induced to neutrophil-associated patterns in severe influenza. Nat Immunol. 2018;19(6):625–35.
76. Michlmayr D, Kim EY, Rahman AH, Raghunathan R, Kim-Schulze S, Che Y, et al. Comprehensive immunoprofiling of pediatric zika reveals key role for monocytes in the acute phase and no effect of prior dengue virus infection. Cell Rep. 2020;31(4):107569.
77. de Araujo LS, Vaas LAI, Ribeiro-Alves M, Geffers R, Mello FCQ, de Almeida AS, et al. Transcriptomic biomarkers for tuberculosis: evaluation of DOCK9, EPHA4, and NPC2 mRNA expression in peripheral blood. Front Microbiol. 2016;7:1586.
78. Figgett WA, Monaghan K, Ng M, Alhamdoosh M, Maraskovsky E, Wilson NJ, et al. Machine learning applied to whole-blood RNA-sequencing data uncovers distinct subsets of patients with systemic lupus erythematosus. Clin Transl Immunol. 2019;8(12):e01093.
79. Shchetynsky K, Diaz-Gallo LM, Folkersen L, Hensvold AH, Catrina AI, Berg L, et al. Discovery of new candidate genes for rheumatoid arthritis through integration of genetic association data with expression pathway analysis. Arthritis Res Ther. 2017;19(1):19.
80. Gray RD, Lucas CD, Mackellar A, Li F, Hiersemenzel K, Haslett C, et al. Activation of conventional protein kinase C (PKC) is critical in the generation of human neutrophil extracellular traps. J Inflamm (Lond). 2013;10(1):12.
81. Rohrbach AS, Slade DJ, Thompson PR, Mowen KA. Activation of PAD4 in NET formation. Front Immunol. 2012;3:360.
82. Carestia A, Kaufman T, Rivadeneyra L, Landoni VI, Pozner RG, Negrotto S, et al. Mediators and molecular pathways involved in the regulation of neutrophil extracellular trap formation mediated by activated platelets. J Leukoc Biol. 2016;99(1):153–62.
83. Denning NL, Aziz M, Gurien SD, Wang P. Damps and nets in sepsis. Front Immunol. 2019;10:2536.
84. McDonald B, Davis RP, Kim SJ, Tse M, Esmon CT, Kolaczkowska E, et al. Platelets and neutrophil extracellular traps collaborate to promote intravascular coagulation during sepsis in mice. Blood. 2017;129(10):1357–67.
85. Jha P, Das H. KLF2 in regulation of NF-κB-mediated immune cell function and inflammation. Int J Mol Sci. 2017;18(11):2383.
86. Németh T, Sperandio M, Mócsai A. Neutrophils as emerging therapeutic targets. Nat Rev Drug Discov. 2020;19(4):253–75.
87. Pilarczyk M, Najafabadi MF, Kouril M, Vasiliauskas J, Niu W, Shamsaei B, et al. Connecting omics signatures of diseases, drugs, and mechanisms of actions with iLINCS. bioRxiv. 2019:826271 [cited 2020 Jun 24]. Available from: http://biorxiv.org/content/early/2019/10/31/826271.abstract.
88. Corsello SM, Bittker JA, Liu Z, Gould J, McCarren P, Hirschman JE, et al. The Drug Repurposing Hub: a next-generation drug library and information resource. Nat Med. 2017;23(4):405–8.
89. Baumann M, Pham CTN, Benarafa C. SerpinB1 is critical for neutrophil survival through cell-autonomous inhibition of cathepsin G. Blood. 2013; 121(19):3900–7.
90. Torriglia A, Martin E, Jaadane I. The hidden side of SERPINB1/leukocyte elastase inhibitor. Semin Cell Dev Biol. 2017;62:178–86.
91. Duplomb L, Rivière J, Jego G, Da Costa R, Hammann A, Racine J, et al. Serpin B1 defect and increased apoptosis of neutrophils in Cohen syndrome neutropenia. J Mol Med. 2019;97(5):633–45.
92. Low-cost dexamethasone reduces death by up to one third in hospitalised patients with severe respiratory complications of COVID-19. 2020 [cited 2020 Jun 24]. Available from: https://www.recoverytrial.net/files/recovery_dexamethasone_statement_160620_v2final.pdf.
93. Fuortes M, Melchior M, Han H, Lyon GJ, Nathan C. Role of the tyrosine kinase pyk2 in the integrin-dependent activation of human neutrophils by TNF. J Clin Invest. 1999;104(3):327–35.
94. Kamen LA, Schlessinger J, Lowell CA. Pyk2 is required for neutrophil degranulation and host defense responses to bacterial infection. J Immunol. 2011;186(3):1656–65.
95. Koff WC, Williams MA. Covid-19 and immunity in aging populations — a new research agenda. N Engl J Med. 2020;383(9):804–5.
96. Bao L, Deng W, Huang B, Gao H, Liu J, Ren L, et al. The pathogenicity of SARS-CoV-2 in hACE2 transgenic mice. Nature. 2020;583(7818):830–3.
97. Lee N, McGeer A. The starting line for COVID-19 vaccine development. Lancet. 2020;395(10240):1815–6.
98. Lurie N, Saville M, Hatchett R, Halton J. Developing covid-19 vaccines at pandemic speed. N Engl J Med. 2020;382(21):1969–73.
99. Callaway E. The race for coronavirus vaccines: a graphical guide. Nature. 2020;580(7805):576–7.
100. Sahin U, Muik A, Derhovanessian E, Vogler I, Kranz LM, Vormehr M, et al. COVID-19 vaccine BNT162b1 elicits human antibody and TH1 T cell responses. Nature. 2020;586(7830):594–9.
101. Walsh EE, Frenck RW, Falsey AR, Kitchin N, Absalon J, Gurtman A, et al. Safety and immunogenicity of two RNA-based covid-19 vaccine candidates. N Engl J Med. 2020;383(25):2439–50.
102. Anderson EJ, Rouphael NG, Widge AT, Jackson LA, Roberts PC, Makhene M, et al. Safety and immunogenicity of SARS-CoV-2 mRNA-1273 vaccine in older adults. N Engl J Med. 2020;383(25):2427–38.
103. Subbarao K, Mahanty S. Respiratory virus infections: understanding COVID-19. Immunity. 2020;52(6):905–9.
104. Vabret N, Britton GJ, Gruber C, Hegde S, Kim J, Kuksin M, et al. Immunology of COVID-19: current state of the science. Immunity. 2020;52(6):910–41.
105. Zeng H-L, Di C, Yan J, Yang Q, Han Q-Q, Li S-S, et al. Proteomic characteristics of bronchoalveolar lavage fluid in critical COVID-19 patients. FEBS J. 2020.
106. Huang YH, Lo MH, Cai XY, Liu SF, Kuo HC. Increase expression of CD177 in Kawasaki disease. Pediatr Rheumatol Online J. 2019;17(1):13.
107. Toubiana J, Poirault C, Corsia A, Bajolle F, Fourgeaud J, Angoulvant F, et al. Kawasaki-like multisystem inflammatory syndrome in children during the covid-19 pandemic in Paris, France: prospective observational study. BMJ. 2020;369:m2094.
108. Viner RM, Whittaker E. Kawasaki-like disease: emerging complication during the COVID-19 pandemic. Lancet. 2020;395(10239):1741–3.
109. Ronconi G, Teté G, Kritas SK, Gallenga CE, Caraffa A, Ross R, et al. SARS-CoV-2, which induces COVID-19, causes kawasaki-like disease in children: role of

pro-inflammatory and anti-inflammatory cytokines. J Biol Regul Homeost Agents. 2020;34(3):767–73.
110. Feldstein LR, Rose EB, Horwitz SM, Collins JP, Newhams MM, Son MBF, et al. Multisystem inflammatory syndrome in U.S. children and adolescents. N Engl J Med. 2020;383(4):334–46.
111. Dufort EM, Koumans EH, Chow EJ, Rosenthal EM, Muse A, Rowlands J, et al. Multisystem inflammatory syndrome in children in New York State. N Engl J Med. 2020;383(4):347–58.
112. Whittaker E, Bamford A, Kenny J, Kaforou M, Jones CE, Shah P, et al. Clinical characteristics of 58 children with a pediatric inflammatory multisystem syndrome temporally associated with SARS-CoV-2. JAMA. 2020;324(3):259–69.
113. Al-Samkari H, Karp Leaf RS, Dzik WH, Carlson JC, Fogerty AE, Waheed A, et al. COVID and coagulation: bleeding and thrombotic manifestations of SARS-CoV2 infection. Blood. 2020;136(4):489–500.
114. Kander T. Coagulation disorder in COVID-19. Lancet Haematol. 2020;7(9):e630–2.
115. Lo MW, Kemper C, Woodruff TM. COVID-19: complement, coagulation, and collateral damage. J Immunol. 2020;205(6):1488–95.
116. Klok FA, Kruip MJHA, van der Meer NJM, Arbous MS, Gommers DAMPJ, Kant KM, et al. Incidence of thrombotic complications in critically ill ICU patients with COVID-19. Thromb Res. 2020;191:145–7.
117. Oxley TJ, Mocco J, Majidi S, Kellner CP, Shoirah H, Singh IP, et al. Large-vessel stroke as a presenting feature of covid-19 in the young. N Engl J Med. 2020;382(20):e60.
118. Ellul MA, Benjamin L, Singh B, Lant S, Michael BD, Easton A, et al. Neurological associations of COVID-19. Lancet Neurol. 2020;19(9):767–83.
119. Creel-Bulos C, Hockstein M, Amin N, Melhem S, Truong A, Sharifpour M. Acute cor pulmonale in critically ill patients with covid-19. N Engl J Med. 2020;382(21):e70.
120. Middleton EA, He X-Y, Denorme F, Campbell RA, Ng D, Salvatore SP, et al. Neutrophil extracellular traps contribute to immunothrombosis in COVID-19 acute respiratory distress syndrome. Blood. 2020;136(10):1169–79.
121. Zuo Y, Yalavarthi S, Shi H, Gockman K, Zuo M, Madison JA, et al. Neutrophil extracellular traps in COVID-19. JCI insight. 2020;5(11):e138999.
122. Tyner JW, Tognon CE, Bottomly D, Wilmot B, Kurtz SE, Savage SL, et al. Functional genomic landscape of acute myeloid leukaemia. Nature. 2018;562(7728):526–31.
123. Rambow F, Rogiers A, Marin-Bejar O, Aibar S, Femel J, Dewaele M, et al. Toward minimal residual disease-directed therapy in melanoma. Cell. 2018;174(4):843–855.e19.
124. Qiu Z, Li H, Zhang Z, Zhu Z, He S, Wang X, et al. A pharmacogenomic landscape in human liver cancers. Cancer Cell. 2019;36(2):179–193.e11.
125. Keenan AB, Jenkins SL, Jagodnik KM, Koplev S, He E, Torre D, et al. The Library of Integrated Network-Based Cellular Signatures NIH Program: system-level cataloging of human cells response to perturbations. Cell Systems. 2018;6(1):13–24.
126. Subramanian A, Narayan R, Corsello SM, Peck DD, Natoli TE, Lu X, et al. A next generation connectivity map: L1000 platform and the first 1,000,000 profiles. Cell. 2017;171(6):1437–1452.e17.
127. Zhou Y, Hou Y, Shen J, Huang Y, Martin W, Cheng F. Network-based drug repurposing for novel coronavirus 2019-nCoV/SARS-CoV-2. Cell Discov. 2020;6:14.
128. Scully EP, Haverfield J, Ursin RL, Tannenbaum C, Klein SL. Considering how biological sex impacts immune responses and COVID-19 outcomes. Nat Rev Immunol. 2020; 20(7):442–7.
129. Shi J, Wen Z, Zhong G, Yang H, Wang C, Huang B, et al. Susceptibility of ferrets, cats, dogs, and other domesticated animals to SARS-coronavirus 2. Science. 2020;368(6494):1016–20.
130. Aschenbrenner AC, Ulas T. COVID-19 blood bulk RNA-seq scripts+data. 2020. Available from: github.com/schultzelab/COVID-19-blood-bulk-RNA-Seq.
131. Ulas T. CoCena[2]. 2019. Available from: https://github.com/Ulas-lab/CoCena2.
132. Aschenbrenner AC, Ulas T. Peripheral immunoprofiling of stratifies COVID-19 patients based on disease-specific neutrophil signatures. EGAS00001004503. 2020. Available from: https://ega-archive.org/studies/EGAS00001004503.
133. Martin JM, Avula R, Nowalk MP, Lin CJ, Horne WT, Chandran UR, et al. Inflammatory mediator expression associated with antibody response induced by live attenuated vs inactivated influenza virus vaccine in children. Open Forum Infect Dis. 2018;5(11):ofy277.
134. Bouquet J, Li T, Gardy JL, Kang X, Stevens S, Stevens J, et al. Whole blood human transcriptome and virome analysis of ME/CFS patients experiencing post-exertional malaise following cardiopulmonary exercise testing. PLoS One. 2019;14(3):e0212193.
135. Spurlock CF, Tossberg JT, Guo Y, Sriram S, Crooke PS, Aune TM. Defective structural RNA processing in relapsing-remitting multiple sclerosis. Genome Biol. 2015;16(1):58.
136. Tornheim JA, Madugundu AK, Paradkar M, Fukutani KF, Queiroz ATL, Gupte N, et al. Transcriptomic profiles of confirmed pediatric tuberculosis patients and household contacts identifies active tuberculosis, infection, and treatment response among Indian children. J Infect Dis. 2020;221(10):1647–58.

## Publisher's Note

Springer Nature remains neutral with regard to jurisdictional claims in published maps and institutional affiliations.

**Ready to submit your research? Choose BMC and benefit from:**

- fast, convenient online submission
- thorough peer review by experienced researchers in your field
- rapid publication on acceptance
- support for research data, including large and complex data types
- gold Open Access which fosters wider collaboration and increased citations
- maximum visibility for your research: over 100M website views per year

**At BMC, research is always in progress.**

**Learn more** biomedcentral.com/submissions

frontiers | Frontiers in Immunology

TYPE Original Research
PUBLISHED 20 November 2023
DOI 10.3389/fimmu.2023.1275136

Check for updates

OPEN ACCESS

EDITED BY
Ying Zhu,
Genentech Inc., United States

REVIEWED BY
Aurobind Vidyarthi,
Yale University, United States
Soumya Panigrahi,
Case Western Reserve University, United States

*CORRESPONDENCE
Anna C. Aschenbrenner
anna.aschenbrenner@dzne.de

†These authors share senior authorship

RECEIVED 09 August 2023
ACCEPTED 18 October 2023
PUBLISHED 20 November 2023

CITATION
Knoll R, Bonaguro L, dos Santos JC, Warnat-Herresthal S, Jacobs-Cleophas MCP, Blümel E, Reusch N, Horne A, Herbert M, Nuesch-Germano M, Otten T, van der Heijden WA, van de Wijer L, Shalek AK, Händler K, Becker M, Beyer MD, Netea MG, Joosten LAB, van der Ven AJAM, Schultze JL and Aschenbrenner AC (2023) Identification of drug candidates targeting monocyte reprogramming in people living with HIV. *Front. Immunol.* 14:1275136. doi: 10.3389/fimmu.2023.1275136

COPYRIGHT
© 2023 Knoll, Bonaguro, dos Santos, Warnat-Herresthal, Jacobs-Cleophas, Blümel, Reusch, Horne, Herbert, Nuesch-Germano, Otten, van der Heijden, van de Wijer, Shalek, Händler, Becker, Beyer, Netea, Joosten, van der Ven, Schultze and Aschenbrenner. This is an open-access article distributed under the terms of the Creative Commons Attribution License (CC BY). The use, distribution or reproduction in other forums is permitted, provided the original author(s) and the copyright owner(s) are credited and that the original publication in this journal is cited, in accordance with accepted academic practice. No use, distribution or reproduction is permitted which does not comply with these terms.

# Identification of drug candidates targeting monocyte reprogramming in people living with HIV

Rainer Knoll[1,2], Lorenzo Bonaguro[1,2], Jéssica C. dos Santos[3,4], Stefanie Warnat-Herresthal[1,2], Maartje C. P. Jacobs-Cleophas[3,4], Edda Blümel[1], Nico Reusch[1], Arik Horne[1,5], Miriam Herbert[1,6], Melanie Nuesch-Germano[1], Twan Otten[3,4], Wouter A. van der Heijden[3,4], Lisa van de Wijer[3,4], Alex K. Shalek[7,8,9], Kristian Händler[10,11], Matthias Becker[1], Marc D. Beyer[1,10], Mihai G. Netea[3,4,12], Leo A. B. Joosten[3,4,13], Andre J. A. M. van der Ven[3,4], Joachim L. Schultze[1,2,10†] and Anna C. Aschenbrenner[1*†]

[1]Systems Medicine, Deutsches Zentrum für Neurodegenerative Erkrankungen (DZNE), Bonn, Germany, [2]Genomics and Immunoregulation, Life and Medical Sciences Institute, University of Bonn, Bonn, Germany, [3]Department of Internal Medicine, Radboud University Medical Center, Nijmegen, Netherlands, [4]Radboud Center for Infectious Diseases, Radboud University Medical Center, Nijmegen, Netherlands, [5]Systems Hematology, Stem Cells & Precision Medicine, Max Delbrück Center - Berlin Institute for Medical Systems Biology (MDCBIMSB), Berlin, Germany, [6]In Vivo Cell Biology of Infection, Max Planck Institute for Infection Biology (MPIIB), Berlin, Germany, [7]Broad Institute at Massachusetts Institute of Technology (MIT) and Harvard, Boston, MA, United States, [8]Ragon Institute of Mass General Hospital (MGH), MIT, and Harvard, Cambridge, MA, United States, [9]Department of Chemistry, Institute for Medical Engineering and Science, Koch Institute, Cambridge, MA, United States, [10]Platform for Single Cell Genomics and Epigenomics (PRECISE), DZNE and University of Bonn, Bonn, Germany, [11]Institute for Human Genetics, University Hospital Schleswig-Holstein, Lübeck, Germany, [12]Immunology and Metabolism, Life and Medical Sciences Institute, University of Bonn, Bonn, Germany, [13]Department of Medical Genetics, Iuliu Hatieganu University of Medicine and Pharmacy, Cluj-Napoca, Romania

**Introduction:** People living with HIV (PLHIV) are characterized by functional reprogramming of innate immune cells even after long-term antiretroviral therapy (ART). In order to assess technical feasibility of omics technologies for application to larger cohorts, we compared multiple omics data layers.

**Methods:** Bulk and single-cell transcriptomics, flow cytometry, proteomics, chromatin landscape analysis by ATAC-seq as well as *ex vivo* drug stimulation were performed in a small number of blood samples derived from PLHIV and healthy controls from the 200-HIV cohort study.

**Results:** Single-cell RNA-seq analysis revealed that most immune cells in peripheral blood of PLHIV are altered in their transcriptomes and that a specific functional monocyte state previously described in acute HIV infection is still existing in PLHIV while other monocyte cell states are only occurring acute infection. Further, a reverse transcriptome approach on a rather small number of PLHIV was sufficient to identify drug candidates for reversing the transcriptional phenotype of monocytes in PLHIV.

10.3389/fimmu.2023.1275136

**Discussion:** These scientific findings and technological advancements for clinical application of single-cell transcriptomics form the basis for the larger 2000-HIV multicenter cohort study on PLHIV, for which a combination of bulk and single-cell transcriptomics will be included as the leading technology to determine disease endotypes in PLHIV and to predict disease trajectories and outcomes.

KEYWORDS

systems immunology, transcriptomics, HIV, monocytes, inflammation, drug repurposing

# Introduction

For people living with HIV (PLHIV), major risk factors for developing cardiovascular diseases (CVDs), neurocognitive impairment, frailty, and cancer are persistent low-grade inflammation and immune dysfunction even under long-term effective antiretroviral therapy (ART) (1–6). Although the adaptive immune system appears to play an important role (7), there is a growing body of evidence that suggests changes in the innate immune system as exemplified by elevated levels of circulating soluble CD163 and sCD14 derived from monocytes are critical (1, 8, 9). We and others have recently demonstrated that concentrations of pro-inflammatory monocyte-derived cytokines are elevated in serum from PLHIV, which was further validated when peripheral blood mononuclear cells were stimulated *ex vivo* with a number of pathogens or their derivatives resulting in increased levels of IL-1β (1, 10–14).

While CMV infection (15), the HIV reservoir itself (16), as well as microbial translocation (17) have been proposed as potential drivers of low-grade inflammation, the complex interplay between the different immune cell compartments in PLHIV is not fully understood. To study the role of different immune cells in the pathophysiology of persistent inflammation in PLHIV it will be necessary to apply higher-resolution single-cell technologies to larger cohorts of PLHIV (18–20). Based on our previous experience applying single-cell technologies to better understand the pathophysiology of COVID-19 (21–23) or chronic obstructive pulmonary disease (COPD) (24), we have recently suggested that large-scale studies should be preceded by smaller optimization studies for clinical application of omics technologies to a particular disease setting (25, 26).

Here, we describe a study using bulk and single-cell transcriptomics technologies as well as chromatin landscaping by ATAC-seq under clinically applicable conditions to assess the reprogramming of the peripheral immune cell compartment in PLHIV cohorts. Despite heterogeneity between individuals, scRNA-seq combined with bulk transcriptomics on a limited number of PLHIV included in this pilot study revealed important new information concerning the involvement of the monocyte compartment in persistent low-grade inflammation. Further, a reverse transcriptome approach in this setup allowed the identification of drug candidates reducing the inflammatory endophenotype, which we validated experimentally in an independent group of PLHIV.

# Results

## Bulk transcriptomes from PBMC of PLHIV are dominated by monocyte-related proinflammatory programs

We previously demonstrated in a cross-sectional study that PLHIV exhibits a proinflammatory profile in monocyte- but not lymphocyte-derived cytokines (1). We recalled five male PLHIV using long-term suppressive ART (mean 7.4 years) from the 200-HIV study with no overt clinical symptoms at the time of blood draw, determined as normal progressors, to investigate whether higher-resolution technologies down to the single-cell level would reveal further information about molecular and functional changes within the peripheral immune system in PLHIV. We generated a multi-layer dataset including selected soluble factors in plasma, multicolor flow cytometry (MCFC), bulk RNA-seq, Assay for Transposase-Accessible Chromatin using sequencing (ATAC-seq) and microwell-based scRNA-seq comparing five age- and sex-matched healthy controls (Figure 1A; Supplementary Table S1).

The MCFC data generated here indicate that the five PLHIV chosen were representative of the 200-HIV cohort with similar alterations in the circulating immune cell compartment (e.g. higher CD8+ and lower CD4+ T as well as NK cell population frequencies in PLHIV versus healthy donors) (11) (Figure S1A). Principal component analysis (PCA) of bulk RNA-seq of PBMC revealed a disease-associated separation of the samples (Figure 1B). Exploration of these alterations by differential gene expression analysis resulted in 287 up- and 914 down-regulated genes in PLHIV compared to control ($|FC|>1.5$, adj p-value $<0.05$, with independent hypothesis weighting (IHW) correction) (Figure S1B). Inspection of those differentially expressed genes (DEGs) in more detail by hierarchical clustering revealed four transcript clusters similarly regulated across the donors (Figure 1C). One cluster revealed a group of commonly upregulated early innate immune response genes for PLHIV and a second cluster contained typical interferon response genes (Figure 1C), which was corroborated by functional enrichment analysis (Figure 1D; Supplementary Table S2). Upregulation of alarmins *S100A8* and *S100A9* (cluster 1), which have been previously associated with inflammation (27, 28) indicated a strong signal from the myeloid cell compartment. In cluster 2, *STAT1*, previously linked to enhanced inflammation in HIV (29, 30), was strongly expressed. Both heatmap visualization (Figure 1C) and

10.3389/fimmu.2023.1275136

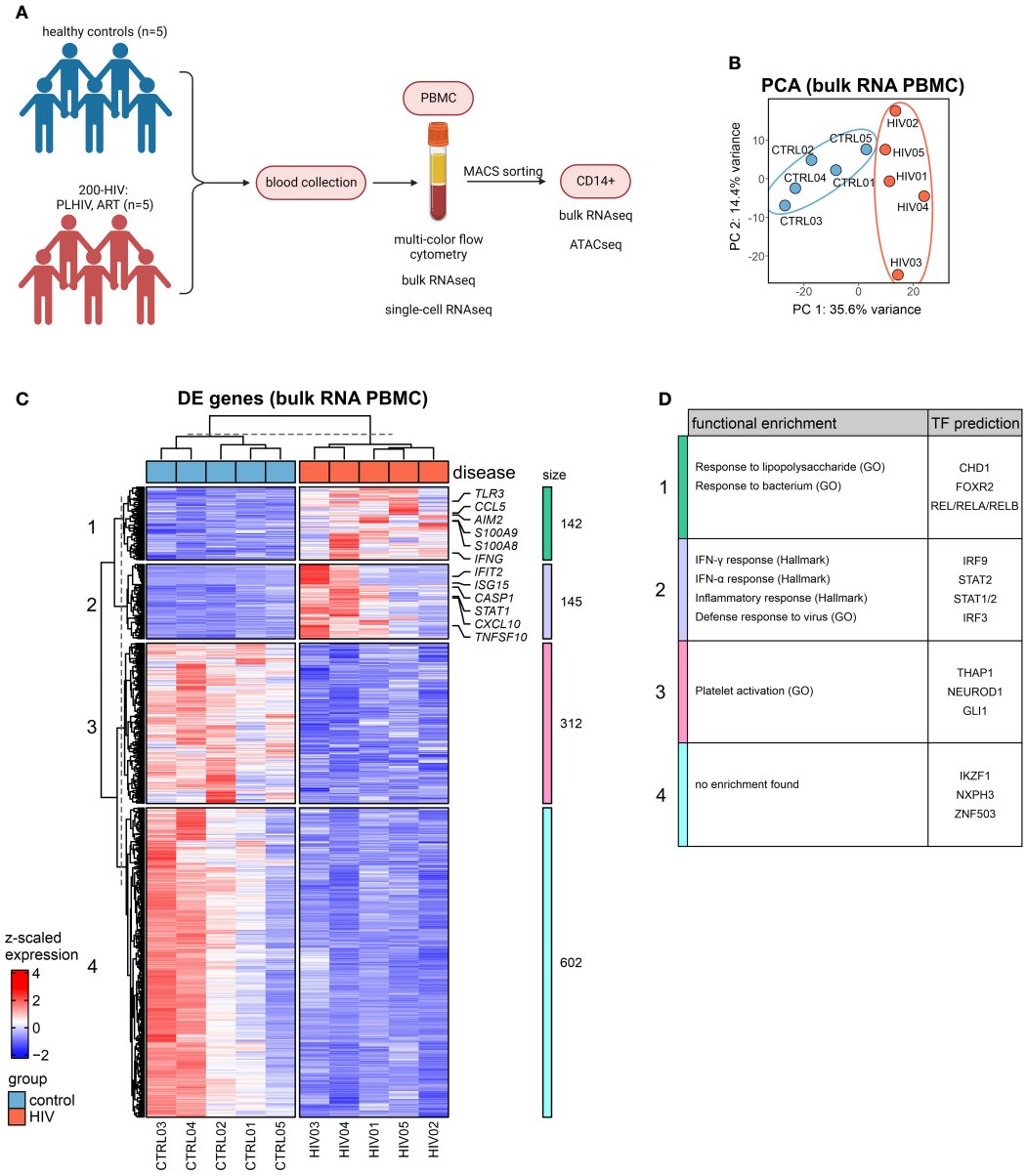


FIGURE 1
Bulk transcriptomes from PBMC in PLHIV are dominated by monocyte-related proinflammatory programs **(A)** Overview of the study design. **(B)** Principal component analysis (PCA) of bulk RNA-seq data from PBMCs. **(C)** Heatmap of DEG (adj. p.val<0.05, |FC|>1.5) from bulk PBMC transcriptomes based on HIV vs. control (see Figure S1C) and hierarchical clustering of genes into 4 clusters. **(D)** Functional enrichment using the GO and Hallmark databases and transcription factor (TF) prediction of gene clusters from **(C)** (full list see Supplementary Table S2).

gene set variation analysis (Figure S1C) showed the highest heterogeneity among the five patients in genes belonging to cluster 2.

Collectively, analysis of bulk transcriptomes from PBMCs of PLHIV revealed upregulation of innate and myeloid proinflammatory gene programs.

## Bulk transcriptomics of monocytes in PLHIV reveals enriched IFN-signaling

The bulk transcriptomes of PBMCs pointed towards the involvement of myeloid cells in PLHIV, and indeed plasma concentrations indicated elevated monocyte-specific soluble factors in circulation such as sCD163 and sCD14, a classical marker of HIV disease progression and monocyte activation (8, 31, 32), while other markers such as liver-derived C-reactive protein (CRP) did not show a significant elevation in these PLHIV (Figure S2A). Consequently, we isolated $CD14^+$ monocytes from the same donors (Figure S2B) and analyzed their transcriptomes. DEGs were calculated for the comparison of PLHIV vs. control, resulting in 65 up- and 6 down-regulated genes (|FC|>1.5, p-value <0.05, IHW) (Figures 2A, S2C). Upregulated genes included several type I IFN-related genes such as *CXCL10*, *STAT2*, *MX2*, and *XAF1* (Figures 2B, S2D). Functional enrichment analysis of the upregulated DEGs

10.3389/fimmu.2023.1275136

supports these findings on the pathway level with IFN response and response to the virus being the most highly enriched terms (Figure 2C). The intersection of the CD14$^+$ DEG with those from the PBMC data revealed 3 shared downregulated (*HERC2P10, HSBP1L1, PHLDB3*) and 21 upregulated (e.g. *CXCL10, SERPING1, GBP1*) genes, most of which belong to cluster 2 of the PBMC DEGs (Figure 2D).

To investigate a possible epigenetic component of the disease-associated changes, we performed ATAC-seq of sorted CD14$^+$ monocytes. Using default analysis criteria (|FC|>1.5, adj. p-value < 0.05), we identified no differentially accessible regions (DARs) when comparing cells from PLHIV with control donors (Figure S2E).

Collectively, the CD14$^+$ monocytes in PLHIV show clear signs of transcriptional activation of IFN-mediated pathways which is not significantly impacted by chromatin packing.

## "Anti-viral" monocyte state is persistent in PLHIV

To address whether changes in the transcriptomes of PBMCs (Figure 1), as well as isolated CD14+ monocytes (Figure 2), are due to general alterations in the transcriptional programs of the myeloid compartment or due to the presence of disease-specific cell states, scRNA-seq was performed on PBMCs of the same individuals (Figure 3). Transcriptomes from 31,566 single cells were produced representing all major immune cell types of the peripheral circulation according to cluster-specific markers known in literature, such as monocytes (*LYZ, S100A9, S100A8*), CD4$^+$ T cells (*IL7R, TRAT1*), CD8$^+$ T cells (*GZMH, CCL5, CD3G*) and NK cells (*GNLY, NKG7, KLRF1*) (Figures 3A; S3A). Density-based coloring of the UMAP for PLHIV and control groups disclosed a major transcriptional shift in the monocyte cluster, in the CD8$^+$ T cell cluster, but not in the CD4$^+$ T cell cluster (Figure 3B). These differences are also reflected in changes in the number of DEG (log2FC=0.25, adj. p-value<0.05, min.pct=0.1) (Figure 3C). Compared to other immune cell populations, monocytes showed the highest number of DEGs comparing PLHIV with controls, 90 up- and 25 down-regulated genes. Functional enrichment analysis on the HIV-specific up-regulated DEG of the monocyte compartment included terms such as 'IFN-γ response", "IFN-α response" and "response to virus" (Figure 3D), in line with the PBMC and CD14 bulk RNA-seq data (Figures 1B, 2C). Similar to the bulk data produced from CD14$^+$ monocytes, 19 genes were also upregulated in the monocyte cluster resulting from scRNA-seq, including *XAF1* and *GBP1* (Figures S3B, E; Supplementary Table S3). To confirm the upregulation of the genes from that intersection, we measured protein levels of SAMD9L, VAMP5, IFIT3, GBP1, SELL, and EIF2AK2, which are

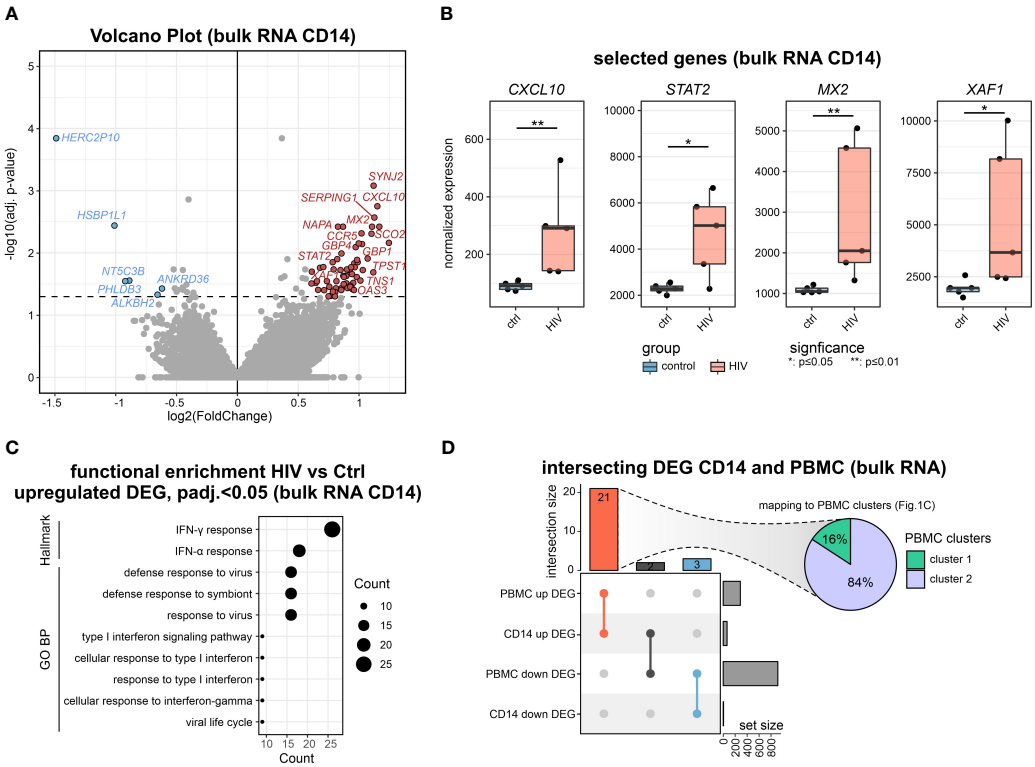


FIGURE 2
Bulk transcriptomics of monocytes in PLHIV mainly reveals IFN-signaling **(A)** Volcano plot showing the DEGs (adj. p.val<0.05, |FC|>1.5) in HIV vs. control of bulk CD14$^+$ monocyte transcriptomes. **(B)** Boxplot and whisker of selected HIV-specific genes. Wilcoxon rank-sum for statistical testing (*: p-value <0.05, **: p-value <0.01). **(C)** Functional enrichment using the GO and Hallmark databases upregulated DEG (HIV vs Ctrl). **(D)** Intersecting DEG for the comparison of HIV vs Ctrl in bulk transcriptomes from CD14$^+$ monocytes and PBMCs. Commonly upregulated DEG mapped to PBMC clusters from Figure 1C.

10.3389/fimmu.2023.1275136

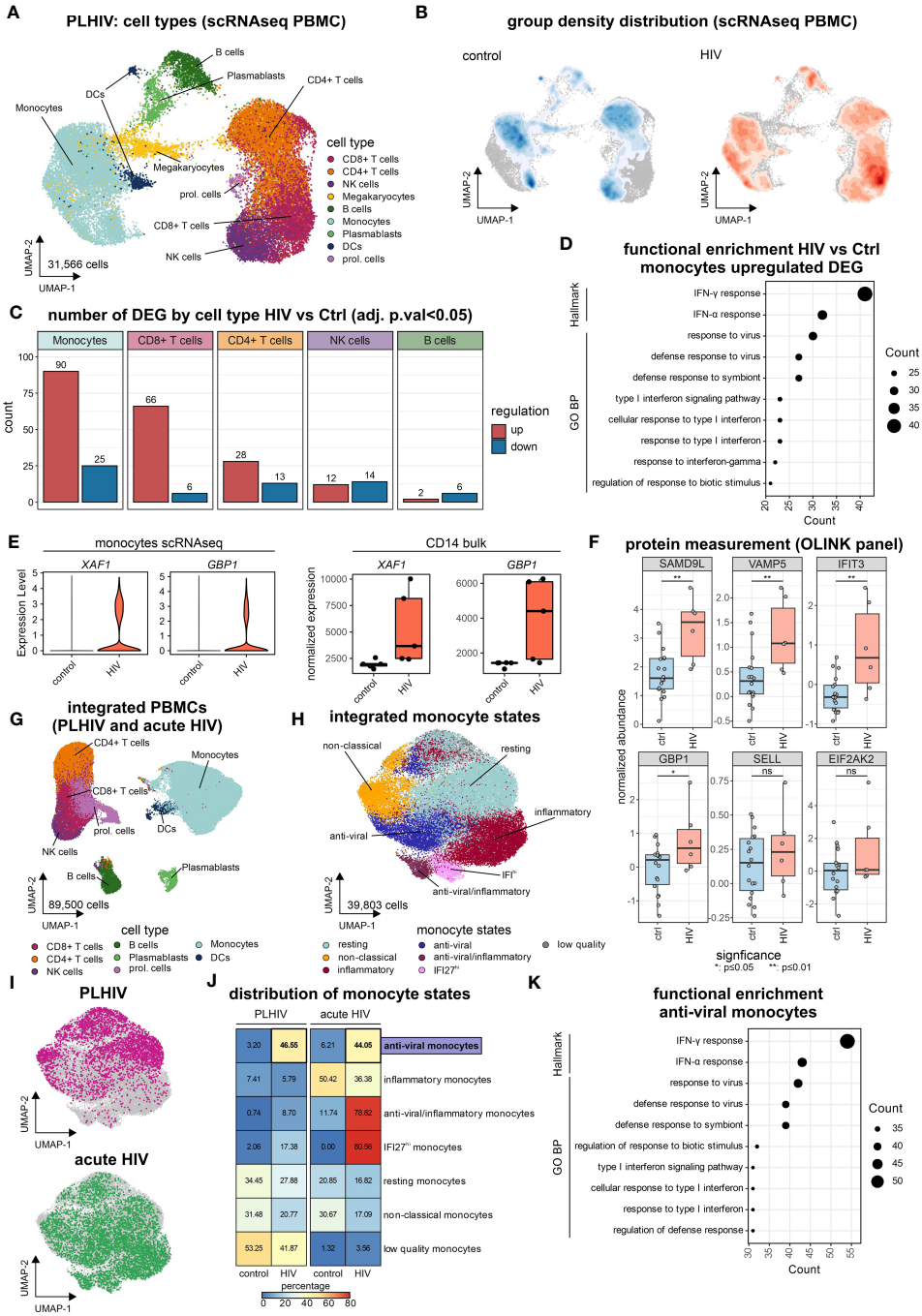


FIGURE 3
"Anti-viral" monocyte state is persistent in PLHIV **(A)** UMAP of PBMCs from PLHIV patients (n= 31,566 cells) indicating identified cell types. **(B)** UMAP from **(A)** colored by disease group density distribution. **(C)** Number of DEG (adj. p.val<0.05, |log2FC|>0.25, min.pct=0.1) by major cell types for the comparison HIV vs Ctrl. **(D)** Functional enrichment using the GO and Hallmark databases for HIV-specific (up-regulated) genes in monocytes. **(E)** Marker expression of *XAF1* and *GBP1* by disease group for monocytes extracted from scRNA-seq data (left panel) and bulk CD14$^{+}$ monocytes (right panel). **(F)** Protein level quantification for SAMD9L, VAMP5, IFIT3, GBP1, SELL, and EIF2AK2 using the Olink system. Wilcoxon rank-sum for statistical testing (ns: not significant, *: p-value <0.05, **: p-value <0.01). **(G)** UMAP of integrated PBMCs from PLHIV **(A)** and acute HIV (Kazer et al., n= 59,286 cells) for commonly present cell types in both datasets, identified cell types are indicated (total dataset n= 89,500 cells). **(H)** UMAP of integrated monocyte subset (n= 39,803 cells) from PLHIV and acute HIV annotated by signatures from Kazer et al. and cluster marker expression. **(I)** UMAP of integrated monocytes colored by dataset origin (PLHIV and acute HIV), each n= 10,000 cells. **(J)** Confusion matrix heatmap showing the distribution of monocyte cell states for disease groups stratified by dataset. **(K)** Functional enrichment using the GO and Hallmark databases for markers (from Figure S3E) of the 'anti-viral' monocyte state.

all related to IFN responses (Figure 3F). In PLHIV, all six proteins showed elevated levels compared to healthy controls with SAMD9L, VAMP5, IFIT3, and GBP1 being significant.

To relate our findings from chronic HIV in PLHIV to acute HIV, in which patients did not yet receive ART and have high viremia, we integrated the newly produced data with our previously published results using the same microwell-based single-cell technology describing several inflammatory monocyte states in acute HIV infection (33) resulting in 89,500 single-cell transcriptomes (Figures 3G, S3C, D). To investigate the possible presence of chronic disease-specific cell states within the monocyte compartment, we subsetted the monocytes of the integrated scRNA-seq dataset (Figure 3H). Clustering of the monocyte compartment resulted in seven monocyte substrates, which could be annotated based on the previously reported acute monocyte states (33). These included several inflammatory monocyte states associated with acute HIV infection, e.g. anti-viral/inflammatory or *IFI27*$^{hi}$ monocytes (Figures 3H, S3E). Monocytes from our new data predominantly exhibited resting and non-classical states, irrespective of HIV group (Figures 3I, J). Chronic HIV was characterized by an 'anti-viral' monocyte state that was also found during acute infection (Figure 3J). This 'anti-viral' monocyte state expresses interferon-related genes, e.g. *IFIT3* and *ISG15* (Figure S3E), and is strongly enriched for the hallmarks 'IFNγ response' and 'IFNα response' as well as the GO term 'response to virus' (Figure 3K), reminiscent of our results in PBMCs (Figures 1C, D) and CD14$^+$ monocytes (Figure 2C).

Even within the resting and non-classical monocyte substates that do not exhibit major changes in proportions between the clinical groups (Figure 3J), differentially expressed genes (log2FC=0.25, adj. p-value<0.05, min.pct=0.1) for PLHIV vs. controls (resting: 70 DEGs, non-classical: 36 DEGs) had a substantial overlay with the DE genes identified from bulk PBMC data, i.e. clusters 1 and 2 (Figures 1C, S3F; Supplementary Table S3). ScRNA-seq also revealed heterogeneity in cell state distribution in the group of the PLHIV, which was not apparent in the healthy individuals (Figure S3G).

Collectively, single-cell transcriptomics identified monocytes as the major cause of changes in PLHIV. Common alterations were evident across all identified cell states, including resting and non-classical monocytes, yet scRNA-seq uncovered elevated numbers of monocytes in the 'anti-viral' cell state in chronic HIV that had been described for acute HIV infection. Thus, pathology in PLHIV is a combination of molecular alterations and proportion changes that could only be revealed by analysis on the single-cell level.

## Drug repurposing to reverse monocyte reprogramming in PLHIV

To illustrate how to identify potential drug targets for reversing a molecular phenotype, here the changes observed in monocytes, we performed a drug repurposing approach (Figure 4A) following a previously established methodology (34). In brief, genes up- and down-regulated in PLHIV who are under ART from scRNA-seq monocytes, bulk RNA-seq PBMCs, and bulk RNA-seq CD14$^+$ monocytes were subjected to the drug prediction databases iLINCS and CLUE (35, 36), resulting in 519 predicted drugs (Supplementary Table S4). From those drugs, 17,641 signatures were retrieved from iLINCS and used as input for GSEA on the bulk RNA-seq CD14$^+$ monocytes and PBMC datasets. Drug signatures were then clustered by their delta normalized enrichment score (ΔNES), resulting in 50 clusters (Figure 4B; Supplementary Table S4). The ΔNES indicates the efficiency of the respective drug signature to reverse the PLHIV-specific signature, with higher ΔNES indicating a more complete reversal. Cluster 43, consisting of 32 signatures, showed the highest ΔNES for CD14$^+$ monocytes and also a high ΔNES for PBMCs (Figure 4C). To decipher the commonalities of those drug responses, we investigated recurring target genes of all drug signatures in the cluster (Figure 4D). A majority of genes were interferon-associated such as *IFI27*, *OAS1*, *MX1*, and *IFI44L*, and the target genes were strongly enriched in the 'anti-viral' and 'anti-viral/inflammatory' monocyte states (Figure S4A).

Of the 32 drug signatures, we chose five among the top 20 drugs according to ΔNES for CD14$^+$ monocytes in PLHIV. Four of them had been studied in the context of HIV infection [trametinib (37), sunitinib (38, 39), sitagliptin (40, 41), clofarabine (42)], but had not been reported to alter transcriptional programs in monocytes. Additionally, the predicted antibiotic doxycycline, for which neither anti-viral nor immune-modulating function has been reported, was chosen as well. Instead of addressing the viral life cycle, this approach predicts a potential impact on the host's immune response to these drugs. To test this hypothesis and validate our predictions, we performed *in vitro* experiments stimulating PBMC from PLHIV with the respective drugs.

Six independent PLHIV were recruited, PBMCs were isolated and co-cultured in the presence of the selected drugs or with DMSO as control (Figure 4A, right panel). After overnight incubation, RNA was extracted and bulk transcriptomics was performed to measure transcriptional changes induced by the respective treatment (Figure S4B). The different *in vitro* treatments resulted in prominent transcriptional changes in the PBMCs, evident in the PCA with the strongest alterations induced by doxycycline followed by trametinib, sunitinib, and clofarabine (Figure 4E). Differential expression analysis reflected this finding in the number of DE genes (Figure S4C). Of note, doxycycline, trametinib, and sunitinib induced a greater number of downregulated DEGs.

Based on our previous findings, we tested the influence of the different treatments by analyzing the reduction of gene signature enrichment for 1) the recurring target genes of cluster 43 identified from the drug repurposing pipeline (n=35), 2) the 'anti-viral monocyte' markers from our integrated single-cell RNA-seq analysis (n=137), and the hallmark terms 3) 'IFNγ response' (n=200) and 4) 'inflammatory response' (n=200) (Figure 4F). Sunitinib and doxycycline showed the most significant impact, strongly reversing the four different HIV-specific gene signatures. Trametinib also showed strong, clofarabine a moderate, and sitagliptin no reductions of the four signatures in our *in vitro* verification experiment. These differential effects of the different

10.3389/fimmu.2023.1275136

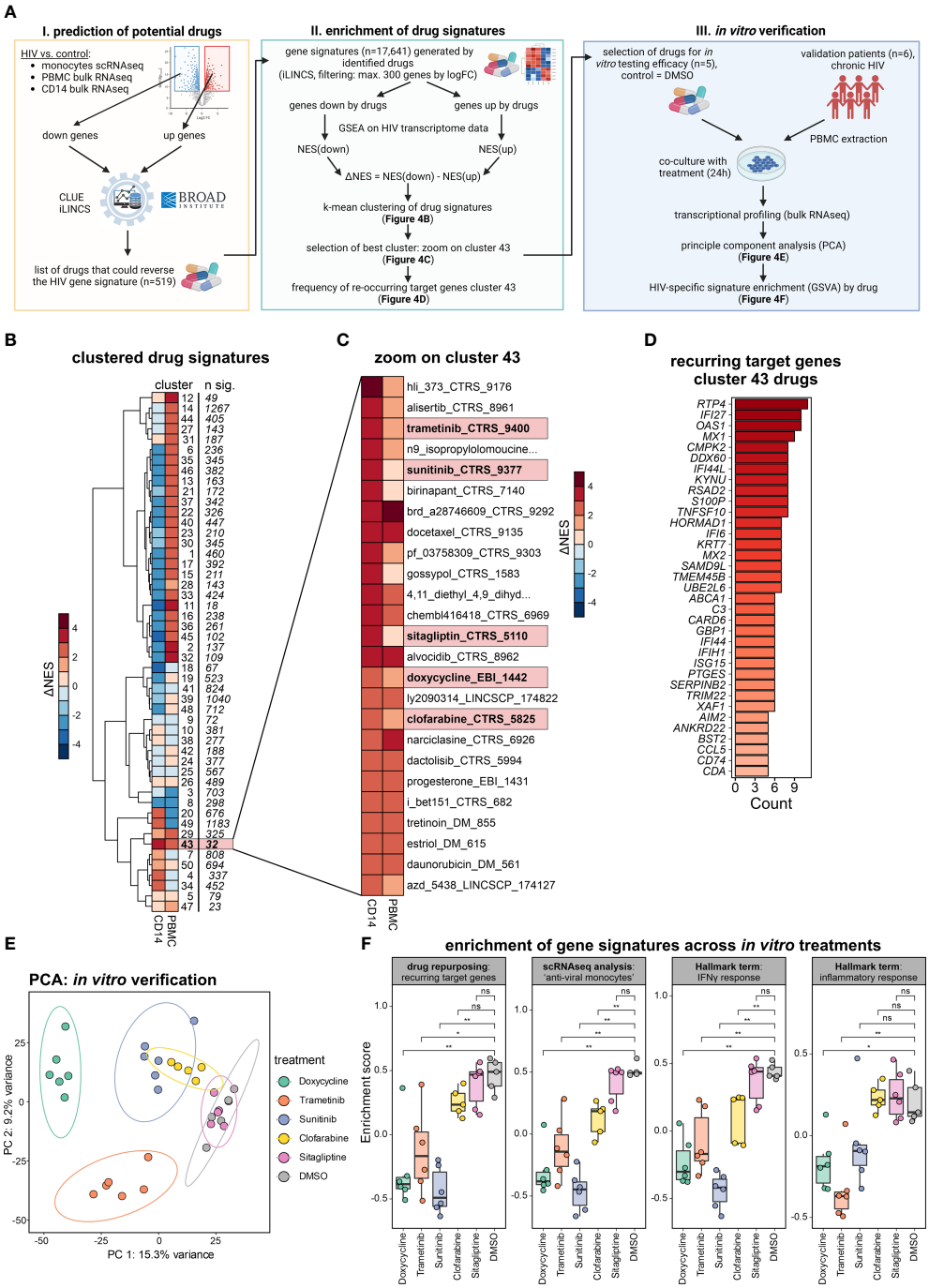


FIGURE 4
Drug repurposing to reverse monocyte reprogramming in PLHIV. **(A)** Drug prediction workflow and follow-up *in vitro* verification, NES=normalized enrichment score. **(B)** Heatmap showing hierarchical clustering (k-mean=50) of ΔNES from all drug signatures (n= 17,641) as groups enriched on transcriptomes from bulk CD14$^+$ monocytes and bulk PBMCs. **(C)** Zoom into cluster 43 from **(B)**, depicting all involved drug signatures. **(D)** Recurring target genes of drug signatures identified in cluster 43 from **(C)**. **(E)** Principal component analysis (PCA) of bulk PBMC transcriptomes of the *in vitro* verification experiment (five HIV donors with six conditions). Samples colored by treatment, DMSO as untreated control. **(F)** Enrichment of gene signatures across *in vitro* treatments, analyzed signatures include the recurring target genes from cluster 43 (drug repurposing), marker for the 'anti-viral' monocytes (integrated scRNA-seq analysis), and the hallmark terms 'IFNγ response' and 'inflammatory response'. Wilcoxon rank-sum for statistical testing (ns: not significant, *: p-value <0.05, **: p-value <0.01).

drugs are also seen on the gene level when investigating the top leading edge genes of the four signatures by each drug (Figure S4D).

Taken together, we predicted drugs that could reverse the altered monocyte-derived signatures and confirmed our repurposing approach *in vitro* with the drugs doxycycline and sunitinib strongly reversing the HIV-specific gene signatures, making them repurposed drug candidates of interest.

## Discussion

In the present study, we illustrate in a small group of PLHIV derived from our previous cross-sectional 200-HIV cohort study (1) that single-cell and bulk transcriptomes of isolated immune cells revealed reprogramming in multiple cellular compartments in PLHIV, with innate immune cells, in particular monocytes, showing most profound changes. We further illustrate that a certain cellular state of monocytes, previously reported in acute HIV infection can be observed in PLHIV, while other cell states associated with acute inflammation are specific for acute HIV and absent in PLHIV. Long-term usage of ART in PLHIV results in undetectable viral loads and restores CD4 cell counts to normal levels, and therefore PLHIV patients differ from people with an acute HIV infection that have high-level viremia and reduced CD4 cell counts (33). Despite the small number of PLHIV studied, which clearly showed heterogeneity in their transcriptional profiles, we also illustrate that combined bulk and single-cell data of these PLHIV was already sufficient to predict drug candidates for reversing the observed transcriptional deviations in the monocyte compartment. While technically applicable to a cohort study setting, ATAC-seq of this small number of PLHIV did not reveal any significant differences, which clearly points towards the need for larger cohorts when assessing chromatin landscape differences. As such the study reported here provides the necessary information to include sophisticated transcriptome and epigenome data generation to be integrated into the larger 2000-HIV cohort study currently recruiting PLHIV including elite controllers.

The combined analysis of bulk transcriptomes from PBMC and purified $CD14^+$ monocytes together with single-cell transcriptomes from blood allowed us already in a rather small number of PLHIV to define major changes within the peripheral immune cell compartment, e.g. the identification of a gene cluster characterized by IFN signaling. The higher-resolution information from scRNA-seq revealed that some of the changes observed in the PBMC-derived transcriptomes was due to molecular changes in monocytes including cell-state differences, but not due to cell-type distribution differences, further supporting the use of higher-resolution technologies in larger cohort studies. While IFN-signaling related molecular changes (cluster 2, Figures 1C, D) were also captured in bulk transcriptomes from purified $CD14^+$ monocytes (Figure 2), the overall information content from purified $CD14^+$ monocytes was surprisingly low, indicating that many of the changes observed in PBMC are derived from other monocyte cell states ($CD14^{low/-}$) and other cell types. Single-cell transcriptomes clearly corroborated this hypothesis showing that basically all immune cell types exhibited transcriptional changes in PLHIV. With the lowest information content and highest technical effort, we concluded that cell-type isolation procedures are not suitable for larger cohort studies on PLHIV. Moreover, when assessing DEG in monocytes using both bulk and single-cell transcriptomes, we detected less DEG in bulk and only a small intersection with single-cell data (n=19, Figure S3B). Differences in experimental sample handling or sequencing resolution could explain this small intersection, however, even though certain genes were not tested to be significantly altered in both methods, the general pathway activation towards IFN responses was uncovered by both methods.

The systemic assessment of single-cell transcriptomes derived from PBMC of PLHIV revealed that major transcriptional reprogramming was mainly observed in monocytes and $CD8^+$ T cells with fewer changes in $CD4^+$ T cells, NK cells, and B cells. Focusing on the cell compartment with the major changes, we revealed a cell state composition in PLHIV including the well-described classical and non-classical monocyte states, but also a cell state we previously termed 'anti-viral monocytes' in acute HIV infection (33). Interestingly, this particular cell state showed high heterogeneity between PLHIV, which will have to be studied in larger cohorts to better define whether there is a pattern reminiscent of PLHIV endotypes or whether this might be explained by individual clinical incidents prior to blood sampling. Despite the heterogeneity of this monocyte state, the assessment of genes enriched in gene clusters derived from bulk transcriptomes indicated that even classical and non-classical monocyte states in PLHIV are characterized by elevated expression of cluster 2 genes, supporting the notion that despite the observed heterogeneity, persistent IFN signaling seems to be a major hallmark of persistent inflammation in PLHIV (43). Based on these informative and promising results we propose to integrate these levels of omics technologies into larger PLHIV studies.

As we identified a major theme for persistent inflammation in this small number of PLHIV, we addressed whether this information would already be sufficient to identify drug candidates by a reverse transcriptome approach (34). Interestingly, while most therapeutic strategies are currently addressing alternative antiviral drugs with less toxicity or treatment strategies aiming at minimizing ART toxicity, fewer drug regimens address immunomodulation itself including the use of purinergic P2X receptor inhibitors (44) or statins (45–49). In clinical studies testing the efficacy of these therapeutic approaches to lower inflammation in PLHIV, mainly soluble mediators (e.g. CRP, sCD14, IL-6, sCD163) measured in plasma or serum were used as readouts, while high-resolution technologies to address molecular changes in immune cells were not reported. We exemplified here, how such an approach could be applied to the identification of drug candidates lowering the inflammatory response observed in PLHIV. We focused on a cluster of drugs with a particularly high probability of reversing the transcriptional alterations observed in monocytes and experimentally validated a small number of drug candidates. A surprising finding was that the antibiotic doxycycline induced the strongest effect mainly reducing gene expression. Together with sunitinib, doxycycline was most effective in reversing gene expression alterations of 1) the major target genes used for drug prediction, 2) of the marker genes expressed in monocytes with the 'antiviral' cell state, 3) of the hallmark genes related to IFN signaling, and 4) hallmark genes related to the pro-inflammatory response. These findings strongly suggested that drugs such as doxycycline might not only function as antibiotics but also modulate host immune responses. This is similarly true for the drug candidates sunitinib and trametinib, which have been developed for completely different purposes (50,

51). Importantly, the modulation of the monocyte-related immune activation should not be considered yet as being unrestrictedly helpful for PLHIV, as it is not yet entirely clear whether these gene programs would play a clinically beneficial role or not. As these findings have to be considered as proof-of-concept, further investigations using more drug candidates, different drug concentrations, and further optimized computational and miniaturized experimental procedures in a larger group of PLHIV are certainly warranted to more quickly identify promising new drug candidates counteracting the inflammatory state in PLHIV under ART therapy.

## Limitations of the study

The present study was conceptualized based on the previous cross-sectional 200-HIV cohort study (1) to determine whether the combination of high-resolution and high-content technologies such as bulk and scRNA-seq data would lead to additional insights into the pathophysiology of immune deviations in PLHI and therefore, only a limited number of individuals were included in this study. As the main purpose was to determine the best strategy to scale these technologies to larger clinical cohorts, we were surprised that despite a rather small number of individuals studied and obvious heterogeneity within the group of PLHIV, we could retrieve important information about major molecular changes on transcriptome level in all immune compartments. However, it became also clear that other layers, e.g. chromatin landscapes as assessed by ATAC-seq require a much larger number of individuals to determine whether immune cells in PLHIV are also altered on this epigenetic level. Based on these initial findings, we have now started to include these technologies in the much larger 2000-HIV cohort study of approx. 2000 PLHIV to study aspects such as disease heterogeneity, potential disease endotypes, and association of cellular changes with clinical trajectories, or to determine potential biomarkers predicting disease outcome. Certainly, the observation that innate immune cells such as monocytes show the most pronounced transcriptional reprogramming in PLHIV was unexpected and will be one major focus within the currently being assembled cohort of PLHIV. Moreover, the identification of these monocyte-derived programs also opens new avenues toward the identification of new mechanisms on how transcriptional alterations contribute to immune dysregulation in PLHIV.

# Methods

## Lead contact

Dr. Anna C. Aschenbrenner, anna.aschenbrenner@dzne.de.

## Materials availability

This study did not generate unique reagents.

## Data and code availability

Bulk RNA-seq datasets and single-cell RNA-seq data have been deposited at the European Genome-phenome Archive (EGA) and are publicly available under the accession numbers.

All original code is stored on FASTGenomics: https://beta.fastgenomics.org/p/HIV_Pilot

Any additional information required to reanalyze the data reported in this paper is available from the lead contact upon request.

## Study cohort

Five PLHIV were recruited from the outpatient HIV clinic of the Radboud University Medical Center on March 26-28th 2019. Included patients were five males of Dutch/Western-European ethnicity who were receiving cART for more than 6 months and latest HIV-RNA levels ≤200 copies/ml. Ethical approval was granted by the Ethical Committee of the Radboud University Medical Center Nijmegen, the Netherlands under registration number NL42561.091.12). Additionally, five age-/sex-matched healthy volunteers were included as controls (age 43-61), and ethical approval was granted by the Ethical Committee of the Radboud University Medical Center Nijmegen, the Netherlands under registration number NL32357.091.10). For the *in vitro* verification experiments of drugs, six additional male PLHIV were recruited (age 26-43, with ethical approval granted by the Ethical Committee of the Radboud University Medical Center Nijmegen, the Netherlands under registration number NL68056.091.18). Written consent was obtained from all participants involved in this study and experiments were conducted according to the Declaration of Helsinki principles.

## PBMC isolation

Human peripheral blood mononuclear cells (PBMCs) were isolated by dilution of blood in pyrogen-free PBS and differential density centrifugation over Ficoll-Paque (GE Healthcare, UK) as previously described by (52). Briefly, the interphase layer was collected, and cells were washed with cold PBS. Cells were resuspended in RPMI 1640 culture medium (Roswell Park Memorial Institute medium; Invitrogen, USA) supplemented with 50 g/mL gentamicin, 2 mM glutamax (Gibco, Life Technologies, USA), and 1 mM pyruvate (Gibco) and quantified. A fraction of PBMCs was viably frozen for later use. The cell suspension was spun down for 5 min at 300g, 4°C, after which all supernatant was removed. Cells were very gently resuspended in freezing medium (90% fetal calf serum, 10% DMSO) and aliquoted into cryovials. They were placed first at -80°C in a CoolCell freezing container (Corning), after which they were transported the next day on dry ice and moved to liquid nitrogen storage. For the thawing of PBMCs,

one vial of 5 million cells was thawed in 10ml RMPI medium supplemented with 10% FCS.

## Preparation of Seq-Well arrays/libraries/sequencing

Seq-Well arrays and libraries were prepared from isolated PBMCs as described previously (24).

## Measurements of plasma markers

Clinical plasma markers were measured using ELISA (Duoset or Quantikine, R&D Systems) for IL18-BP, IL-18, hsCRP, sCD14, sCD163 or using SimplePlex Cartridges (Protein Simple) for IL-6, all performed according to manufacturers' instructions. As a reference, the mean of healthy controls from van der Heijden et al. (1) were used.

## Isolation of CD14+ monocytes

CD14+ monocytes were isolated from PBMC by magnetic-activated cell sorting (MACS) positive selection with CD14 microbeads (Miltenyi Biotec), according to the manufacturer's instructions. Depending on the available PBMC counts used as input, either MS or LS columns were used (Miltenyi Biotec). After isolation, cells were again resuspended in a Dutch modified RPMI culture medium (Invitrogen) supplemented with 50 µg/mL gentamycin, 2 mM glutamax and 1 mM pyruvate (Gibco, Life Technologies).

## Flow cytometry

Frozen PBMCs were thawed then stained for surface markers (Supplementary Table S1) in DPBS with BD Horizon Brilliant Stain Buffer (Becton Dickinson) for 30min at 4°C. To distinguish live from dead cells, the cells were incubated with LIVE/DEAD Fixable Yellow Dead Cell Stain Kit (1:1000 – Thermo Scientific). Following staining and washing, the cell suspension was fixed with 4% PFA for 10 min at room temperature to prevent any possible risk of contamination due to aerosol formation during sample handling and acquisition. Flow cytometry analysis was performed on a BD Symphony instrument (Becton Dickinson) configured with 5 lasers (UV, violet, blue, yellow-green, red).

## ATAC-seq

Frozen PBMCs were thawed and sorted on a BD FACSAria III (Blue, Yellow-Green, Red, and Violet lasers), and 20,000 live $CD14^+$ cells were sorted and spun down at 500×g for 5 min at 4°C. The cell pellet was washed with 50 µL of cold 1x PBS buffer and spun down at 500 ×g for 5 min at 4°C. The pellet was then resuspended in 50 µL of cold lysis buffer (10 mM Tris-HCl, pH 7.4, 10 mM NaCl, 3 mM MgCl2, 0.1% IGEPAL CA-630) and spun down immediately at 500×g for 10 min at 4°C. The supernatant was then discarded, and the transposition reaction was immediately performed. To perform the transposition reaction, a mixture of transposase, 5x TAPS-DMF buffer (50mM TAPS (T5130 SIGMA), 25mM MgCl2, 50% DMF (N, N-Dimethylformamide)), and water was combined and added to the cell pellet. The transposition reaction was incubated at 37°C for 30 min. Following transposition, the DNA was purified using a Qiagen MinElute Kit. The transposed DNA was eluted in 10 µL of water, and purified DNA was stored at 4°C until the following day or at -20°C.

To amplify the transposed DNA fragments, a PCR mixture was prepared using the purified DNA, nuclease-free water, customized Nextera PCR primers, and NEBNext High-Fidelity 2x PCR Master Mix. The PCR mixture was cycled as follows: 72°C for 5 min, 98°C for 30 sec, 98°C for 10 sec, 63°C for 30 sec, and 72°C for 1 min. Steps 3-5 were then repeated 11 times for a total of 12 cycles. The PCR products were then purified using a Qiagen MinElute Kit and eluted in 12 µL of water. To validate the quality and concentration of the PCR products, gel electrophoresis was performed using the TapeStation and Agilent High Sensitivity D1000 kit.

## Protein measurements

Proteomic profiling of selected markers was performed as described before (53). In brief, venous whole-blood samples were collected in EDTA tubes and centrifuged into plasma, and then stored at -80°C. Protein measurements were performed by Olink Proteomics AB using the Olink Explore platform. QC and normalization were performed by Olink services. For this study, protein markers of interest were selected.

## *In vitro* verification of selected drugs

To verify the effectiveness of predicted drugs, six different PLHIV from the 200-HIV cohort were re-called, and the PBMCs were extracted and seeded in triplicates with 500,000 cells per replicate. The PBMCs were cultured for 24 hours in the presence of a selected subset of drugs from cluster 43, including trametinib (50 mM in 0.000002% DMSO), sunitinib (100 mM in 0.0001% DMSO), clofarabine (100 mM in 0.00001% DMSO), doxycycline (100 mM in $H_2O$) and sitagliptin (100 mM in 0.0001% DMSO) or DMSO (0.001%) as control. After incubation, replicates were collected in a total of 1 ml TRIzol reagent and processed for bulk RNA-seq.

## Quantification and statistical analysis

### RNA-sequencing analysis (bulk RNA PBMC, CD14)

Sequenced reads were aligned and quantified using STAR: ultrafast universal RNA-seq aligner (v2.7.3a) (54) and the human reference genome, GRCh38p13, from the Genome Reference Consortium. Raw counts were imported using the DESeqDataSetFromMatrix function

from DESeq2 (v1.32.0) (55) and rlog transformed according to the DESeq2 pipeline. DESeq2 was used for the calculation of normalized counts for each transcript using default parameters. All normalized transcripts with a maximum overall row mean lower than 10 were excluded resulting in 26,920 present transcripts. All present transcripts were used as input for principal component analysis (PCA). Differentially expressed genes were calculated for HIV vs. control using an independent hypothesis weighting (IHW) adjusted p-value cutoff of 0.05 and an absolute fold change (|FC|) of 1.5. DEGs were used as input for the k-mean clustered heatmap (k=4), generating four clusters.

## RNA-sequencing analysis (drug verification analysis)

Sequenced reads were aligned and quantified using kallisto v0.44.0 (56) and the human reference genome, GRCh38p13, from the Genome Reference Consortium. Raw counts were imported using the DESeqDataSetFromTximport function from DESeq2 (v1.32.0) (55) and vst-transformed according to the DESeq2 pipeline. DESeq2 was used for the calculation of normalized counts for each transcript using default parameters. All normalized transcripts with a maximum overall row mean lower than 10 were excluded resulting in 37,952 present transcripts. Variation in the data was identified using the SVA package (v3.40) (57), and batch effects were removed with limma (v3.48.3) (58) using the first six surrogate variables (SVs), which were also added in the design of the dds object. All present transcripts were used as input for principal component analysis (PCA) of the batch-corrected data. Differentially expressed genes were calculated for HIV vs. control using a p-value cutoff of 0.05, an adjusted p-value (IHW) < 0.05 (independent hypothesis weighting), and a |FC|>2. DEGs were used as input for the clustered heatmap.

## Transcription factor prediction analysis

The R package RcisTarget (version 1.12.0) (59) was used to predict the transcription factors potentially regulating heatmap cluster-specifically contained gene sets. The genomic regions of TF-motif search were limited to 10kb around the respective transcriptional start sites by using the RcisTarget-implemented "hg19-tss-centered-10kb-7species.mc9nr.feather" motifRanking file. Prediction was performed using the cisTarget function and the resulting top 3 predicted TF, according to their normalized enrichment scores (NES), were selected for each heatmap cluster.

## Gene set ontology enrichment analysis

Gene set ontology enrichment analysis using the heatmap clusters as input was performed on the gene sets from the Gene Ontology (GO) biological process (BP) database (60, 61) and the Hallmark gene sets (62) using the R package clusterProfiler (version 4.0.5) (63). Ontologies with the highest and statistically significant enrichment were used for presentation.

## Gene set variation analysis

For the enrichment of the genes included in the four different clusters of the DE heatmap (PBMC data) and for the enrichment of the four different transcriptional signatures for the *in vitro* verification of drugs, the GSVA package (version 1.40.1) (64) was applied.

## Flow analysis

After pre-processing, compensated fluorescence intensities were exported from FlowJo (BD, v. 10.7.1). Exported.fcs files were imported in R with the flowCore package (v. 2.2.0). Fluorescence intensities were auto-logicle transformed, used for dimensionality reduction using the UMAP algorithm (umap package v. 0.2.7.0) (65) and clustered using the Phenograph package (v. 0.99.1) (66). Cell types were annotated for each cluster by respective marker expression. For visualization, the proportions of main cell types were calculated and stratified by disease group.

## ATAC-seq analysis

Reads were aligned to human hg38 reference with bowtie2 (67). Samtools (68) was used to remove adapter offset and to create bam files. Open chromatin peaks were called using MACS2 (69), blacklisted regions (hg38-blacklist.v2.bed.gz, https://sites.google.com/site/anshulkundaje/projects/blacklists), the low covered peaks were excluded, and then the peaks were annotated with gene models from TxDb.Hsapiens.UCSC.hg38.knownGene using the ChIPseeker package (applying annotatePeaks function) (70). Downstream analysis was performed with the DESeq2 (v1.26.0) package (55). Differentially accessible regions (DAR) were detected with a |FC|>1.5 and a corrected p-value > 0.05. With these standard parameters, no DAR were identified.

## ScRNA-seq data analysis

ScRNA-seq UMI count matrices were imported to R 4.1 and gene expression data analysis was performed using the Seurat package 4.0.4 (71, 72). Cells with more than 10% mitochondrial reads and less than 200 expressed genes were excluded from the analysis and only those genes present in more than 3 cells were considered for downstream analysis. Moreover, the genes *MT-RNR1* and *MT-RNR2* were excluded. Log-normalization, scaling, and dimensionality reduction steps were performed using the Seurat implemented functions. For scaling, the number of detected transcripts per cell was regressed out to correct for heterogeneity associated with differences in sequencing depth. For dimensionality reduction, PCA was performed on the top 2,000 variable genes identified using the vst method implemented in Seurat. Subsequently, UMAP was used for two-dimensional representation of the data structure using the first 30 PCs. Cell type annotation was based on the respective clustering results combined with the expression of known marker genes. DEG by celltype were calculated for the comparison of HIV vs control with a |log2FC|>0.25, adj. p-value<0.05 and min.pct=0.1.

## Data integration

Data integration of the PLHIV PBMCs (this study) and the acute HIV PBMC dataset (33) were integrated using the harmony algorithm (73) based on the first 15 principal components. Prior to integration, the PLHIV dataset was subsetted for major cell types

present in acute HIV. Cell type annotation was based on the respective clustering results combined with the expression of known marker genes.

### Integrated scRNA-seq monocyte analysis

The monocyte compartment was subsetted from the integrated PBMCs and subsequently normalized, scaled, and subjected to PCA calculation. For UMAP visualization, the first 10 harmony PCs were used. After clustering the integrated monocytes with the FindNeighbors and FindClusters function from Seurat, monocyte states were annotated according to the signatures described in acute HIV (33) and cluster-specific markers, separating the monocyte population into anti-viral (*TNFSF10, ISG15, IFIT2, IFIT3*), inflammatory (*IL8, IL1B, EREG*), anti-viral/inflammatory (*CCL2, CCL4*), IFI27/30$^{hi}$ (*IFI27, IFI30*), HLA$^{hi}$ (*HLA-DRB1, HLA-DQA1*), resting (*S100A8, S100A9, LYZ*) and non-classical (*FCGR3A, C1QA*) monocytes.

### Confusion matrix

For each monocyte cell state, the relative proportion across the groups (HIV, control) was visualized as a fraction of samples from the respective condition contributing to the monocyte cell state stratified by dataset (PLHIV vs. acute HIV).

### Drug prediction

To identify drugs that reverse the gene expression signature observed in the comparison HIV vs. control for bulk RNA-seq PBMCs, bulk RNA-seq CD14 monocytes, and scRNA-seq monocytes, the drug prediction databases iLINCS (http://www.ilincs.org/ilincs/), and CLUE (https://clue.io/) were accessed. As input for the drug prediction, the top 1000 (iLINCS) or the top 100 (CLUE) DEGs were used. Drugs reversing the HIV gene expression signature (defined by a negative score) comprised a total of 519 unique drugs. Using the iLINCS API (https://github.com/uc-bd2k/ilincsAPI/blob/master/usingIlincsApis.Rmd), every gene expression signature from each drug listed in the signature libraries iLINCS chemical perturbagens (LINCSCP), iLINCS targeted proteomics signatures (LINCSTP), Disease-related signatures (GDS), Connectivity Map signatures (CMAP), DrugMatrix signatures (DM), Transcriptional signatures from EBI Expression Atlas (EBI), Cancer therapeutics response signatures (CTRS), and Pharmacogenomics transcriptional signatures (PG) was downloaded. Labeling was performed in the following principle: "drug name"_"database"_"database ID". Signatures were ordered by fold change, and only the top 300 genes were used. This resulted in a total of 17,641 unique drug signatures each with an up- and downregulated set. Subsequently, GSEA was performed on the sequencing data for every up- and down-regulated set for each drug and each cluster comparison. The resulting normalized enrichment scores (NES) were used to calculate the delta NES for each drug, defined as ΔNES = NES (down) – NES (up), ergo the difference of the NES from the downregulated set and the NES from the upregulated set of each respective drug. These ΔNES values were then k-mean clustered (k = 40). The cluster with the highest ΔNES values for both CD14 and PBMCs was chosen and uniquely present drugs were shown. The leading edge genes of the downregulation signatures of these drugs (cluster 43) were examined, and the frequency was counted (recurring target genes).

### Data visualization

For data visualization, the R packages Seurat, ggplot2 (version 3.3.5) (74), (https://ggplot2.tidyverse.org), pheatmap (version 1.0.12), and ComplexHeatmap (version 2.8.0) (75) were used.

## Data availability statement

The datasets presented in this study can be found in online repositories. Bulk RNA-seq datasets and single-cell RNA-seq data have been deposited at the European Genome-phenome Archive (EGA) and are publicly available under the accession number EGAS00001007460.

All original code is stored on FASTGenomics: https://beta.fastgenomics.org/p/HIV_Pilot. Any additional information required to reanalyze the data reported in this paper is available from the lead contact upon request.

## Ethics statement

Ethical approval was granted by the Ethical Committee of the Radboud University Medical Center Nijmegen, the Netherlands under registration number NL68056.091.18). Written consent was obtained from all participants involved in this study and experiments were conducted according to the Declaration of Helsinki principles. The studies were conducted in accordance with the local legislation and institutional requirements. The participants provided their written informed consent to participate in this study. Written informed consent was obtained from the individual(s) for the publication of any potentially identifiable images or data included in this article.

## Author contributions

RK: Writing – original draft, Writing – review & editing, Data curation, Formal Analysis, Investigation, Visualization. LB: Data curation, Formal Analysis, Investigation, Writing – review & editing. JS: Data curation, Investigation, Validation, Writing – review & editing, Formal Analysis. SW-H: Data curation, Formal Analysis, Investigation, Writing – review & editing. MJ-C: Data curation, Investigation, Project administration, Resources, Writing – review & editing. EB: Writing – review & editing, Investigation. NR: Data curation, Formal Analysis, Investigation, Writing – review & editing. AH: Investigation, Writing – review & editing. MH: Investigation, Writing – review & editing, Formal Analysis. MN-G: Investigation, Formal Analysis, Writing – review & editing. TO: Writing – review & editing, Resources. WH: Resources, Writing – review & editing, Data curation, Investigation. LW: Resources,

Writing – review & editing. AS: Resources, Writing – review & editing, Methodology. KH: Writing – review & editing, Investigation. MB: Data curation, Writing – review & editing. MDB: Resources, Supervision, Writing – review & editing. MN: Resources, Supervision, Conceptualization, Funding acquisition, Writing – review & editing. LJ: Conceptualization, Funding acquisition, Resources, Supervision, Writing – review & editing. AV: Conceptualization, Funding acquisition, Resources, Supervision, Writing – review & editing. JS: Conceptualization, Funding acquisition, Resources, Supervision, Writing – review & editing, Writing – original draft, Investigation. AA: Conceptualization, Funding acquisition, Resources, Supervision, Writing – original draft, Writing – review & editing, Project administration, Data curation, Investigation.

## Funding

The author(s) declare financial support was received for the research, authorship, and/or publication of this article. This work was supported by the German Research Foundation (DFG) (INST 37/1049-1, INST 216/981-1, INST 257/605-1, INST 269/768-1, INST 217/988-1, INST 217/577-1, EXC2151 – 390873048; and SFB1454 – 432325352 to JS); Helmholtz-Gemeinschaft Deutscher Forschungszentren, Germany (sparse2big to JS and MN); EU projects SYSCID (733100 to JS); ERA CVD (00160389 to JS); ImmunoSep (847422 to JS); AA is supported by DFG under AS 637/1-1; AS 637/2-1; AS 637/3-1 and SFB1454 (432325352) and by the BMBF under IMMME/01EJ2204D. The 2000-HIV study is supported by an unrestricted grant from ViiV Healthcare (to AV, M.G.N., LJ). MN is supported by an ERC Advanced Grant (833247) and a Spinoza Grant of the Netherlands Organization for Scientific Research.

## Acknowledgments

We are grateful to the patients and donors volunteering to participate in this study making this research possible.

## Conflict of interest

The authors declare that the research was conducted in the absence of any commercial or financial relationships that could be construed as a potential conflict of interest.

The author(s) declared that they were an editorial board member of Frontiers, at the time of submission. This had no impact on the peer review process and the final decision.

## Publisher's note

All claims expressed in this article are solely those of the authors and do not necessarily represent those of their affiliated organizations, or those of the publisher, the editors and the reviewers. Any product that may be evaluated in this article, or claim that may be made by its manufacturer, is not guaranteed or endorsed by the publisher.

## Supplementary material

The Supplementary Material for this article can be found online at: https://www.frontiersin.org/articles/10.3389/fimmu.2023.1275136/full#supplementary-material

SUPPLEMENTARY FIGURE 1
Blood transcriptomes of PLHIV are dominated by monocyte-related proinflammatory gene programs. **(A)** Overview of age and sex of the cohort by disease group. **(A)** Multicolor flow cytometry (MCFC) cell distribution for HIV and controls. **(B)** Number of DEG for the comparison HIV vs. Ctrl in bulk PBMCs transcriptomes; IHW multiple comparison adjustment and false discovery rate (FDR) cutoff of 5%, significant fold change of >|1.5|. **(C)** Gene set variation analysis (GSVA) of the genes from the four clusters of the DE heatmap (from ).

SUPPLEMENTARY FIGURE 2
Bulk transcriptomics of monocytes in PLHIV mainly reveals IFN-signaling. **(A)** Boxplots of clinically relevant markers measured in the serum of PLHIV. References as blue bars (1). **(B)** Overview of MACS CD14 positive selection. **(C)** Number of DEG for the comparison HIV vs. Ctrl in bulk RNA-seq CD14; IHW multiple comparison adjustment and false discovery rate (FDR) cutoff of 5%, significant fold change of >|1.5|. **(D)** Boxplot and whisker of selected genes.

SUPPLEMENTARY FIGURE 3
'Anti-viral' monocyte state is persistent in PLHIV. **(A)** Cell type marker expression of the PLHIV dataset for all identified cell types. **(B)** Overlap of up-regulated DEG from monocytes extracted from scRNAseq and bulk $CD14^+$ transcriptomes (Supplementary Table S3). Genes contributing to the IFN-γ or IFN-α response pathways are indicated for the intersection as well as the uniquely identified DEG. **(C)** UMAP of integrated PBMCs from PLHIV and acute HIV split by dataset (total n= 89,500 cells, each 30,000 cells depicted). **(D)** Cell type marker expression of the integrated HIV dataset for all included cell types. **(E)** Monocyte cell state marker of the integrated monocytes from PLHIV and acute HIV. **(F)** Mapping of HIV-specific (upregulated) DEG of resting and non-classical monocyte states (for DEG see Supplementary Table S3) to PBMC clusters from . **(G)** Integrated monocyte UMAP subsetted for chronic HIV and stratified by donor.

SUPPLEMENTARY FIGURE 4
Drug repurposing to reverse monocyte reprogramming in PLHIV. **(A)** Enrichment of recurring target genes from cluster 43 in monocyte states of the integrated monocyte analysis (see ). **(B)** Included samples by treatment condition after quality control (QC) for the *in vitro* verification experiment. **(C)** Number of DEG (adj. p-value<0.05, |FC|>2, IHW) for each treatment vs. control (DMSO). **(D)** Heatmap showing the union of top leading edge genes of each signature (from ) for each treatment ranked by adj. p-value.

SUPPLEMENTARY TABLE 1
Donor overview.

SUPPLEMENTARY TABLE 2
Functional enrichment (GO and Hallmark) and transcription factor (TF) prediction of bulk RNA-seq PBMC heatmap clusters (related to Figure 1) and MCFC marker.

SUPPLEMENTARY TABLE 3
ScRNA-seq monocytes DEG (related to Figure 3).

SUPPLEMENTARY TABLE 4
Predicted drug clusters and signatures (related to Figure 4).

# References


1. van der Heijden WA, Van de Wijer L, Keramati F, Trypsteen W, Rutsaert S, Horst RT, et al. Chronic HIV infection induces transcriptional and functional reprogramming of innate immune cells. *J Clin Invest Insight* (2021) 6(7). doi: 10.1172/jci.insight.145928

2. Deeks SG, Tracy R, Douek DC. Systemic effects of inflammation on health during chronic HIV infection. *Immunity* (2013) 39(4):633–45. doi: 10.1016/j.immuni.2013.10.001

3. INSIGHT START Study Group, Lundgren JD, Babiker AG, Gordin F, Emery S, Grund B, et al. Initiation of antiretroviral therapy in early asymptomatic HIV infection. *New Engl J Med* (2015) 373(9):795–807. doi: 10.1056/NEJMoa1506816

4. Hunt PW, Lee SA, Siedner MJ. Immunologic biomarkers, morbidity, and mortality in treated HIV infection. *J Infect Dis* (2016) 214 Suppl 2(Suppl 2):S44–50. doi: 10.1093/infdis/jiw275

5. Zicari S, Sessa L, Cotugno N, Ruggiero A, Morrocchi E, Concato C, et al. Immune activation, inflammation, and non-AIDS co-morbidities in HIV-infected patients under long-term ART. *Viruses* (2019) 11(3):200. doi: 10.3390/v11030200

6. Dirajlal-Fargo S, Funderburg N. HIV and cardiovascular disease: the role of inflammation. *Curr Opin HIV AIDS* (2022) 17(5):286–92. doi: 10.1097/COH.0000000000000755

7. Freeman ML, Shive CL, Nguyen TP, Younes S-A, Panigrahi S, Lederman MM. Cytokines and T-cell homeostasis in HIV infection. *J Infect Dis* (2016) 214 Suppl 2 (Suppl 2):S51–7. doi: 10.1093/infdis/jiw287

8. Sandler NG, Wand H, Roque A, Law M, Nason MC, Nixon DE, et al. Plasma levels of soluble CD14 independently predict mortality in HIV infection. *J Infect Dis* (2011) 203(6):780–90. doi: 10.1093/infdis/jiq118

9. Mensching L, Hoelzemer A. NK cells, monocytes and macrophages in HIV-1 control: impact of innate immune responses. *Front Immunol* (2022) 13:883728. doi: 10.3389/fimmu.2022.883728

10. McKibben RA, Margolick JB, Grinspoon S, Li X, Palella FJ, Kingsley LA, et al. Elevated levels of monocyte activation markers are associated with subclinical atherosclerosis in men with and those without HIV infection. *J Infect Dis* (2015) 211 (8):1219–28. doi: 10.1093/infdis/jiu594

11. Van de Wijer L, van der Heijden WA, Ter Horst R, Jaeger M, Trypsteen W, Rutsaert S, et al. The architecture of circulating immune cells is dysregulated in people living with HIV on long term antiretroviral treatment and relates with markers of the HIV-1 reservoir, cytomegalovirus, and microbial translocation. *Front Immunol* (2021) 12:661990. doi: 10.3389/fimmu.2021.661990

12. van der Heijden WA, Wan J, Van de Wijer L, Jaeger M, Netea MG, van der Ven AJ, et al. Plasmatic coagulation capacity correlates with inflammation and abacavir use during chronic HIV infection. *JAIDS J Acquired Immune Deficiency Syndromes* (2021) 87(1):711–9. doi: 10.1097/QAI.0000000000002633

13. van der Heijden WA, van de Wijer L, Jaeger M, Grintjes K, Netea MG, Urbanus RT, et al. Long-term treated HIV infection is associated with platelet mitochondrial dysfunction. *Sci Rep* (2021) 11(1):6246. doi: 10.1038/s41598-021-85775-5

14. Navas A, Van de Wijer L, Jacobs-Cleophas M, Schimmel-Naber AM, van Cranenbroek B, van der Heijden WA, et al. Comprehensive phenotyping of circulating immune cell subsets in people living with HIV. *J Immunol Methods* (2022) 507:113307. doi: 10.1016/j.jim.2022.113307

15. Gianella S, Letendre S. Cytomegalovirus and HIV: A dangerous pas de deux. *J Infect Dis* (2016) 214 Suppl 2(Suppl 2):S67–74. doi: 10.1093/infdis/jiw217

16. Hatano H. Immune activation and HIV persistence: considerations for novel therapeutic interventions. *Curr Opin HIV AIDS* (2013) 8(3):211–6. doi: 10.1097/COH.0b013e32835f9788

17. Brenchley JM, Price DA, Schacker TW, Asher TE, Silvestri G, Rao S, et al. Microbial translocation is a cause of systemic immune activation in chronic HIV infection. *Nat Med* (2006) 12(12):1365–71. doi: 10.1038/nm1511

18. Rajewsky N, Almouzni G, Gorski SA, Aerts S, Amit I, Bertero MG, et al. LifeTime and improving European healthcare through cell-based interceptive medicine. *Nature* (2020) 587(7834):377–86. doi: 10.1038/s41586-020-2715-9

19. Liu N, Jiang C, Cai P, Shen Z, Sun W, Xu H, et al. Single-cell analysis of COVID-19, sepsis, and HIV infection reveals hyperinflammatory and immunosuppressive signatures in monocytes. *Cell Rep* (2021) 37(1):109793. doi: 10.1016/j.celrep.2021.109793

20. Rood JE, Maartens A, Hupalowska A, Teichmann SA, Regev A. Impact of the human cell atlas on medicine. *Nat Med* (2022) 28(12):2486–96. doi: 10.1038/s41591-022-02104-7

21. Bernardes JP, Mishra N, Tran F, Bahmer T, Best L, Blase JI, et al. Longitudinal multi-omics analyses identify responses of megakaryocytes, erythroid cells, and plasmablasts as hallmarks of severe COVID-19. *Immunity* (2020) 53(6):1296–1314.e9. doi: 10.1016/j.immuni.2020.11.017

22. Schulte-Schrepping J, Reusch N, Paclik D, Baßler K, Schlickeiser S, Zhang B, et al. Severe COVID-19 is marked by a dysregulated myeloid cell compartment. *Cell* (2020) 182(6):1419–1440.e23. doi: 10.1016/j.cell.2020.08.001

23. Krämer B, Knoll R, Bonaguro L, ToVinh M, Raabe J, Astaburuaga-García R, et al. Early IFN-α signatures and persistent dysfunction are distinguishing features of NK cells in severe COVID-19. *Immunity* (2021) 54(11):2650–2669.e14. doi: 10.1016/j.immuni.2021.09.002

24. Baßler K, Fujii W, Kapellos TS, Dudkin E, Reusch N, Horne A, et al. Alveolar macrophages in early stage COPD show functional deviations with properties of impaired immune activation. *Front Immunol* (2022) 13:917232. doi: 10.3389/fimmu.2022.917232

25. Bonaguro L, Schulte-Schrepping J, Ulas T, Aschenbrenner AC, Beyer M, Schultze JL. A guide to systems-level immunomics. *Nat Immunol* (2022) 23 (10):1412–23. doi: 10.1038/s41590-022-01309-9

26. Carraro C, Bonaguro L, Schulte-Schrepping J, Horne A, Oestreich M, Warnat-Herresthal S, et al. Decoding mechanism of action and sensitivity to drug candidates from integrated transcriptome and chromatin state. *eLife* (2022) 11. doi: 10.7554/eLife.78012

27. Wang S, Song R, Wang Z, Jing Z, Wang S, Ma J. S100A8/A9 in inflammation. *Front Immunol* (2018) 9:1298. doi: 10.3389/fimmu.2018.01298

28. Knoll R, Schultze JL, Schulte-Schrepping J. Monocytes and macrophages in COVID-19. *Front Immunol* (2021) 12:720109. doi: 10.3389/fimmu.2021.720109

29. Chaudhuri A, Yang B, Gendelman HE, Persidsky Y, Kanmogne GD. STAT1 signaling modulates HIV-1-induced inflammatory responses and leukocyte transmigration across the blood-brain barrier. *Blood* (2008) 111(4):2062–72. doi: 10.1182/blood-2007-05-091207

30. Appelberg KS, Wallet MA, Taylor JP, Cash MN, Sleasman JW, Goodenow MM. HIV-1 infection primes macrophages through STAT signaling to promote enhanced inflammation and viral replication. *AIDS Res Hum Retroviruses* (2017) 33(7):690–702. doi: 10.1089/AID.2016.0273

31. Lien E, Aukrust P, Sundan A, Müller F, Frøland SS, Espevik T. Elevated levels of serum-soluble CD14 in human immunodeficiency virus type 1 (HIV-1) infection: correlation to disease progression and clinical events. *Blood* (1998) 92(6):2084–92. doi: 10.1182/blood.V92.6.2084

32. Shive CL, Jiang W, Anthony DD, Lederman MM. Soluble CD14 is a nonspecific marker of monocyte activation. *AIDS* (2015) 29(10):1263–5. doi: 10.1097/QAD.0000000000000735

33. Kazer SW, Aicher TP, Muema DM, Carroll SL, Ordovas-Montanes J, Miao VN, et al. Integrated single-cell analysis of multicellular immune dynamics during hyperacute HIV-1 infection. *Nat Med* (2020) 26(4):511–8. doi: 10.1038/s41591-020-0799-2

34. Aschenbrenner AC, Mouktaroudi M, Krämer B, Oestreich M, Antonakos N, Nuesch-Germano M, et al. Disease severity-specific neutrophil signatures in blood transcriptomes stratify COVID-19 patients. *Genome Med* (2021) 13(1):7. doi: 10.1186/s13073-020-00823-5

35. Subramanian A, Narayan R, Corsello SM, Peck DD, Natoli TE, Lu X, et al. A next generation connectivity map: L1000 platform and the first 1,000,000 profiles. *Cell* (2017) 171(6):1437–1452.e17. doi: 10.1016/j.cell.2017.10.049

36. Pilarczyk M, Fazel-Najafabadi M, Kouril M, Shamsaei B, Vasiliauskas J, Niu W, et al. Connecting omics signatures and revealing biological mechanisms with iLINCS. *Nat Commun* (2022/) 13:4678/. doi: 10.1038/s41467-022-32205-3

37. Dochi T, Akita A, Kishimoto N, Takamune N, Misumi S. Trametinib suppresses HIV-1 replication by interfering with the disassembly of human immunodeficiency virus type 1 capsid core. *Biochem Biophys Res Commun* (2018) 495(2):1846–50. doi: 10.1016/j.bbrc.2017.11.177

38. Guo J, Xu X, Rasheed TK, Yoder A, Yu D, Liang H, et al. Genistein interferes with SDF-1- and HIV-mediated actin dynamics and inhibits HIV infection of resting CD4 T cells. *Retrovirology* (2013) 10:62. doi: 10.1186/1742-4690-10-62

39. Fields JA, Metcalf J, Overk C, Adame A, Spencer B, Wrasidlo W, et al. The anticancer drug sunitinib promotes autophagyand protects from neurotoxicity in an HIV-1 Tat model of neurodegeneration. *J Neurovirology* (2017) 23(2):290–303. doi: 10.1007/s13365-016-0502-z

40. Best C, Struthers H, Laciny E, Royal M, Reeds DN, Yarasheski KE. Sitagliptin reduces inflammation and chronic immune cell activation in HIV+ adults with impaired glucose tolerance. *J Clin Endocrinol Metab* (2015) 100(7):2621–9. doi: 10.1210/jc.2015-1531

41. Dubé MP, Chan ES, Lake JE, Williams B, Kinslow J, Landay A, et al. A randomized, double-blinded, placebo-controlled trial of sitagliptin for reducing inflammation and immune activation in treated and suppressed human immunodeficiency virus infection. *Clin Infect Dis* (2019) 69(7):1165–72. doi: 10.1093/cid/ciy1051

42. Daly MB, Roth ME, Bonnac L, Maldonado JO, Xie J, Clouser CL, et al. Dual anti-HIV mechanism of clofarabine. *Retrovirology* (2016) 13:20. doi: 10.1186/s12977-016-0254-0

43. Soper A, Kimura I, Nagaoka S, Konno Y, Yamamoto K, Koyanagi Y, et al. Type I interferon responses by HIV-1 infection: association with disease progression and control. *Front Immunol* (2017) 8:1823. doi: 10.3389/fimmu.2017.01823

44. Soare AY, Durham ND, Gopal R, Tweel B, Hoffman KW, Brown JA, et al. P2X antagonists inhibit HIV-1 productive infection and inflammatory cytokines interleukin-10 (IL-10) and IL-1β in a human tonsil explant model. *J Virology* (2019) 93(1):e01186-18. doi: 10.1128/JVI.01186-18

45. Calza L, Trapani F, Bartoletti M, Manfredi R, Colangeli V, Borderi M, et al. Statin therapy decreases serum levels of high-sensitivity C-reactive protein and tumor necrosis factor-α in HIV-infected patients treated with ritonavir-boosted protease inhibitors. *HIV Clin Trials* (2012) 13(3):153–61. doi: 10.1310/hct1303-153

46. Eckard AR, Jiang Y, Debanne SM, Funderburg NT, McComsey GA. Effect of 24 weeks of statin therapy on systemic and vascular inflammation in HIV-infected subjects receiving antiretroviral therapy. *J Infect Diseases* (2014) 209(8):1156–64. doi: 10.1093/infdis/jiu012

47. Lo J, Lu MT, Ihenachor EJ, Wei J, Looby SE, Fitch KV, et al. Effects of statin therapy on coronary artery plaque volume and high-risk plaque morphology in HIV-infected patients with subclinical atherosclerosis: a randomised, double-blind, placebo-controlled trial. *Lancet HIV* (2015) 2(2):e52–63. doi: 10.1016/S2352-3018(14)00032-0

48. Eckard AR, Meissner EG, Singh I, McComsey GA. Cardiovascular disease, statins, and HIV. *J Infect Dis* (2016) 214 Suppl 2(Suppl 2):S83–92. doi: 10.1093/infdis/jiw288

49. Fitch KV, Fulda ES, Grinspoon SK. Statins for primary cardiovascular disease prevention among people with HIV: emergent directions. *Curr Opin HIV AIDS* (2022) 17(5):293–300. doi: 10.1097/COH.0000000000000752

50. Faivre S, Demetri G, Sargent W, Raymond E. Molecular basis for sunitinib efficacy and future clinical development. *Nat Rev Drug Discov* (2007) 6(9):734–45. doi: 10.1038/nrd2380

51. Lian T, Li C, Wang H. Trametinib in the treatment of multiple Malignancies harboring MEK1 mutations. *Cancer Treat Rev* (2019) 81:101907. doi: 10.1016/j.ctrv.2019.101907

52. Domínguez-Andrés J, Arts RJW, Bekkering S, Bahrar H, Blok BA, de Bree LCJ, et al. In vitro induction of trained immunity in adherent human monocytes. *STAR Protoc* (2021) 2(1):100365. doi: 10.1016/j.xpro.2021.100365

53. Vadaq N, Zhang Y, Vos WA, Groenendijk A, Blaauw M, Eekeren L, et al. High-throughput proteomic analysis reveals systemic dysregulation in virally suppressed people living with HIV. *J Clin Invest Insight* (2023) 8(11):e166166. doi: 10.1172/jci.insight.166166

54. Dobin A, Davis CA, Schlesinger F, Drenkow J, Zaleski C, Jha S, et al. STAR: ultrafast universal RNA-seq aligner. *Bioinformatics* (2013) 29(1):15–21. doi: 10.1093/bioinformatics/bts635

55. Love MI, Huber W, Anders S. Moderated estimation of fold change and dispersion for RNA-seq data with DESeq2. *Genome Biol* (2014) 15(12):550. doi: 10.1186/s13059-014-0550-8

56. Bray NL, Pimentel H, Melsted P, Pachter L. Near-optimal probabilistic RNA-seq quantification. *Nat Biotechnol* (2016) 34(5):525–7. doi: 10.1038/nbt.3519

57. Leek JT, Johnson WE, Parker HS, Jaffe AE, Storey JD. The sva package for removing batch effects and other unwanted variation in high-throughput experiments. *Bioinformatics* (2012) 28(6):882–3. doi: 10.1093/bioinformatics/bts034

58. Ritchie ME, Phipson B, Wu D, Hu Y, Law CW, Shi W, et al. limma powers differential expression analyses for RNA-sequencing and microarray studies. *Nucleic Acids Res* (2015) 43(7):e47. doi: 10.1093/nar/gkv007

59. Aibar S, González-Blas CB, Moerman T, Huynh-Thu VA, Imrichova H, Hulselmans G, et al. SCENIC: single-cell regulatory network inference and clustering. *Nat Methods* (2017) 14(11):1083–6. doi: 10.1038/nmeth.4463

60. Ashburner M, Ball CA, Blake JA, Botstein D, Butler H, Cherry JM, et al. Gene Ontology: tool for the unification of biology. *Nat Genet* (2000) 25(1):25–9. doi: 10.1038/75556

61. The Gene Ontology Consortium. The Gene Ontology Resource: 20 years and still GOing strong. *Nucleic Acids Res* (2019) 47(D1):D330–8. doi: 10.1093/nar/gky1055

62. Liberzon A, Birger C, Thorvaldsdóttir H, Ghandi M, Mesirov JP, Tamayo P. The Molecular Signatures Database (MSigDB) hallmark gene set collection. *Cell Systems* (2015) 1(6):417–25. doi: 10.1016/j.cels.2015.12.004

63. Yu G, Wang L-G, Han Y, He Q-Y. clusterProfiler: an R package for comparing biological themes among gene clusters. *Omics: J Integr Biol* (2012) 16(5):284–7. doi: 10.1089/omi.2011.0118

64. Hänzelmann S, Castelo R, Guinney J. GSVA: gene set variation analysis for microarray and RNA-seq data. *BMC Bioinf* (2013) 14:7. doi: 10.1186/1471-2105-14-7

65. McInnes L, Healy J, Saul N, Großberger L. UMAP: uniform manifold approximation and projection for dimension reduction. *J Open Source Softw* (2018) 3(29):861. doi: 10.21105/joss.00861

66. Levine JH, Simonds EF, Bendall SC, Davis KL, Amir ED, Tadmor MD, et al. Data-driven phenotypic dissection of AML reveals progenitor-like cells that correlate with prognosis. *Cell* (2015) 162(1):184–97. doi: 10.1016/j.cell.2015.05.047

67. Langmead B, Salzberg SL. Fast gapped-read alignment with Bowtie 2. *Nat Methods* (2012) 9(4):357–9. doi: 10.1038/nmeth.1923

68. Danecek P, Bonfield JK, Liddle J, Marshall J, Ohan V, Pollard MO, et al. Twelve years of SAMtools and BCFtools. *GigaScience* (2021) 10(2). doi: 10.1093/gigascience/giab008

69. Zhang Y, Liu T, Meyer CA, Eeckhoute J, Johnson DS, Bernstein BE, et al. Model-based analysis of chIP-seq (MACS). *Genome Biol* (2008) 9(9):R137. doi: 10.1186/gb-2008-9-9-r137

70. Yu G, Wang L-G, He Q-Y. ChIPseeker: an R/Bioconductor package for ChIP peak annotation, comparison and visualization. *Bioinformatics* (2015) 31(14):2382–3. doi: 10.1093/bioinformatics/btv145

71. Butler A, Hoffman P, Smibert P, Papalexi E, Satija R. Integrating single-cell transcriptomic data across different conditions, technologies, and species. *Nat Biotechnol* (2018) 36(5):411–20. doi: 10.1038/nbt.4096

72. Stuart T, Butler A, Hoffman P, Hafemeister C, Papalexi E, Mauck WM, et al. Comprehensive integration of single-cell data. *Cell* (2019) 177(7):1888–1902.e21. doi: 10.1016/j.cell.2019.05.031

73. Korsunsky I, Millard N, Fan J, Slowikowski K, Zhang F, Wei K, et al. Fast, sensitive and accurate integration of single-cell data with Harmony. *Nat Methods* (2019) 16(12):1289–96. doi: 10.1038/s41592-019-0619-0

74. Wickham H. ggplot2: Elegant Graphics for Data Analysis. Springer-Verlag New York. (2016). Available at: https://ggplot2.tidyverse.org.

75. Gu Z, Eils R, Schlesner M. Complex heatmaps reveal patterns and correlations in multidimensional genomic data. *Bioinformatics* (2016) 32(18):2847–9. doi: 10.1093/bioinformatics/btw313

Cell

Article

# The life-saving benefit of dexamethasone in severe COVID-19 is linked to a reversal of monocyte dysregulation

## Graphical abstract

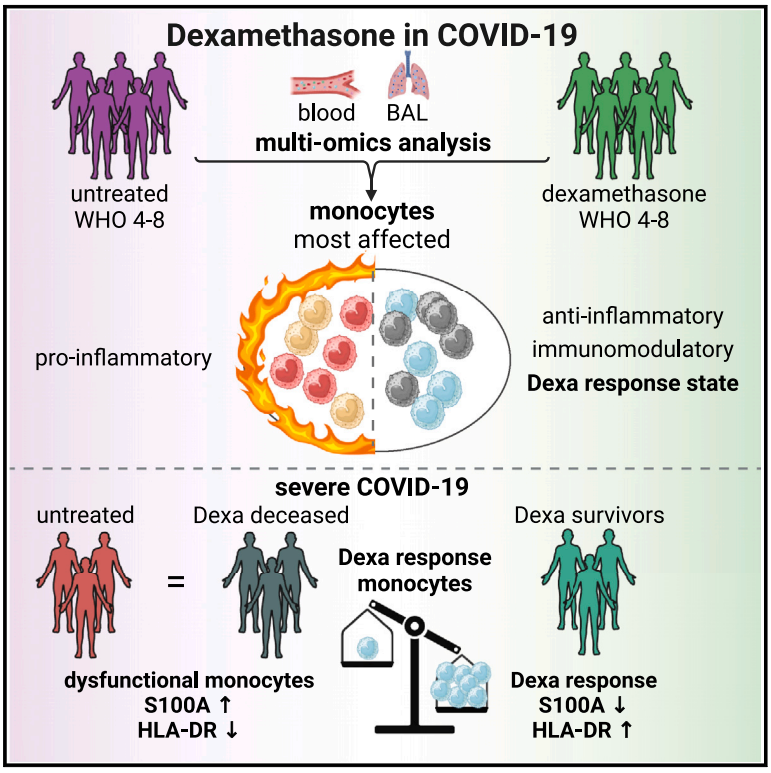


## Highlights

- Dexamethasone-induced transcriptional changes were confined to a specific monocyte state
- Molecular treatment responses in monocytes were directly linked to clinical outcome
- Reversal of dysregulated monocyte signatures in dexamethasone-treated COVID-19 survivors
- Monocyte single-cell signatures stratified blood samples for treatment response

## Authors

Rainer Knoll, Elisa T. Helbig, Kilian Dahm, ..., Joachim L. Schultze, Anna C. Aschenbrenner, Florian Kurth

## Correspondence

anna.aschenbrenner@dzne.de

## In brief

Dexamethasone was used as an effective drug for severe COVID cases during the pandemic. A study integrating single-cell and bulk transcriptomics in clinical cohorts reveals the molecular basis of its immunomodulatory effect and also provides a framework for the future development of companion diagnostics for patient stratification in precision medicine.

Knoll et al., 2024, Cell *187*, 4318–4335
August 8, 2024 © 2024 The Authors. Published by Elsevier Inc.
https://doi.org/10.1016/j.cell.2024.06.014

CellPress

CellPress
OPEN ACCESS

Cell

Article

# The life-saving benefit of dexamethasone in severe COVID-19 is linked to a reversal of monocyte dysregulation

Rainer Knoll,[1,20] Elisa T. Helbig,[2,20] Kilian Dahm,[1,3] Olufemi Bolaji,[4] Frederik Hamm,[5] Oliver Dietrich,[6] Martina van Uelft,[1,7] Sophie Müller,[1,7,8] Lorenzo Bonaguro,[1,9] Jonas Schulte-Schrepping,[1,9] Lev Petrov,[4] Benjamin Krämer,[10] Michael Kraut,[9] Paula Stubbemann,[2] Charlotte Thibeault,[2,11] Sophia Brumhard,[2] Heidi Theis,[9] Gudrun Hack,[10] Elena De Domenico,[9] Jacob Nattermann,[10] Matthias Becker,[1] Marc D. Beyer,[1,9,12] David Hillus,[2] Philipp Georg,[2] Constantin Loers,[2] Janina Tiedemann,[2] Pinkus Tober-Lau,[2] Lena Lippert,[2] Belén Millet Pascual-Leone,[2] Frank Tacke,[13] Gernot Rohde,[14,15,16] Norbert Suttorp,[2,16,17] Martin Witzenrath,[2,16,17] CAPNETZ Study Group, Pa-COVID-19 Study Group, Antoine-Emmanuel Saliba,[6,18] Thomas Ulas,[1,7,9] Julia K. Polansky,[5,19] Birgit Sawitzki,[4] Leif E. Sander,[2,5,17,20] Joachim L. Schultze,[1,7,9,20] Anna C. Aschenbrenner,[1,20,21,*] and Florian Kurth[2,17,20]

[1]Systems Medicine, Deutsches Zentrum für Neurodegenerative Erkrankungen (DZNE), Bonn, Germany
[2]Department of Infectious Diseases and Critical Care Medicine, Charité - Universitätsmedizin Berlin, Berlin, Germany
[3]Translational Pediatrics, Department of Pediatrics, University Hospital Würzburg, Würzburg, Germany
[4]Institute of Medical Immunology, Charité - Universitätsmedizin Berlin, Berlin, Germany
[5]BIH Center for Regenerative Therapies (BCRT), Berlin Institute of Health at Charité - Universitätsmedizin Berlin, Berlin, Germany
[6]Helmholtz Institute for RNA-based Infection Research (HIRI), Helmholtz-Center for Infection Research (HZI), Würzburg, Germany
[7]Genomics & Immunoregulation, Life & Medical Sciences Institute, University of Bonn, Bonn, Germany
[8]Department of Microbiology and Immunology, The University of Melbourne at the Peter Doherty Institute for Infection and Immunity, Melbourne, VIC, Australia
[9]PRECISE Platform for Single Cell Genomics and Epigenomics, DZNE, University of Bonn, and West German Genome Center, Bonn, Germany
[10]Department of Internal Medicine I, University Hospital Bonn, Bonn, Germany
[11]BIH Biomedical Innovation Academy, BIH Charité Clinician Scientist Program, Berlin Institute of Health at Charité - Universitätsmedizin Berlin, Berlin, Germany
[12]Immunogenomics & Neurodegeneration, Systems Medicine, Deutsches Zentrum für Neurodegenerative Erkrankungen (DZNE), Bonn, Germany
[13]Department of Hepatology and Gastroenterology, Charité - Universitätsmedizin Berlin, Berlin, Germany
[14]Department of Respiratory Medicine, Medical Clinic I, Goethe-Universität Frankfurt am Main, Frankfurt, Germany
[15]Biomedical Research in Endstage and Obstructive Lung Disease Hannover (BREATH), Member of the German Center for Lung Research (DZL), Hannover, Germany
[16]CAPNETZ STIFTUNG, 30625 Hannover, Germany
[17]German Center for Lung Research (DZL), Germany
[18]Faculty of Medicine, Institute of Molecular Infection Biology (IMIB), University of Würzburg, Josef-Schneider-Str. 2, 97080 Würzburg, Germany
[19]German Rheumatism Research Centre (DRFZ) Berlin, Berlin, Germany
[20]These authors contributed equally
[21]Lead contact
*Correspondence: anna.aschenbrenner@dzne.de
https://doi.org/10.1016/j.cell.2024.06.014

## SUMMARY

Dexamethasone is a life-saving treatment for severe COVID-19, yet its mechanism of action is unknown, and many patients deteriorate or die despite timely treatment initiation. Here, we identify dexamethasone treatment-induced cellular and molecular changes associated with improved survival in COVID-19 patients. We observed a reversal of transcriptional hallmark signatures in monocytes associated with severe COVID-19 and the induction of a monocyte substate characterized by the expression of glucocorticoid-response genes. These molecular responses to dexamethasone were detected in circulating and pulmonary monocytes, and they were directly linked to survival. Monocyte single-cell RNA sequencing (scRNA-seq)-derived signatures were enriched in whole blood transcriptomes of patients with fatal outcome in two independent cohorts, highlighting the potential for identifying non-responders refractory to dexamethasone. Our findings link the effects of dexamethasone to specific immunomodulation and reversal of monocyte dysregulation, and they highlight the potential of single-cell omics for monitoring *in vivo* target engagement of immunomodulatory drugs and for patient stratification for precision medicine approaches.

 © 2024 The Authors. Published by Elsevier Inc.
This is an open access article under the CC BY-NC-ND license (http://creativecommons.org/licenses/by-nc-nd/4.0/).

## INTRODUCTION

Dexamethasone represents the first and most effective treatment against severe COVID-19,[1] with likely millions of lives saved worldwide during the COVID-19 pandemic. Based on transcriptome-based reverse drug target prediction, we had identified dexamethasone as a potential drug candidate for a subgroup of patients with severe disease courses.[2] As early as June 2020, preliminary data from the Randomized Evaluation of COVID-19 Therapy (RECOVERY) platform trial demonstrated a significant clinical benefit of dexamethasone, reducing the relative risk of 28-day mortality by approximately 30% in patients with severe COVID-19 requiring mechanical ventilation.[1] The benefit of glucocorticoid (GC) treatment in severe COVID-19 was subsequently validated in further trials[1,3,4] and dexamethasone quickly became the standard of care (SOC) for all patients with COVID-19 requiring supplemental oxygen or mechanical ventilation.[5] The survival benefit was lower in patients requiring supplemental oxygen therapy without invasive ventilation, whereas no benefit and even harm was observed in patients without respiratory failure and no need for supplemental oxygen, particularly at higher doses.[1,6,7] Although no impact of dexamethasone on severe acute respiratory syndrome coronavirus 2 (SARS-CoV-2) viral load kinetics, antibody and T cell response was observed with the standard dexamethasone dose used in the RECOVERY trial,[8,9] negative effects of corticosteroid use have previously been reported for patients with viral pneumonia caused by SARS-CoV and Middle East respiratory syndrome-related coronavirus (MERS-CoV),[10] where delayed viral clearance was observed, as well as for influenza, where corticosteroid therapy is associated with higher mortality.[11]

As no mechanistic studies were conducted in the pivotal clinical efficacy trials, smaller experimental studies have elaborated on the potential effects of corticosteroids on the immune system. A recent study demonstrated that dexamethasone treatment of patients with severe COVID-19 affected circulating neutrophils. The study revealed transcriptional alteration of several of the known neutrophil cell states in peripheral blood, mainly counteracting sustained interferon (IFN) activation and reinforcing suppressor states, suggesting limitation of neutrophil pathogenicity.[12] In two hamster models, a strong anti-inflammatory effect of dexamethasone was postulated as a major effect of therapy, which was also linked to a specifically responsive subpopulation of neutrophils.[13] Downregulation of STAT1 target genes in monocytes[14] as well as suppression of T cell function[15] were two other potential modes of action of dexamethasone in COVID-19, yet a link of these transcriptomic changes to treatment response and clinical outcome is missing.

Despite the proven clinical effectiveness of dexamethasone, a substantial number of patients progresses to critical illness and die from COVID-19 with apparently little or no response to dexamethasone treatment. Overall, the mechanisms of action of dexamethasone in severe COVID-19 are unknown, and biomarkers of treatment response or treatment failure are missing. Early prediction of treatment failure, however, would be valuable to guide early step-up of immunomodulatory therapy, and results from recent clinical trials assessing efficacy of dexamethasone in COVID-19 further support the need for biomarker-supported clinical decision processes, even for such well-known and widely used drugs as corticosteroids.[6,16]

Here, we provide a framework to identify molecular modes of action and markers of treatment response of repurposed drugs, exemplified by dexamethasone in COVID-19. We identified patients treated with and without dexamethasone according to criteria of the RECOVERY trial during the first months of the COVID-19 pandemic from a large observational cohort study.[17] We generated single-cell omics profiles from peripheral blood-derived immune cells, deciphered cellular, molecular, and functional changes to dexamethasone treatment, and linked the observed changes to clinical outcomes. We found that dexamethasone specifically reverses the dysfunctional molecular phenotypes associated with severe COVID-19 in monocytes of patients with a clinical response to treatment but not those with a fatal outcome. Based on these outcome-specific single-cell gene expression data, we generated transcriptomic signatures that we transferred to whole blood transcriptomes of two independent COVID-19 cohorts, demonstrating their potential as predictive biomarkers for treatment response in clinical studies. We reveal molecular hallmarks that are linked to the life-saving effects of dexamethasone and demonstrate, in general, the feasibility of single-cell transcriptomics to assess *in vivo* drug target engagement and treatment responses in clinical studies.

## RESULTS

### Dexamethasone treatment leads to immunomodulation in circulating immune cells

To determine cellular and molecular changes induced by dexamethasone treatment in COVID-19 patients, we identified all patients enrolled in our central phenotyping platform study[17] who were infected during the first two waves of the COVID-19 pandemic (i.e., infected with SARS-CoV-2 D614G strain) and who were either GC naive (first wave from March to May 2020, termed control patients, short "ctrl") or who were treated with dexamethasone (second wave from October 2020 to February 2021) (Figure 1A; Table S1).[17] We carefully selected patients who met the criteria for dexamethasone treatment as identified in the RECOVERY trial. Of note, all selected patients did not receive any other immunomodulatory or any antiviral treatment. We selected patients who received dexamethasone or were treatment-naive and matched them for sex, age, disease severity, and time from symptom onset to blood sampling, resulting in comparable baseline characteristics and disease severity (Table S1). Whole blood and peripheral blood mononuclear cells (PBMCs) were taken on average 8 days after treatment initiation and subjected to high-dimensional single-cell analyses utilizing cytometry by time of flight (CyTOF), single-cell RNA sequencing (scRNA-seq), and multi-color flow cytometry.

Assessment of compositional alterations of the major immune cell types (Figure 1B) by CyTOF revealed significantly increased leukocytes in dexamethasone-treated patients with moderate disease severity (Figure 1C). Increased leukocyte frequencies were mainly due to alterations in B cells and neutrophils in moderately ill patients (hospitalized patients requiring oxygen supplementation but no mechanical ventilation), while there

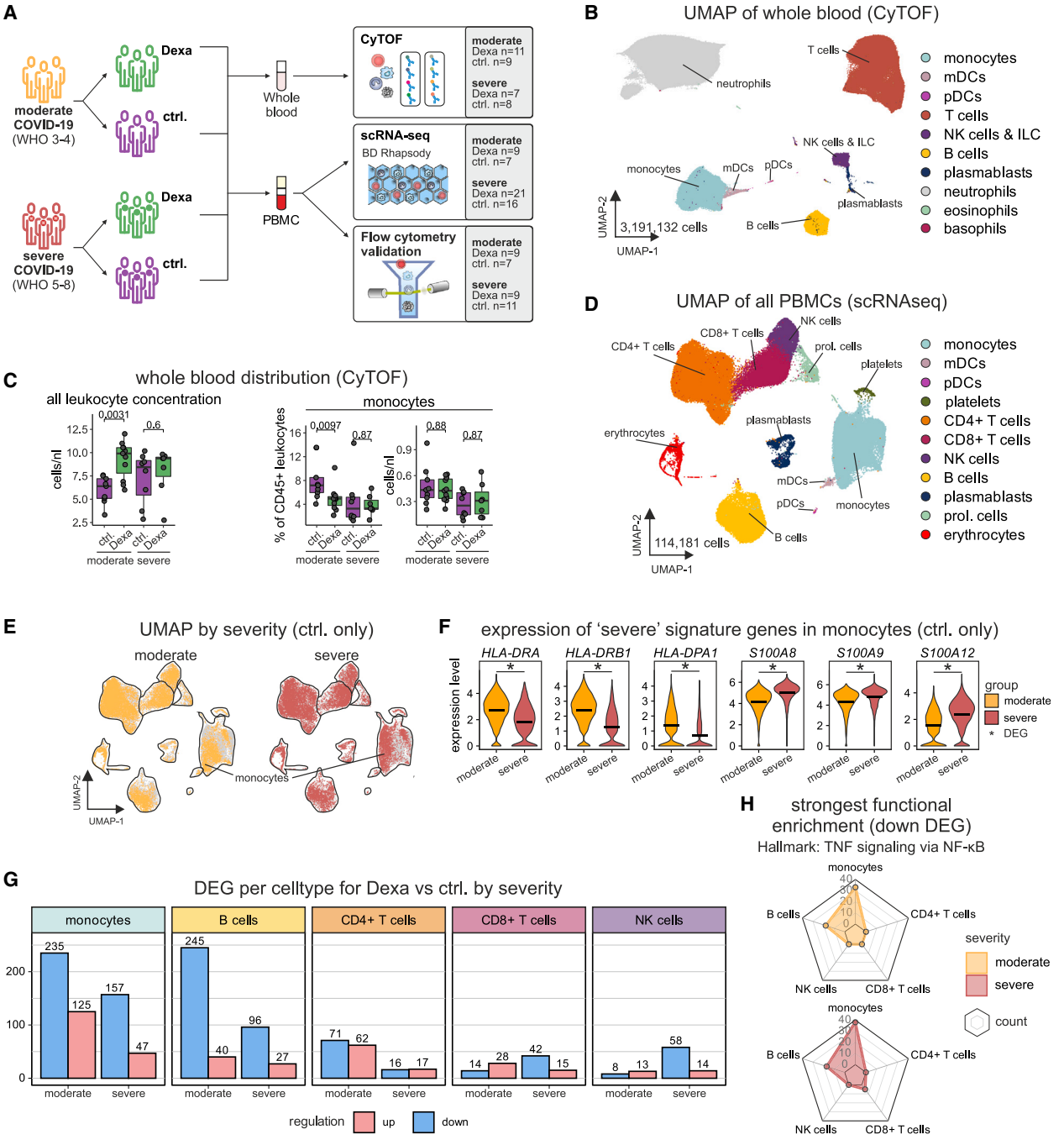


**Figure 1. Dexamethasone treatment leads to immunomodulation in circulating immune cells**

(A) Study design: hospitalized moderately (supplemental oxygen needed) and severely affected (i.e., intensive care unit treatment) patients with COVID-19 treated with dexamethasone were matched for sex, age, disease severity, and time from symptom onset to blood sampling with treatment-naive COVID-19 patients (ctrl.). Samples were obtained prior to treatment or corresponding time points for controls ("early"), respectively, and toward the end of the treatment period and corresponding time points for controls ("late"). Whole blood leukocytes were analyzed by CyTOF, and purified PBMCs were analyzed by scRNA-seq and flow cytometry for marker validation. Included sample numbers are indicated. See Table S1.

(B) UMAP of whole blood cells (downsampled from $n$ = 3,191,132 to $n$ = 986,030 cells for better visualization) from CyTOF with identified cell types indicated.

(C) Absolute leukocyte counts from differential blood count, monocyte percentages, and concentration of whole blood cells from CyTOF. Wilcoxon test for statistical significance, and resulting $p$ value is indicated.

(D) UMAP visualization of the entire PBMC space ($n$ = 114,181 cells) from scRNA-seq with indicated major cell types.

*(legend continued on next page)*

was no difference in dexamethasone-treated severely ill patients (Figure S1A). Further, there was a relative decrease of monocytes in dexamethasone-treated patients with moderate disease (Figure 1C). Altogether, the compositional changes indicated cell-type-related immunomodulatory alterations of dexamethasone treatment.

Next, we defined molecular phenotypes and treatment-related transcriptional alterations of a total of 114,181 PBMCs by scRNA-seq. All major blood-derived immune cell types were present in our dataset (Figures 1D and S1B). Overlaying time of sampling after symptom onset ($\leq$10 and >10 days, Figure S1C) or disease severity onto the uniform manifold approximation and projection (UMAP) (Figure 1E) revealed global distribution shifts, as previously described,[18] particularly within the monocyte compartment. Specifically, we observed profound disease severity-related alterations in expression of human leukocyte antigen (HLA) and S100A genes (Figure 1F) and the IFN system (Figure S1D), as previously described.[18] In order to reveal transcriptional effects of dexamethasone treatment, we quantified differentially expressed genes (DEGs) by cell type (Figure 1G). We observed the strongest treatment-dependent transcriptional changes in monocytes, followed by B cells and $CD4^+$ T cells, with all other cell types showing a moderate gene regulation. Of note, we observed an upregulation of a substantial number of genes associated with dexamethasone treatment in monocytes in moderate and severe disease (Figure 1G). Despite clear differences in the magnitude of transcriptional alterations between cell types, we identified a small set of DEGs shared across cell types in severe COVID-19, including the well-known GC receptor target genes *TSC22D3*[19] and *TXNIP*[20] among the commonly upregulated genes, while *IFITM1* and *FTH1* were among the downregulated genes (Figure S1E). Functional enrichment analysis across all major cell types using all up- and downregulated genes revealed that a large number of genes are tumor necrosis factor alpha (TNF)-mediated nuclear factor κB (NF-κB) target genes, particularly within downregulated DEGs (Figures 1H and S1F), which corroborates previous findings that corticosteroids can inhibit NF-κB transcription factor family members.[21,22] The importance of dexamethasone-related changes in the monocyte compartment was further illustrated by the strongest enrichment scores of many other cellular functions when assessing upregulated DEGs in patients with severe disease (Figure S1F, right panel).

In summary, we observed transcriptional changes associated with dexamethasone treatment that were quantitatively most prominent in monocytes and B cells and exhibited cell-type-specific modulations in addition to common transcriptional changes.

## Dexamethasone treatment elicits a unique cell state in a subset of monocytes

To determine disease severity-dependent commonalities and differences in the transcriptional response of monocytes to treatment, we compared DEGs in monocytes from dexamethasone-treated (Dexa) vs. untreated (ctrl.) patients with severe and moderate COVID-19 (Figure 2A). Dexamethasone treatment suppressed expression of several proinflammatory genes, including *IL1B*, *CCL3*, *CCL4*, *CCL3L3*, and *CCL4L2*, irrespective of disease severity, and induced a disease severity-independent gene program, which included known GC-response genes such as *IL1R2*, the decoy receptor for interleukin (IL)-1 in line with the anti-inflammatory effect of dexamethasone, as well as *TSC22D3, CD163*, *SAP30*, *PER1*, and *ZFP36L2*[19,23–25] (Figure 2B). Based on these *in vivo* changes, we compiled a dexamethasone treatment gene signature composed of both down- and upregulated genes (Figure 2C). Upregulated genes were functionally related to hypoxia and regulation of catabolic processes, while downregulated genes enriched for NF-κB signaling and terms related to immune activation (Figure 2D). Further, we found a GC signature derived from monocytes treated with a synthetic GC *in vitro*[26] to be strongly enriched in monocytes during dexamethasone treatment in our dataset (Figure 2E).

Next, we sub-clustered the 23,416 transcriptomes of the monocyte space into ten different cell states (Figures 2F and 2G), showing enrichment of seven cell state signatures derived from acute COVID-19 prior to introduction of dexamethasone therapy[18] (Figure S2A). Despite the enrichment of the GC-response gene signature upon dexamethasone treatment in the monocyte space overall (Figure 2E), cell state-specific analysis revealed the strongest enrichment of the GC signature in one selected cluster, which we termed "Dexa response" cell state (Figures 2H and S2B). These findings were validated with gene sets based on the Gene Ontology (GO) term "response to GC" and "response to steroid hormone" (Figures 2I and 2J). Manual assessment of individual genes corroborated the Dexa response state to be related to dexamethasone treatment as several known GC target genes were elevated including *TSC22D3*,[19] *SAP30*,[24] *FKBP5*,[27] and *CD163*[23] (Figure 2G). To cross-validate our results, we analyzed 2,350 monocyte transcriptomes included in a recently published dataset of dexamethasone-treated patients,[12] revealing similar changes in monocytes from this independent dataset (Figures S2C and S2D).

Dexamethasone treatment elicited a transcriptional core signature in monocytes in COVID-19 patients, independent of disease severity. Single-cell analysis revealed that these

(E) UMAP of the entire PBMC space by scRNA-seq colored by COVID-19 severity with indicated cell types subsetted for untreated controls. Shift in monocytes is indicated.
(F) Violin plots indicating the expression of selected MHC class II (*HLA-DRA*, *HLA-DRB1*, and *HLA-DPA1*) and alarmin (*S100A8*, *S100A9*, and *S100A12*) genes by severity in monocytes of untreated controls. Significant differential expression is indicated with asterisks.
(G) Number of differentially expressed (DE) genes (DEGs) by major cell type with at least 2,000 cells for dexamethasone vs. control by COVID-19 severity (DE parameters: $\log_2$FC = 0.25, min.pct = 0.1).
(H) Spider plots depicting the Hallmark TNF signaling via NF-κB, the most prominent term of functional enrichment analysis for the dexamethasone downregulated genes by cell types extracted from Figure S1F.
See also Figure S1.

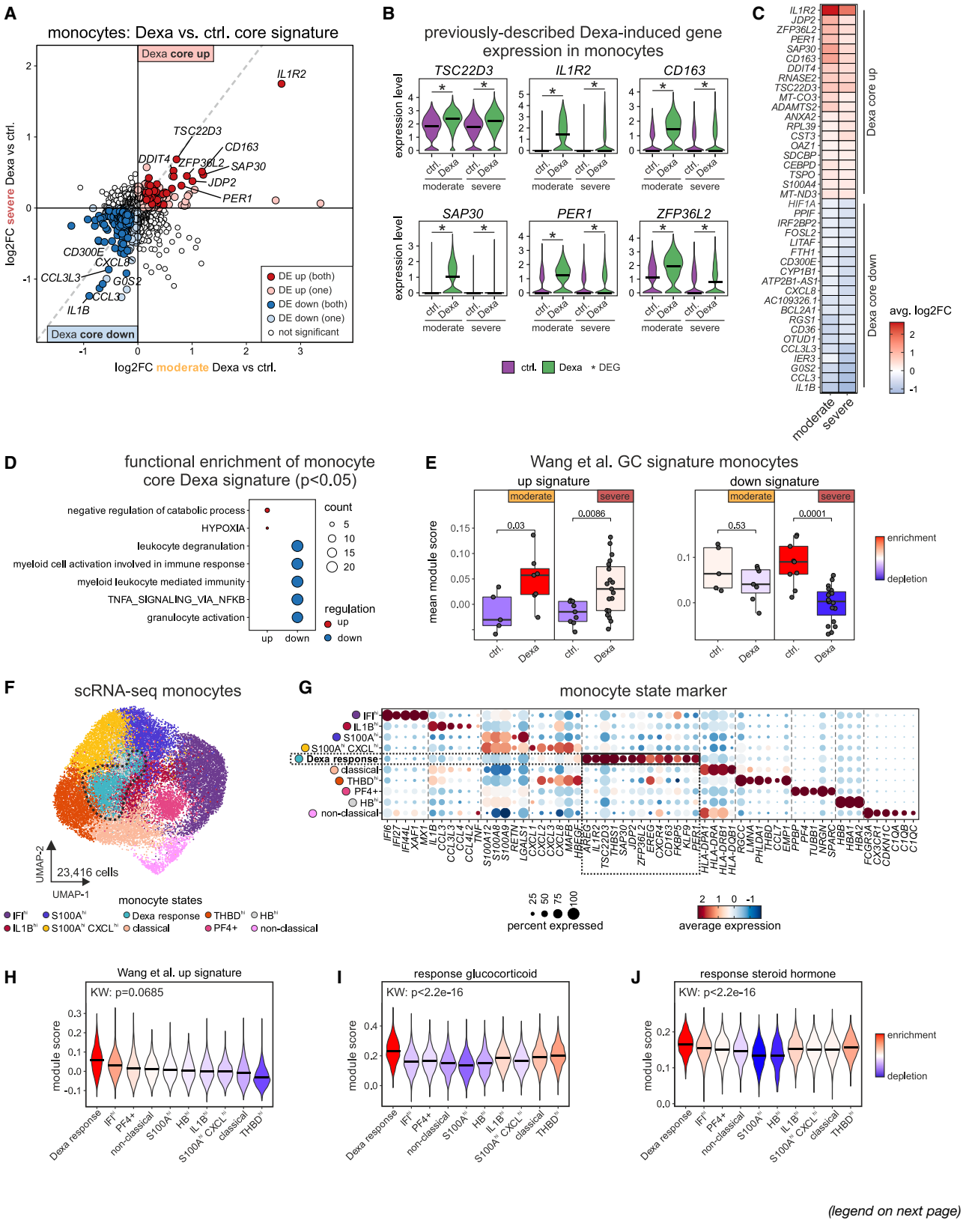


*(legend on next page)*

transcriptional changes were not present evenly across all monocytes, but that a specific monocyte substate elicited upon dexamethasone treatment showed the highest enrichment of GC-response genes (Dexa response monocyte state).

## Dexamethasone-induced transcriptional modulation of monocytes is linked to clinical outcome

Although clinical trials have demonstrated a strong clinical benefit of dexamethasone in patients with moderate and severe COVID-19, a substantial number of patients—almost 30% in the RECOVERY trial—died despite dexamethasone treatment.[1] It is unclear whether the unfavorable outcome in these patients is caused by a failure to adequately respond to treatment and which mechanisms contribute to a treatment benefit. We therefore assessed whether the distribution of treatment-related monocyte cell states was linked to disease severity and to the clinical outcome. The Dexa response monocyte state was prevalent in up to 80% of all monocytes in dexamethasone-treated patients with moderate COVID-19 (hospitalized patients requiring oxygen supplementation but no mechanical ventilation) and less pronounced in dexamethasone-treated patients with severe COVID-19 (Figure 3A). Similarly, protein expression of CD163, a prominent marker gene of the dexamethasone response cluster, was elevated on monocytes in dexamethasone-treated COVID-19 patients (Figure S3A). Analysis of whole blood samples by CyTOF (Figure S3B) revealed that cluster abundance of the $CD14^{+}CD16^{-}CD163^{hi}$ classical monocytes (Figure 3B) and signal intensity of CD163 (Figure 3C) were significantly elevated in dexamethasone-treated patients, whereas the $CD14^{+}$ and $CD16^{+}$ $CD69^{+}PD\text{-}L1^{+}$ activated classical and non-classical monocyte subpopulations were significantly downregulated by dexamethasone treatment (Figure S3C), with potentially beneficial effects on T cell functionality, similar to programmed cell death ligand-1 (PD-L1) blockade in SARS-CoV-2 infection.[28]

Further stratification of dexamethasone-treated patients with severe COVID-19 by clinical outcome (survival) revealed a significantly higher frequency of Dexa response monocytes in survivors compared with patients who later died during the course of their disease (deceased), in whom Dexa response state monocytes were low to undetectable (Figures 3D and S3D).

Given the outcome-dependent transcriptional changes, we next contrasted the DEGs in all monocytes focusing on dexamethasone-treated surviving patients (i.e., responders) and untreated control survivors (Figure 3E). Beyond the downregulation of proinflammatory genes observed in the dexamethasone core signature, selective analysis of monocyte gene expression in survivors revealed that dexamethasone treatment was associated with a reversal of the previously reported transcriptional dysregulation in monocytes in severe COVID-19.[18] Dexamethasone treatment led to a downregulation of alarmins, cytokines, and chemokines and reconstitution of *HLA-DRB1*, *HLA-DRA*, *HLA-DPA1*, and *CD74* expression (Figure 3F). Alarmin expression in monocytes was lower at 7 days compared with 3 days after initiation of dexamethasone treatment[12] (Figure S3E), indicating a time-dependent effect of dexamethasone on alarmin gene expression.

In line with these findings, dexamethasone treatment significantly reduced the frequency of $S100A^{hi}$ monocytes in survivors, but not in non-survivors (Figure 3G). Differential gene expression analysis of patients with severe COVID-19 (all treated with dexamethasone) showed that dexamethasone induced the upregulation of genes associated with a milder course of disease, specifically in survivors, whereas monocytes in non-survivors expressed higher levels of alarmins associated with monocyte dysregulation (Figure 3H), resembling untreated patients with severe COVID-19 (Figure S3F). These data indicated that a non-favorable clinical outcome, i.e., death from COVID-19, was associated with a failure of monocytes to respond to dexamethasone. We had previously identified a dysregulated monocyte state marked by low major histocompatibility complex (MHC)-II expression and high levels of alarmins, termed "$HLA\text{-}DR^{lo}S100A^{hi}$," which was strongly associated with COVID-19 severity.[18] Gene set enrichment analysis (GSEA) showed that dexamethasone treatment reversed this dysfunctional monocyte phenotype in survivors, whereas monocytes from deceased patients did not show a reversal of this transcriptional signature, hence failed to respond to treatment (Figure 3I).

In addition to monocytes, we also tested B cells for outcome-specific signatures, as they also showed profound transcriptional changes to dexamethasone (Figure 1G). However, only a

**Figure 2. Dexamethasone elicits a unique cell state in a fraction of monocytes**

(A) Fold change-fold change (FC-FC) plot showing the $\log_2$ fold changes of differentially expressed genes (DEGs) in monocytes from the comparisons of severe COVID-19 Dexa vs. control (y axis) and moderate COVID-19 Dexa vs. control (x axis). Genes that are DE in both or only one comparison are indicated.

(B) Violin plots depicting expression of previously described dexamethasone-induced genes (*TSC22D3*, *IL1R2*, *CD163*, *SAP30*, *PER1*, and *ZFP36L2*) in monocytes stratified by severity and treatment. Significant differential expression is indicated with asterisks.

(C) Heatmap of the average $\log_2$ fold change in monocytes from genes identified in (A) stratified by the severity comparisons. For representation, the top 20 upregulated and downregulated genes were selected.

(D) Functional enrichment of the Dexa core signature genes from (A) and (C) using the GO and Hallmark databases (Bonferroni-adjusted $p$ value < 0.05).

(E) Enrichment of the *in vitro* generated glucocorticoid signatures from Wang et al.[26] in monocytes stratified by COVID-19 severity and treatment represented as mean module score per donor. Statistical testing using Wilcoxon test.

(F) UMAP visualization of the entire monocyte space ($n$ = 23,416 cells) with identified monocyte states. The Dexa response state is highlighted.

(G) Marker gene expression levels for identified monocyte states from (F). Markers for the Dexa response state are highlighted.

(H) Enrichment of the *in vitro* generated glucocorticoid up signatures from Wang et al.[26] in all monocyte states. Kruskal-Wallis (KW) test between mean module scores by donor and cell states, and the resulting $p$ value is indicated.

(I) Enrichment of the GO term response to glucocorticoid in all monocyte states. Kruskal-Wallis (KW) test between mean module scores by donor and cell states, and the resulting $p$ value is indicated.

(J) Enrichment of the GO term response to steroid hormone in all monocyte states. Kruskal-Wallis (KW) test between mean module scores by donor and cell states, and the resulting $p$ value is indicated.

See also Figure S2.

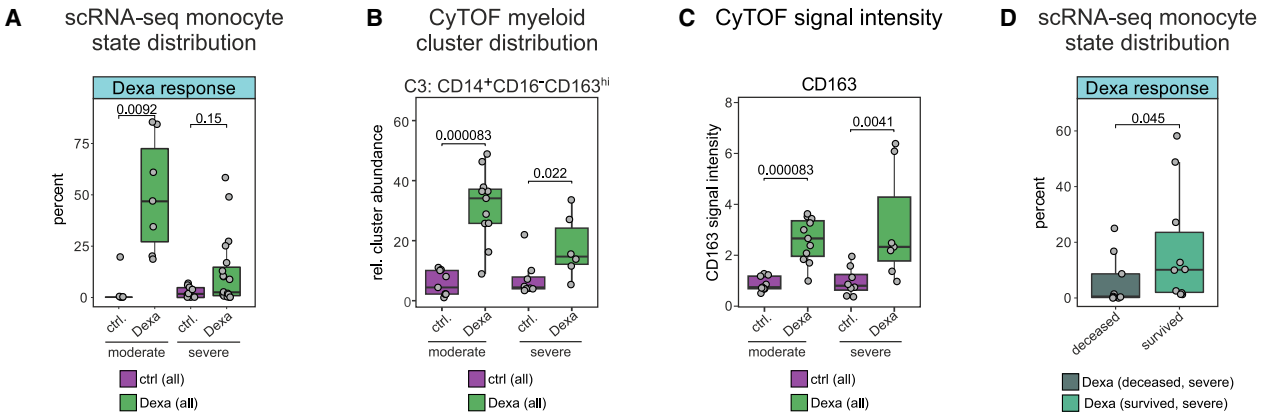


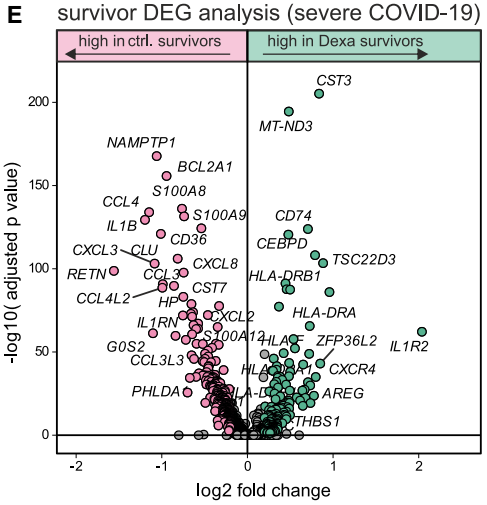


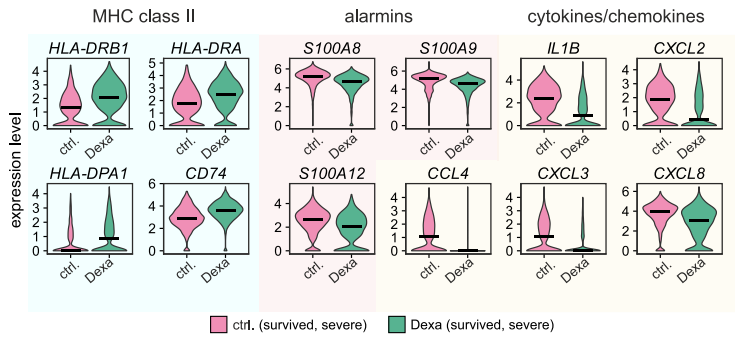


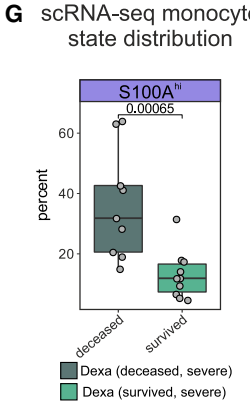


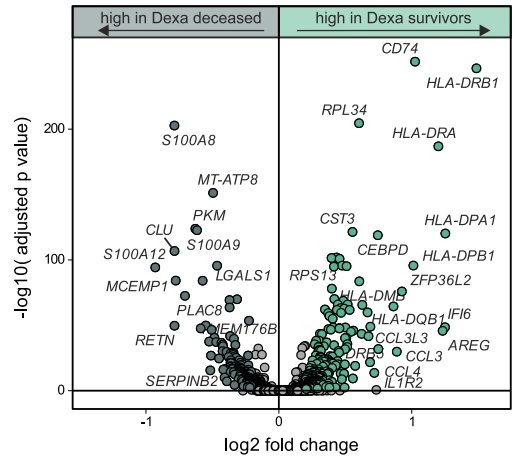


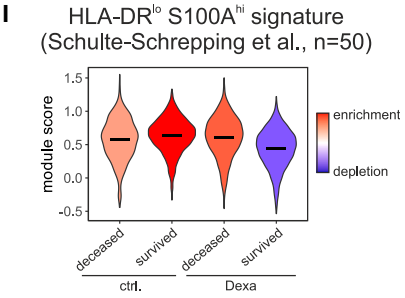


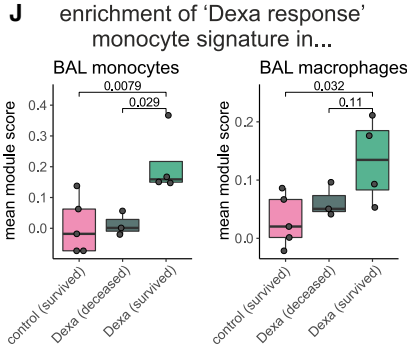


*(legend on next page)*

comparatively small fraction of genes was associated with outcome, indicating that B cells are not informative in contrast to the monocytes for stratifying treatment response (Figure S3G).

To evaluate if similar treatment effects as detected in blood monocytes were also detectable in the lungs and therefore potentially directly related to organ failure and disease progression, we analyzed cells from bronchoalveolar lavage (BAL) of patients with severe COVID-19. First, we analyzed published single-cell transcriptomes of BAL[29] including a total of six patients with severe COVID-19 patients, four of whom were treated with the synthetic GC methylprednisolone. We recovered similar patterns as we found in blood monocytes in response to dexamethasone treatment. Disease outcome-stratifying markers from the blood monocytes (Figure 3E) were also highly expressed in BAL myeloid cells of methylprednisolone-treated survivors ($n$ = 2), while blood monocyte markers associated with treatment failure were higher in treated deceased patients ($n$ = 2, Figure S3H). As the cohort size in this published dataset was too limited for robust statistical analysis, we generated single-cell transcriptomes from BAL samples collected from twelve patients with severe COVID-19 in the first two waves in Germany, including seven dexamethasone-treated and five untreated patients. The dataset comprised a total of 67,439 cells (Figure S3I; Table S1) and recovered all major cell types expected in BAL (Figures S3J and S3K). In order to investigate similarities of the transcriptional responses to dexamethasone between circulating and pulmonary immune cells, we analyzed the enrichment of the signature of Dexa response monocytes from blood in BAL monocytes and macrophages, stratified by treatment (dexa vs. untreated) and outcome (survival vs. deceased) (Figure 3J). The Dexa response signature was significantly enriched in BAL monocytes from dexamethasone-treated survivors, but it was neither enriched in monocytes from untreated patients nor in dexamethasone-treated deceased patients. A similar stratification was observed in BAL macrophages, albeit to a lesser extent (Figure 3J). These data indicate that transcriptional responses to dexamethasone treatment detected in circulating monocytes are preserved in the lung and likely contribute to outcome benefits of dexamethasone.

In conclusion, induction of a Dexa response monocyte state in patients with severe COVID-19 treated with dexamethasone was associated with clinical benefit (survival). In addition, dexamethasone treatment exerted specific modulatory effects by reversing the dysregulated monocyte phenotype in patients with severe COVID-19, whereas fatal outcome was associated with a failure to revert the dysregulated monocyte phenotype. These data link the clinical effect of a pharmacological intervention (dexamethasone) to a molecular phenotype in immune cells in the blood and in the lung. The data also demonstrate the versatility of scRNA-seq to reveal mechanisms of action of therapeutic interventions and to identify non-responders to a specific treatment prior to the clinical endpoint. The results underscore the causal relevance of monocyte responses in the pathophysiology of severe COVID-19.[18,30]

## Dexamethasone treatment response is reflected in the epigenome of CD14$^{+}$ monocytes early after treatment initiation

To investigate whether the observed differences in the dexamethasone treatment response on the transcriptional level are reflected by epigenetic profiles in monocytes, we selected patients with supplemental oxygen but without invasive mechanical ventilation at treatment start (World Health Organization (WHO) score of 4–5) and generated genome-wide DNA methylation profiles of blood samples at an earlier stage of treatment (median 2 days after initiation of dexamethasone treatment) than for the transcriptome analysis (median of 8 days) (Figure 4A). Patients were matched in pairs according to clinical status at treatment initiation and classified based on their future WHO score (median 9 days later) as either dexamethasone non-responders (increased WHO score, i.e., clinical deterioration to intubation and invasive mechanical ventilation, need for additional organ replacement, or death) or dexamethasone responders (stable or improved clinical status and WHO score). DNA methylation profiles of fluorescence-activated cell sorting

**Figure 3. Dexamethasone-induced transcriptional modulation of monocytes is linked to clinical outcome**

(A) Percentages of Dexa response monocyte state of all monocytes stratified by severity and treatment with each dot representing one donor. Statistical testing using Wilcoxon test, resulting $p$ values are indicated.

(B) Monocyte relative cluster distribution from CyTOF analysis for cluster 3 (CD14$^{+}$CD16$^{-}$CD163$^{hi}$, clustering see Figure S3B). Wilcoxon test for statistical testing, and resulting $p$ values are indicated.

(C) Mean scaled signal intensity of CD163 in myeloid cells (CyTOF) by treatment group and severity. Wilcoxon test for statistical testing, and resulting $p$ values are indicated.

(D) Percentages of Dexa response monocyte state of all monocytes in severe patients with dexamethasone treatment stratified by outcome. Statistical testing using Wilcoxon test, and resulting $p$ values are indicated.

(E) Volcano plot showing the differentially expressed genes (DEGs) for Dexa vs. control in severe COVID-19 survivors (DE parameters: $\log_2$FC = 0.25, min.pct = 0.1).

(F) Violin plots for a selection of genes from (E) belonging to the MHC class II, alarmins, or cytokines/chemokines group.

(G) Percentages of "*S100A*$^{hi}$" monocyte state of all monocytes stratified by outcome in dexamethasone-treated severe COVID-19 patients. Statistical testing using Wilcoxon test, and resulting $p$ values are indicated.

(H) Volcano plot showing the DEG between severe COVID-19 patients treated with dexamethasone who survived vs. those who were treated but deceased in monocytes (DE parameters: $\log_2$FC = 0.25, min.pct = 0.1).

(I) Signature enrichment of the *HLA-DR*$^{lo}$*S100A*$^{hi}$ monocytes from Schulte-Schrepping et al.[18] in monocytes of severe COVID-19 patients stratified by treatment and outcome.

(J) Enrichment of the Dexa response monocyte signature ($n$ = 30) in both bronchoalveolar lavage (BAL) COVID-19 monocytes (left) and macrophages (right), cohort overview in Figure S3G. Statistical testing using the Wilcoxon test (alternative = "greater"), and resulting $p$ values are indicated.

See also Figure S3.

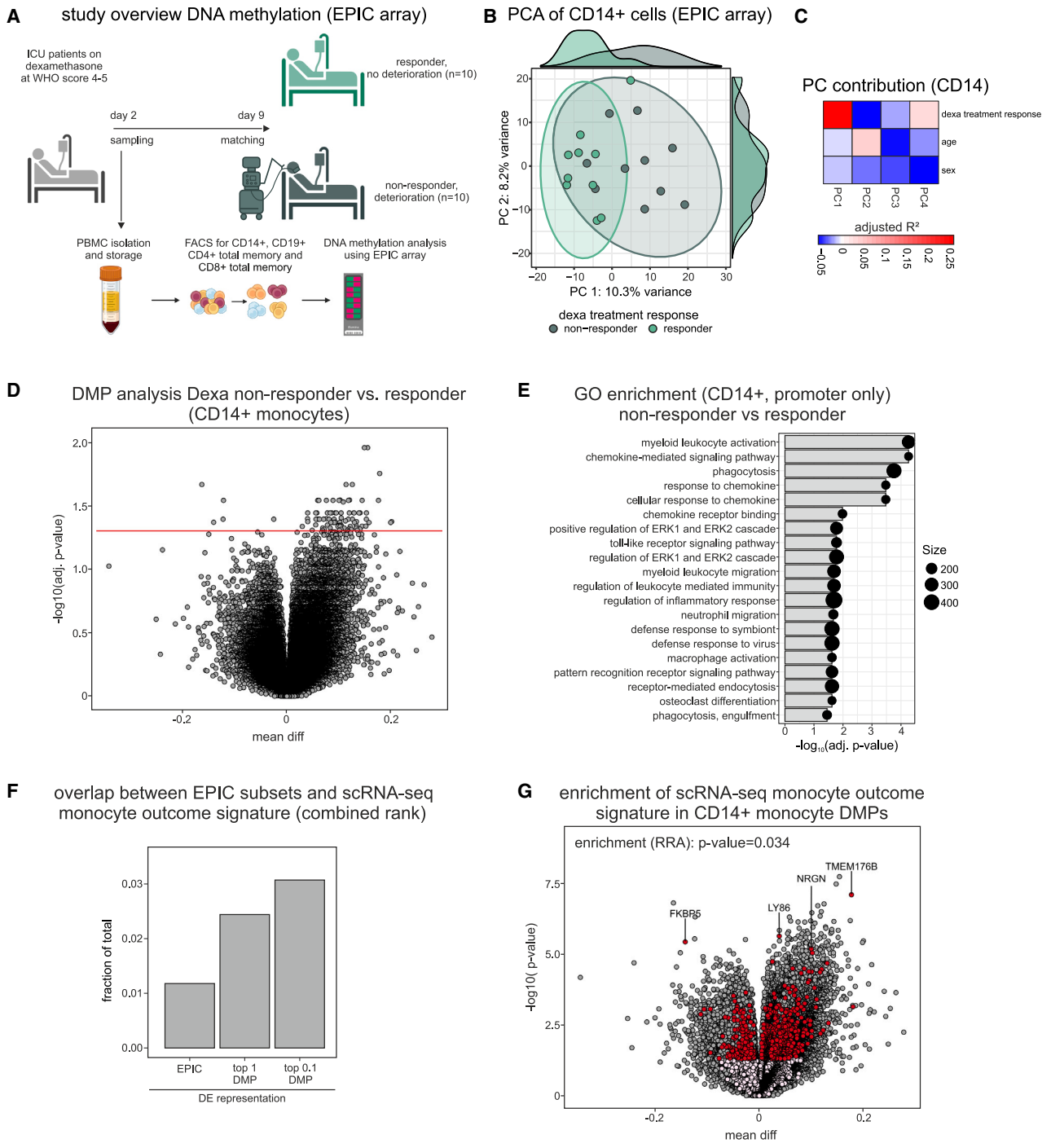


**Figure 4. Treatment response is reflected in the epigenome of CD14⁺ monocytes early after treatment initiation**

(A) Study design: PBMCs were isolated from patients (WHO score of 4–5 at dexamethasone treatment start) 1–4 days after the start of Dexa treatment. Ten matching pairs of treatment non-responders/responders were selected based on their increased/not-increased WHO score 5–11 days after Dexa treatment, respectively. $CD14^{+}CD16^{-}$ monocytes, $CD19^{+}$ B cells, $CD4^{+}$ memory T cells, and $CD8^{+}$ memory T cells were purified using flow cytometry (FACS) and analyzed on the Infinium MethylationEPIC BeadChip array for genome-wide DNA methylation.

(B) Principal-component analysis (PCA) was performed on the genome-wide DNA methylation datasets of $CD14^{+}$ monocytes. Histograms on the axes show the distribution of dexamethasone treatment response group samples.

(C) PC linear regression analysis of covariates. Contribution of dexamethasone treatment response, age, and sex are displayed for PCs 1–4.

*(legend continued on next page)*

(FACS)-purified CD14$^+$CD16$^-$ monocytes, CD19$^+$ B cells, CD4$^+$ memory T cells, and CD8$^+$ memory T cells (Figure S4A) showed the strongest differences by cell type without differentiating between responders and non-responders in the global principal-component analysis (PCA, Figure S4B). To define treatment response-related differences, each cell compartment was subsetted and analyzed individually. A separation between responders and non-responders was observed in the PCA for CD14$^+$ monocytes (Figure 4B), which was not seen in CD19$^+$ B cells or CD4$^+$ and CD8$^+$ memory T cells (Figure S4C). PC linear regression analysis of the CD14$^+$ monocytes confirmed the highest influence to be the dexamethasone treatment-response group on the first principal component (Figures 4B and 4C). To further explore the epigenetic differences within CD14$^+$ monocytes between non-responding and responding patients, we determined significantly differentially methylated positions (DMPs, Figure 4D). Functional enrichment analysis of promoter-associated DMPs revealed high association of GO terms such as "myeloid leukocyte activation," "response to chemokine," "myeloid leukocyte migration," and "regulation of inflammatory response," displaying epigenetic remodeling of promoter elements of genes contributing to a proinflammatory program in CD14$^+$ monocytes (Figure 4E).

Comparing these results to our findings on the transcriptome level (~8 days after treatment initiation), outcome-specific monocyte signature genes for severe dexamethasone-treated COVID-19 patients who deceased (Figure 3H) were overrepresented in the top 1% DMPs (based on combined rank) with an even stronger overrepresentation in the top 0.1% DMPs, indicating significant differential methylation changes in these signature genes (Figure 4F). This was supported by a significant robust rank aggregation (RRA) enrichment analysis (Figure 4G).

Taken together, we observed profound epigenetic differences in monocytes of dexamethasone non-responders vs. responders early after treatment initiation, thus preceding the observed transcriptional changes. Differences were mainly associated with a proinflammatory program and also showed enrichment of the outcome signature retrieved from single monocyte transcriptomes, further supporting the importance of this gene program to be targeted if dexamethasone therapy is to become clinically effective.

## Dexamethasone-induced monocyte signatures enrich in whole blood transcriptomes of two clinical cohorts and stratify outcome

Given the clear outcome-associated transcriptional changes, particularly in the monocyte compartment, we next investigated whether these changes could be recapitulated in whole blood transcriptomes and whether transcriptome information from early time points after dexamethasone treatment initiation would be informative to stratify patients according to their clinical outcome.

To this end, we generated whole blood bulk transcriptomes from 92 patients of our single-center COVID-19 cohort (Charité, Pa-COVID-19), sampled at 4 days after treatment initiation (Figure 5A), 4 days earlier than for the scRNA-seq analysis. PCA revealed expression differences between moderately ill patients, severely ill patients who survived, and severely ill patients who later died (Figure 5B), indicating the feasibility to detect outcome-related differences from whole blood transcriptomes. We compiled two transcriptome signatures related to fatal outcome, i.e., for up- and downregulated transcripts, based on the single-cell monocyte transcriptomes (Figures 2 and 3). Enrichment scores for these signatures were calculated for each patient and integrated for each patient group. We observed significant disease severity- and outcome-dependent differences, with enrichment of the "deceased upregulated" signature in deceased patients and highest enrichment of the "deceased downregulated" signature in patients with the lowest disease severity (moderate COVID-19) (Figure S5A). These findings indicated that outcome-associated monocyte-specific gene signatures are detectable in whole blood transcriptomes, even at an earlier time point after treatment initiation (4 vs. 8 days), and that these signatures could stratify patients by outcome (Figure S5A).

Next, we utilized samples collected from 90 patients in a German multi-center cohort (CAPNETZ cohort) at an even earlier time point after initiation of dexamethasone treatment (2 vs. 4 days, Figure 5C). Also in this cohort, we identified differences between patients according to disease severity and outcome (moderate, severe survived, and severe deceased) by PCA (Figure 5D), albeit less clear than in the samples from the single-center cohort collected at a later time point of 4 days post treatment initiation. Accordingly, the single monocyte transcriptome-derived deceased upregulated signature was not significantly enriched, but the deceased downregulated signature enriched with statistically significant differences between the three groups (Figure S5B).

To assess the likelihood of obtaining an enrichment of the single monocyte transcriptome-derived signatures of that size with the respective significance, we performed a permutation test with 500 gene sets randomly drawn from each dataset, respectively, and calculated the enrichment scores in deceased and surviving patients. In contrast to the vast majority of these random gene sets, we observed a highly specific enrichment of our original single monocyte transcriptome-derived signatures in both cohorts, particularly of the deceased upregulated

(D) Volcano plot of differentially methylated positions (DMPs) in CD14$^+$ monocytes comparing both dexamethasone response groups. The red line indicates the false discovery rate (FDR) of 0.05 (Benjamini-Hochberg).
(E) Gene Ontology enrichment analysis performed on promoter-associated DMPs for CD14$^+$ monocytes comparing dexamethasone response groups.
(F) Fraction of outcome signature genes from monocytes (deceased vs. survivors, Figure 3H) within all samples on the EPIC array, the top 1% of DMPs (based on combined rank), and the top 0.1% of DMPs.
(G) Volcano plot with marked sites of monocyte outcome signature genes displaying differential methylation (red dots: $p$ value < 0.05; pink dots: not significant). Gene names were displayed for DEG sites with an FDR < 0.05. Statistical significance of the overlap between differential DNA methylation and differential gene expression was calculated (robust rank aggregation [RRA], $p$ value = 0.034).
See also Figure S4.

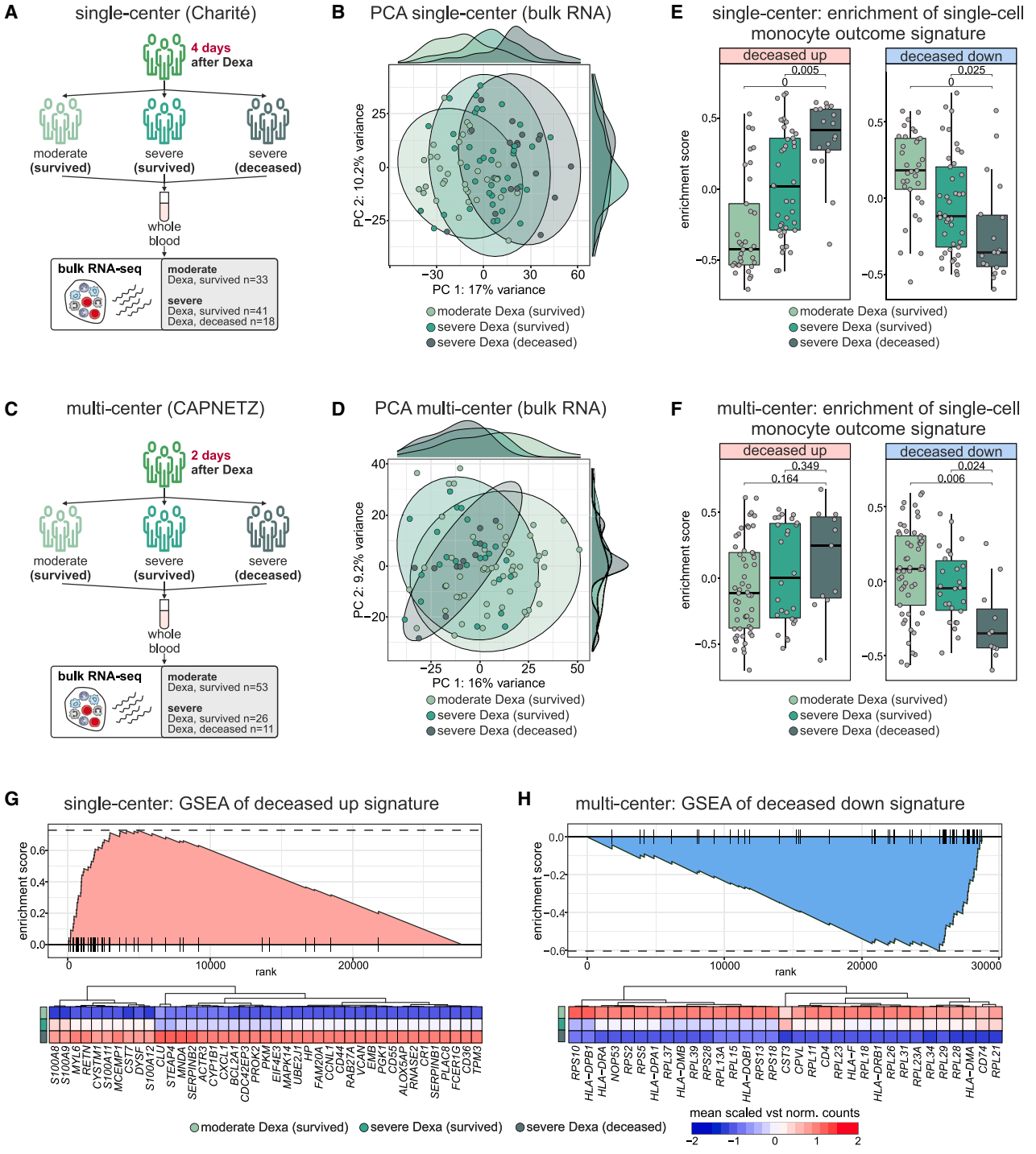


**Figure 5. Monocyte-specific signatures enrich in whole blood transcriptomes of two validation cohorts and stratify outcome**

(A) Schematic representation of the single-center (Charité) COVID-19 cohort used for whole blood transcriptome data analysis sampled on average at 4 days after dexamethasone treatment initiation. Included sample numbers are indicated.

(B) Principal-component analysis (PCA) plot showing the distribution of the top 5,000 most variable genes present in the single-center cohort, color-coded according to COVID-19 severity and outcome.

(C) Schematic representation of the multi-center (CAPNETZ) cohort used for whole blood transcriptome data analysis sampled on average 2 days after dexamethasone treatment initiation. Included sample numbers are indicated.

*(legend continued on next page)*

signature in the single-center cohort and of the deceased downregulated signature in the multi-center cohort. (Figures S5C and S5D.) To further increase the robustness of the enrichment analysis, we varied the number of genes to be included in the gene signature and optimized the signature size based on the calculated enrichment scores and different enrichment between the groups in both cohorts (Figures S5E and S5F). These optimized signatures showed a high robustness for stratifying patients according to disease severity and outcome in the two independent cohorts, at early time points after treatment initiation (Figures 5E and 5F). Investigation of the driving genes of the enrichment of the outcome-related signature (Figures 5G, 5H, S5G, and S5H) revealed that the leading edge of the GSEA included the chemokine *CXCL1* together with the alarmins *S100A8*, *S100A9*, *S100A11*, and *S100A12*, resembling the monocyte phenotype in patients with severe acute COVID-19 for the deceased upregulated signature in the original single-center cohort (Figure 5G) and that enrichment of the deceased downregulated signature in the deceased patients was strongly driven by many MHC class II genes (Figure S5G). In the whole blood transcriptomes of the multi-center cohort sampled at 2 days post treatment initiation, the leading edge of the enrichment of the deceased upregulated signature did not yet contain the complete signature at this early time point in patients who later died, but already showed changes in *S100A12* and *CXCL1* (Figure S5H). Yet, the edge of the deceased downregulated signature was already enriched in MHC class II genes such as *CD74*, *HLA-DQB1*, *HLA-DRB1*, and *HLA-DRA* for patients who later died (Figure 5H). These results further emphasize the role of dexamethasone in reversing the severe acute COVID-19 phenotype, as early as 2 days after initiation of treatment.

Taken together, clinical outcome-related single monocyte transcriptome-based gene signatures derived from COVID-19 patients on average 8 days after initiation of dexamethasone treatment were enriched in whole blood bulk transcriptomes obtained at day 4 post treatment initiation and accurately stratified patients according to disease severity and outcome. In whole blood transcriptomes collected 2 days after treatment initiation in an independent cohort, we could only detect an enrichment of the gene signature based on downregulated genes, indicating that dexamethasone treatment effects become apparent in whole blood transcriptomes between 2 and 4 days after treatment initiation.

The results demonstrate the versatility of single-cell sequencing of clinical samples to reveal *in vivo* effects of pharmacological treatment and that gene signatures derived from these analyses can be applied to larger clinical cohorts to stratify study patients by outcome, even at early time points after treatment initiation.

## DISCUSSION

GCs are among the most widely prescribed drugs worldwide and a cornerstone for the treatment of a variety of acute and chronic inflammatory conditions. In clinical practice, they are often regarded as effective yet rather nonspecific immunosuppressants, despite an established molecular understanding that both naturally occurring and pharmacologically designed GCs are acting via specific binding to GC receptors.[31,32] Responsiveness to GC treatment is known to be heterogeneous among patients, possibly influenced by the variety of diverse GC receptor isoforms, which mediate their differential genomic and non-genomic effects.[26,33]

To better understand the specificity and the molecular mode of action of GC treatment in COVID-19, we applied high-content bulk transcriptomics and high-resolution single-cell technologies in two clinical cohorts of patients with COVID-19. We provide evidence that dexamethasone treatment in severe COVID-19 leads to a highly specific immune modulation. Major changes of molecular phenotypes occur mainly in the myeloid cell compartment, where dexamethasone elicits a treatment-specific cell state in a fraction of monocytes, with induction of genes with well-known regulatory functions including cell surface receptors, transcriptional regulators, and translational regulators, while many chemokines and *IL-1B* are decreased in expression. Defining qualitative and quantitative effects of dexamethasone treatment on the cellular and molecular level supported a specific immunomodulatory effect, with many changes induced irrespective of disease severity. Importantly, these effects are reminiscent of changes described previously in other therapeutic settings, such as rheumatoid arthritis, inflammatory bowel diseases, or allergic asthma,[32] for example, the increase of expression of certain genes with regulatory function including Thrombospondin 1 (*THBS1*), *IL1R2*, or GC-induced leucine zipper protein GILZ (*TSC22D3*). Functional enrichment across cell types pointed toward strong interference with NF-κB signaling, which is one of the well-known mechanisms downstream of GC receptor signaling.[21,22]

(D) PCA illustrating the distribution of the top 5,000 most variable genes present in the multi-center cohort, color-coded according to COVID-19 severity and outcome.
(E) Boxplots displaying the gene set variation analysis (GSVA) enrichment scores of the optimized deceased upregulated signature (left plot) and deceased downregulated signature (right plot) in the single-center cohort, split and colored by the COVID-19 severity status and outcome. Wilcoxon test and Benjamini-Hochberg adjustment were utilized for statistical analysis.
(F) Boxplots displaying the GSVA enrichment scores of the optimized deceased upregulated signature (left plot) and deceased downregulated signature (right plot) in the multi-center cohort, split and colored by the COVID-19 severity status and outcome. Wilcoxon test and Benjamini-Hochberg adjustment were utilized for statistical analysis.
(G) Gene set enrichment analysis (GSEA) of the optimized deceased upregulated signature in the deceased patient group of the Charité cohort. Ranking of samples is based on expression-level statistics, and the running sum is visualized. The heatmap depicts the scaled variance-stabilized mean expression per COVID-19 severity status and outcome of the genes included in the leading edge.
(H) GSEA of the optimized deceased downregulated signature in the deceased patient group of the multi-center cohort. Ranking of samples is based on expression-level statistics, and the running sum is visualized. The heatmap depicts the scaled batch-corrected variance-stabilized mean expression per COVID-19 severity status and outcome of the genes included in the leading edge.
See also Figure S5.

Most strikingly, the molecular response to dexamethasone was linked to clinical treatment response and outcome, as the previously described dysfunctional molecular phenotype associated with severe acute COVID-19 (*HLA-DR*$^{lo}$*S100A*$^{hi}$ monocytes)[18] was reversed in patients surviving severe COVID-19. This illustrates that dexamethasone therapy in this clinical situation is not only immunosuppressive but rather immunomodulatory since expression of genes related to effective immune function was re-established. In fact, a specific Dexa response state within monocytes, uncovered by single-cell transcriptome analysis, revealed that not all monocytes respond to treatment. Patients succumbing to the disease did not show a reversal of the dysfunctional molecular phenotype in the monocyte compartment (*HLA-DR*$^{lo}$*S100A*$^{hi}$ monocytes), accompanied by a lack of the dexamethasone response monocyte cell state in most of these patients.

The dexamethasone response signature from blood monocytes also enriched in monocytes and macrophages from BAL samples of dexamethasone-treated survivors, but not of treated non-survivors or GC-naive patients of our cohort. The role of inflammatory and potentially profibrotic monocytes and monocyte-derived macrophages for the development of acute respiratory distress syndrome (ARDS) in COVID-19 has been documented in numerous studies.[34] The reversal of the dysfunctional molecular phenotype of monocytes in the lung, associated with dexamethasone treatment and positive outcome (survival), links our findings in circulating immune cells to dexamethasone treatment-induced protection.

The differences in transcriptional changes following treatment were preceded by epigenetic changes in the proinflammatory program of CD14$^+$ monocytes, which also differed between responders and non-responders. An outcome-related signature generated from the monocyte transcriptomes (8 days post treatment initiation) was successfully applied to whole blood transcriptomes sampled even earlier within two larger observational single-center and multi-center cohorts, respectively. The signature was enriched in whole blood transcriptomes from patients succumbing to COVID-19 in our single-center study already at 4 days post treatment initiation, indicating early treatment failure. Testing for generalizability of this potential predictor of treatment response and outcome in a national multi-center cohort at an even earlier time point revealed that more than 2 days of treatment are required for molecular outcome stratification.

Several attempts have been made to identify subgroups of patients with severe COVID-19 who are likely to respond differently to anti-inflammatory treatment. Two distinct groups of patients with COVID-related ARDS, similar to the previously described hypoinflammatory and hyperinflammatory ARDS subphenotypes,[35] were reported to show differential response to corticosteroid treatment[36] and have been proposed for a biomarker-guided corticosteroid dosing in COVID-19.[37] Similarly, peripheral blood transcriptomes have been used to identify two different endotypes of patients with severe COVID-19 based on IFN-related or checkpoint genes, who showed cluster-specific effects of corticosteroid treatment.[38] Attempts to identify different COVID-19 endotypes or phenotypes in terms of their response to anti-inflammatory treatment are particularly important in light of the fact that several clinical trials initially failed to demonstrate a clear survival benefit of corticosteroid treatment in COVID-19,[4,39] in addition to the fact that only about one-third of the mechanically ventilated severe COVID-19 patients benefit from dexamethasone therapy.[1] There is a long history of research investigating GC responsiveness,[40] based on the known heterogeneity in treatment response and the variety of unfavorable effects of corticosteroids, particularly associated with their long-term use. In asthma, distinct endotypes have been defined based on the level of type 2 inflammation, known to predict response to GC treatment.[41] Also in other clinical conditions, e.g., community-acquired pneumonia, the significance of steroid treatment is not fully evident, with clear signs that certain patient groups benefit more from adjunct corticosteroid treatment than others, thus emphasizing the importance of early patient stratification.[42,43] In our view, the approach presented in this study goes one step beyond molecular stratification and definition of disease endotypes by providing direct information on therapy response as a form of molecular therapy monitoring. The potential of whole blood transcriptome-based signatures to optimize dexamethasone treatment regimens should be evaluated in a prospective pivotal trial in the future.

## Limitations of the study

Our analysis of the effects of dexamethasone treatment was based on a large prospective, single-center cohort study and an independent prospective, multi-center cohort study for validation of the transcriptional signature enrichment associated with fatal outcome. One important limitation of this approach is the fact that both cohorts were observational and not primarily designed to study the effect of dexamethasone treatment. However, we took advantage of the fact that dexamethasone treatment was only introduced into SOC in the second wave, thus allowing for a well-matched comparison of COVID-19 patients of similar demographics and disease severity, infected with the same viral variant (D614G), that differed only by treatment. Nonetheless, it would be preferable to conduct studies of this nature within the setting of randomized controlled trials, designed to study clinical endpoints as well as mechanisms of action of the investigated drugs. Thus, adaptive platform trials, such as the RECOVERY study, designed to rapidly test the effectiveness of repurposed drugs or new therapies in public health emergencies, would benefit from incorporating high-resolution biomarker studies to uncover mechanisms and to identify target and risk populations who would benefit most from the respective treatment or alternative therapies. To this end, global networks of specialized medical institutions capable of performing highly standardized, high-resolution methods on study samples at high throughput are needed to facilitate this accelerated treatment development. While our approach included well-matched cohorts, the study period was restricted to the early phase of the pandemic. This is a limitation since immunological and virological characteristics have changed during the course of the pandemic. Dexamethasone remains the SOC for patients with moderate to severe COVID-19, yet, it is unknown whether it is still equally effective in re- and breakthrough infections. The use of corticosteroids in other respiratory infections has been controversial, with potentially detrimental effects in influenza infections and mixed results in community-acquired pneumonia. However, it will be difficult to generate new data since it would not be

ethical to withhold dexamethasone in patients with severe COVID-19.

Our study has several implications. First, GC treatment in acute COVID-19 is better characterized as an immunomodulatory rather than immunosuppressive therapy. Second, early outcome predictors could guide personalized therapy by identifying patients not responding adequately to GCs, necessitating early addition of other immunomodulators such as Janus kinase inhibitors or IL-6 receptor blockers.[44] As high-dose GC therapy has been reported to increase mortality in hypoxic moderate to severe patients not requiring mechanical ventilation,[6] prolonged dexamethasone treatment in severe COVID-19 patients might also increase the risk for secondary infections[45] and thereby might contribute to reduced survival rates in this subgroup of patients.[46] Third, a more precise use of GCs in other medical conditions would be highly desirable, and a more precise stratification could be achieved based on clinical trials that incorporate single-cell resolution biomarker studies.

Taken together, we provide single-cell-level resolved molecular phenotype information for the immunomodulatory effect of dexamethasone treatment in patients with COVID-19, which could be utilized for clinical decision-making regarding therapy reevaluation for dexamethasone treatment in the future. Combined with transcriptome-based reverse drug target prediction approaches and randomized controlled trials, this approach can form the basis for faster drug repurposing solutions for future emerging infectious diseases, and it may even be a blueprint for the development of precision medicine for other infectious and non-infectious diseases.

## STAR★METHODS

Detailed methods are provided in the online version of this paper and include the following:



## SUPPLEMENTAL INFORMATION

Supplemental information can be found online at https://doi.org/10.1016/j.cell.2024.06.014.

## CONSORTIA

### Pa-COVID-19 Study Group

Stefan Hippenstiel, Saskia Zvorc, Christof von Kalle, Mirja Mittermaier, Fridolin Steinbeis, Tilman Lingscheid, Bettina Temmesfeld-Wollbrück, Thomas Zoller, Holger Müller-Redetzky, Alexander Uhrig, Daniel Grund, Miriam S. Stegemann, Katrin M. Heim, Ralf H. Hübner, Bastian Opitz, Kai-Uwe Eckardt, Martin Möckel, Victor Corman, Felix Balzer, Claudia Spies, Steffen Weber-Carstens, Chantip Dang-Heine, Michael Hummel, Georg Schwanitz, Uwe D. Behrens, Maria Rönnefarth, Sein Schmidt, Linda Jürgens, Sophy Denker, Moritz Pfeiffer, Luisa Mrziglod, Felix Machleidt, Sebastian Albus, Felix Bremer, Jan-Moritz Doehn, Tim Andermann, Carmen Garcia, Philipp Knape, Philipp M. Krause, Liron Lechtenberg, Yaosi Li, Panagiotis Pergantis, Till Jacobi, Teresa Ritter, Berna Yedikat, Lennart Pfannkuch, Christian Zobel, Ute Kellermann, Susanne Fieberg, Laure Bosquillon de Jarcy, Anne Wetzel, Michael Ney, Simon Ronicke, Maria Roth, Christoph Tabeling, Moritz Müller-Plathe, Jan M. Kruse, Daniel Zickler, Andreas Edel, Gianluca Barbone, Marius Eckart, Martin Kluge, Tobias Püngel, Münevver Demir, Robert Röhle, Theresa Keller, Christoph Jochum, Britta Stier, Roland Körner, Nils B. Mueller, Stefan Schaller, Viktor Wegener, Lucie Kretzler, Lil A. Meyer-Arndt, Linna Li, Isabelle Wirsching, Denise Treue, Dana Briesemeister, Jenny Schlesinger, Lara Bardtke, Kai Pohl, Daniel Wendisch, Anna L. Hiller, Sophia Brumhard, Marie Luisa Schmidt, Leonie Meiners, and Patricia Tscheak and all study nurses.

### CAPNETZ Study Group except the authors

A. Fuchs, M. Engelmann (Augsburg); D. Stolz (Basel/Freiburg); W. Bauer, H.C. Mücke (Berlin); S. Schmager (Cottbus); B. Schaaf, J. Kremling, D. Nickoleit-Bitzenberger, H. Azzaui, M. Hower, F. Hempel, K. Prebeg, K. Popkirova (Dortmund); M. Kolditz(Dresden); C. Bellinghausen, A. Grünewaldt (Frankfurt), M. Panning (Freiburg); T. Welte, T. Fühner, M. van't Klooster, G. Barten-Neiner, W. Kröner, O. Unruh, N. Adaskina, F. Eberhardt, C. Julius, T. Illig, N. Klopp (Hannover); M. Pletz, B.T. Schleenvoigt, C. Forstner, A. Moeser, J. Ankert (Jena); D. Drömann, P. Parschke, K. Franzen, J. Rupp, N. Käding, F. Waldeck (Lübeck); C. Spinner, J. Erber, F. Voit, J. Schneider (Munich); D. Heigener, I. Hering (Rotenburg/Wümme); W. Albrich, M. Seneghini, F. Rassouli, S. Baldesberger (St. Gallen); A. Essig, S. Stenger, M. Wallner (Ulm); H. Burgmann, L. Traby, L. Schubert, R. Chen (Vienna); and all study nurses.

## ACKNOWLEDGMENTS

We thank all the patients who have participated in the study and donated their blood. We thank Anne Schulze for expert technical assistance; Gilles Gasparoni for sharing protocols; Olesya Unruh, Grit Barten, and Frank Eberhardt from CAPNETZ for assistance during provision of samples and data; BIH Flow & Mass Cytometry Core facility for flow-cytometric cell sorting; the German Cancer Consortium (DKTK), Site Berlin (AG Capper) for access to the iScan instrument; and Sach Mukherjee for critical discussion of the manuscript.

K.D. is supported by the DFG via HA 6409/5-1. C.T. is a participant in the BIH Charité Clinician Scientist Program funded by the Charité-Universitätsmedizin and the Berlin Institute of Health at Charité (BIH). F.T. has received funding

from Allergan for a COVID-19-related IIT. N.S. reports grants from the German Research Foundation (SFB-TR84 C09) and from the German Ministry of Education and Research (BMBF) in the framework of CAPSyS (01ZX1604B and 01ZX1304B). A.-E.S. and O.D. thank the DFG – GRK2157 for support. A.-E.S. thanks FOR-COVID initiative funded by the Bayerisches Staatsministerium für Wissenschaft und Kunst. This work was supported by the Stiftung Charité to J.K.P. CAPNETZ was founded by a BMBF grant (FKZ 01KI07145) 2001–2011 and has been an associated member of the German Center for Lung Research (FKZ 82DZL002B4) since 2013. B.S. is supported by the German Research Foundation (DFG) via the SFB 1444 - project #427826188 and by the German Federal Ministry of Education and Research (BMBF) via FKZ 01IK20337 - RECAST; FKZ 01KX2021 - COVIM; FKZ 01EP2201 – NKSG; and FKZ 01KX2121 – NAPKON TIP. J.L.S. is supported by the DFG via the GRK2168 – #272482170, BMBF-funded project iTREAT (01ZX2202B), and Helmholtz-funded project sparse2big (ZT-I-0007). A.C.A., M.B., and J.L.S. are members of the excellence cluster ImmunoSensation (EXC 2151) funded by the German Research Foundation (DFG) under grant agreement #390873048 and are supported by the DFG via the SFB 1454 – project number #432325352, grant #466168337, and grant #466168626; the BMBF-funded project IMMME (01EJ2204D) and National Clinical Study Group (NKSG) (FKZ 01EP2201); and the EU-funded project ImmunoSep (#847422) and NEUROCOV, receiving funding from the RIA HORIZON Research and Innovation under GA No. 101057775. A.C.A. is supported by the Deutsche Forschungsgemeinschaft (DFG, German Research Foundation) via grant #458854699. F.K. is supported by the German Ministry of Education and Research (BMBF) in the framework of CAP-TSD (031L0286B). L.E.S and F.K. are supported by the COVIM platform of Netzwerk Universitätsmedizin (01KX2021, 01KX2121) and by the German Federal Institute for Dugs and Medical Devices (V-2021.3 / 1503_68403 / 2021–2022).

## AUTHOR CONTRIBUTIONS

Conceptualization: E.T.H., L.E.S., J.L.S., A.C.A., and F.K.; investigation: R.K., E.T.H., K.D., O.B., F.H., O.D., M.v.U., S.M., L.B., J.S.-S., L.P., B.K., M.K., S.B., H.T., G.H., E.D.D., J.N., M.D.B., P.G., and J.T.; resources: E.T.H., P.S., C.T., P.G., L.L., B.M.P.-L., F.T., G.R., N.S., and M.W., CAPNETZ Study Group, Pa-COVID-19 study group, A.-E.S., J.K.P., B.S., L.E.S., J.L.S., A.C.A., and F.K.; data curation: R.K., E.T.H., D.H., P.T.L., K.D., O.B., F.H., O.D., M.v.U., P.S., C.T., and C.L.; data analysis: R.K., E.T.H., K.D., O.B., F.H., L.B., J.S.-S., L.P., B.K., M.B., T.U., and A.-E.S.; visualization: R.K., K.D., O.B., F.H., O.D., and L.P.; writing – original draft: R.K., E.T.H., K.D., F.H., J.K.P., B.S., L.E.S., J.L.S., A.C.A., and F.K.; writing – review & editing: R.K., E.T.H., K.D., F.H., P.S., C.T., A.E.S., J.K.P., L.E.S., J.L.S., A.C.A., and F.K.

## DECLARATION OF INTERESTS

The authors declare no competing interests.

Received: July 24, 2023
Revised: February 27, 2024
Accepted: June 10, 2024
Published: July 3, 2024

## REFERENCES

1. RECOVERY Collaborative Group, Horby, P., Lim, W.S., Emberson, J.R., Mafham, M., Bell, J.L., Linsell, L., Staplin, N., Brightling, C., Ustianowski, A., et al. (2021). Dexamethasone in Hospitalized Patients with Covid-19. N. Engl. J. Med. *384*, 693–704. https://doi.org/10.1056/NEJMoa2021436.
2. Aschenbrenner, A.C., Mouktaroudi, M., Krämer, B., Oestreich, M., Antonakos, N., Nuesch-Germano, M., Gkizeli, K., Bonaguro, L., Reusch, N., Baßler, K., et al. (2021). Disease severity-specific neutrophil signatures in blood transcriptomes stratify COVID-19 patients. Genome Med. *13*, 7. https://doi.org/10.1186/s13073-020-00823-5.
3. WHO Rapid Evidence Appraisal for COVID-19 Therapies (REACT) Working Group, Sterne, J.A.C., Murthy, S., Diaz, J.V., Slutsky, A.S., Villar, J., Angus, D.C., Annane, D., Azevedo, L.C.P., Berwanger, O., et al. (2020). Association Between Administration of Systemic Corticosteroids and Mortality Among Critically Ill Patients With COVID-19: a Meta-analysis. JAMA *324*, 1330–1341. https://doi.org/10.1001/jama.2020.17023.
4. Tomazini, B.M., Maia, I.S., Cavalcanti, A.B., Berwanger, O., Rosa, R.G., Veiga, V.C., Avezum, A., Lopes, R.D., Bueno, F.R., Silva, M.V.A.O., et al. (2020). Effect of Dexamethasone on Days Alive and Ventilator-Free in Patients With Moderate or Severe Acute Respiratory Distress Syndrome and COVID-19: The CoDEX Randomized Clinical Trial. JAMA *324*, 1307–1316. https://doi.org/10.1001/jama.2020.17021.
5. National Institutes of Health. National Institutes of Health COVID-19 Treatment Guidelines Panel. Coronavirus Disease 2019 (COVID-19) Treatment Guidelines. https://www.covid19treatmentguidelines.nih.gov/.
6. RECOVERY Collaborative Group. Electronic address: recoverytrial@ndph.ox.ac.uk; RECOVERY; Collaborative Group (2023). Higher dose corticosteroids in patients admitted to hospital with COVID-19 who are hypoxic but not requiring ventilatory support (RECOVERY): a randomised, controlled, open-label, platform trial. Lancet *401*, 1499–1507. https://doi.org/10.1016/S0140-6736(23)00510-X.
7. Les, I., Loureiro-Amigo, J., Capdevila, F., Oriol, I., Elejalde, I., Aranda-Lobo, J., Modesto, J., Güell-Farré, E., García, R., Murgadella-Sancho, A., et al. (2022). Methylprednisolone Pulses in Hospitalized COVID-19 Patients Without Respiratory Failure: A Randomized Controlled Trial. Front. Med. (Lausanne) *9*, 807981. https://doi.org/10.3389/fmed.2022.807981.
8. Thibeault, C., Bardtke, L., Vanshylla, K., di Cristanziano, V., Eberhardt, K.A., Stubbemann, P., Hillus, D., Tober-Lau, P., Mukherjee, P., Münn, F., et al. (2023). Short- and long-term T cell and antibody responses following dexamethasone treatment in COVID-19. JCI Insight *8*, e166711. https://doi.org/10.1172/jci.insight.166711.
9. Mühlemann, B., Thibeault, C., Hillus, D., Helbig, E.T., Lippert, L.J., Tober-Lau, P., Schwarz, T., Müller, M.A., Pa-COVID-19 collaborative study group, and Witzenrath, M., et al. (2021). Impact of dexamethasone on SARS-CoV-2 concentration kinetics and antibody response in hospitalized COVID-19 patients: results from a prospective observational study. Clin. Microbiol. Infect. *27*, 1520.e7–1520.e10. https://doi.org/10.1016/j.cmi.2021.06.008.
10. Arabi, Y.M., Mandourah, Y., Al-Hameed, F., Sindi, A.A., Almekhlafi, G.A., Hussein, M.A., Jose, J., Pinto, R., Al-Omari, A., Kharaba, A., et al. (2018). Corticosteroid Therapy for Critically Ill Patients with Middle East Respiratory Syndrome. Am. J. Respir. Crit. Care Med. *197*, 757–767. https://doi.org/10.1164/rccm.201706-1172OC.
11. Ni, Y.-N., Chen, G., Sun, J., Liang, B.-M., and Liang, Z.-A. (2019). The effect of corticosteroids on mortality of patients with influenza pneumonia: a systematic review and meta-analysis. Crit. Care *23*, 99. https://doi.org/10.1186/s13054-019-2395-8.
12. Sinha, S., Rosin, N.L., Arora, R., Labit, E., Jaffer, A., Cao, L., Farias, R., Nguyen, A.P., de Almeida, L.G.N., Dufour, A., et al. (2022). Dexamethasone modulates immature neutrophils and interferon programming in severe COVID-19. Nat. Med. *28*, 201–211. https://doi.org/10.1038/s41591-021-01576-3.
13. Wyler, E., Adler, J.M., Eschke, K., Teixeira Alves, G., Peidli, S., Pott, F., Kazmierski, J., Michalick, L., Kershaw, O., Bushe, J., et al. (2022). Key benefits of dexamethasone and antibody treatment in COVID-19 hamster models revealed by single-cell transcriptomics. Mol. Ther. *30*, 1952–1965. https://doi.org/10.1016/j.ymthe.2022.03.014.
14. Jeong, H.-W., Lee, J.S., Ko, J.-H., Hong, S., Oh, S.T., Choi, S., Peck, K.R., Yang, J.H., Chung, S., Kim, S.-H., et al. (2023). Corticosteroids reduce pathologic interferon responses by downregulating STAT1 in patients with high-risk COVID-19. Exp. Mol. Med. *55*, 653–664. https://doi.org/10.1038/s12276-023-00964-8.
15. Mazer, M.B., Davitt, E., Turnbull, I.R., Caldwell, C.C., Brakenridge, S.C., Remy, K.E., and Hotchkiss, R.S. (2021). In vitro-Administered Dexamethasone Suppresses T Cell Function With Reversal by Interleukin-7 in

Coronavirus Disease 2019. Crit. Care Explor. *3*, e0378. https://doi.org/10.1097/CCE.0000000000000378.

16. Wong, C.K.H., Lau, K.T.K., Au, I.C.H., Xiong, X., Chung, M.S.H., Leung, B.Y.C., Lau, E.H.Y., and Cowling, B.J. (2022). Initiation of Tocilizumab or Baricitinib Were Associated With Comparable Clinical Outcomes Among Patients Hospitalized With COVID-19 and Treated With Dexamethasone. Front. Pharmacol. *13*, 866441. https://doi.org/10.3389/fphar.2022.866441.
17. Kurth, F., Roennefarth, M., Thibeault, C., Corman, V.M., Müller-Redetzky, H., Mittermaier, M., Ruwwe-Glösenkamp, C., Heim, K.M., Krannich, A., Zvorc, S., et al. (2020). Studying the pathophysiology of coronavirus disease 2019: a protocol for the Berlin prospective COVID-19 patient cohort (Pa-COVID-19). Infection *48*, 619–626. https://doi.org/10.1007/s15010-020-01464-x.
18. Schulte-Schrepping, J., Reusch, N., Paclik, D., Baßler, K., Schlickeiser, S., Zhang, B., Krämer, B., Krammer, T., Brumhard, S., Bonaguro, L., et al. (2020). Severe COVID-19 Is Marked by a Dysregulated Myeloid Cell Compartment. Cell *182*, 1419–1440.e23. https://doi.org/10.1016/j.cell.2020.08.001.
19. D'Adamio, F., Zollo, O., Moraca, R., Ayroldi, E., Bruscoli, S., Bartoli, A., Cannarile, L., Migliorati, G., and Riccardi, C. (1997). A new dexamethasone-induced gene of the leucine zipper family protects T lymphocytes from TCR/CD3-activated cell death. Immunity *7*, 803–812. https://doi.org/10.1016/s1074-7613(00)80398-2.
20. Wang, Z., Rong, Y.P., Malone, M.H., Davis, M.C., Zhong, F., and Distelhorst, C.W. (2006). Thioredoxin-interacting protein (txnip) is a glucocorticoid-regulated primary response gene involved in mediating glucocorticoid-induced apoptosis. Oncogene *25*, 1903–1913. https://doi.org/10.1038/sj.onc.1209218.
21. Auphan, N., DiDonato, J.A., Rosette, C., Helmberg, A., and Karin, M. (1995). Immunosuppression by glucocorticoids: inhibition of NF-kappa B activity through induction of I kappa B synthesis. Science *270*, 286–290. https://doi.org/10.1126/science.270.5234.286.
22. Petta, I., Dejager, L., Ballegeer, M., Lievens, S., Tavernier, J., De Bosscher, K., and Libert, C. (2016). The interactome of the glucocorticoid receptor and its influence on the actions of glucocorticoids in combatting inflammatory and infectious diseases. Microbiol. Mol. Biol. Rev. *80*, 495–522. https://doi.org/10.1128/MMBR.00064-15.
23. Ehrchen, J.M., Roth, J., and Barczyk-Kahlert, K. (2019). More than suppression: glucocorticoid action on monocytes and macrophages. Front. Immunol. *10*, 2028. https://doi.org/10.3389/fimmu.2019.02028.
24. Ehrchen, J., Steinmüller, L., Barczyk, K., Tenbrock, K., Nacken, W., Eisenacher, M., Nordhues, U., Sorg, C., Sunderkötter, C., and Roth, J. (2007). Glucocorticoids induce differentiation of a specifically activated, anti-inflammatory subtype of human monocytes. Blood *109*, 1265–1274. https://doi.org/10.1182/blood-2006-02-001115.
25. Reddy, T.E., Pauli, F., Sprouse, R.O., Neff, N.F., Newberry, K.M., Garabedian, M.J., and Myers, R.M. (2009). Genomic determination of the glucocorticoid response reveals unexpected mechanisms of gene regulation. Genome Res. *19*, 2163–2171. https://doi.org/10.1101/gr.097022.109.
26. Wang, C., Nanni, L., Novakovic, B., Megchelenbrink, W., Kuznetsova, T., Stunnenberg, H.G., Ceri, S., and Logie, C. (2019). Extensive epigenomic integration of the glucocorticoid response in primary human monocytes and in vitro derived macrophages. Sci. Rep. *9*, 2772. https://doi.org/10.1038/s41598-019-39395-9.
27. Zannas, A.S., Wiechmann, T., Gassen, N.C., and Binder, E.B. (2016). Gene-Stress-Epigenetic Regulation of FKBP5: Clinical and Translational Implications. Neuropsychopharmacology *41*, 261–274. https://doi.org/10.1038/npp.2015.235.
28. Duhalde Vega, M., Olivera, D., Gastão Davanzo, G., Bertullo, M., Noya, V., Fabiano de Souza, G., Primon Muraro, S., Castro, I., Arévalo, A.P., Crispo, M., et al. (2022). PD-1/PD-L1 blockade abrogates a dysfunctional innate-adaptive immune axis in critical β-coronavirus disease. Sci. Adv. *8*, eabn6545. https://doi.org/10.1126/sciadv.abn6545.
29. Liao, M., Liu, Y., Yuan, J., Wen, Y., Xu, G., Zhao, J., Cheng, L., Li, J., Wang, X., Wang, F., et al. (2020). Single-cell landscape of bronchoalveolar immune cells in patients with COVID-19. Nat. Med. *26*, 842–844. https://doi.org/10.1038/s41591-020-0901-9.
30. Wendisch, D., Dietrich, O., Mari, T., von Stillfried, S., Ibarra, I.L., Mittermaier, M., Mache, C., Chua, R.L., Knoll, R., Timm, S., et al. (2021). SARS-CoV-2 infection triggers profibrotic macrophage responses and lung fibrosis. Cell *184*, 6243–6261.e27. https://doi.org/10.1016/j.cell.2021.11.033.
31. Buttgereit, F., Burmester, G.-R., and Lipworth, B.J. (2005). Optimised glucocorticoid therapy: the sharpening of an old spear. Lancet *365*, 801–803. https://doi.org/10.1016/S0140-6736(05)17989-6.
32. Reichardt, S.D., Amouret, A., Muzzi, C., Vettorazzi, S., Tuckermann, J.P., Lühder, F., and Reichardt, H.M. (2021). The role of glucocorticoids in inflammatory diseases. Cells *10*, 2921. https://doi.org/10.3390/cells10112921.
33. Ramamoorthy, S., and Cidlowski, J.A. (2016). Corticosteroids: mechanisms of action in health and disease. Rheum. Dis. Clin. North Am. *42*, 15–31,vii. https://doi.org/10.1016/j.rdc.2015.08.002.
34. Chen, S.T., Park, M.D., Del Valle, D.M., Buckup, M., Tabachnikova, A., Thompson, R.C., Simons, N.W., Mouskas, K., Lee, B., Geanon, D., et al. (2022). A shift in lung macrophage composition is associated with COVID-19 severity and recovery. Sci. Transl. Med. *14*, eabn5168. https://doi.org/10.1126/scitranslmed.abn5168.
35. Calfee, C.S., Delucchi, K., Parsons, P.E., Thompson, B.T., Ware, L.B., and Matthay, M.A.; NHLBI ARDS Network (2014). Subphenotypes in acute respiratory distress syndrome: latent class analysis of data from two randomised controlled trials. Lancet Respir. Med. *2*, 611–620. https://doi.org/10.1016/S2213-2600(14)70097-9.
36. Sinha, P., Furfaro, D., Cummings, M.J., Abrams, D., Delucchi, K., Maddali, M.V., He, J., Thompson, A., Murn, M., Fountain, J., et al. (2021). Latent Class Analysis Reveals COVID-19-related Acute Respiratory Distress Syndrome Subgroups with Differential Responses to Corticosteroids. Am. J. Respir. Crit. Care Med. *204*, 1274–1285. https://doi.org/10.1164/rccm.202105-1302OC.
37. Odeyemi, Y.E., Chalmers, S.J., Barreto, E.F., Jentzer, J.C., Gajic, O., and Yadav, H. (2022). Early, biomarker-guided steroid dosing in COVID-19 Pneumonia: a pilot randomized controlled trial. Crit. Care *26*, 9. https://doi.org/10.1186/s13054-021-03873-2.
38. López-Martínez, C., Martín-Vicente, P., Gómez de Oña, J., López-Alonso, I., Gil-Peña, H., Cuesta-Llavona, E., Fernández-Rodríguez, M., Crespo, I., Salgado Del Riego, E., Rodríguez-García, R., et al. (2023). Transcriptomic clustering of critically ill COVID-19 patients. Eur. Respir. J. *61*, 2200592. https://doi.org/10.1183/13993003.00592-2022.
39. Dequin, P.-F., Heming, N., Meziani, F., Plantefève, G., Voiriot, G., Badié, J., François, B., Aubron, C., Ricard, J.-D., Ehrmann, S., et al. (2020). Effect of Hydrocortisone on 21-Day Mortality or Respiratory Support Among Critically Ill Patients With COVID-19: A Randomized Clinical Trial. JAMA *324*, 1298–1306. https://doi.org/10.1001/jama.2020.16761.
40. Brown, H.M. (1958). Treatment of chronic asthma with prednisolone; significance of eosinophils in the sputum. Lancet *2*, 1245–1247. https://doi.org/10.1016/S0140-6736(58)91385-0.
41. Busse, W.W., Kraft, M., Rabe, K.F., Deniz, Y., Rowe, P.J., Ruddy, M., and Castro, M. (2021). Understanding the key issues in the treatment of uncontrolled persistent asthma with type 2 inflammation. Eur. Respir. J. *58*, 2003393. https://doi.org/10.1183/13993003.03393-2020.
42. Saleem, N., Kulkarni, A., Snow, T.A.C., Ambler, G., Singer, M., and Arulkumaran, N. (2023). Effect of Corticosteroids on Mortality and Clinical Cure in Community-Acquired Pneumonia: A Systematic Review, Meta-analysis, and Meta-regression of Randomized Control Trials. Chest *163*, 484–497. https://doi.org/10.1016/j.chest.2022.08.2229.
43. Dequin, P.-F., Meziani, F., Quenot, J.-P., Kamel, T., Ricard, J.-D., Badie, J., Reignier, J., Heming, N., Plantefève, G., Souweine, B., et al. (2023). Hydrocortisone in Severe Community-Acquired Pneumonia. N. Engl. J. Med. *388*, 1931–1941. https://doi.org/10.1056/NEJMoa2215145.

44. Ely, E.W., Ramanan, A.V., Kartman, C.E., de Bono, S., Liao, R., Piruzeli, M.L.B., Goldman, J.D., Saraiva, J.F.K., Chakladar, S., Marconi, V.C., et al. (2022). Efficacy and safety of baricitinib plus standard of care for the treatment of critically ill hospitalised adults with COVID-19 on invasive mechanical ventilation or extracorporeal membrane oxygenation: an exploratory, randomised, placebo-controlled trial. Lancet Respir. Med. *10*, 327–336. https://doi.org/10.1016/S2213-2600(22)00006-6.

45. Lingscheid, T., Lippert, L.J., Hillus, D., Kruis, T., Thibeault, C., Helbig, E.T., Tober-Lau, P., Pfäfflin, F., Müller-Redetzky, H., Witzenrath, M., et al. (2022). Characterization of antimicrobial use and co-infections among hospitalized patients with COVID-19: a prospective observational cohort study. Infection *50*, 1441–1452. https://doi.org/10.1007/s15010-022-01796-w.

46. Leistner, R., Schroeter, L., Adam, T., Poddubnyy, D., Stegemann, M., Siegmund, B., Maechler, F., Geffers, C., Schwab, F., Gastmeier, P., et al. (2022). Corticosteroids as risk factor for COVID-19-associated pulmonary aspergillosis in intensive care patients. Crit. Care *26*, 30. https://doi.org/10.1186/s13054-022-03902-8.

47. Dobin, A., Davis, C.A., Schlesinger, F., Drenkow, J., Zaleski, C., Jha, S., Batut, P., Chaisson, M., and Gingeras, T.R. (2013). STAR: ultrafast universal RNA-seq aligner. Bioinformatics *29*, 15–21. https://doi.org/10.1093/bioinformatics/bts635.

48. Martin, M. (2011). Cutadapt removes adapter sequences from high-throughput sequencing reads. EMBnet J. *17*, 10. https://doi.org/10.14806/ej.17.1.200.

49. Andrews S. FastQC: A Quality Control Tool for High Throughput Sequence Data. 2010. http://www.bioinformatics.babraham.ac.uk/projects/fastqc/. Accessed Jan 19, 2024.

50. Zheng, G.X.Y., Terry, J.M., Belgrader, P., Ryvkin, P., Bent, Z.W., Wilson, R., Ziraldo, S.B., Wheeler, T.D., McDermott, G.P., Zhu, J., et al. (2017). Massively parallel digital transcriptional profiling of single cells. Nat. Commun. *8*, 14049. https://doi.org/10.1038/ncomms14049.

51. Butler, A., Hoffman, P., Smibert, P., Papalexi, E., and Satija, R. (2018). Integrating single-cell transcriptomic data across different conditions, technologies, and species. Nat. Biotechnol. *36*, 411–420. https://doi.org/10.1038/nbt.4096.

52. Hafemeister, C., and Satija, R. (2019). Normalization and variance stabilization of single-cell RNA-seq data using regularized negative binomial regression. Genome Biol *20*, 296. https://doi.org/10.1186/s13059-019-1874-1.

53. Stuart, T., Butler, A., Hoffman, P., Hafemeister, C., Papalexi, E., Mauck, W.M., 3rd, Stoeckius, M., Smibert, P., and Satija, R. (2019). Comprehensive Integration of Single-Cell Data. Cell *177*, 1888–1902.e21. https://doi.org/10.1016/j.cell.2019.05.031.

54. Korsunsky, I., Millard, N., Fan, J., Slowikowski, K., Zhang, F., Wei, K., Baglaenko, Y., Brenner, M., Loh, P.-R., and Raychaudhuri, S. (2019). Fast, sensitive and accurate integration of single-cell data with Harmony. Nat. Methods *16*, 1289–1296. https://doi.org/10.1038/s41592-019-0619-0.

55. Yu, G., Wang, L.-G., Han, Y., and He, Q.-Y. (2012). clusterProfiler: an R package for comparing biological themes among gene clusters. OMICS *16*, 284–287. https://doi.org/10.1089/omi.2011.0118.

56. Haghverdi, L., Lun, A.T.L., Morgan, M.D., and Marioni, J.C. (2018). Batch effects in single-cell RNA-sequencing data are corrected by matching mutual nearest neighbors. Nat. Biotechnol. *36*, 421–427. https://doi.org/10.1038/nbt.4091.

57. Aibar, S., González-Blas, C.B., Moerman, T., Huynh-Thu, V.A., Imrichova, H., Hulselmans, G., Rambow, F., Marine, J.-C., Geurts, P., Aerts, J., et al. (2017). SCENIC: single-cell regulatory network inference and clustering. Nat. Methods *14*, 1083–1086. https://doi.org/10.1038/nmeth.4463.

58. Love, M.I., Huber, W., and Anders, S. (2014). Moderated estimation of fold change and dispersion for RNA-seq data with DESeq2. Genome Biol. *15*, 550. https://doi.org/10.1186/s13059-014-0550-8.

59. Hänzelmann, S., Castelo, R., and Guinney, J. (2013). GSVA: gene set variation analysis for microarray and RNA-seq data. BMC Bioinformatics *14*, 7. https://doi.org/10.1186/1471-2105-14-7.

60. Korotkevich, G., Sukhov, V., Budin, N., Shpak, B., Artyomov, M.N., and Sergushichev, A. (2016). Fast gene set enrichment analysis. Preprint at bioRxiv. https://doi.org/10.1101/060012.

61. Wickham, H. (2016). ggplot2 - Elegant Graphics for Data Analysis, Second Edition (Springer International Publishing) https://doi.org/10.1007/978-3-319-24277-4.

62. Kolde, R., Laur, S., Adler, P., and Vilo, J. (2012). Robust rank aggregation for gene list integration and meta-analysis. Bioinformatics *28*, 573–580. https://doi.org/10.1093/bioinformatics/btr709.

63. Leek, J.T., Johnson, W.E., Parker, H.S., Jaffe, A.E., and Storey, J.D. (2012). The sva package for removing batch effects and other unwanted variation in high-throughput experiments. Bioinformatics *28*, 882–883. https://doi.org/10.1093/bioinformatics/bts034.

64. Fortin, J., Labbe, A., Lemire, M., Zanke, B.W., Hudson, T.J., Fertig, E.J., Greenwood, C.M., and Hansen, K.D. (2014). Functional normalization of 450k methylation array data improves replication in large cancer studies. Genome Biology *15*, 503. https://doi.org/10.1186/s13059-014-0503-2.

65. Ritchie, M.E., Phipson, B., Wu, D., Hu, Y., Law, C.W., Shi, W., and Smyth, G.K. (2015). limma powers differential expression analyses for RNA-sequencing and microarray studies. Nucleic Acids Res. *43*, e47. https://doi.org/10.1093/nar/gkv007.

66. Van Gassen, S., Callebaut, B., Van Helden, M.J., Lambrecht, B.N., Demeester, P., Dhaene, T., and Saeys, Y. (2015). FlowSOM: Using self-organizing maps for visualization and interpretation of cytometry data. Cytometry A *87*, 636–645. https://doi.org/10.1002/cyto.a.22625.

67. Gu, Z., Eils, R., and Schlesner, M. (2016). Complex heatmaps reveal patterns and correlations in multidimensional genomic data. Bioinformatics. https://doi.org/10.1093/bioinformatics/btw313.

68. Sekhon, J.S. (2011). Multivariate and Propensity Score Matching Software with Automated Balance Optimization: The Matching Package for R. J. Stat. Softw. *42*, 1–52. https://doi.org/10.18637/jss.v042.i07.

69. World Health Organiztion. COVID 19 Therapeutic Trial Synopsis. 2020. https://www.who.int/docs/default-source/blue-print/covid-19-therapeutic-trial-synopsis.pdf. Accessed Jul 23, 2023.

70. Krämer, B., Knoll, R., Bonaguro, L., ToVinh, M., Raabe, J., Astaburuaga-García, R., Schulte-Schrepping, J., Kaiser, K.M., Rieke, G.J., Bischoff, J., et al. (2021). Early IFN-$\alpha$ signatures and persistent dysfunction are distinguishing features of NK cells in severe COVID-19. Immunity *54*, 2650–2669.e14. https://doi.org/10.1016/j.immuni.2021.09.002.

71. Kurth, F., Helbig, E.T., Lippert, L.J., Thibeault, C., Barbone, G., Eckart, M.A., Kluge, M., Puengel, T., Demir, M., Röhle, R., et al. (2023). Cenicriviroc for the treatment of COVID-19: first interim results of a randomised, placebo-controlled, investigator-initiated, double-blind phase II trial. J. Glob. Antimicrob. Resist. *32*, 44–47. https://doi.org/10.1016/j.jgar.2022.12.004.

72. De Domenico, E., Bonaguro, L., Schulte-Schrepping, J., Becker, M., Händler, K., and Schultze, J.L. (2020). Optimized workflow for single-cell transcriptomics on infectious diseases including COVID-19. Star Protoc. *1*, 100233. https://doi.org/10.1016/j.xpro.2020.100233.

73. Hao, Y., Hao, S., Andersen-Nissen, E., Mauck, W.M., Zheng, S., Butler, A., Lee, M.J., Wilk, A.J., Darby, C., Zager, M., et al. (2021). Integrated analysis of multimodal single-cell data. Cell *184*, 3573–3587.e29. https://doi.org/10.1016/j.cell.2021.04.048.

74. Ashburner, M., Ball, C.A., Blake, J.A., Botstein, D., Butler, H., Cherry, J.M., Davis, A.P., Dolinski, K., Dwight, S.S., Eppig, J.T., et al. (2000). Gene Ontology: tool for the unification of biology. The Gene Ontology Consortium. Nat. Genet. *25*, 25–29. https://doi.org/10.1038/75556.

75. The Gene Ontology Consortium (2019). The Gene Ontology Resource: 20 years and still GOing strong. Nucleic Acids Res. *47*, D330–D338. https://doi.org/10.1093/nar/gky1055.

76. Kanehisa, M. (2019). Toward understanding the origin and evolution of cellular organisms. Protein Sci. *28*, 1947–1951. https://doi.org/10.1002/pro.3715.

77. Liberzon, A., Birger, C., Thorvaldsdóttir, H., Ghandi, M., Mesirov, J.P., and Tamayo, P. (2015). The Molecular Signatures Database (MSigDB) hallmark gene set collection. Cell Syst. *1*, 417–425. https://doi.org/10.1016/j.cels.2015.12.004.

78. Fabregat, A., Jupe, S., Matthews, L., Sidiropoulos, K., Gillespie, M., Garapati, P., Haw, R., Jassal, B., Korninger, F., May, B., et al. (2018). The Reactome Pathway Knowledgebase. Nucleic Acids Res. *46*, D649–D655. https://doi.org/10.1093/nar/gkx1132.

79. Gillespie, M., Jassal, B., Stephan, R., Milacic, M., Rothfels, K., Senff-Ribeiro, A., Griss, J., Sevilla, C., Matthews, L., Gong, C., et al. (2022). The reactome pathway knowledgebase 2022. Nucleic Acids Res. *50*, D687–D692. https://doi.org/10.1093/nar/gkab1028.

80. Wu, T., Hu, E., Xu, S., Chen, M., Guo, P., Dai, Z., Feng, T., Zhou, L., Tang, W., Zhan, L., et al. (2021). clusterProfiler 4.0: A universal enrichment tool for interpreting omics data. Innovation (Camb) *2*, 100141. https://doi.org/10.1016/j.xinn.2021.100141.

81. Waltman, L., and van Eck, N.J. (2013). A smart local moving algorithm for large-scale modularity-based community detection. Eur. Phys. J. B *86*, 471. https://doi.org/10.1140/epjb/e2013-40829-0.

82. Subramanian, A., Tamayo, P., Mootha, V.K., Mukherjee, S., Ebert, B.L., Gillette, M.A., Paulovich, A., Pomeroy, S.L., Golub, T.R., Lander, E.S., et al. (2005). Gene set enrichment analysis: a knowledge-based approach for interpreting genome-wide expression profiles. Proc. Natl. Acad. Sci. USA *102*, 15545–15550. https://doi.org/10.1073/pnas.0506580102.

83. Pidsley, R., Zotenko, E., Peters, T.J., Lawrence, M.G., Risbridger, G.P., Molloy, P., Van Djik, S., Muhlhausler, B., Stirzaker, C., and Clark, S.J. (2016). Critical evaluation of the Illumina MethylationEPIC BeadChip microarray for whole-genome DNA methylation profiling. Genome Biol. *17*, 208. https://doi.org/10.1186/s13059-016-1066-1.

84. Ren, X., and Kuan, P.F. (2019). methylGSA: a Bioconductor package and Shiny app for DNA methylation data length bias adjustment in gene set testing. Bioinformatics *35*, 1958–1959. https://doi.org/10.1093/bioinformatics/bty892.

## STAR★METHODS

### KEY RESOURCES TABLE

| REAGENT or RESOURCE | SOURCE | IDENTIFIER |
|---|---|---|
| Antibodies | | |
| CD3 BV421 (clone UCHT1) | Biolegend | Cat# 300434; RRID:AB_10962690 |
| CD4 APCFire750 (clone RPA-T4) | Biolegend | Cat# 300560; RRID:AB_2629693 |
| CD8a BV711 (clone RPA-T8) | Biolegend | Cat# 301044; RRID:AB_2562906 |
| CD14 PerCP (clone TÜK4) | Miltenyi | Cat# 130-113-150; RRID:AB_2725978 |
| CD16 BV605 (clone 3G8) | Biolegend | Cat# 302040; RRID:AB_2562990 |
| CD19 PE (clone HIB19) | Biolegend | Cat# 302208; RRID:AB_314238 |
| CD45RA BV785 (clone HI100) | Biolegend | Cat# 304140; RRID:AB_2563816 |
| CD66b APC (clone G10F5) | Biolegend | Cat# 305118; RRID:AB_2566607 |
| CCR7 AF488 (clone G042H7) | Biolegend | Cat# 353206; RRID:AB_10916389 |
| CD45 89Y (Hi30) | Fluidigm | Cat# 3089003; RRID:AB_2938863 |
| CCR2 113In (K036C2) | Biolegend | N/A |
| CD3 115In (UCHT1) | Biolegend | Cat# 300443; RRID:AB_2562808 |
| CD196 141Pr (G034E3) | Fluidigm | Cat# 3141003A; RRID:AB_2687639 |
| CD49d 141Pr (9F10) | Fluidigm | Cat# 3141004B; RRID:AB_2892684 |
| CD19 142Nd (HIB-19) | Fluidigm | Cat# 3142001B; RRID:AB_2651155 |
| CD123 143Nd (6H6) | Fluidigm | Cat# 3143014B; RRID:AB_2811081 |
| CD15 144Nd (W6D3) | Fluidigm | Cat# 3144019B; RRID:AB_2892685 |
| CD21 145Nd (Bu-15) | Biolegend | Cat# 354902; RRID:AB_11219188 |
| CD138 145Nd (DL101) | Fluidigm | Cat# 3145003B |
| CD226 146Nd (REA1040) | Miltenyi Biotec | N/A |
| CD64 146Nd (10.1) | Fluidigm | Cat# 3146006B; RRID:AB_2661790 |
| IgD 147Sm (IgD26) | Biolegend | Cat# 348235; RRID:AB_2563775 |
| CXCR2 147Sm (5E8) | Fluidigm | Cat# 3147010B |
| ICOS 148Nd (C398.4A) | Fluidigm | Cat# 3148019B; RRID:AB_2756435 |
| CD206 purified (152) | Biolegend | Cat# 321127; RRID:AB_2563729 |
| CD96 purified (REA195) | Miltenyi Biotec | Produced at request |
| KLRG1 purified (REA261) | Miltenyi Biotec | Produced at request |
| TCRgd purified (11F2) | Miltenyi Biotec | Produced at request |
| FceRI 150Nd (AER-37) | Fluidigm | Cat# 3150027B |
| CD155 purified (REA1081) | Miltenyi Biotec | Produced at request |
| CD95 purified (DX2) | Biolegend | Cat# 305631; RRID:AB_2563766 |
| CD66b 152Sm (80H3) | Fluidigm | Cat# 3152011B; RRID:AB_2661795 |
| TIGIT 153Eu (MBSA43) | Fluidigm | Cat# 3153019B; RRID:AB_2756419 |
| CD62L purified (DREG56) | Biolegend | Cat# 304835; RRID:AB_2563758 |
| CD1c purified (L161) | Biolegend | Cat# 331502; RRID:AB_1088995 |
| CD27 155Gd (L128) | Fluidigm | Cat# 3155001B; RRID:AB_2687645 |
| CXCR3 156Gd (G025H7) | Fluidigm | Cat# 3156004B; RRID:AB_2687646 |
| CCR5 156Gd (NP-6G4) | Fluidigm | Cat# 3156015A; RRID:AB_2938860 |
| KLRF1 purified (REA845) | Miltenyi Biotec | Produced at request |
| CD10 158Gd (HI10a) | Fluidigm | Cat# 3158011B; RRID:AB_2921314 |
| CD33 158Gd (WM53) | Fluidigm | Cat# 3158001; RRID:AB_2661799 |
| CD14 160Gd (RMO52) | Fluidigm | Cat# 3160006; RRID:AB_2661801 |
| CD28 purified (L293) | BD Bioscience | Cat# 348040; RRID:AB_400367 |

(*Continued on next page*)

*Continued*

| REAGENT or RESOURCE | SOURCE | IDENTIFIER |
|---|---|---|
| CD69 162Dy (FN50) | Fluidigm | Cat# 3162001B; RRID:AB_3096016 |
| CD294 163Dy (BM16) | Fluidigm | Cat# 3163003B; RRID:AB_2810253 |
| Anti-APC 163Dy | Fluidigm | Cat# 3163001B; RRID:AB_2687636 |
| CXCR5 164Dy (RF8B2) | Fluidigm | Cat# 3164029B |
| Siglec 8 164Dy (7C9) | Fluidigm | Cat# 3164017B |
| CD163 165Ho (GHI/61) | Fluidigm | Cat# 3165017B; RRID:AB_2810250 |
| CD34 166Er (581) | Fluidigm | Cat# 3166012B; RRID:AB_2756424 |
| CD38 167Er (HIT2) | Fluidigm | Cat# 3167001B; RRID:AB_2802110 |
| Ki67 168Er (Ki-67) | Fluidigm | Cat# 3168007B; RRID:AB_2800467 |
| CD25 169Tm (2A3) | Fluidigm | Cat# 3169003; RRID:AB_2938861 |
| CD24 169Tm (ML5) | Fluidigm | Cat# 3169004B; RRID:AB_2688021 |
| Lag3 purified (11C3C65) | Biolegend | Cat# 369302; RRID:AB_2616876 |
| RANK purified (80704) | R&D Systems | Cat# MAB683; RRID:AB_2205330 |
| CD161 purified (HP-3G10) | Biolegend | Cat# 339919; RRID:AB_2562836 |
| CD11b purified (ICRF44) | Biolegend | Cat# 301337; RRID:AB_2562811 |
| CD45RO purified (4G11) | DRFZ Berlin | N/A |
| CD44 purified (BJ18) | Biolegend | Cat# 338811; RRID:AB_2562835 |
| CD137 173Yb (4B4-1) | Fluidigm | Cat# 3173015B |
| HLA-DR purified (L243) | Biolegend | Cat# 307602; RRID:AB_314680 |
| PD-1 175Lu (EH12.2H7) | Fluidigm | Cat# 3175008; RRID:AB_2687629 |
| PD-L1 175Lu (29.E2A3) | Fluidigm | Cat# 3175017B; RRID:AB_2687638 |
| CD56 176Yb (NCAM16.2) | Fluidigm | Cat# 3176008; RRID:AB_2661813 |
| CD8 purified (GN11) | DRFZ Berlin | N/A |
| IgM purified (MHM-88) | Biolegend | Cat# 314502; RRID:AB_493003 |
| CD11c purified (Bu15) | Biolegend | Cat# 337221; RRID:AB_2562834 |
| CD16 209Bi (3G8) | Fluidigm | Cat# 3209002B; RRID:AB_2756431 |
| CD14-BV421 (clone M5E2) | Biolegend | Cat# 301830; RRID:AB_10959324 |
| CD163-PercP-Vio700 (clone REA812) | Miltenyi | Cat# 130-112-133; RRID:AB_2655489 |
| CD3-FITC (clone UCHT1) | Biolegend | Cat# 300406; RRID:AB_314060 |
| CD94-FITC (clone DX22) | Biolegend | Cat# 305504; RRID:AB_314534 |
| NKp80-FITC (clone 4A4.D10) | Miltenyi | Cat# 130-094-843; RRID:AB_10829948 |
| TCRab-FITC (clone IP26) | Biolegend | Cat# 306706; RRID:AB_314644 |
| TCRgd-FITC (clone B1) | Biolegend | Cat# 331208; RRID:AB_1575108 |
| CD20-FITC (clone 2H7) | Biolegend | Cat# 302304; RRID:AB_314252 |
| CD19-FITC (clone HIB19) | Biolegend | Cat# 302206; RRID:AB_314236 |
| Amphiregulin-APC (clone AREG559) | Ebioscience | Cat# 17-5370-42; RRID:AB_2716941 |
| **Chemicals, peptides, and recombinant proteins** | | |
| FcR Blocking Reagent, human | Miletnyi Biotec | Cat# 130-059-901; RRID:AB_2892112 |
| Proteinase K | Sigma-Aldrich | Cat# 3115828001 |
| Tempus™ Blood RNA Tube | ThermoFisher Scientific | Cat# 4342792 |
| PAXgene® Blood RNA Tube | Becton Dickinson | Cat# 762165 |
| SPRIselect | Beckmann Coulter | Cat# B23318 |
| BD Vacutainer® Lithium Heparin Tubes | Becton Dickinson | Cat# 367526 |
| **Critical commercial assays** | | |
| BD Single-Cell Multiplexing Kit (human) | Becton Dickinson | Cat# 633781 |
| BD Rhapsody WTA Amplification Kit | Becton Dickinson | Cat# 633801 |
| BD Rhapsody Cartridge Kit | BectonDickinson | Cat# 633733 |

(*Continued on next page*)

*Continued*

| REAGENT or RESOURCE | SOURCE | IDENTIFIER |
|---|---|---|
| BD Rhapsody cDNA Kit | BectonDickinson | Cat# 633773 |
| High Sensitivity D5000 ScreenTape | Agilent | Cat# 5067-5592 |
| High Sensitivity D1000 ScreenTape | Agilent | Cat# 5067-5584 |
| Qubit dsDNA HS Assay Kit | ThermoFisher | Cat# Q32851 |
| High Sensitivity DNA Kit | Agilent | Cat# 5067-4626 |
| NovaSeq 6000 S2 Reagent Kit (200 cycles) | Illumina | Cat# 20040326 |
| NovaSeq 6000 S4 Reagent Kit (200 cycles) | Illumina | Cat# 20028313 |
| Chromium Next GEM Single Cell 3′ GEM, Library & Gel Bead Kit v3.1 | 10x Genomics | Cat# 1000121 |
| Chromium Next GEM Chip G Single Cell Kit | 10x Genomics | Cat# 1000120 |
| Single Index Kit T Set A | 10x Genomics | Cat# 1000213 |
| TruSeq Stranded Total RNA with Ribo-Zero Globin | Illumina | Cat# 20020613 |
| Maxpar® X8 Antibody Labeling Kit | Fluidigm | Cat# 201146B |
| Quick-DNA Microprep Kit | Zymo Research | Cat# D3020 |
| EZ DNA Methylation-Gold Kit | Zymo Research | Cat# D5006 |
| Infinium MethylationEPIC BeadChip Kit | Illumina | Cat# WG-317-1002 |
| Zombie Aqua™ Fixable Viability Kit | BioLegend | Cat# 423101 |
| BD Cytofix/Cytoperm™ Fixation/ Permeabilization Kit | Becton, Dickinson | Cat# 554714 |
| SeraSpot Anti-SARS-CoV-2 IgG microarray | Seramun Diagnostica | SP-015-4 G-S12 RUO |
| **Deposited data** | | |
| scRNA-seq raw data | This paper | EGAS00001007461, EGAS50000000203 |
| bulk RNA-seq raw data | This paper | EGAS00001007461 |
| processed scRNA-seq count data and code | This paper | https://github.com/knollr/COVID_Dexa |
| processed bulk RNA-seq count data and code | This paper | https://github.com/knollr/COVID_Dexa |
| DNA methylation data | This paper | GSE270901 |
| Code for DNA methylation data analysis | This paper | https://github.com/knollr/COVID_Dexa |
| **Software and algorithms** | | |
| Bcl2fastq2 | Illumina | v2.20 |
| STAR | Dobin et al.[47] | v2.7.3a |
| Cutadapt | Martin et al.[48] | v1.16 |
| Dropseq-tools | https://github.com/broadinstitute/Drop-seq/ | v2.0.0 |
| fastQC | Andrews et al.[49] | 0.11.8 |
| 10x Genomics Cell Ranger (Software) | Zheng et al.,[50] 10X Genomics | 7.0.0 |
| R (bulk and scRNA-seq blood analysis) | https://www.cran.r-project.org | v4.1.0 |
| R (DNA methylation analysis) | https://www.cran.r-project.org | v4.2.1 |
| R (scRNA-seq BAL analysis) | https://www.cran.r-project.org | v4.3.1 |
| Seurat (scRNA-seq blood, R package) | Butler et al.,[51] Hafemeister et al.,[52] Stuart et al.[53] | v4.3.0 |
| Seurat (scRNA-seq BAL, R package) | Butler et al.,[51] Hafemeister et al.,[52] Stuart et al.[53] | v4.4.0 |
| Harmony (R package) | Korsunsky et al.[54] | v0.1.0 |
| ClusterProfiler (R package) | Yu et al.[55] | v4.0.5 |
| batchelor (R package) | Haghverdi et al.[56] | v1.16.0 |
| AUCell (R package) | Aibar et al.[57] | v1.22.0 |
| DESeq2 (R package) | Love et al.[58] | v1.32.0 |

(*Continued on next page*)

*Continued*

| REAGENT or RESOURCE | SOURCE | IDENTIFIER |
|---|---|---|
| GSVA (R package) | Hänzelmann et al.[59] | v1.40.1 |
| fgsea (R package) | Korotkevich et al.[60] | v1.18.0 |
| ggplot2 (R Package; bulk RNA-seq analysis) | Wickham et al.[61] | v3.3.5 |
| ggplot2 (R package; DNA methylation analysis) | Wickham et al.[61] | v3.3.6 |
| pheatmap (R package) | Kolde et al.[62] | v1.0.12 |
| sva (R package) | Leek et al.[63] | v3.44.0 |
| minfi (R package) | Fortin et al.[64] | v1.42.0 |
| limma (R package; DNA methylation analysis) | Ritchie et al.[65] | v3.52.2 |
| limma (R package; bulk RNA-seq analysis) | Ritchie et al.[65] | v3.48.3 |
| methylGSA (R package) | Fortin et al.[64] | v1.14.0 |
| FlowSOM (R package) | Van Gassen et al.[66] | v3.17 |
| uwot (R package) | https://cran.r-project.org/web/packages/uwot/index.html | v0.1.8 |
| ComplexHeatmap (R package) | Gu et al.[67] | v1.20.0 |
| FlowJo | https://www.flowjo.com | v10.8 |
| JMP Pro | SAS Institute inc. | V 16.2.0 |
| Matching (R package) | Sekhon et al.[68] | v4.9-7 |
| OMIQ | www.omiq.ai | N/A |

## RESOURCE AVAILABILITY

### Lead contact

Further information and requests for resources and reagents should be directed to and will be fulfilled by the lead contact, Anna C. Aschenbrenner (anna.aschenbrenner@dzne.de).

### Materials availability

This study did not generate new unique reagents.

### Data and code availability

scRNA-seq and bulk RNA-seq data generated during this study are deposited at the European Genome-phenome Archive (EGA) under access numbers EGAS00001007461 and EGAS50000000203, which is hosted by the EBI and the CRG. DNA methylation data are deposited on the GEO database under access number GSE270901. All original code has been deposited at GitHub (https://github.com/knollr/COVID_Dexa) and is publicly available as of the date of publication. Any additional information required to reanalyze the data reported in this paper is available from the lead contact upon request.

## EXPERIMENTAL MODEL AND STUDY PARTICIPANT DETAILS

### Patient cohorts and study flow overview

To determine dexamethasone-specific molecular signatures, samples from patients with dexamethasone treatment and matched controls enrolled into the Pa-COVID-19 study, a prospective, observational study on patients with COVID-19 conducted at Charité Universitätsmedizin Berlin[17] were analyzed using single-cell transcriptomics, CyTOF and flow cytometry. In addition, matched samples from patients with stable versus progressive disease under dexamethasone treatment from the same cohort were assessed for possible influence of the patient's DNA-methylation status on responsiveness to dexamethasone treatment. In a last step, to assess if treatment-related signatures can be used to stratify outcome, bulk-sequencing was performed on samples from patients treated with dexamethasone recruited into the Pa-COVID-19 study and an independent study, PROVID-CAPNETZ, a prospective, observational, multi-centered cohort study with adult SARS-CoV-2 positive hospitalized patients to evaluate clinical data, molecular and functional biomarkers for prognosis, pathomechanisms and treatment strategies of COVID-19 (PROVID) recruited within the competence network community-acquired pneumonia (CAPNETZ, https://capnetz.de). Grouping and selection of patients and a synopsis on clinical characteristics of all included patients and controls per analysis is given in Table S1.

### Single-cell transcriptomics, CyTOF, and FACS

In order to determine dexamethasone-specific molecular signatures, all 543 patients included from 1 March 2020 to February 28, 2021 into the Pa-COVID-19 study were screened to identify patients treated with dexamethasone (from June 2020 onwards, following publication of the results of the recovery trial[1]) and comparable patients without dexamethasone treatment (from March to May 2020). Disease severity was stratified using the 8-point WHO ordinal scale[69] of improvement: WHO score 1 and 2 = ambulatory; WHO score 3 = hospitalized without supplemental oxygen; WHO score 4 = hospitalized with low-flow supplemental oxygen; WHO score 5 = hospitalized with requirement of non-invasive ventilation or high-flow oxygen; WHO score 6 = hospitalized with invasive ventilation; WHO score 7 = hospitalized with invasive ventilation and additional organ support; WHO score 8 = death. For analysis WHO grade $\leq$4 was considered as moderate disease, whereas WHO grade $\geq$ 5 was considered as severe disease. WHO score at time point of sampling was used to determine disease severity for these analyses.

Patients meeting one of the following criteria were excluded: age <18 years, no biosamples available, mild disease (maximum WHO score $\leq$3), chronic immunosuppression according to medical history, dexamethasone treatment not following treatment criteria of the recovery trial[1] or any steroid-treatment of control patients recruited early in the pandemic (e.g. hydrocortisone-treatment for septic shock). We also excluded all patients receiving additional immunosuppressive treatments (e.g. TNF-inhibitors, JAK-inhibitors, antimetabolites). This resulted in a total of 153 patients. Sampling timepoints were selected towards the end of the dexamethasone treatment period, and at corresponding time points based on symptom onset for patients without dexamethasone treatment, respectively. To obtain comparable groups (glucocorticoid-naïve controls vs. treated patients), multivariate matching was employed to identify the most suitable matches between groups. Specifically, we used exact matching for treatment with/without dexamethasone, sex, and maximum recorded value of WHO Ordinal Scale during hospitalization and greedy matching with Mahalanobis distance[68] for age and time interval (in days) between symptom onset and acquisition of blood sample closest to the end of dexamethasone treatment. If several equivalent matches were available, patient data was reviewed by two clinically experienced physicians for further details on course of disease (e.g. organ replacement therapy) and pre-existing comorbidities to find the best matches. The most appropriate matches were selected for the respective analyses depending on sample quality (e.g. PBMC count), using the same pairs for scRNASeq, CyTOF, and FACS analysis. If needed for CyTOF and FACS analysis, individual donors were replaced as equivalent as possible and sampling timepoints were adapted to a maximum of +2 days (for CyTOF) and +3 days (for FACS, 1 donor only), respectively.

### Subject details blood sc transcriptomics subgroup

A total of 66 PBMC samples from 48 male patients of the Pa-COVID-19 study were selected, with additional 4 samples included from 2 glucocorticoid-naïve patients from an observational study performed at Bonn university hospital fulfilling the same inclusion criteria as described above for the Pa-COVID-19 study.[70]

For analysis of dexamethasone-related signatures, 40 samples collected towards the end of the dexamethasone treatment period of 40 individuals were analyzed. These included 14 treatment-naive (5 moderately ill, 9 severely ill) and 26 dexamethasone-treated patients (7 moderately ill, 19 severely ill). The median age of all patients was 62 years (IQR range 55.25-69.75 years). All moderately affected patients survived, whereas 12 severely ill patients died. Three untreated controls and nine patients treated with dexamethasone. Samples included in analysis of dexamethasone treatment effects were obtained at a median of 8 days (IQR 6.75-9 days) after initiation of dexamethasone treatment and at a median of 15.5 days (IQR 13.75-18 days) after symptom onset. Control samples were obtained at a median of 16 days (IQR 14.75-18 days) after symptom onset.

An additional 26 samples from moderately and severely ill patients were included for comparison and validation of our dataset with previously defined expression changes, but not for analysis of dexamethasone-related signatures. These include samples collected during the early phase of hospitalization of glucocorticoid-naive patients (median 9 days (IQR 7.5-10 days) post symptom onset) and dexamethasone-treated patients (median 6 days (IQR 5-9 days) post symptom onset), as well as early (median 6 days (IQR 5-9 days) post symptom onset) and late (median 13.5 days (IQR 12.25-16.75 days) post symptom onset) samples of patients treated with dexamethasone and the CCR2/CCR5 inhibitor cenicriviroc (CVC[71]), which showed no major effects on single-cell transcriptomes in our analyses.

### Subject details FACS subgroup

A total of 36 PBMC samples from 36 male individuals (18 treatment-naive and 18 dexamethasone-treated patients) recruited within Pa-COVID-19 study were analyzed, of which 12 were moderately ill and 24 severely ill. The median age of included patients was 61.5 years (IQR 54-72.25). Samples of dexamethasone-treated patients were obtained at a median of 8 days (IQR 7-10 days) after treatment initiation. Samples were collected at a median of 17 days (IQR 14-18.25 days) after symptom onset for dexamethasone-treated patients vs. 16.5 days (IQR 15-19.25 days) in the untreated control group. Five severely affected patients died, four of whom were in the dexamethasone group and one in the control group.

### Subject details CyTOF subgroup

Due to expected decreasing sample quality with storage time and therefore reduced processability, optimization of the sample processing protocol of whole blood samples was applied (see below) and allowed the analysis of limited available samples taken during

the very early pandemic phase before dexamethasone and during the early phase of dexamethasone treatment within this study. Therefore, partial adoption of sampling time points and analyzed individuals was necessary.

A total of 35 samples from 35 patients (1 female, 34 males) recruited within the Pa-COVID-19 study were included into this analysis, 17 of whom were treatment-naive (9 moderately ill, 8 severely ill) and 18 treated with dexamethasone (11 moderately ill, 7 severely ill). The median age of all patients was 61 years (IQR range 54-73 years). All moderately affected patients survived, three severely ill patients deceased, one untreated patient and two patients treated with dexamethasone.

For determination of dexamethasone-related signatures, samples included into analysis were obtained at a median of nine days (IQR 6.75 - 9 days) after initiation of dexamethasone treatment and maximum 24 hours after the last dose. Samples from the dexamethasone-treated group were collected at a median of 15.5 days (IQR 13.75 - 17.25 days) after symptom onset. Control samples were obtained at a median of 15 days (IQR 12.5 - 18 days) after symptom onset.

### Subject details BAL sc-transcriptomics subgroup

In order to validate our findings from the blood in lung tissue we furthermore analyzed bronchoalveolar lavages (BAL) obtained from 12 patients recruited in the Pa-COVID-19 study. Due to the limited number of available samples, no matching was performed. In line with the other groups or cohorts, respectively, only immunocompetent glucocorticoid-naive and dexamethasone-treated patients without any additional immunomodulatory COVID-19-specific treatment were included. Samples from dexamethasone-treated patients were included into analysis when collected up to 10 days after the end of treatment. Three patients of the BAL analyses (2 treatment-naive, 1 dexamethasone-treated) were also part of the study population analyzed by blood scRNA-seq.

BALs were obtained during bronchoscopy of invasively ventilated COVID-19 patients at the Department of Infectious Diseases and Respiratory Medicine, Charité Universitätsmedizin Berlin according to standard operating procedures. Among the 12 patients 5 were glucocorticoid-naive (3 males, 2 females), who all survived; 7 received dexamethasone treatment (4 males, 3 females) of whom 4 survived and 3 died. The median age of all patients was 59 years (IQR 33-70 years). BALs were collected at a median of 14 days (IQR 9.5-25 days) after symptom onset from the treatment-naive group and at a median of 23 days (IQR 13-28 days) after symptom onset or 14 days (IQR 8-18 days) after initiation of dexamethasone treatment, respectively, from treated patients.

### Epigenetics

To assess the possible influence of patient's DNA-methylation status on responsiveness to dexamethasone treatment, we performed comparative analysis of the included patients from the Pa-COVID-19 study cohort with stable versus progressive disease under treatment, i.e. which progressed from moderate to severe disease or death after having received at least 2 days of treatment with a sample collected within the first 4 days of treatment. Control patients without disease progression under treatment were matched for sex, age, and available early samples after initiation of dexamethasone treatment. If more than one equivalent match was available, data was reviewed by at least two clinically experienced physicians for pre-existing comorbidities to find the most appropriate match.

### Subject details epigenetics

A total of 20 samples from 20 dexamethasone-treated patients, 10 males and 10 females, recruited within the Pa-COVID-19 study were analyzed. All 20 patients required supplemental oxygen at treatment initiation without need of invasive mechanical ventilation (WHO score 4-5). The median age of all patients was 62 years (IQR 57.25-69.75 years). Ten out of 20 patients (50%) recovered and did not worsen after initiation of dexamethasone treatment, whereas 10 patients (10/20, 50%) progressed under treatment reflected by the need of invasive ventilation and/or death. Four patients died. Sampling date for analysis was at a median of 2 days (IQR 2-3.75 days) after initiation of dexamethasone and median 9.5 days (IQR 7.25-11.75 days) after symptom onset.

### Bulk transcriptomics

To assess if the treatment-related signatures of dexamethasone-treated patients can be used to stratify outcome, bulk-sequencing was performed from the earliest available sample of whole blood collected under dexamethasone treatment from moderately (maximum WHO score $\leq$4) to severely ill (maximum WHO score $\geq$5) COVID-19 patients recruited into two independent cohorts. Patients were grouped according to disease severity as described above. First, patients recruited into the Pa-COVID-19 study in Berlin between 03/2020 and 12/2021 were included into the single-center (Charité) bulk subgroup.

Second, for the independent multi-center (CAPNETZ) cohort, samples were obtained from the CAPNETZ foundation. These patients were recruited across 11 centers (Berlin-Campus Benjamin Franklin, Cottbus, Jena, Bad Arolsen, Dortmund, Bonn, Rotenburg, Dresden, Gerlingen, Berlin-Charité, Berlin-Neukölln) between 06/2020 and 12/2021.

### Subject details single-center bulk subgroup

A total of 92 samples from 92 dexamethasone-treated patients (68 males, 24 females) included into the Pa-COVID-19 study were included into this subgroup (single-center, Charité). The median age of all patients was 61 years (IQR 49.75-69 years). Thirty-three patients were moderately ill and 59 patients severely ill, 18 of whom died. Samples for this analysis were obtained at a median 12 days (IQR 9-15 days) after symptom onset and of 4 days (IQR 3-5 days) after the initiation of dexamethasone treatment, respectively.

### Subject details multi-center bulk subgroup

A total of 90 samples obtained from 90 dexamethasone-treated patients (65 males, 25 females) included into the multi-center (CAPNETZ) cohort were included into this subgroup. The median age of all patients was 61 years (IQR 52-68 years). A total of 53 patients (65.5%) were moderately ill and 37 (34.4%) were severely ill, 11 of whom (35.5%) died. Samples for this analysis were obtained at a median of 2 days (IQR 1-3) after the initiation of dexamethasone treatment. Symptom onset was not documented in the case reporting form of PROVID-CAPNETZ.

### Ethics

The Ethics Committee of Charité Universitätsmedizin Berlin approved the following studies: Pa-COVID-19: EA2/066/20, COV-IMMUN: EA1/068/20. The Ethics Committee of the State Office for Health and Social Affairs Berlin: CVC for COVID-19: 20/0118 – A1 (AMG). The Institutional Review board of the University Hospital Bonn (073/19 and 134/20) approved the study conducted at University Hospital Bonn. The Ethics Committee of Hannover Medical School approved PROVID-CAPNETZ (Nr. 301-2008).

The Pa-COVID-19 study is registered in the German and the WHO international registry for clinical studies (DRKS00021688). The CVC for COVID-19 trial (NCT04500418) and PROVID-CAPNETZ study (NCT04952337) are registered at ClinicalTrials.gov.

The studies were conducted in accordance with the Declaration of Helsinki and current guidelines of Good Clinical Practice. Informed consent was obtained from all participants or their respective legal representatives. All patients were treated according to national and international guidelines.

## METHOD DETAILS

### Details for blood single-cell transcriptomics

#### *Isolation of blood cells for scRNA-seq*

scRNA-seq was performed on frozen PBMCs. Briefly, PBMCs were isolated from heparinized peripheral blood by density centrifugation over Pancoll or Ficoll-Paque density centrifugation (density: 1.077 g/ml). Cells were then cryopreserved at -150°C in RPMI1640 with 40% FBS and 10% DMSO.

#### *BD Rhapsody blood single-cell RNA-seq*

Frozen PBMCs were recovered by rapidly thawing frozen cell suspensions in a 37°C water bath followed by immediate serial dilution in pre-warmed RPMI1640+10% FBS (GIBCO) and centrifugation at 300 g for 5 min. After centrifugation, the cells were resuspended in RPMI1640+10% FBS and processed for whole transcriptome analyses, using the BD Rhapsody Single-Cell Analysis System (BD, Biosciences) as previously described[72]. Cells from each sample were labeled with hashtag-oligonucleotide-coupled antibodies, sample tags (BD Human Single-Cell Multiplexing Kit) following the manufacturer's protocol. Briefly, a total number of $1x10^6$ cells were resuspended in 90 μl of Stain Buffer (FBS) (BD PharMingen). The sample tags were added to the respective samples and incubated for 20 min at room temperature. After incubation, 500 μl stain buffer was added to each sample and centrifuged for 5 min at 300 g and 4°C. Samples were washed one more time. Subsequently cells were resuspended in 300 μl of cold BD Sample Buffer and counted using Improved Neubauer Hemocytometer (INCYTO). Labeled samples were pooled equally in 650 μl cold BD Sample Buffer. For each pooled sample two BD Rhapsody cartridges were super-loaded with approximately 60,000 cells each. Single cells were isolated using Single-Cell Capture and cDNA Synthesis with the BD Rhapsody Express Single-Cell Analysis System according to the manufacturer's recommendations (BD Biosciences). cDNA libraries were prepared using the BD Rhapsody Whole Transcriptome Analysis Amplification Kit following the BD Rhapsody System mRNA Whole Transcriptome Analysis (WTA) and Sample Tag Library Preparation Protocol (BD Biosciences). The final libraries were quantified using a Qubit Fluorometer with the Qubit dsDNA HS Kit (ThermoFisher) and the size-distribution was measured using the Agilent high sensitivity D5000 assay on a TapeStation 4200 system (Agilent technologies). Sequencing was performed in paired-end mode (2*75 cycles) on a NovaSeq 6000 with NovaSeq 6000 S2 or S4 Reagent Kit v1.5 (200 cycles) chemistry.

### Details for DNA methylation

#### *PBMC isolation for methylation analysis*

All samples were obtained in Berlin and subjected to standardized processing and stored by the Central Biobank of Charité (ZeBanC) according to SOPs of the Pa-COVID-19 study.

#### *FACS-based cell isolation for methylation analysis*

Frozen PBMC samples were taken up in 37°C RPMI1640 medium (Gibco) containing 20% BSA Fraction V (PAN-Biotech), 1% 10,000 U/ml Penicillin Streptomycin (Thermo Fisher Scientific) and 10 mM Hepes buffer (Biochrom) to quickly thaw. Cells were washed with PBS (Gibco).

PBMCs were stained using the following fluorescently conjugated monoclonal antibodies: CD3 BV421 (clone UCHT1), CD4 APCFire750 (clone RPA-T4), CD8a BV711 (clone RPA-T8), CD14 PerCP (clone TÜK4), CD16 BV605 (clone 3G8), CD19 PE (clone HIB19), CD45RA (clone HI100), CD66b APC (clone G10F5), CCR7 AF488 (clone G042H7).

$CD14^+$ Monocytes ($CD14^+$, $CD16^-$, $CD66b^-$), $CD19^+$ B cells ($CD3^-$, $CD19^+$), $CD4^+$ total memory T cells ($CD3^+$, $CD4^+$, $CD45RA^-$ and $CD3^+$, $CD4^+$, $CD45RA^+$, $CCR7^-$) and $CD8^+$ total memory T cells ($CD3^+$, $CD8^+$, $CD45RA^-$ and $CD3^+$, $CD8^+$, $CD45RA^+$, $CCR7^-$) were

sorted via FACS with a BD FACSAria II SORP (Becton Dickinson). Checks for sort purity were performed and ranged between 90%–99%. Following FACS, cell pellets were flash-frozen in liquid nitrogen.

#### *DNA methylation profiling*

From purified cell samples frozen as pellets, genomic DNA was extracted using Zymo's Quick-DNA MicroPREP Kit (Zymo Research) following instructions provided by the manufacturer. DNA concentration was measured using the Qubit dsDNA HS Assay Kit and the Qubit Fluorometer (Molecular Probes/Life Technologies).

Samples with cell counts <25,000 cells were not subjected to DNA extraction. Instead, the cell pellets were directly taken up in a mix of 40 μl lysate buffer from the Zymo's Quick-DNA MicroPREP Kit (Zymo Research) with 1.25 mg/ml Proteinase K (Sigma-Aldrich 3115828001) and incubated for 3 hours at room temperature. Cell lysate was directly used for bisulfite conversion as described below.

Isolated genomic DNA and cell lysates from Proteinase K digestion were subjected to bisulfite conversion using Zymo's EZ DNA Methylation-Gold Kit (Zymo Research) according to manufacturer's instructions. DNA methylation was assessed using the Infinium MethylationEPIC Kit (Illumina EPIC-8 BeadChip) following manufacturer's instructions. Illumina EPIC-8 BeadChips were imaged using Illumina's Microarray Scanner iScan.

### Details for CyTOF

#### *Antibodies used for CyTOF*

All anti-human antibodies pre-conjugated to metal isotopes were obtained from Fluidigm Corporation (San Francisco, USA). All remaining antibodies were obtained from the indicated companies as purified antibodies and in-house conjugation was done using the MaxPar X8 labeling kit (Fluidigm, USA). Antibodies are listed in the key resource table.

#### *Sample processing and antigen staining for CyTOF*

Sample processing, cell staining and acquisition was done as previously described.[18] In brief, whole blood samples were thawed, tagged with barcoding antibodies conjugated with different isotopes of Pd or Pt for 30min at 4°C and up to 10 samples were pooled for surface and intracellular staining. For surface staining, samples were incubated with primary and secondary anti-APC163Dy antibodies for 30min at 4°C, respectively, washed with PBS and fixed overnight. For intracellular staining, samples were permeabilized with permeabilization buffer (eBiosciecne, San Diego, US), stained with the respective antibodies for 30min at room temperature, and washed and stained with iridium intercalator (Fluidigm) for 20min at room temperature. After staining, cells were washed and stored at 4°C. Mass cytometry measurement was performed on a CyTOF2/Helios mass cytometer (Fluidigm).

### Details for bulk transcriptomics

#### *Whole blood RNA isolation*

For the single-center (Charité Berlin) and multi-center cohort (CAPNETZ), whole blood RNA isolation strategies were applied. In cohort 1, whole blood was collected and stored in Tempus tubes (Applied Biosystems), while cohort 2 used the PAXgene system (BD Medical). RNA was extracted according to the manufacturer's information.

#### *Bulk RNA sequencing*

After RNA extraction, total RNA libraries were generated using the TruSeq Stranded Total RNA with Ribo-Zero Globin kit (Illumina). In brief, ribosomal and globin mRNA were depleted from 750 ng purified total RNA using biotinylated, target-specific oligos combined with Ribo-Zero rRNA removal beads; after depletion remaining RNA was purified, fragmented, and primed for cDNA synthesis. 3′ ends were adenylated and index adapters were ligated to the ends of the ds cDNA. Selective enrichment of DNA fragments with ligated adaptor molecules on both ends was performed using Illumina PCR primers in a 15-cycle PCR reaction, followed by a purification step using SPRIBeads (Beckman Coulter). Libraries were quantified by Qubit dsDNA HS Assay (Thermo Fisher Scientific), and fragment size distribution was determined using the HS D1000 assay on a Tapestation 4200 system (Agilent). Sequencing was performed in paired-end mode (2*50 cycles) on a NovaSeq 6000 with NovaSeq 6000 S2 Reagent Kit v 1.5 (200 cycles) chemistry. Data was converted into fastq files using bcl2fastq2 v2.20.

### BAL single-cell processing and sequencing

BALs were processed and sequenced as described before.[30] BAL fluid was filtered through a 70 μm mesh and centrifuged (400 g, 10 min, 4°C). The supernatant was removed and cells were washed once with DPBS (GIBCO). Erythrocytes were then removed using the Red Blood Cell (RBC) lysis buffer (Biolegend). The cells were washed twice and either processed for subsequent scRNA-seq or cryopreserved in FCS+10% DMSO at -150°C.

Frozen BAL cells were thawed using pre-warmed medium (RPMI 1640, Gibco; 2% FCS, Sigma; 0.01% Pierce Universal Nuclease, Thermo Fisher, USA). For multiplexing of multiple BAL donors, cells were labeled with 0.5μg of TotalSeq-A Hashtag antibodies for 30 min at 4°C. Subsequently cells were washed three times and up to 4 donors were pooled in equal proportions and passed through a 40 μm mesh (Flowmi™ Cell Strainer, Merck).

The cell suspension was then adjusted to an appropriate concentration to load 16.500- 50.000 cells/reaction into the 10x Genomics Chromium Controller for scRNA-seq. Single Cell 3′ reagent kit v3.1 was used for reverse transcription, cDNA amplification and library construction according to the detailed protocol provided by 10x Genomics and Biolegend. Libraries were quantified by QubitTM 2.0 Fluorometer (ThermoFisher) and quality was checked using 2100 Bioanalyzer or Tapestation 4150 with High Sensitivity

DNA kit (Agilent). Sequencing was performed in paired-end mode with SP, S1, S2 (2x50 cycles) and S4 (2x100 cycles) flowcells using NovaSeq 6000 sequencer (Illumina).

### Monocyte FACS verification

CD163 and amphiregulin expression in monocytes was assessed by flow cytometry. Briefly, after treatment with Zombie Aqua viability dye (Biolegend, USA), FC receptor blockade (FC Block, Miltenyi), thawed PBMCs were incubated with following surface antibodies: CD14-BV421 (clone M5E2), CD163-PercP-Vio770 (clone REA812), and for exclusion CD3-FITC (clone UCGT1), CD94-FITC (clone DX22), NKp80-FITC (clone 4A4.D10), TCRab-FITC (clone IP26), TCRgd-FITC (clone B1), CD20-FITC (clone 2H7), and CD19-FITC (clone HIB19). Samples were analyzed using a BD Canto II flow cytometer and FlowJo 10.8 software (BD).

### SARS-CoV-2 spike protein ELISA

SARS-CoV-2 spike protein-specific antibodies were detected by SeraSpot Anti-SARS-CoV-2 IgG microarray-based multiparameter immunoassay. Samples were processed and measured according to the manufacturer's instructions (Seramun Diagnostica GmbH, https://www.seramun.com). In brief, serum samples were pre-diluted 1:101 and added to microarray plates pre-coated with the SARS-COV-2 receptor-binding domain (RBD) epitope, with negative and positive controls as capture antibodies. Samples were measured with the accompanying SpotSight plate scanner and results above 160 BAU/ml were regarded as positive, as per the manufacturer.

## QUANTIFICATION AND STATISTICAL ANALYSIS

### Analysis of blood single-cell transcriptome data

#### *Data pre-processing of blood scRNA-seq data*

After demultiplexing of bcl files using Bcl2fastq2 V2.20 from Illumina and quality control, paired-end scRNA-seq reads were filtered for valid cell barcodes using the barcode whitelist provided by BD. Cutadapt 1.16 was then used to trim NexteraPE-PE adaptor sequences where needed and to filter reads for a PHRED score of 20 or above.[48] Then, STAR 2.7.3a was used for alignment against the Gencode v27 reference genome.[47] Dropseq-tools 2.0.0 were used to quantify gene expression and collapse to UMI count data (https://github.com/broadinstitute/Drop-seq/). For hashtag-oligo based demultiplexing of single-cell transcriptomes and subsequent assignment of cell barcodes to their sample of origin the respective multiplexing tag sequences were added to the reference genome and quantified as well.

#### *Blood scRNA-seq quality control and annotation*

Samples were selected and grouped as described above. Analysis of scRNA-seq data was performed using the Seurat pipeline (v4.3.0).[51,73] During preprocessing and quality control (QC), cells that were considered as doublets or negatives after demultiplexing using the HTODemux function from Seurat (positive.quantile 0.99), singlets that did not exceed 300 unique molecular identifiers (UMIs), had more than 30% mitochondrial genes, showed less than 300 and more than 3500 features per cell or were present in small contaminating clusters were excluded from downstream analysis. Additionally, genes that were expressed in less than 5 cells per cartridge were removed. After QC, a total of 114,181 single-cell transcriptomes of PBMCs were analyzed. The entire dataset was normalized, scaled, and dimensional reduction was calculated using the standard Seurat functions. For normalization, the gene expression values were normalized by total UMI counts per cell, multiplied by 10,000 (TP10K) and then log transformed by $\log_{10}$(TP10k+1). Subsequently, the data was scaled, centered, and regressed against the number of detected transcripts per cell to correct for heterogeneity associated with differences in sequencing depth. For dimensionality reduction, PCA was performed on the top 2,000 variable genes identified using the vst method. For two-dimensional representation of the data structure, uniform manifold approximation and projection (UMAP) was calculated using the first 30 principle components (PCs). Subsequently, the cells were clustered using the Louvain algorithm based on the first 30 PCs using a resolution of 0.4. Cluster-specific marker genes were calculated with the Wilcoxon rank sum test using the FindAllMakers function (min.pct=0.2, logfc.threshold=0.5). Using the combined information of cluster marker and literature-known markers, present cell types were annotated: Monocytes (*LYZ, S100A8, S100A9*), mDCs (*FCER1A, CD1C*), pDCs (*ITM2C, SOX4*), platelets (*PPBP, PF4*), $CD4^+$ T cells (*TCF7, IL7R*), $CD8^+$ T cells (*CD8A, GZMH*), NK cells (*KLRF1, PRF1*), B cells (*MS4A1, CD79A*), plasmablasts (*JCHAIN, IGKC*), proliferating cells (*MKI67, STMN1*) and erythrocytes (*HBB, HBA1, HBA2*).

#### *Selection of monocytes*

Blood monocytes were selected and annotated in a three-step process. First, all monocyte transcriptomes were subsetted from the PBMC data. This subset was subsequently normalized and scaled, and dimensional reduction was calculated using the standard Seurat functions. For normalization, the gene expression values were normalized by total UMI counts per cell, multiplied by 10,000 (TP10K) and then log transformed by $\log_{10}$(TP10k+1). Subsequently, the data was scaled, centered, and regressed against the number of detected transcripts per cell to correct for heterogeneity associated with differences in sequencing depth. For dimensionality reduction, PCA was performed on the top 1000 variable genes identified using the vst method. To adjust for a batch-effect observed by experimental day, the harmony algorithm (v0.1.0) was applied.[54] For two-dimensional representation of the data structure, uniform manifold approximation and projection (UMAP) was calculated using the first 15 harmony components. Next, monocytes were cleaned from non-monocytes. For this, the cells were clustered using the Louvain algorithm based on the first 15 harmony

reductions. Clusters showing expression of other cell types (such as NK cells, T cells and B cells) were excluded. Finally, after cleaning, the basic Seurat steps were applied again and clusters were calculated using a resolution of 0.7. Cluster-specific marker genes were calculated with the Wilcoxon rank sum test using the FindAllMakers function (min.pct=0.2, logfc.threshold=0.5). The resulting monocyte clusters were annotated as IFI$^{hi}$ (*IFI6, IFI27, IFI44L*), IL1B$^{hi}$ (*IL1B, CCL3, CCL4L2*), S100A$^{hi}$ (*S100A12, S100A8, S100A9*), S100A$^{hi}$CXCL$^{hi}$ (*CXCL1, CXCL2, CXCL3, CXCL8*), Dexa response (*AREG, IL1R2, CD163, TSC22D3*), HLA$^{hi}$ (*HLA-DPA1, HLA-DRA, HLA-DRB1*), THBD$^{hi}$ (*THBD, RGCC, LMNS*), PF4$^{+}$ (*PF4*), HB$^{hi}$ (*HBB*) and CD16 C1Q$^{+}$ (*FCGR3A, C1QB, C1QA*) monocytes.

#### Module score calculation

For the module score calculation, the AddModuleScore function from Seurat was applied with the respective gene signatures.

For the interferon enrichment a set of 15 interferon-response genes was used including *IFI6, ISG15, IFITM1, ISG20, IFI27, IFI30, IFIH1, IFIT1, IFIT2, IFIT3, IFITM2, IFITM3, XAF1, MX1* and *MX2*. For the glucocorticoid signature the top 100 up- and downregulated genes from Wang et al.[26] were extracted and enriched by blood monocyte states.

To check for statistical differences, a Kruskal-Wallis (KW) test was applied for the mean module score per donor against the respective category of interest, e.g. monocyte states.

#### Differential gene expression

Differential expression (DE) tests in the blood data were performed using FindMarkers function from Seurat with the Wilcoxon rank sum test. Genes with a log-fold change greater than 0.25, at least 10% expressed in tested groups and with a bonferroni-corrected $p$ value $\leq$0.05 were considered as significantly differentially expressed genes (DEGs). For calculation of DEGs by cell types, only cell types with more than 2,000 cells were considered.

#### Functional enrichment analysis

Gene set ontology enrichment analysis (GOEA) using the DEGs as input was performed on the gene sets from the Gene Ontology (GO) biological process (BP) database,[74,75] the Kyoto Encyclopedia of Genes And Genomes (KEGG) database,[76] the Hallmark gene sets[77] and the Reactome gene sets[78,79] using the R package clusterProfiler (version 4.0.5).[55,80] Ontologies with statistical significance (bonferroni-adjusted $p$ value $\leq$0.05) were used for presentation. For the common terms in multiple cell types, terms were filtered for enrichment in at least three different cell types.

#### Quantification of monocyte states

To compare shifts in the blood monocyte states stratified by group and treatment as well as outcome, the percentages of each cluster were quantified per sample of the respective groups and visualized together in boxplots. For determination of statistical significant differences in the distribution a Wilcox test was performed for severity or outcome groups.

#### Core Dexa signature identification

To identify DEGs common for Dexa treatment despite COVID-19 severity, a fold change (FC) comparison was performed for DEGs calculated between Dexa vs. ctrl. for both severities independently. Resulting FCs were plotted against each other and commonly up- and downregulated genes were indicated.

### Analysis of BAL single-cell transcriptome data

#### Re-analysis of BAL monocytes from Sinha et al.

To verify our findings from our scRNA-seq monocyte analysis, we inspected the single-cell whole blood dataset generated by Sinha et al.[12] The monocyte compartment was subsetted based on the original 'celltype1' annotation. Subsequently, the monocytes were normalized, scaled, and visualized using 'patient'-corrected harmony and UMAP dimensionality reductions. After removal of contaminating clusters, defined as cells that express cell type markers unrelated to monocytes, a total of 2,350 monocytes were present. By *CD14* and *FCGR3A* (CD16) expression, the monocytes were annotated as classical or non-classical monocytes. In all monocytes, the average expression of selected Dexa-related genes was calculated stratified by the "time_split_status" information provided by the authors (including treatment group and duration) and visualized in a heatmap.

#### Re-analysis of BAL myeloid cells from Liao et al.

To check specific genes identified in this study in the lung, we inspected the single-cell bronchoalveolar lavage (BAL) dataset generated by Liao et al.[29] Here, a total of 6 severe COVID-19 patients were included with n=2 untreated survivors and n=4 methylprednisolone-treated patients, of which n=2 deceased. The macrophage and monocyte compartment was subsetted based on the original cell type annotation, cells were cleaned from contamination and gene expression of 32 selected markers was assessed in a total of 25,191 cells.

#### BAL scRNA-seq pre-processing, quality control, and annotation

Raw expression data in form of FASTQ files were collected, read quality was assessed using fastQC (version 0.11.8)[49] and alignment/counting was performed using 10x Genomics Cell Ranger (version 7.0.0)[50] using a custom reference created from the GRCh38 human genome reference available from 10x Genomics (refdata-gex-GRCh38-2020-A) and a number of viral genomes including SARS-CoV-2 (RefSeq:NC_045512.2).

For quality control, transcriptomes were clustered using library size, number of genes, percentage of mitochondrial (%MT) and ribosomal (%RP) counts. Clusters with %MT > 5 were excluded from the analysis. After QC, a total of 67,439 single-cell transcriptomes of BAL cells remained.

Data was loaded into R (version 4.3.1) and stored in a SeuratObject (version 4.1.4). Seurat (version 4.4.0)[51,73] was used to normalize counts, find variable genes, scale data, and compute a PCA embedding. FastMNN from the batchelor package (version 1.16.0)[56] was used to integrate data using "library" as a batch. For annotation, clusters were computed using the Seurat implementation of the smart local moving algorithm for large-scale modularity-based community detection,[81] cell type AUCs were computed using the AUCell package (version 1.22.0)[57] and automatic assignment of cell type identity to clusters was performed using annotate_maxAUC of the SeuratHelper package (version 1.0.0). Annotation was refined using cluster averages of AUC scores and quality metrics. Cell types annotation markers: Monocytes (*CD14, VCAN, FCGR3A*), macrophages (*MARCO, CD68*), DCs (*TCF4, CD1C*), T cells (*CD8A, CD3D, CD3E*), plasmablasts (*JCHAIN, IGHGP*), neutrophils (*CSF3R, NAMPT*), erythrocytes (*HBA1, HBB*) and epithelia (*KRT8, KRT19*).

Custom code used for the analysis is available under github.com/saliba-lab/covid19-bal-atlas-integration.

#### *Differential gene expression*

Differential expression (DE) tests in the BAL data were performed using FindMarkers function from Seurat with the Wilcoxon rank sum test. Genes with a log-fold change greater than 0.25, at least 10% expressed in tested groups and with a bonferroni-corrected $p$ value $\leq 0.05$ were considered as significantly differentially expressed genes (DEGs). For calculation of DEGs by cell types, erythrocytes and low-quality cells were excluded.

#### *Module score calculation*

For the module score calculation in BAL monocytes and macrophages, the AddModuleScore function from Seurat was applied with the "Dexa response" monocyte state markers (n=30) as a signature. For statistical testing, a Wilcoxon test was performed based on the mean module score per donor by the respective treatment groups and outcome.

### Bulk RNA-sequencing analysis

The 'STAR: ultrafast universal RNA-seq aligner' (v2.7.3a)[47] was used to align the sequenced reads against the human GENCODE reference genome v33. Total reads were randomly downsampled to a maximum of 34,195,155 reads per sample. Following the import of the raw counts using the DESeq2[58] function DESeqDataSetFromMatrix, genes with a lower total count number than the included number of samples were excluded from the analysis resulting in 27,669 and 28,784 genes for cohort 1 and cohort 2, respectively. The count matrices were DESeq2 normalized and a variance stabilizing transformation (vst) was applied. To minimize the variance introduced by the different study sites in cohort 2, the transformed data was limma batch-corrected[65] setting the study sites and the seasonality as the batch variables. Patient groups were defined as described above. A gene set variation analysis (GSVA)[59] was performed on the transformed data with default parameters using the single-cell RNA-seq monocyte outcome signature, which was based on the comparison of dexamethasone-treated but deceased patients vs. treated survivors ('deceased upregulated' with 379 genes and 'deceased downregulated' with 282 genes). Wilcoxon tests were calculated between the different conditions and the resulting $p$ values were adjusted utilizing the Benjamini-Hochberg (BH) method. Permutation tests were performed by drawing 500 random, unique gene sets with the same size as the respective signature. For each gene set, GSVA enrichment scores were calculated per sample and BH-adjusted $p$ values were computed between surviving and deceased patients. The likelihood of the enrichment results of the single-cell signatures was computed by dividing the number of gene sets with lower adjusted $p$ values by the number of permutations. To identify the optimal signature length, signature genes measured in both cohorts (366 genes in the 'deceased upregulated'-signature and 275 genes in the 'deceased downregulated'-signature) were ordered based on their average log2FC in the scRNA-seq data and a GSVA was performed for all possible signature sizes in each cohort (starting with an initial size of 10 signature genes). The optimal signature length was defined as the minimum of the mean adjusted $p$ value distribution of the two cohorts. Genes representing the leading edge of each signature enrichment were assessed by calculating the expression level statistics from a non-parametric kernel estimation of the cumulative density function of each gene expression profile per sample and cohort as previously described.[59] After computing the mean of the expression level statistic for each gene over all samples of the deceased patient group of the respective cohort and centering the resulting ranks around 0, a gene set enrichment analysis (GSEA) was performed per signature and cohort and the leading edge defined as the subset of the signature including those genes that appear in the ranked list at or before the point at which the running sum reaches its maximum[82] was computed using fgsea (v1.18.0).[60]

### CyTOF: Cell identification and cluster analysis

Major leukocyte populations were identified from two antibody panels designed for CyTOF. Myeloid cells were identified from panel 2. Monocytes and DCs were obtained from the exclusion of $CD3^-$, $CD19^-$ and $CD56^-$ cells, and expression of $CD14^+$ and $HLA\text{-}DR^+$ cells. The Monocytes and DCs batch-normalized CyTOF values (described in Schulte-Schrepping et al.[18]) were first transformed with the inverse hyperbolic sine function (asinh) and then z-score normalized per marker across all samples and all cells. They were then clustered using FlowSOM,[66] with 25 meta clusters (FlowSOM_k). Clusters were merged in pairs when their marker expressions were similar, which resulted in 19 clusters (Figure S3B). Similarly, UMAPs were calculated with the selected markers mentioned above using the R package 'uwot' with default parameters (https://github.com/jlmelville/uwot). The frequency of each cluster was calculated as the percentage of cells in each cluster for each sample in each compartment.

Statistical testing for the difference in the frequency of each cluster per severe or moderate category was calculated with the Wilcoxon test. Granulocytes in panel 2 were identified based on the expression or exclusion of $CD3^{-}CD19^{-}CD56^{-}CD14^{-}CD15^{+}$. Populations obtained from panel 1 include:

$CD4^{+}$ T cells ($CD3^{+}CD45^{+}CD19^{-}CD15^{+}CD14^{+}CD8^{-}TCRgd^{-}$), $CD8^{+}$ T cells ($CD3^{+}CD45^{+}CD19^{-}CD15^{+}CD14^{+}CD8^{-}TCRgd^{-}$) and $TCRgd^{+}$ cells ($CD3^{+}CD45^{+}CD19^{-}CD15^{+}CD14^{+}TCRgd^{+}$). Other populations include the B cells ($CD45^{+}CD19^{+}CD3^{-}CD14^{-}CD15^{-}$) and NK cells ($CD45^{+}CD3^{-}CD19^{-}CD56^{+}CD14^{-}$).

## Analysis of DNA methylation data

### *Pre-processing raw methylation data*

The raw intensity data files (IDAT) were preprocessed using minfi version 1.42.0 by quantile normalization. Probes were filtered based on not meeting the detection *p* value threshold against the background ($p<0.01$), being reported as cross-reactive,[83] revisions of Illumina's manifest (Infinium MethylationEPIC v1.0 13.03.2020), or being at a SNP, using the minfi function dropLociWithSnps. To account for differences between the 10 matched responder/non-responder pairs (e.g. matched comorbidities, age, sex, etc.) batch correction was performed using the ComBat function from the sva package version 3.44.0.[63]

### *Differential DNA methylation analysis*

As the cohort included both female and male donors, CpGs on sex chromosomes were removed before differential methylation analysis. Differential methylated positions (DMPs) were identified using the limma package version 3.52.2.[65]

## Enrichment analysis for DNA methylation data

Gene set ontology enrichment analysis adjusting for CpG number per gene using DMPs as input was performed using the methylglm function from the mehylGSA package version 1.14.0[84] on gene sets from the Gene Ontology (GO) biological process (BP) database.[75]

Enrichment of differentially expressed genes from the scRNA-seq dataset was calculated using the methylRRA function from the same package. The function utilizes robust rank aggregation (RRA) to adjust multiple *p* values of each gene for enrichment analysis.[62]

## Data visualization

For data visualization the R packages Seurat (version 4.3.0),[73] ggplot2 (version 3.3.5),[61] pheatmap (version 1.0.12) or fmsb (version 0.7.5) were used.

CellPress
OPEN ACCESS

# Supplemental figures

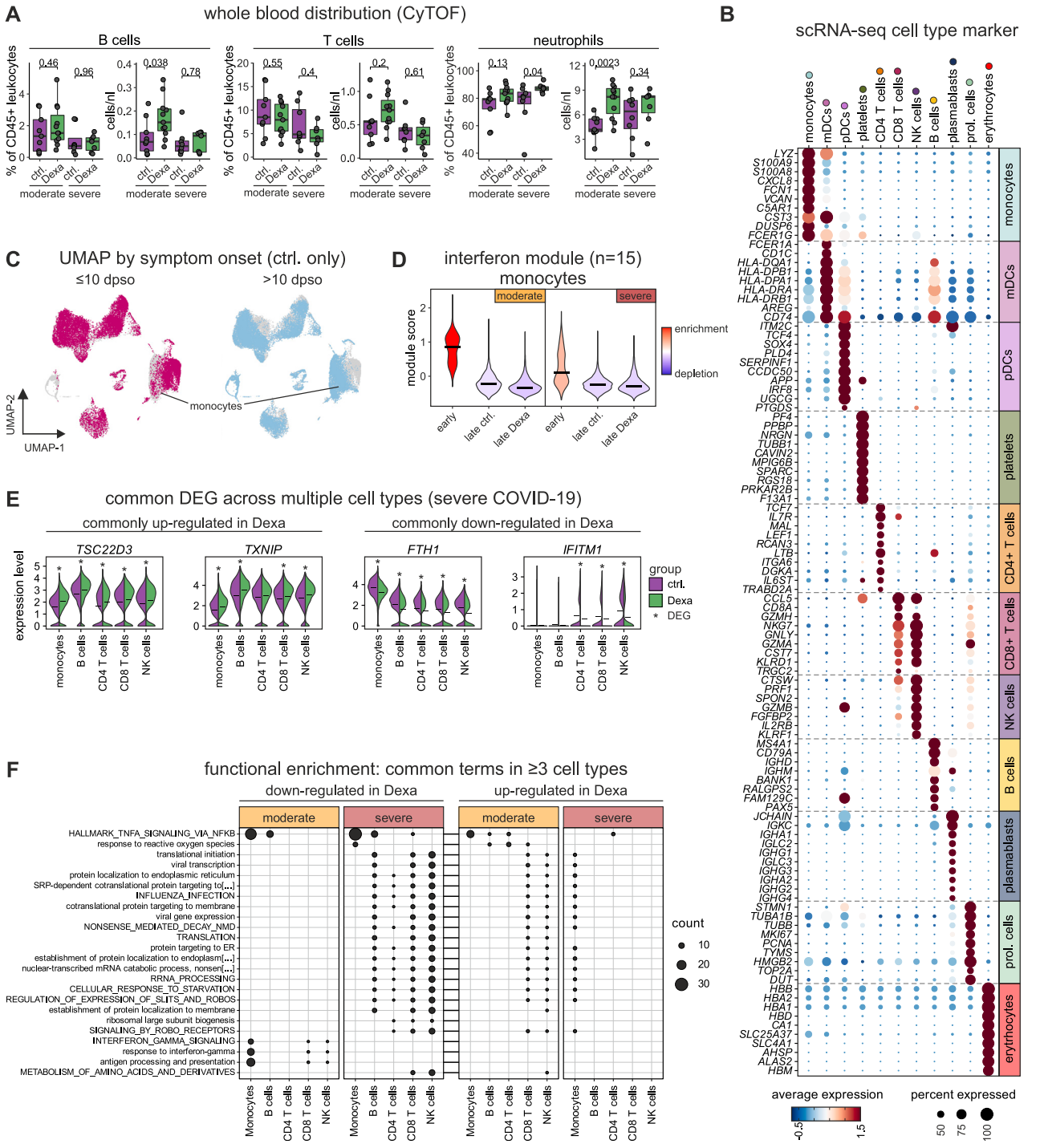


**Figure S1. Shared effect of dexamethasone treatment across circulating immune cells, related to Figure 1**

(A) Percentages of CD45$^{+}$ leukocytes and concentration of B cells, T cells, and neutrophils in whole blood from CyTOF stratified by treatment and COVID-19 severity. Wilcoxon test for statistical significance, and resulting *p* values are indicated.

(B) Marker gene expression for identified major cell types in the PBMC space from single-cell RNA-seq data.

*(legend continued on next page)*

(C) UMAP of the entire PBMC space from scRNA-seq colored by symptom onset in days after onset ($\leq$10 or >10) for untreated patients (control).
(D) Enrichment of the interferon module ($n$ = 15 genes) described for acute COVID-19 monocytes[18] in monocytes by time points.
(E) Common differentially expressed genes (DEGs, from Figure 1G) in at least 3 cell types in severe COVID-19. Significant differential expression is indicated with asterisks.
(F) Functional enrichment of DEGs identified in Figure 1G using the GO biological processes (BP) and Hallmark databases. Displayed terms were common in at least three cell types.

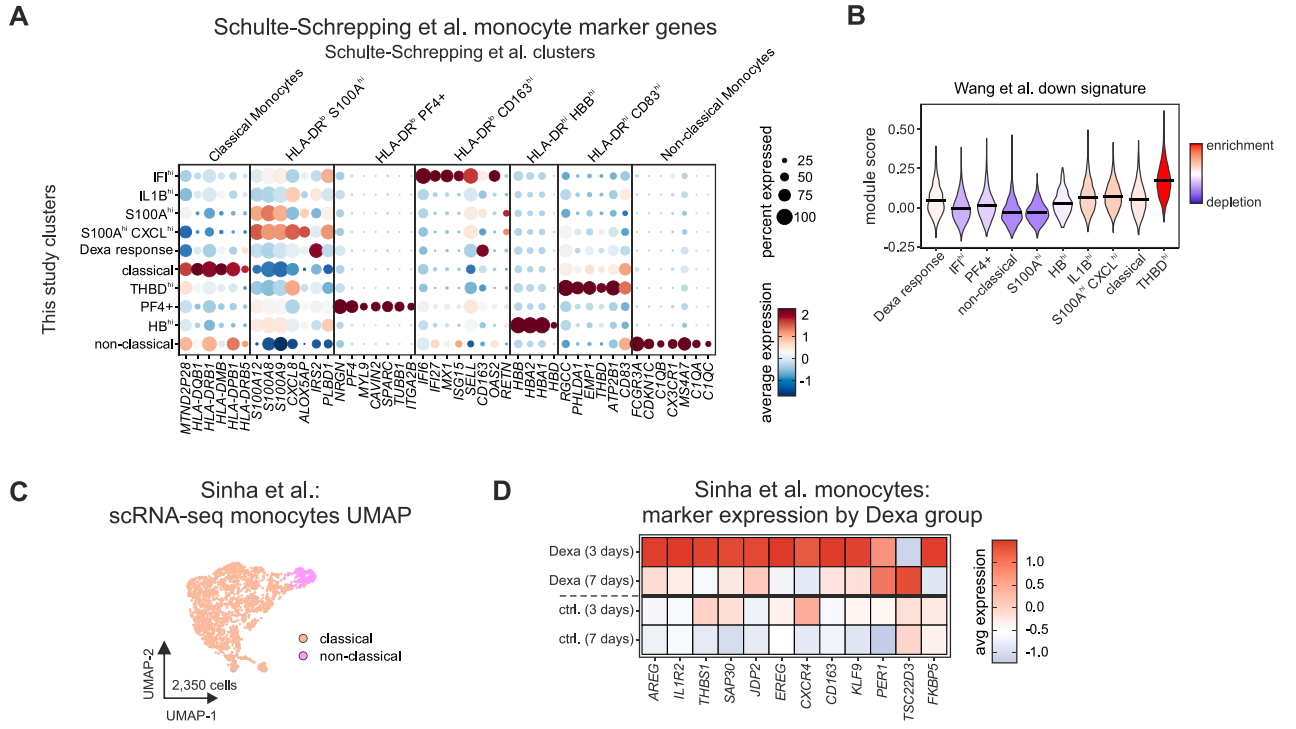


**Figure S2. Mapping of monocyte states to acute COVID-19 and validation of dexamethasone effects, related to Figure 2**

(A) Expression of monocyte-state markers from Schulte-Schrepping et al.[18] by monocyte states identified in this study.

(B) Enrichment of the *in vitro* generated glucocorticoid down signatures from Wang et al.[26] in all monocyte states.

(C) UMAP visualization of all monocytes extracted from the whole blood scRNA-seq dataset from Sinha et al. ($n$ = 2,350 cells).[12]

(D) Dexa-inducible gene expression in whole blood monocytes of dexamethasone-treated and control patients separated for time points (3 and 7 days) from Sinha et al.[12]

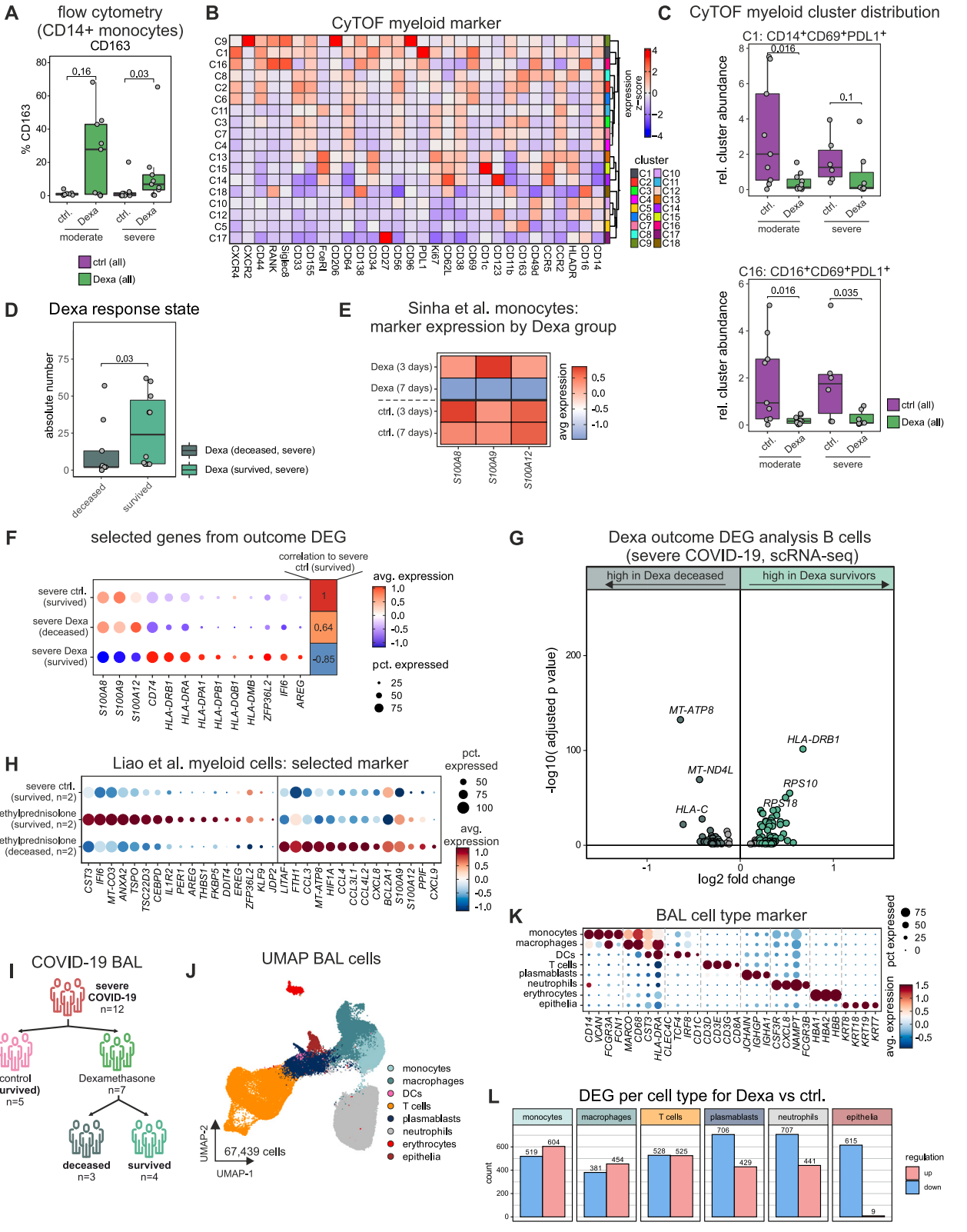


*(legend on next page)*

**Figure S3. Proteomics analysis of monocytes and overview of the BAL dexamethasone cohort, related to Figure 3**

(A) CD163 protein expression by flow cytometry on $CD14^+$ monocytes of COVID-19 patients who survived stratified by severity and dexamethasone treatment. Wilcoxon test for statistical testing, and resulting *p* values are indicated.

(B) Clustered marker heatmap of the CyTOF analysis from myeloid cells with a total of 18 clusters defined by 31 protein markers. Resulting clusters are indicated.

(C) Monocyte relative cluster distribution from CyTOF analysis for clusters 1 ($CD14^+CD69^+PD\text{-}L1^+$) and 16 ($CD16^+CD69^+PD\text{-}L1^+$) in COVID-19 patients who survived stratified by severity and dexamethasone treatment. Wilcoxon test for statistical testing, and resulting *p* values are indicated.

(D) Absolute numbers of monocyte in the Dexa response state in severe patients with dexamethasone treatment stratified by outcome. Statistical testing using Wilcoxon test, and resulting *p* values are indicated.

(E) Alarmin (*S100A8*, *S100A9*, and *S100A12*) gene expression in whole blood monocytes selected from Sinha et al. (see Figure S2C).[12]

(F) Gene expression of selected genes from the monocyte outcome signature (Figure 3H) by COVID-19 severity status and outcome in monocytes. Correlation of the average gene expression of those genes compared with severe controls that survived is indicated.

(G) Volcano plot showing the outcome DEGs between severe COVID-19 patients treated with dexamethasone who survived vs. those who were treated but deceased in B cells.

(H) Expression of selected markers identified in this study in the bronchoalveolar lavage (BAL) COVID-19 macrophages and monocytes from Liao et al.[29] comprising $n = 6$ severe COVID-19 patients with $n = 2$ untreated survivors and $n = 4$ methylprednisolone-treated patients of which 2 deceased.

(I) COVID-19 BAL cohort overview. A total of 12 severe COVID-19 patients were included of which $n = 5$ were untreated controls and $n = 7$ received dexamethasone of which 3 deceased (for cohort details see Table S1).

(J) UMAP visualization of the cell types identified in the BAL of severe COVID-19 patients ($n = 67{,}439$ cells).

(K) Cell type marker for identification of present cell types identified in (H).

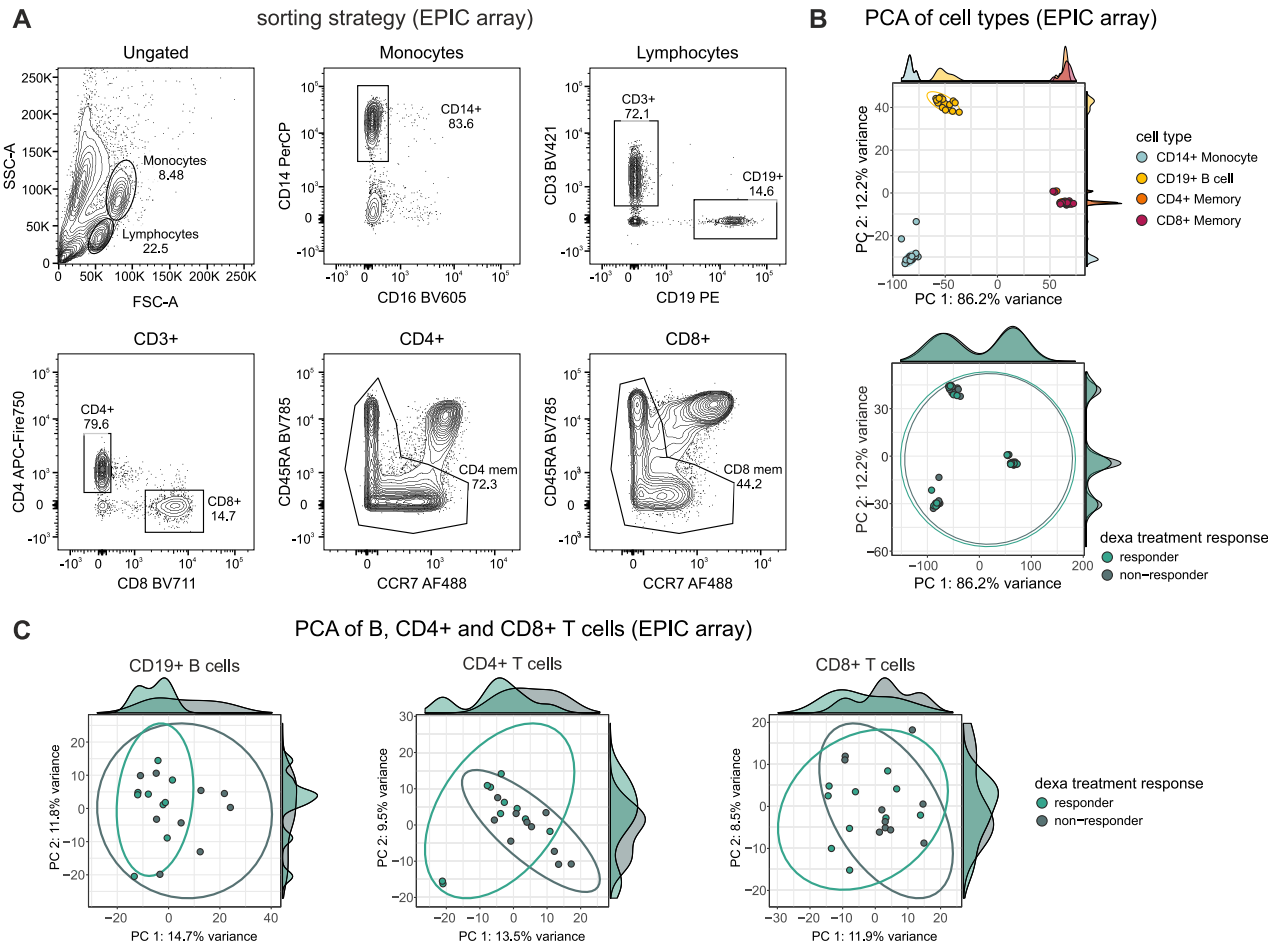


**Figure S4. Gating strategy for cell sorting and PCA by treatment response of the epigenetic data, related to Figure 4**

(A) FACS sorting strategy for the isolation of $CD14^{+}CD16^{-}$ monocytes, $CD19^{+}$ B cells, and $CD4^{+}$ or $CD8^{+}$ memory T cells for DNA methylation analysis.

(B) PCA of DNA methylomes of all samples analyzed, colored by cell types (upper) and dexamethasone treatment response group (lower).

(C) PCA of DNA methylomes of B cells, $CD4^{+}$ and $CD8^{+}$ memory T cells by dexamethasone treatment response.

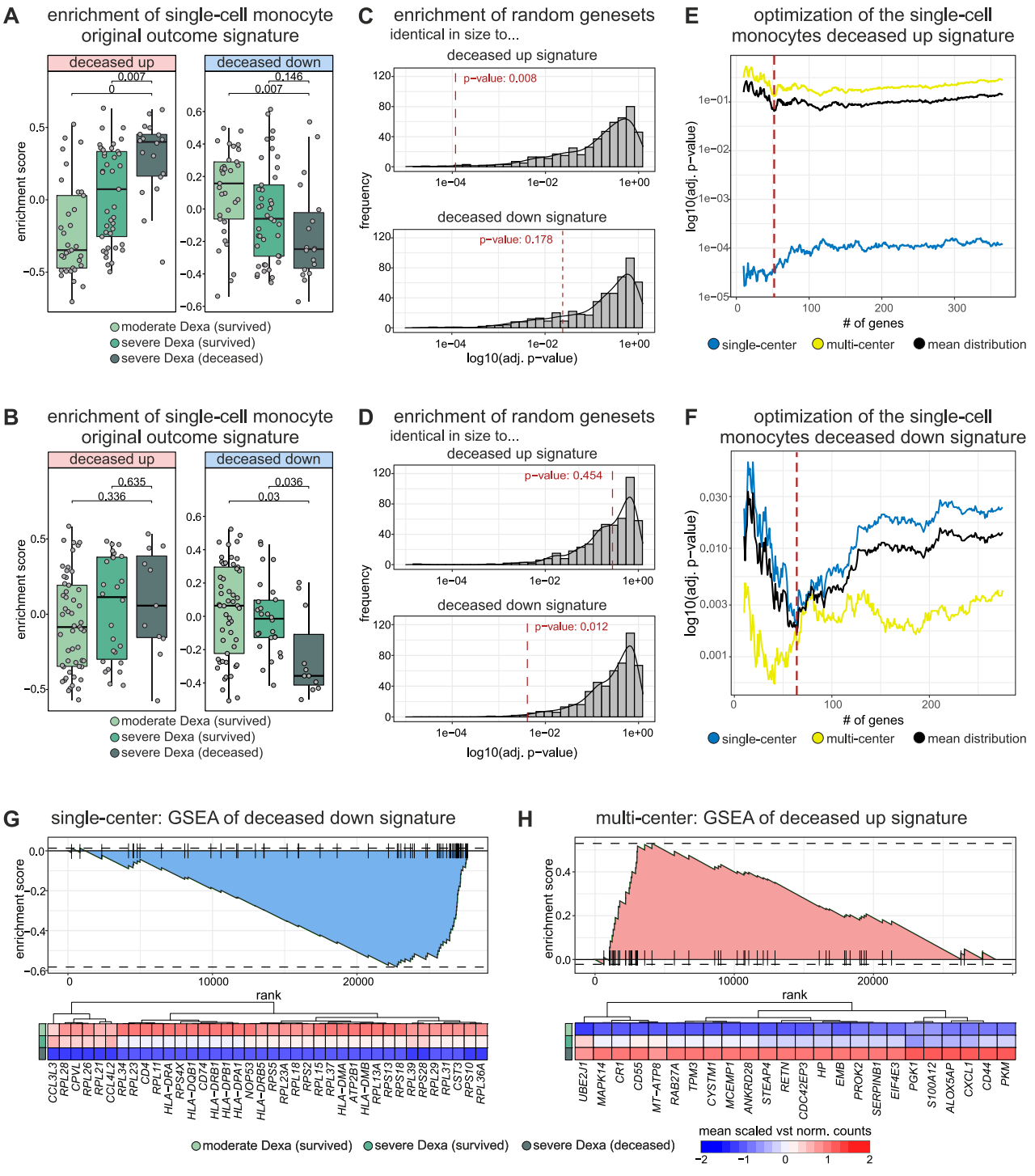


**Figure S5. Optimization of the single-cell signature for enrichment in whole blood data, related to Figure 5**

(A) Boxplots displaying the gene set variation analysis (GSVA) enrichment scores of the original deceased upregulated signature (left plot) and original deceased downregulated signature (right plot) in the single-center (Charité) cohort split and colored by the COVID-19 severity status and outcome. Wilcoxon test and Benjamini-Hochberg adjustment were utilized for statistical analysis.

(B) Boxplots displaying the GSVA enrichment scores of the original deceased upregulated signature (left plot) and original deceased downregulated signature (right plot) in the multi-center (CAPNETZ) cohort split and colored by the COVID-19 severity status and outcome. Wilcoxon test and Benjamini-Hochberg adjustment were utilized for statistical analysis.

*(legend continued on next page)*

(C) *p* value distribution of GSVA enrichment results of 500 random, unique gene sets in the single-center cohort on a $\log_{10}$ scale. Gene set size was based on the size of the original deceased upregulated signature (upper plot) and the original deceased downregulated signature (lower plot). *p* values were computed with a Wilcoxon test comparing deceased and surviving patients and were Benjamini-Hochberg adjusted. The red dashed line represents the adjusted *p* value from GSVA enrichment of the original deceased upregulated and the original deceased downregulated signatures, respectively.
(D) *p* value distribution of GSVA enrichment results of 500 random, unique gene sets in the multi-center cohort on a $\log_{10}$ scale. Gene set size was based on the size of the original deceased upregulated signature (upper plot) and the original deceased downregulated signature (lower plot). *p* values were computed with a Wilcoxon test comparing deceased and surviving patients and were Benjamini-Hochberg adjusted. The red dashed line represents the adjusted *p* value from GSVA enrichment of the original deceased upregulated and the original deceased downregulated signatures, respectively.
(E) Line plot of the deceased upregulated signature optimization illustrating the GSVA *p* value distribution between deceased and surviving patients with varying signature size based on the average $\log_2$FC from the scRNA-seq data. Signature size varied from 10 to the number of signature genes expressed in both cohorts, and the distributions were color-coded according to the single-center cohort (blue), the multi-center cohort (yellow), and the mean of the single- and multi-center cohorts (black). The red dashed line indicates the optimal gene signature size.
(F) Line plot of the deceased downregulated signature optimization illustrating the GSVA *p* value distribution between deceased and surviving patients with varying signature size based on the average log2FC from the scRNA-seq data. Signature size varied from 10 to the number of signature genes expressed in both cohorts, and the distributions were color-coded according to the single-center cohort (blue), the multi-center cohort (yellow), and the mean of the single- and multi-center cohorts (black). The red dashed line indicates the optimal gene signature size.
(G) Gene set enrichment analysis (GSEA) of the optimized deceased downregulated signature in the deceased patient group of the single-center cohort. Ranking of samples is based on expression-level statistics, and the running sum is visualized. The heatmap depicts the scaled variance-stabilized mean expression per COVID-19 severity status and outcome of the genes included in the leading edge.
(H) GSEA of the optimized deceased upregulated signature in the deceased patient group of the multi-center cohort. Ranking of samples is based on expression-level statistics, and the running sum is visualized. The heatmap depicts the scaled variance-stabilized mean expression per COVID-19 severity status and outcome of the genes included in the leading edge.